A N N U A L R E P O R T

2002

and list of publications

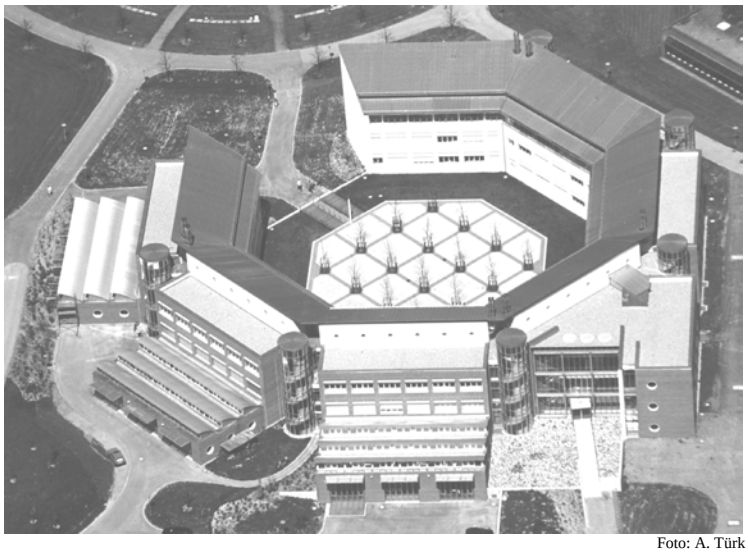

Foto: A. Türk

Bayerisches Forschungsinstitut
für Experimentelle Geochemie und Geophysik
Universität Bayreuth

Bayerisches Geoinstitut
Universität Bayreuth
D-95440 Bayreuth
Germany

Telephone: +49-(0)921-55-3700
Telefax: +49-(0)921-55-3769
e-mail: bayerisches.geoinstitut@uni-bayreuth.de
www: http://www.bgi.uni-bayreuth.de

Editorial compilation by: Stefan Keyssner and Petra Ständner
Section editors: Tiziana Boffa Ballaran, Natalia Dubrovinskaia, Leonid Dubrovinsky, Dan Frost, Florian Heidelbach, Falko Langenhorst, Catherine McCammon, Burkhard Schmidt, Friedrich Seifert

Staff and guests of the Bayerisches Geoinstitut in **July 2002**:

Die Mitarbeiter und Gäste des Bayerischen Geoinstituts im **Juli 2002**:

First/second row, from left (1./2. Reihe, v. links) Anke Markert, Petra Ständner, Jibamitra Ganguly, Kai Neufeld, Hidenori Terasaki, Patrick Cordier, Hélène Couvy, Takehiko Yagi, Sylvie Demouchy, Steve Mackwell, Xavier Helluy, Christian Liebske, Tiziana Boffa Ballaran, Julian Mecklenburgh, Bettina Schmickler, Paul Balog, Natalia Dubrovinskaia, Juliane Hopf, Catherine McCammon, Anastasia Kantor, Geoffrey Bromiley, Oskar Leitner, Stefan Keyssner, Dave Rubie

Third/fourth row, from left (3./4. Reihe, v. links) Kenji Mibe, Akio Suzuki, Johannes Krämer, Friedrich Seifert, Steven Jacobsen, Sven Linhardt, Kurt Klasinski, Ulrich Bläß, Christian Holzapfel, Fabrice Gaillard, Fiona Bromiley, Georg Herrmannsdörfer, Dan Frost, Fred Marton, Astrid Holzheid, Michael Terry, Leonid Dubrovinsky, Hisako Hirai, Falko Langenhorst, Gerti Gollner, Florian Heidelbach, Innokenty Kantor, Lydia Kison-Herzing, Heinz Fischer

Absent (Es fehlten) Matthias Bechmann, Ulrich Böhm, Wolfgang Böss, Detlef Krauße, Holger Kriegl, Jie Yuan Ning, Gerd Ramming, Oliver Rausch, Burkhard Schmidt, Hubert Schulze, Angelika Sebald, Iona Stretton

Contents

Foreword/Vorwort 9/I

1. Advisory Board and Directorship 11
   1.1 Advisory Board 11
   1.2 Leadership 11

2. Staff, Funding and Facilities 13
   2.1 Staff 13
   2.2 Funding 13
   2.3 Laboratory and office facilities 15
   2.4 Experimental equipment 16

3. Forschungsprojekte - Zusammenfassung in deutscher Sprache III
3. Research Projects 19
   3.1 *Physical and Chemical Properties of Minerals and Rocks* 19
      a. High-pressure elasticity of (Mg,Fe)O (S.D. Jacobsen) 20
      b. Structure and elasticity of natural magnetite (S.D. Jacobsen, T. Boffa Ballaran, L.S. Dubrovinsky, N.A. Dubrovinskaia, in collaboration with H. Reichmann/Potsdam) 21
      c. Sound velocities and elastic constants of Fo_{89} hydrous ringwoodite (S.D. Jacobsen and D.J. Frost, in collaboration with J. Smyth, H. Spetzler and C. Holl/Boulder) 24
      d. Rheology of $(Ca,Sr)TiO_3$ perovskite (J. Mecklenburgh, F. Heidelbach, S.J. Mackwell and F. Seifert) 25
      e. Mechanical behaviour and fabric development in experimentally deformed magnesiowüstite (Mg,Fe)O as a function of Fe-content (F. Heidelbach, I.C. Stretton and S.J. Mackwell) 27
      f. Plastic deformation of forsterite under high pressure and high temperature: An experimental study in the multianvil apparatus (H. Couvy, S.J. Mackwell, P. Cordier/Lille, D.J. Frost and F. Heidelbach) 28
      g. Lattice preferred orientation in wet dunite (S. Majumder and D.L. Kohlstedt/ Minneapolis, in collaboration with F. Heidelbach) 30
      h. Electrical conductivity of garnets: The effect of Fe-Mg substitution in the system pyrope ($Mg_3Al_2Si_3O_8$) – almandine ($Fe_3Al_2Si_3O_8$) (B.T. Poe, C. Romano and N. Kreidie/Rome, in collaboration with C.A. McCammon) 32
      i. Temperature and mineralogy of subducting slabs: The effects of variable thermal conductivity (F.C. Marton and D.C. Rubie, in collaboration with T.J. Shankland/Los Alamos) 34
      j. Effects of the phase transformation on the stress state of deep subducted slabs (J.-Y. Ning, F.C. Marton and D.C. Rubie) 35

k. Effects of latent heat and kinetics of phase transformations on the topography of phase boundaries and dynamic surface topography (B. Steinberger, D.C. Rubie and F.C. Marton) 36
l. Ultrahigh-temperature deformation textures in the contact aureole of the Chilka Lake anorthosite, India (C. Dobmeier/Berlin, in collaboration with F. Heidelbach) 37
m. Orientation of exsolution rods in antiperthite from a shear zone within the Bolangir anorthosite, India (C. Dobmeier/Berlin, in collaboration with F. Heidelbach) 38
n. Micrometer- and nanometer-scale mineral chemistry of hemo-ilmenite in relation to magnetism (S. McEnroe and P. Robinson/Trondheim, in collaboration with F. Langenhorst and G. Bromiley) 40
o. Magnetic remanence, oxide-silicate mineralogy, and lattice-preferred orientation in ilmenite norite of the Heskestad anomaly, Bjerkreim-Sokndal layered intrusion, Rogaland, Norway (S. McEnroe and P. Robinson/ Trondheim, in collaboration with F. Langenhorst and F. Heidelbach) 42
p. The colouring and constitution of New Zealand jade (C.A. McCammon, in collaboration with C.J. Wilkins†, W.C. Tennant and B.E. Williamson/ Christchurch) 44

3.2 *Mineralogy, Crystal Chemistry and Phase Transformations*..... 46
a. Crystal chemistry of Fe^{3+} in Al-containing majorite and implications for the transition zone (C.A. McCammon, in collaboration with N.L. Ross/ Blacksburg, USA) 47
b. Incorporation of the trivalent cations Fe^{3+} and Al^{3+} into $CaSiO_3$ – perovskite at transition zone conditions (U.W. Bläß, T. Boffa Ballaran, D.J. Frost, F. Langenhorst, C.A. McCammon and F. Seifert, in collaboration with P.A. van Aken/Darmstadt) 48
c. High-pressure structural phase transition in hematite (Fe_2O_3) (L.S. Dubrovinsky, in collaboration with G. Rozenberg/Tel Aviv and R. Ahuja/Uppsala) 50
d. New high-pressure Fe-Si phases (D.P. Dobson, L.S. Dubrovinsky, N.A. Dubrovinskaia, F. Langenhorst and C.A. McCammon, in collaboration with L. Vocadlo and I.G. Wood/London) 53
e. Structure of iron-nickel alloys at conditions of Earth's core (L.S. Dubrovinsky, N.A. Dubrovinskaia, F. Langenhorst and F. Seifert) 54
f. A class of new high-pressure silica polymorphs (L.S. Dubrovinsky, N.A. Dubrovinskaia, F. Seifert and F. Langenhorst, in collobaration with V. Prakapenka/Chicago, V. Dmitriev and H.-P. Weber/Grenoble) 56
g. Mixing behaviour of the magnesite-otavite ($MgCO_3$-$CdCO_3$) solid solution (F.A. Bromiley, T. Boffa-Ballaran and F. Langenhorst) 59

h. Investigations on the stability of Na-K-disilicates at elevated pressures (V. Kahlenberg and S. Rakic/Bremen, in collaboration with B.C. Schmidt) 61
i. Spontaneous strain at the C2/m $\leftrightarrow$ $P2_1/m$ transition in cummingtonite (T. Boffa Ballaran, in collaboration with M.A. Carpenter/Cambridge and K. Knight/Chilton) 62
j. The high-pressure $P2_1/c$-$C2/c$ phase transition in $Ca_{0.15}Mg_{1.85}Si_2O_6$ clinopyroxene (F. Nestola/Torino and T. Boffa Ballaran, in collaboration with M. Tribaudino/Torino) 63
k. The compressibility of $CaNiSi_2O_6$ (F. Nestola/Torino and T. Boffa Ballaran, in collaboration with M. Tribaudino/Torino) 65
l. Equation of state of bismuthinite (L. Lundegaard/Copenhagen and T. Boffa Ballaran) 66
m. Compressibility of baddeleyite-type TiO_2 from static compression to 40 GPa (N.A. Dubrovinskaia and L.S. Dubrovinsky, in collaboration with V. Swamy/Montreal) 67
n. Microstructure of radiation-damaged zircon and its behaviour as a function of pressure (S. Ríos/Cambridge and T. Boffa Ballaran) 69

3.3 *Geochemistry*..... 72
a. Fractionation of siderophile elements resulting from metal-silicate separation during core formation: The role of magma ocean convection dynamics (D.C. Rubie, in collaboration with H.J. Melosh and K. Righter/Tucson) 73
b. Iron-silicon alloy at extreme conditions (L.S. Dubrovinsky, N.A. Dubrovinskaia, F. Langenhorst, D.P. Dobson, D.C. Rubie, in collaboration with I. Abrikosov and B. Johansson/Uppsala) 75
c. The behaviour of sulphur in metal-silicate core segregation experiments under reducing conditions (J. Siebert, V. Malavergne, R. Combes/ Marne La Vallée and F. Guyot/Paris, in collaboration with D.J. Frost) 78
d. Effect of high pressure on Fe-Mg interdiffusion in ferropericlase (C. Holzapfel, D.C. Rubie, S.J. Mackwell and D.J. Frost) 80
e. Melting of Mg_2SiO_4 between 10-24 GPa (C. Liebske, D.J. Frost and D.C. Rubie, in collaboration with R.G. Trønnes/Reykjavik) 82
f. Oxygen fugacity profile of the Slave cratonic mantle (C.A. McCammon, in collaboration with M. Kopylova/Vancouver) 84
g. Fe-Mg partitioning between magnesiowüstite, olivine and wadsleyite (D.J. Frost) 85
h. The stability of anhydrous phase B (J. Ganguly and D.J. Frost) 88
i. Preparation and investigation of solid Xe compounds relevant to the Earth (C. Sanloup/Paris, in collaboration with B.C. Schmidt) 89
j. Supersilicic clinopyroxenes at high P and T in simplified and natural bulk compositions (J. Konzett/Innsbruck, in collaboration with D.J. Frost) 90

3.4 *Metamorphism at different Time-Scales* 92
a. Insight into deformation mechanisms in garnet from high-pressure granulite shear zones (M.P. Terry and F. Heidelbach) 92
b. UHP metamorphism of a kyanite-garnet gneiss from Fjørtoft, Western Norway (P. Robinson/Trondheim, F. Langenhorst and M.P. Terry) 95
c. Microstructure of metamorphic coesite from Dora Maira, Alps (F. Langenhorst and J.-P. Poirier, in collaboration with H.-P. Schertl/Bochum) 96
d. A transparent, very hard and dense form of carbon in heavily shocked gneisses from Popigai, Russia (A. El Goresy/Mainz, L.S. Dubrovinsky, P. Gillet/Lyon, V.L. Masaitis/St. Petersburg) 98
e. Formation of ringwoodite in high-explosive experiments on muscovite-biotite-quartz slates (E. Kozlov/Snezhinsk, L. Sazonova and V. Feldman/ Moscow, N.A. Dubrovinskaia and L.S. Dubrovinsky) 100
f. Experimental study of shock deformation and decomposition of anhydrite (F. Langenhorst, in collaboration with A. Deutsch/Münster and U. Hornemann/Efringen-Kirchen)..... 101
g. Evidence for degassing of anhydrite in drill cores from the Chicxulub impact crater, Yucatan, Mexico (F. Langenhorst, in collaboration with A. Deutsch/Münster and E. Lounejeva/Mexico City) 103

3.5 *Fluids and their Interactions with Melts and Minerals* 105
a. Full characterisation of modes of hydrogen incorporation in synthetic, water-saturated jadeite and jadeite-rich pyroxenes (G.D. Bromiley, in collaboration with H. Keppler/Tübingen) 105
b. Structural systematics of hydrous ringwoodite (J.R. Smyth and C.M. Holl/ Boulder, in collaboration with D J. Frost, S.D. Jacobsen, F. Langenhorst and C.A. McCammon) 108
c. Raman investigations of deuterated ringwoodite (A.P. Jephcoat and A.K. Kleppe/Oxford, in collaboration with J.R. Smyth/Boulder and D. J. Frost) 109
d. Kinetics of hydration into synthetic iron-free forsterite (S. Demouchy and S.J. Mackwell) 111
e. Water in nominally anhydrous minerals: First water diffusion profiles in xenolithic olivine (S. Demouchy, S.J. Mackwell, F. Gaillard and S.D. Jacobsen, in collaboration with C. Stern/Boulder) 113
f. Hydrogen profiles in olivine as a geospeedometer of magma ascent rate (F. Gaillard, F.A. Bromiley and S. Demouchy, in collaboration with K. Roggensack/Tempe) 115
g. Deformation and dehydration interactions in serpentinite under orogenic conditions (K. Neufeld, I.C. Stretton, S.J. Mackwell and J. Mecklenburgh) 116

h. Experimental investigation of diamond growth in high-pressure fluids (H. Bureau/Saclay, F. Langenhorst and D.J. Frost, in collaboration with C. Shaw/Fredricton and J.-P. Gallien/Saclay) 117
i. Melting curve of water studied in an externally heated diamond anvil cell (N.A. Dubrovinskaia and L.S. Dubrovinsky) 119

3.6 *Physics and Chemistry of Melts and Magmas* 121
a. Determination of peridotite liquid transport properties at high pressure (B. Schmickler, D.C. Rubie, C. Liebske, A. Suzuki, H. Terasaki and B.T. Poe) 121
b. Thermal diffusivity of $CaMgSi_2O_6$ glass at high pressure (A. Suzuki and D.C. Rubie) 123
c. Electrical conductivity of water-bearing magmas as a tool for estimating magmas water content? (F. Gaillard) 124
d. Redox history of magma ascent (F. Gaillard, B.C. Schmidt and C.A. McCammon) 126
e. Oxygen fugacity gradients in high-silica rhyolites of the Rattlesnake Tuff, Oregon (C.A. McCammon, in collaboration with M. Streck/Portland) 127
f. On the water solubility mechanisms in hydrous aluminosilicate glasses: Information from ^{27}Al MAS and MQMAS NMR (D. Padro and R. Dupree/Warwick, in collaboration with B.C. Schmidt) 128
g. Effect of boron on the water speciation in (alumino)silicate melts and glasses (B.C. Schmidt and F. Gaillard) 129
h. The effect of time and melt fraction on connectivity of liquid Fe-S alloy in olivine under high pressure (H. Terasaki, D.C. Rubie and D.J. Frost) 132

3.7 *Materials Science* 134
a. FCC–HCP phase boundary in lead (L.S. Dubrovinsky, in collaboration with A. Kuznetov, V. Dmitriev and H.-P. Weber/Grenoble) 135
b. Titanium metal at high pressure: Synchrotron experiments and *ab initio* calculations (L.S. Dubrovinsky, N.A. Dubrovinskaia, in collaboration with R. Ahuja, J.M. Osorio Guillen, B. Johansson/Uppsala) 137
c. *In situ* study of C_{60} polymerisation at high-pressure/high-temperature conditions (A. Talyzin/Uppsala and L.S. Dubrovinsky) 140
d. High-pressure Raman study of $C_{60}S_{16}$ (A. Talyzin/Uppsala and L.S. Dubrovinsky) 141
e. Compression behaviour of nanocrystalline anatase TiO_2 (L.S. Dubrovinsky and N.A. Dubrovinskaia, in collaboration with V. Swamy/Montreal) 143
f. Pressure-induced structural transformations in the Mott insulator FeI_2 (L.S. Dubrovinsky, in collaboration with G. Rozenberg/Tel Aviv and R. Ahuja/Uppsala) 145

g. Oxygen vacancies in Fe^{3+}-substituted barium titanate (E. Mashkina/ Erlangen, in collaboration with F. Seifert and C.A. McCammon) 148
h. Stabilization of Ni-containing layered oxides under high-oxygen pressure (G.D. Bromiley and T. Boffa-Ballaran, in collaboration with R. Stoyanova/Sofia) 150
i. Combined isotope substitution and pressure-tuning Raman study of the spin-crossover complex Fe(pyridine)$_2$[Ni(CN)$_4$] (G. Molnar and A. Boussekso/Toulouse, T. Kitazawa/Toho and L.S. Dubrovinsky) 152
j. *In situ* Raman study of pressure-induced amorphization in $Eu_2(MoO_4)_3$ single crystal (D. Machon and V. Dmitriev/Grenoble, L.S. Dubrovinsky, F. Langenhorst; V. Sinitsin and E. Ponyatovsky/Chernogolovka) 153
k. Optical and A.T.E.M. investigations of sintered alumina transformed under excimer laser irradiation (C. Dupas-Bruzek, L.D. Laude, K. Kolev/ Mons and F. Langenhorst) 157

3.8 *Methodological Developments* 161
a. Gigahertz ultrasonic interferometry at Bayerisches Geoinstitut: Where sound and optical wavelengths meet (S.D. Jacobsen, H. Schulze, G. Herrmansdörfer, S. Linhardt and K. Klasinski, in collaboration with K. Müller and H. Ohlmeyer/ZT Uni-Bayreuth, H. Reichmann/Potsdam, H. Spetzler and J. Smyth/Boulder) 161
b. A new methodology for multianvil acoustic emissions experiments (D.P. Dobson, in collaboration with P.G. Meredith and S.A. Boon/London) ... 164
c. Development of an opposed anvil type high-pressure and high-temperature apparatus using sintered diamond (T. Yagi, D.J. Frost and D.C. Rubie, in collaboration with H. Goto/Tokyo) 165
d. High-temperature heater for diamond anvil cells (N.A. Dubrovinskaia and L.S. Dubrovinsky) 168
e. Solubility of hydroxyl in pyroxenes under mantle conditions: A novel method for annealing natural samples at high pressure (G.D. Bromiley, H. Keppler, F. Bromiley and S.J. Jacobsen) 170
f. ALCHEMI study of perovskite by electron energy dispersive X-ray spectroscopy (EDXS) (N. Miyajima/Tokyo, in collaboration with F. Langenhorst) 172
g. New solid-state NMR results (M. Bechmann, X. Helluy and A. Sebald) 173

4. Publications, Conference Presentations, Seminars, Visiting Scientists 177
4.1 Publications (published) 177
a. Refereed international journals 177
b. Conference proceedings 182
4.2 Publications (submitted, in press) 182
4.3 Presentations at scientific institutions and at congresses 187

4.4 Lectures and seminars at Bayerisches Geoinstitut 200
4.5 Scientific conferences organized by/with assistance of Bayerisches Geoinstitut 201
4.6 Visiting scientists 202
a. Visiting scientists funded by the Bayerisches Geoinstitut 202
b. Visiting scientists funded by EU Programme "Access to Large-Scale Facilities" 203
c. Visiting scientists supported by other externally funded BGI projects 206
d. Visitors (externally funded) 206
4.7 Theses 208
4.8 Honours and awards 208
4.9 Editorship of scientific journals 208
4.10 Membership of scientific advisory bodies 209
4.11 Public relations and press reports 209

5. Scientific and Technical Personnel 211

Index 214

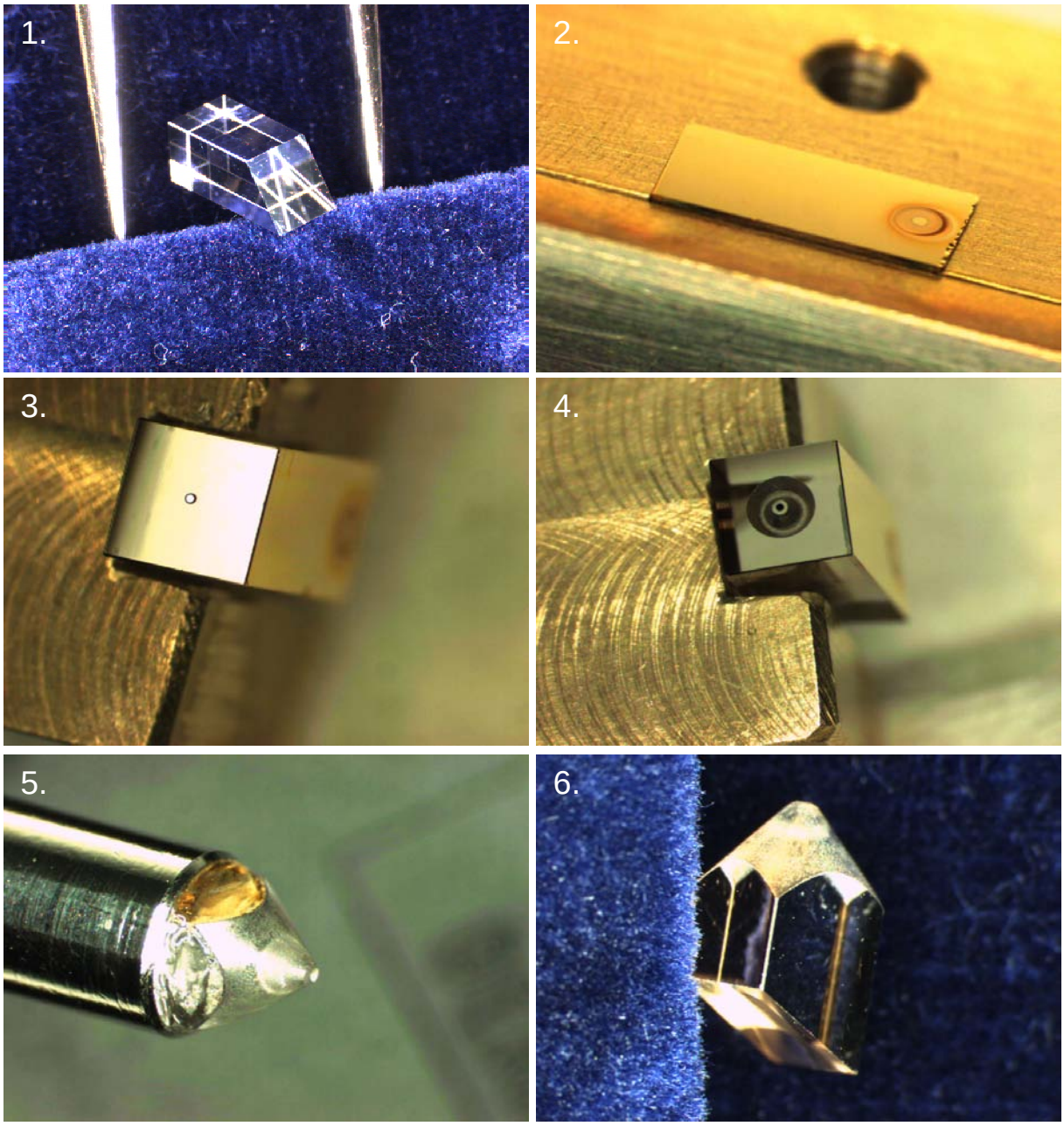

Pictured here is a unique ultrasonic buffer rod that converts high-frequency P-waves into S-waves for measuring the shear elasticity of minerals at high pressures in the diamond anvil cell (see contribution page 161).

Ultraschall-Wandler hochfrequenter P-Wellen in S-Wellen, um die Scherelastizität von Mineralen unter hohen Drücken in einer Diamantstempelzelle zu bestimmen (siehe Beitrag S. 161).

1. Faceting the oriented Yttrium Aluminium garnet crystal (3 x 3 x 6 mm).
2. Sputtering the P-wave transducer.
3. Locating the shear signal with a test sample (0.2 mm diameter).
4. Coring around the test sample where the signal is observed.
5. Coning for access into the diamond anvil cell.
6. The working P-to-S conversion buffer rod.

1. Facettierung des orientierten YAG Kristalls.
2. Aufdampfen des P-Wellen-Signalgebers.
3. Lokalisierung des Scherwellensignals mit einer Testprobe (0,2 mm Durchmesser).
4. Kreisförmige Ausbohrung dort, wo das Signal der S-Welle auf die Kristallfläche trifft.
5. Der konusförmige Kristall, fertig zur Einpassung in eine Diamantstempelzelle.
6. Der fertige Kristall, der P- in S-Wellen umwandelt.

Foreword

The research aims of the Bayerisches Geoinstitut are to understand the structure, composition, evolution and dynamics of the Earth's interior by studying Earth materials experimentally at high pressures and temperatures. The contributions contained in this Annual Report describe the results of experimental studies that pertain to a wide range of problems in the Earth Sciences and demonstrate that these aims are being achieved. The research reports cover a wide spectrum of topics such as the early differentiation of the Earth, the present structure of the silicate mantle (such as the causes of seismic discontinuities), the incorporation and transport of water in the Earth's mantle, the nature of the Earth's core and chemical interactions at the core-mantle boundary. Of relevance to shallower parts of the Earth, there are contributions on crustal metamorphism and the consequences of large impacts on the Earth.

A crucial aspect of maintaining progress in experimental studies is the development of new experimental technologies and strategies. In the last twelve years, the multianvil apparatus has become standard in studies of the Earth's mantle to 25 GPa (750 km depth) and 3000 K. In the course of 2002, a new diamond anvil cell laboratory has been set up in which, with the use of laser heating, conditions of 150 GPa and 4000 K can be achieved, corresponding to a depth of about 3000 km. During the coming year, this facility will be greatly enhanced through the installation of an ultra-high intensity X-ray system for in situ studies to megabar pressures. This new facility will make it possible to investigate materials under pressure-temperature conditions of the Earth's metallic core, enabling studies to be pursued, for example, of the chemical interactions that occur at the core-mantle boundary between metal and silicates.

A major breakthrough during 2002 has been the successful measurement of acoustic shear wave velocities in small single crystals at high pressure in the diamond anvil cell using gigahertz ultrasonic interferometry (see page 8). This achievement, which has been the culmination of years of work, will greatly facilitate interpretations of seismic wave velocities in terms of mantle mineralogy (a major goal of mineral physics). In the future, such experiments will be developed further to significantly higher pressures with the simultaneous application of high temperatures. Other technological developments have led to an understanding of deep earthquakes through the monitoring of acoustic emissions from samples at high pressure and temperature in the multianvil apparatus. These experiments have greatly strengthened the case for dehydration reactions, and the consequent release of water, as being the cause of intermediate depth earthquakes (*e.g.* at depths of 200-300 km).

An important event of 2002 has been the appointment of a Junior Professor in the field of computational mineral physics. This scientific field is complementary to experimental studies and is concerned with calculating, from first principles, the structure and properties of materials under extreme conditions of pressure and temperature. Combining theoretical and experimental studies will have significant synergistic effects in catalysing progress towards

understanding material properties at extreme conditions. Another major development is the recent move of the previous Director, Prof. Stephen Mackwell, to the Lunar and Planetary Institute (Houston, USA). Consequently the Professorship for *Experimental Geophysics of the Solid Earth* is currently being refilled.

Part of the success in realising research goals at the Bayerisches Geoinstitut results from collaborations with scientists in Europe, North America, Japan and Australia etc. Together with our wide range of experimental facilities, such collaborations have established the Bayerisches Geoinstitut as an international centre for high-pressure research. At the European level, support by the EU since 1994 under the "Large Scale Facility" and "Access to Research Infrastructure" programmes has been highly successful and beneficial. These programmes have enabled scientists from more than 100 research groups in 17 European countries to visit and take advantage of the experimental facilities. The visiting scientists who have been supported under these programmes number up to 90 per year, and originate from the Earth sciences, physics, chemistry and materials sciences. The outcome has been wide ranging interdisciplinary scientific collaborations and more than 180 publications in international scientific journals.

As in previous years, and also on behalf of my colleagues, I would like to thank the *Free State of Bavaria* as represented by the *Bayerisches Staatsministerium für Wissenschaft, Forschung und Kunst* as well as the *Kommission für Geowissenschaftliche Hochdruckforschung* of the *Bavarian Academy of Science* for their continuing support and strong commitment to the Bayerisches Geoinstitut. We also gratefully acknowledge generous support from external funding agencies, in particular the *Alexander von Humboldt Foundation*, the *European Union*, and the *German Science Foundation*, which have also contributed greatly to the development and success of the Institute.

Bayreuth, February 2003 David C. Rubie

Vorwort

Die Forschungsziele des Bayerischen Geoinstituts sind, Erkenntnisse über die Struktur, Zusammensetzung, Entwicklung und Dynamik des Erdinneren durch experimentelle Untersuchungen an der Erdmaterie unter hohen Drücken und Temperaturen zu gewinnen. Die Beiträge dieses Jahresberichts beschreiben die Ergebnisse solcher Forschung zu einer weiten Spanne von Fragestellungen in den Erdwissenschaften und erläutern, dass und wie Antworten gefunden wurden. Die Artikel zu den einzelnen Projekten umfassen ein breites Themenspektrum, von der frühen Differentiation der Erde über die gegenwärtige Struktur des silikatischen Erdmantels (einschließlich z. B. der Ursachen seismischer Diskontinuitäten), über die Aufnahme und den Transport von Wasser im Erdmantel, die Natur des Erdkerns und chemische Wechselbeziehungen an der Mantel-Kern-Grenze. Auf oberflächennähere Bereiche der Erde zielen Artikel über Metamorphose der Erdkruste und Auswirkungen von Einschlägen großer Himmelskörper.

Eine wesentliche Voraussetzung für kontinuierliche experimenteller Fortschritte ist die Entwicklung neuer Versuchstechniken und -strategien. In den vergangenenen 12 Jahren wurde die Multianvil-Apparatur als Standardwerkzeug und -Methode für Untersuchungen des Erdmantels bis in ca. 750 km Tiefe (25 GPa) und 3000 K etabliert. Im Laufe des Jahres 2002 ist ein neues Diamantstempelzellen-Labor in Betrieb genommen worden, wo unter Einsatz von Laser-Heiztechnik Versuchsbedingungen nachgestellt werden können, die im tieferen Erdinneren in ca. 3000 km herrschen. Im kommenden Jahr wird die Apparatur noch einmal durch die Verknüpfung mit einer ultra-intensiven Röntgenquelle für in situ-Studien unter Drücken im Megabar-Bereich erheblich erweitert und aufgewertet werden. Mit dieser Apparatur lässt sich Materie unter Druck-/Temperaturbedingungen des metallischen Erdkerns studieren, so dass zum Beispiel die Untersuchung chemischer Wechselwirkungen zwischen Silikaten und Metall an der Mantel/Kern-Grenze ermöglicht wird.

Einen Durchbruch stellte im Verlauf des Jahres 2002 die erfolgreiche Messung von akustischen Scherwellengeschwindigkeiten in sehr kleinen Einkristallen unter hohem Druck dar. Diese Messungen werden in Diamantstempelzellen mit Hilfe der Ultraschall-Interferometrie im Gigahertz-Bereich durchgeführt (siehe auch Abb. auf Seite 8). Dieser Erfolg als Frucht langer experimenteller Vorbereitungen wird Interpretationen von seismischen Wellengeschwindigkeiten hinsichtlich der Mineralogie des Erdmantels (einem wesentlichen Ziel der Mineralphysik) sehr erleichtern. In der Zukunft werden derartige Versuche in signifikant höhere Druckbereiche geführt werden, mit der zusätzlichen Option, simultan hohe Temperaturen anzulegen. Weitere technische Entwicklungen des Jahres 2002 verbesserten unser Verständnis über tiefe Erdbeben durch die Aufzeichnung akustischer Emissionen von Proben in einer Multianvil-Apparatur bei hohen Drücken und Temperaturen. Diese Experimente haben Dehydratisierungsreaktionen bestätigt und auch, dass die stetige Freisetzung von Wasser Erdbeben in mittleren Tiefen (z. B. zwischen 200-300 km) generieren kann.

Ein weiteres maßgebliches Ereignis des Jahres 2002 ist die Berufung eines Juniorprofessors auf dem Gebiet der "computational" Mineralphysik. Diese Fachrichtung ergänzt die experimentelle Forschung und befasst sich mit Berechnung und Modellierung von Grundprinzipien, Strukturen und Eigenschaften von Materie unter extremen Druck- und Temperaturbedingungen. Eine Kombination von theoretischer mit experimenteller Forschung wird signifikante Synergieeffekte freisetzen und als Katalysator für Fortschritte im Verständnis von Materialeigenschaften unter extremen Bedingungen wirken. Ein weiteres nachhaltiges Ereignis stellte der Weggang des bisherigen Leiters des Instituts, Prof. Stephen Mackwell, an das *Lunar and Planetary Institute* (Houston, USA) dar. Daher wird derzeit versucht, die Professur für *Experimentelle Geophysik der Festen Erde* neu zu besetzen.

Ein Teil des Erfolgs des Bayerischen Geoinstituts in der Realisierung der gesteckten Forschungsziele beruht auf der engen Zusammenarbeit mit Wissenschaftlern in Europa, Nordamerika, Japan und Australien etc. In Verbindung mit unserer umfangreichen experimentellen Ausstattung hat diese Kollaboration das Bayerische Geoinstitut als ein internationales Zentrum für die Hochdruck-Forschung etabliert. Auf der europäischen Ebene ist die Förderung im Rahmen der EU-Programme *Large Scale Facility* und *Access to Research Infrastructure* seit 1994 äußerst erfolgreich und nützlich gewesen. Diese Förderprogramme haben es Wissenschaftlern von mehr als 100 Forschergruppen in 17 europäischen Ländern ermöglicht, die experimentellen Einrichtungen zu besuchen und zu nutzen. Die Zahl der Wissenschaftler, die aus diesen Programmen gefördert wurden, beläuft sich auf bis zu 90 pro Jahr. Es handelt sich um Geowissenschaftler, Physiker, Chemiker und Materialwissenschaftler. Es entstanden daraus wissenschaftliche Kooperationen mit einem breiten interdisziplinären Spektrum und mehr als 180 Publikationen in internationalen Fachzeitschriften.

Wie in den vorangegangenen Jahren möchte ich auch im Namen meiner Kollegen dem Freistaat Bayern, vertreten durch das *Bayerische Staatsministerium für Wissenschaft, Forschung und Kunst*, als auch der *Kommission für Geowissenschaftliche Hochdruckforschung* der *Bayerischen Akademie der Wissenschaften* meinen Dank für ihre fortwährende Unterstützung und ihre enge Verbundenheit mit dem Bayerischen Geoinstitut aussprechen. Wir sind auch für die großzügige Förderung durch externe Geldgeber, insbesondere durch die *Alexander von Humboldt-Stiftung*, die *Europäische Union* und die *Deutsche Forschungsgemeinschaft*, die ebenfalls wesentlich zur Entwicklung und zum Erfolg des Bayerischen Geoinstituts beigetragen hat, sehr dankbar.

Bayreuth, im Februar 2003 David C. Rubie

1. Advisory Board and Directorship

1.1 Advisory Board

The *Kommission für Geowissenschaftliche Hochdruckforschung* der *Bayerischen Akademie der Wissenschaften* advises on the organisation and scientific activities of the Institute. Members of this board are:

Prof. Dr. Drs. h. c. E. ALTHAUS	Mineralogisches Institut der Universität Karlsruhe
Prof. Dr. Drs. h. c. mult. H. AUTRUM	Bayerische Akademie der Wissenschaften
Prof. Dr. H. BERCKHEMER[1]	Emeritus, Institut für Meteorologie und Geophysik der Universität Frankfurt
Prof. Dr. Drs. h. c. E. U. FRANCK	Emeritus, Institut für Physikalische Chemie der Universität Karlsruhe
Prof. Dr. Dr. h. c. G. NEUWEILER (Chairman)	Zoologisches Institut der Universität München
Prof. Dr. H. PALME	Institut für Mineralogie und Geochemie der Universität zu Köln
Prof. Dr. R. RUMMEL	Institut für Astronomische und Physikalische Geodäsie der TU München
Prof. Dr. E. SALJE	Department of Earth Sciences, University of Cambridge
Prof. Dr. Drs. h. c. W. SCHREYER	Emeritus, Institut für Mineralogie der Ruhr-Universität Bochum
Prof. Dr. H. SOFFEL	Institut für Allgemeine und Angewandte Geophysik der Universität München

[1] resigned from the *Kommission* in 2002

The Advisory Board held meetings in Bayreuth (18.-19.03.2002) and in Munich (14.11.2002).

1.2 Leadership

Prof. Dr. Stephen MACKWELL (Director to 30.11.2002)
Prof. Dr. David C. RUBIE (Director from 01.12.2002)
Prof. Dr. Friedrich SEIFERT

2. Staff, Funding and Facilities

2.1 Staff

At the end of 2002 the following staff positions existed in the Institute:

- Scientific staff: **12**
- Technical staff: **12**
- Administrative staff: **2**
- Administrative officer: **1**

During 2002, 13 scientific and 1 technical positions were funded by grants raised externally by staff members of the institute.

In addition 10 long-term scientific positions were funded by the resources of the BGI Visiting Scientists' Program (see Sect. 5) which also supported short-term visits for discussing future projects or presenting research results (see Sect. 4.6). Eight scientists were funded by personal grants (stipends).

2.2 Funding

In 2002, the following financial resources were available from the Free State of Bavaria:

- Investment Funding: 1.263.000 €
- Visiting Scientists' Program: 437.000 €
- Consumables: 363.000 €

The total amount of national/international external funding („*Drittmittel*") used for ongoing research projects in 2002 was 922.000 € (Positions: 482.000 €, equipment, consumables and travel grants: 440.000 €).

	positions	**equipment, consumables, travel grants**	**total**
• AvH	169.000 €	165.200 €	334.200 €
• DAAD		2.600 €	2.600 €
• DFG	134.200 €	128.300 €	262.500 €
• EU	172.200 €	128.200 €	300.400 €
• Others	6.600 €	15.600 €	22.200 €
			921.900 €

(AvH = Alexander von Humboldt Foundation; DAAD = German Academic Exchange Program; DFG = German Science Foundation; EU = European Union; "Others" in 2002: Rhône-Poulenc Rorer, France; Funds of the Chemical Industry; University of Bayreuth)

In the following list only the BGI part of the funding is listed in cases where joint projects involved other research institutions. Principal investigators and duration of the grants are listed in brackets.

Funding institution	Project, Funding	Total Project Funding
DFG	Ba 814/16-1 (H. Spetzler – 10.01 - 6.02) Positions: Travel funding:	 36.100 € 2.100 €
DFG	Fr 1555/1-1 (D.J. Frost, D.C. Rubie – 9.01 - 8.03) Positions: BAT IIa/2, 24 months Consumables:	 11.800 €
DFG	La 830/4-4 (F. Langenhorst – 1.02 - 12.02) Positions: studentische Hilfskraft, 24 months Consumables and travel funding:	 9.500 €
DFG	La 830/5-1,2 (F. Langenhorst – 1.02 – 12.02) Consumable and travel funding:	 5.400 €
DFG	Ma 801/7-1 (A. Magerl and M. Göbbels/Erlangen, F. Seifert/ Bayreuth) Positions: BAT IIa, 24 months Consumables and travel funding: 18.400 € (Erlangen)	
DFG	Ru 437/6-1 (D.C. Rubie, D. Frost, F. Langenhorst, A. Holzheid – 4.02 - 3.04) Positions: BAT IIa/2, 24 months studentische Hilfskraft, 24 months Consumables and travel funding:	 13.800 €
DFG	Ru 437/7-1 (D.C. Rubie, B.T. Poe – 9.01 - 8.03) Positions: BAT IIa/2, 24 months Consumables and travel funding:	 22.500 €
DFG	Schm 1622/1-1 (B.C. Schmidt – 10.01 - 9.03) Consumables and travel funding:	 14.900 €
DFG	Se 301/24-1 and -2 (F. Seifert, D. Frost, F. Langenhorst, C. McCammon – 1.01 - 12.03) Positions: BAT IIa/2, 36 months Consumables: Travel funding:	 15.900 € 2.100 €
DFG	Wr15/20-1 (A. Sebald, B. Wrackmeyer/Bayreuth, joint project – 7.00 - 6.02) Positions: BAT IIa, 24 months, BAT IIa/2, 24 months Consumables and travel funding:	 7.700 €

Funding institution	Project, Funding	Total Project Funding
DFG	Wr15/20-2 and Wr15/20-3 (A. Sebald, B. Wrackmeyer/ Bayreuth, joint project – 7.02 - 6.03) Positions: BAT IIa, 12 months, BAT IIa/2, 12 months Consumables and travel funding:	3.400 €
DFG	Travel funding (F. Heidelbach)	1.250 €
DAAD	Travel funding (J. Mecklenburgh)	2.000 €
EU	Hydrospec-Network (H. Keppler – 9.00 - 8.04) Positions/Consumables:	181.000 €
EU	"Access to Research Infrastructures" Programme (D.C. Rubie – 5.00 - 4.03) Positions, consumables, equipment, travel:	825.000 €
EU	Marie Curie Fellowships (Training Center) (S. Mackwell – 01.02. - 01.06) Positions, consumables, equipment, travel:	150.000 €
AvH	Sofia-Kovalevskaja-Programm (T. Boffa Ballaran – 8.01 - 7.04) Positions, consumables, equipment, travel:	843.740 €
FCI	(F. Seifert – 1997 - 2003) Consumables: Equipment:	23.500 € 51.100 €

2.3 Laboratory and office facilities

The institute occupies an area of

ca. 1200 m^2 laboratory space
ca. 480 m^2 infrastructural areas (machine shops, computer facilities, seminar room, library)
ca. 460 m^2 office space
in a building which was completed in 1994.
A laboratory of the *Institut für Anorganische Chemie (Prof. Herberhold)* is used by the NMR spectroscopy group.

2.4 Experimental equipment

The following major equipment is available at Bayerisches Geoinstitut:

I. High-pressure apparatus

5000 tonne multianvil press (25 GPa, 3000 K)
1200 tonne multianvil press (25 GPa, 3000 K)
1000 tonne multianvil press (25 GPa, 3000 K)
500 tonne multianvil press (20 GPa, 3000 K)
3 piston-cylinders (0.5" and 0.75"; 4 GPa, 2100 K)
1 piston cylinder (5 GPa, 2000 K)
Cold-seal vessels (700 MPa, 1000 K, H_2O), TZM vessels (300 MPa, 1400 K, gas), rapid-quench equipment
Internally-heated autoclave (1 GPa, 1600 K)

II. Structural and chemical analysis

2 X-ray powder diffractometers
1 X-ray powder diffractometer with furnace and cryostat
X-ray powder microdiffractometer
Single-crystal X-ray cameras
2 automated single-crystal X-ray diffractometers
2 Mössbauer spectrometers (1.5 - 1300 K)
Mössbauer millispectrometer
FTIR spectrometer with IR microscope
FEG transmission electron microscope, 200 kV analytical, with EDS and PEELS
FEG scanning electron microscope with BSE detector, EDS, EBSD and CL
3 high-resolution solid-state NMR spectrometers (100, 200, 300 MHz)
2 Micro-Raman spectrometers
JEOL JXA-8200 electron microprobe; fully-automated with 14 crystals, 5 spectrometer configuration, EDX, capability for light elements
Cameca SX-50 electron microprobe
ICP-AES sequential spectrometer
Water content determination by Karl-Fischer titration

III. *In situ* determination of properties

1 calorimeter (77 - 1000 K) scanning
1 dilatometer (to 1800 K)

Diamond anvil cells for powder and single crystal X-ray diffraction, Mössbauer, IR, Raman, optical spectroscopy and electrical resistivity measurements at megabar pressure range

Facility for *in situ* hydrothermal studies in DAC

Externally electrically heated DACs for *in situ* studies at pressures to 100 GPa and 1200 K

1-atm furnace (to 1873 K, gas mixing) equipped with zirconia *f*O2 probes

Paterson HP/HT deformation apparatus

1-atm high-temperature creep apparatus

2 high frequency ultrasonic interferometers (crystalline and molten materials)

Gigahertz ultrasonic interferometer with interface to resistance-heated diamond-anvil cells

Heating stage for fluid inclusion studies

Impedance/gain-phase analyser for electrical conductivity studies

Apparatus for *in situ* measurements of thermal diffusivity at high P and T

The Geoinstitut is provided with well equipped machine shops, electronic workshop and sample preparation laboratories. It has also access to the university computer centre.

3. Forschungsprojekte

Es wird an dieser Stelle nur über die wichtigsten, derzeit laufenden Projekte berichtet. Informationen über abgeschlossene Teilprojekte sind in den Abschnitten 4.1 und 4.2 in Form von Literaturzitaten angegeben. Die Beiträge des Kapitels 3 sollen nicht zitiert werden.

3.1 Physikalische und chemische Eigenschaften fester Materie

Geologische Ereignisse wie Vulkanausbrüche oder Erdbeben, die an bzw. dicht unter der Erdoberfläche auftreten, belegen die dynamische Natur des Planeten Erde. Eines der Hauptziele der Geowissenschaften besteht darin, die Antriebskräfte dieser dynamischen Prozesse zu verstehen und sichtbar zu machen. Da das tiefe Erdinnere für unsere direkten Beobachtungen und eine Beprobung allgemein unerreichbar ist, müssen zu seiner Erforschung indirekte Methoden der Geophysik und Geochemie herangezogen werden. Die Interpretation dieser Messdaten ist nur möglich, wenn man sie mit Daten aus Experimenten vergleicht, in denen die physikalischen und chemischen Bedingungen in der tiefen Erde nachgeahmt wurden. Dieser experimentelle Ansatz bildet einen wesentlichen Schwerpunkt der Forschung des Geoinstituts.

Aus der seismologischen Erforschung der Erde erhalten wir Kenngrößen zur Verteilung von Geschwindigkeiten seismischer Wellen und der Dichte im Erdinneren; diese Werte müssen mit Labormessungen verglichen werden, die Daten zu elastischen Eigenschaften für charakteristische Minerale aus unterschiedlichen Erdtiefen liefern. In den vergangenen Jahren wurden hier große experimentelle Fortschritte gemacht. Wir können jetzt Laufzeiten akustischer Wellen in Millimeter großen Einkristallen unter hohen Drücken im Labor direkt bestimmen und daraus den elastischen Tensor vollständig ableiten. Neben dem elastischen Verhalten ist ebenso die plastische Verformung von Mineralen des Erdmantels von großem Forschungsinteresse, da sie für die Bildung anisotroper Strukturen und damit für seismische Anisotropien im Erdinneren verantwortlich gemacht werden kann. Die Rheologie verschiedener Komponenten des Erdmantels ist also von großer Bedeutung; sie wird deshalb in Verformungsexperimenten untersucht. Die unter den Bedingungen des Erdmantels durchzuführenden Verformungsversuche stellen immer noch eine große experimentelle Herausforderung dar. Neben dem mechanischen Verhalten der beteiligten Phasen muss man weitere Faktoren, wie zum Beispiel erhöhte Fluidgehalte oder Veränderungen der kristallographischen Struktur (Phasenübergänge) beachten. Unsere Kenntnisse über den Wertebereich der elektrischen Leitfähigkeit im Erdmantel gelten aufgrund von Vergleichsdaten aus Leitfähigkeitsmessungen unter hohen Drücken im Labor im Wesentlichen als gesichert. Für eine genaue Interpretation ist jedoch eine noch detailliertere Kenntnis über die Eisenverteilung sowohl in den Phasen des oberen und unteren Erdmantels, als auch in der dazwischen liegenden Übergangszone wichtig.

Weiterhin gehen physikalische und chemische Kenngrößen von Mineralen und Gesteinen in die Berechnungen ein, mit denen das Erdinnere unter verschiedenen Aspekten modelliert wird, wie z. B. Konvektion im Erdmantel oder das Verhalten von Teilen der Erdkruste bei der Subduktion. Besonders das Auftreten von Erdbeben bis in eine Tiefe von 600 km in den

abtauchenden Krustensegmenten bleibt weiterhin ein rätselhaftes Phänomen, da die Materie unter den hohen Drücken und Temperaturen in diesen Tiefen plastische und keine bruchhaften Verformungseigenschaften aufweisen sollte. Metastabiler Olivin in den abtauchenden Platten mag zumindest teilweise als Erklärung für das Auftreten tiefer Erdbeben gelten. Sein Auftreten ist jedoch von vielen physikalischen Parametern abhängig, wie z. B. thermischer Leitfähigkeit, latenter Wärme, Kinetik von Phasenübergängen, als auch von der Spannungsverteilung in der abtauchenden Platte.

Die Bildungsbedingungen natürlicher Gesteine spiegeln sich in ihren physikalischen und chemischen Eigenschaften wider. Mikrostrukturen und kristallographische Vorzugsorientierungen sind ein Speicher für frühere Metamorphosen und Verformungen unter hohen Temperaturen und/oder Drücken. Sie erlauben eine Abschätzung der Bildungs- bzw. Umwandlungsbedingungen. Die magnetischen Eigenschaften von Gesteinen stellen das Ergebnis einer komplexen Bildungsgeschichte dar; sie können große Anomalien in dem heutigen Magnetfeld der Erde erzeugen. Optische Mineral- und Gesteinseigenschaften spielen bei der Charakterisierung von Edelsteinen eine wichtige Rolle; sie können aber auch durch sich ändernde chemische Bildungsbedingungen beeinflusst werden.

3.2 Mineralogie, Kristallchemie und Phasenübergänge

Die Mineralogie ist eine Zentraldisziplin der Geowissenschaften. Ihr elementares Ziel ist die Bestimmung der physikalischen und chemischen Eigenschaften von Materie, die Struktur und thermischen Zustand, Prozesse und Entwicklung der Erde steuern bzw. von diesen Faktoren beeinflusst werden. Als Konsequenz stetiger Innovationen in der Hochdruck-/Hochtemperatur-Technologie ist heute der gesamte Erdkörper von der Kruste bis zum inneren Kern in das wissenschaftliche Interesse der Mineralogen gerückt. Die Arbeiten zum Verständnis und Quantifizierung von Mineraleigenschaften als Funktion von Temperatur, Druck, Kationenaustausch und -ordnung haben die Bedeutung des Begriffs „Mineralogie“ erweitert, und zwar in Richtung eines interdisziplinären Fachgebietes, das die Kristallographie, die Festkörperphysik und -chemie sowie auch die Materialwissenschaften umfasst. Es ist daher nicht überraschend, dass die in diesem Kapitel vorgestellten Untersuchungen ein weites Spektrum an Materialien und ihren Eigenschaften zum Thema haben.

Die Natur von Eisen (in Hinsicht auf seine Ladung, als Spurenelement oder als Hauptbestandteil) spielt bei der Bestimmung der Eigenschaften von Mantelmineralen und des metallischen Erdkerns eine wichtige Rolle. Daher befassen sich einige der laufenden Projekte mit diesem Element, von seiner Substitution als dreiwertiges Kation in Hauptphasen des Erdmantels, wie Majorit-Granat oder Perowskit, bis zu den Hochdruck-/Hochtemperatur-Übergängen seiner Legierungen, die für das Verständnis des tieferen Erdinneren von Bedeutung sind.

Die meisten natürlichen Minerale sind keine chemisch reinen Phasen. Vielmehr weisen sie wegen des Austauschs von Atomen auf verschiedenen Plätzen des Kristallgitters in der Zusammensetzung eine große Streubreite auf. Ein derartiger Kationenaustausch kann die Struktur-Eigenschaftsbeziehungen eines Minerals stark beeinflussen. So ist zum Beispiel eine

Struktur vom „Dolomit-Typ“, die aus geordnetem Einbau von Mg und Cd zwischen den Karbonatlagen resultiert, bei mittleren Zusammensetzungen zwischen $MgCO_3$ und $CdCO_3$ stabil. Neue, abweichende Strukturen wurden bei hohen Drücken in Abhängigkeit der K-Konzentration in den Na-Disilikat-Komponenten entdeckt. Kritische Temperatur- und Druckwerte (d. h. Temperatur- und Druckwerte, bei denen Phasenübergänge auftreten) werden auch durch den Kationenaustausch beeinflusst, wie im Falle des Klinoenstatit, der sich bei erheblich niedrigeren Temperaturen in seine Hochdruck-Modifikation umwandelt, wenn Spuren von Ca in seine Struktur eingebaut werden.

Andere Untersuchungen befassen sich mit der Kompressibilität von Materie. Die Volumenänderung der Einheitszelle des Kristallgitters als Funktion des Druckes kann derzeit sehr präzise mit Hochdruck-Röntgenmethoden *in situ* bestimmt werden. Unter den hohen Drücken und Temperaturen des Erdinnern ist es wichtig, nicht nur die bei diesen Bedingungen stabilen Phasen zu kennen, sondern auch deren Reaktionen auf Veränderungen der Umgebungsbedingungen.

3.3 Geochemie

Aus der Erforschung radiogener Isotope wissen wir, dass sich der Metallkern der Erde in den ersten 30 Millionen Jahren der Erdgeschichte von seinem Silikatmantel abgetrennt hat. Die Tatsache, dass der größte Teil der Erde zu jener Zeit aufgeschmolzen war, mag eine schnelle Abscheidung gefördert haben. So konnte die dichtere Metallschmelze zum Erdzentrum absinken, wobei sie einen silikatischen Magmaozean zurückließ, der als Erdmantel auskristallisierte. Sogenannte primitive chondritische Meteorite bestehen möglicherweise aus dem Material, aus dem auch der Großteil der Erde gebildet wurde. Im Vergleich mit Chondriten erweist sich die heutige Zusammensetzung des Erdmantels als abgereichert an den sogenannten siderophilen Elementen. Diese Elemente bewahren ihren metallischen Zustand über eine große Spannbreite von Umgebungsbedingungen. Gold ist zum Beispiel hoch siderophil, da es seinen Metall-Zustand auch bei sehr hohen Sauerstoff-Partialdrücken beibehält. Heute ist obere Erdmantel in Bezug auf Gold stark verarmt, da das Metall bei der Bildung des Erdkerns dorthin extrahiert wurde. Zahlreiche andere Elemente treten über einen weiten Bildungsbereich als Oxide auf. Man bezeichnet sie als gesteinsbildende oder lithophile Elemente. Silizium und Calzium sind zum Beispiel lithophile Elemente, die in metallischem Zustand lediglich bei extrem niedrigen Sauerstoff-Partialdrücken existent sind. Es besteht ein fließender Übergang zwischen lithophilen und hoch-siderophilen Elementen, was sich im Verhältnis widerspiegelt, in dem jedes Element als Folge der Erdkernbildung aus dem Erdmantel extrahiert wurde. Diese einfache Deutung der Elementverteilung zwischen Mantel und Kern erscheint auf den ersten Blick völlig hinreichend. Jedoch tauchen bei einer detaillierteren Untersuchung viele ungeklärte Fragen auf. Die Konzentration zahlreicher Elemente ist im Mantel weit höher als die Metall-Silikat-Verteilungskoeffizienten vemuten ließen. Umgekehrt ist der Erdmantel an einigen Elemente wie Silizium übermäßig abgereichert. Ein möglicher Grund für diese Ungereimtheiten ist, dass unsere Kenntnisse des siderophilen oder lithophilen Charakters im Allgemeinen auf Verteilungsdaten bei relativ niedrigen Drücken basieren. Aus thermodynamischer Sicht lässt sich der Druckeinfluss auf die Elementverteilung über die Volumenänderung zwischen Oxiden und Metallphasen

bestimmen. Die Volumenänderung ist infolge der elastischen Kompression und von Phasenumwandlungen ebenfalls druckabhängig, sodass sich das Wesen der Elementverteilung bei hohen Drücken potentiell stark ändert. Viele in diesem Kapitel vorgestellte experimentelle Untersuchungen unter den hohen Drücken und Temperaturen des Erdinneren sollen unser Verständnis der Einzelheiten der Erdkernbildung und der Kristallisation des Erdmantels verbessern.

Diskontinuitäten in den elastischen Eigenschaften des Mantels erzeugen Reflektion und Refraktion seismischer Wellen in 410, 520 und 660 km Tiefe. Es gilt weithin als gesichert, dass Phasenumwandlungen in Mantelmineralen diese Diskontinuitäten erzeugen. Die Diskontinuität in 660 km Tiefe wurde als scharf abgegrenzter Tiefenabschnitt von ca. 6 km Mächtigkeit identifiziert, wohingegen für die Diskontinuität in 410 km eine variable Dicke zwischen 4 und über 10 km beobachtet wurde. Phasenübergänge in einfachen Ein-Komponenten-Systemen sind scharf begrenzt, da sie bei vorgegebenem Druck bei einer genau definierten Temperatur ablaufen. Als einfachstes und bekanntestes Beispiel ist reines H_2O zu nennen, das ausschließlich bei 0 °C und 1 bar schmilzt. Der Erdmantel ist jedoch als ein komplexes Gemenge von Elementen anzusehen, deren Hauptphasen als Mischkristalle vorliegen, die Fe und Mg enthalten. So wie H_2O-NaCl-Gemische über einen größeren Temperaturbereich schmelzen (im Gegensatz zu reinem H_2O), so werden Phasenübergänge im Erdmantel über tiefenabhängige Druckintervalle auftreten. Experimentelle Untersuchungen zur Bestimmung Transformationsintervalls von Mantelmineralen unter unterschiedlichen Bedingungen können mit seismischen Beobachtungen verglichen werden und daraus grundlegende Informationen über die Natur des Erdmantels in diesen Tiefen gewonnen werden.

3.4 Metamorphose

Metamorphose tritt im Zusammenhang mit zwei grundsätzlich verschiedenen geologischen Prozessen auf: (a) mit Gebirgsbildung/Plattentektonik und (b) mit Asteroideneinschlägen. Diese beiden geologischen Prozesse unterscheiden sich erheblich im zeitlichen Maßstab der metamorphen Überprägung. Gebirgsbildung oder Orogenese ist ein endogener, d. h. von Kräften im Erdinneren kontrollierter Prozess. Er wird von der träge im Erdmantel ablaufenden Mantelkonvektion angetrieben und kann sich über Millionen von Jahren erstrecken. Dieser langsame Prozess führt zu massiven Veränderungen von Gesteinstexturen und zu metamorphen Reaktionen, die neue Mineralvergesellschaftungen hervorrufen. Im Gegensatz dazu ist die Impakt-Metamorphose ein exogener Prozess, der als Folge von Einschlägen großer Himmelskörper in nur wenigen Sekunden abläuft. Die Minerale reagieren nach bestimmten Um- und Verformungsmustern, die für den kurzzeitigen Prozess diagnostisch sind. Typische Gesteinsvertreter sind Impakt-Brekzien, die aus einer chaotischen Mischung von Schmelzklumpen und Mineral- und Gesteinsbruchstücken aus unterschiedlichem Ausgangsmaterial und mit verschiedenem Schockmetamorphose-Grad aufgebaut sind.

In den vergangenen Jahren wurden bedeutende Entdeckungen und Fortschritte in beiden Bereichen der Metamorphose erzielt. Unter regionalmetamorphen Aspekten sind die

eindruckvollsten Gesteine wohl die metamorphen Hochdruck- und Ultrahochdruck-Gesteine (Gneise und Eklogite), die nun weltweit zunehmend in metamorphen Gesteinsgürteln unterschiedlichen Alters identifiziert werden. Diese Gesteine sind für Petrologen besonders attraktiv, da sie spektakuläre Mineralvergesellschaftungen z. B. mit Diamant und Coesit enthalten. Die metamorphen Gesteine wurden einer tiefen Subduktion mit anschließender schneller Heraushebung unterzogen und bieten nun einzigartige Einblicke in Prozesse, die tief in der Erdkruste in Kontinent-Kontinent-Kollisionszonen abgelaufen sind. So liefern z. B. hochauflösende Untersuchungen von Gesteinstexturen und die Charakterisierungen von Mikro-Defektstrukturen in metamorphen Mineralen mit Hilfe der Raster- und Transmissions-elektronenmikroskopie (REM und TEM) wesentliche Informationen zum Verformungs-verhalten von tief subduzierten Gesteinen.

Forschungen auf dem Gebiet der Schockmetamorphose konzentrieren sich auf die Ausbildung neuer Hochdruck-Modifikationen in Impakt-Brekzien und auf das Zersetzungsverhalten von geschockten Mineralen mit leichtflüchtigen Bestandteilen. Kontrollierte Schockexperimente haben wesentlich zu einem besseren Verständnis über Bildungsmechanismen von Hochdruck-Mineralen und Entgasungsphänomene von Karbonaten und Sulfaten beigetragen. Letzteres ist für das Verständnis der Klimaentwicklung auf der Erde und die Rolle der schockbedingten Freisetzung toxischer Klimagase beim Massensterben an der Kreide-Tertiär-Grenze von Bedeutung.

3.5 Fluide und ihre Wechselwirkung mit Schmelzen und Materie

Die Entstehung einer Hydrosphäre war in der Erdgeschichte eines der tiefgreifendsten Ereignisse für das irdische Leben. Die Ausbildung der Hydrosphäre ist eng mit Fluid-prozessen im Erdmantel verbunden. Wasser und weitere leichtflüchtige Komponenten wurden durch vulkanische Aktivitäten und andere nicht-magmatische Vorgänge über geologische Zeiträume zur Erdoberfläche transportiert und in Subduktionsprozessen erneut wieder in den Erdmantel verbracht. Während Wasser im oberen Mantel lediglich als Spurenkomponente auftritt, gibt es Hinweise darauf, dass die Gehalte in der Übergangszone und im unteren Mantel erhöht sind.

Ein erster Schritt zur Quantifizierung des Einflusses von Wasserstoff, sowohl auf die physikalischen und chemischen Eigenschaften des Erdmantels als auch auf Prozesse im Erdmantel, ist die Beschreibung des Wasserstoffeinbaus in Mineralphasen des Erdmantels. Da der Wasserstoffeinbau durch vorhandene Punktdefekte und geringe Gehalte bestimmter Elemente beeinflusst werden kann, müssen diese Untersuchungen an natürlichen und synthetischen Proben die entsprechenden Zusammensetzungen des Mantels berücksichtigen. Kürzlich wurden Untersuchungen begonnen, die den Einfluss von Hydratation auf physikalische Eigenschaften wie Elastizität und Rheologie einschließen. Diese Studien führen auf der Basis geophysikalischer Gesamtmessungen zu klaren Eingrenzungen des Chemismus des Erdmantels. Aus der Kinetik der Hydratation lässt sich abschätzen, inwieweit natürliche Proben ihre Geschichte konserviert haben könnten. Die Wasserstoff-Profile in natürlichen Proben ermöglichen also, die Entwicklung von Xenolithen und Magmen unter zeitlichen und thermischen Aspekten aufzuklären. Direkte Untersuchungen von Fluiden im Labor sind für

das Verständnis von Prozessen (z. B. Diamantwachstum) von Bedeutung, aber auch für die Eingrenzung der physikalischen Grundeigenschaften wie z. B. Aufschmelzung.

3.6 Physikalische und chemische Eigenschaften von Schmelzen und Magmen

Schmelzphasen sind wichtige, im Erdinneren allgegenwärtige Komponenten und haben bedeutenden Einfluss auf die Entwicklung unseres Planeten. Silikat- und Metallschmelzen ermöglichten erst eine Differentiation der Erde in Kruste, Mantel und Kern. Auch danach spielten sie eine Schlüsselrolle im dynamischen Verhalten der Erde. Obwohl zwar oberflächennahe Schmelzen bei Vulkanausbrüchen beobachtet werden können, lassen sich die physikalischen und chemischen Eigenschaften von Schmelzen des Erdinneren nur experimentell im Labor untersuchen.

Die Beiträge in diesem Abschnitt decken einen weiten Bereich von Schmelzen ab, der für die ganze Erde maßgeblich ist. Untersuchungen von Viskosität und Transporteigenschaften von Schmelzen, wie Ionen- oder thermische Leitfähigkeit unter den hohen Drücken des Erdmantels, stellen experimentell eine große Herausforderung dar, sind jedoch für die Eingrenzung der Eigenschaften eines Magmaozeans in der Frühgeschichte der Erde oder für die Diskussion des Wärme- und Materie-Transports im Inneren der Planeten entscheidend. Trotz der experimentellen Problematik konnte die Impedanz-Spektroskopie erfolgreich zur Bestimmung elektrischer Leitfähigkeiten in wasserhaltigen Silikatschmelzen unter Erdkrustendruck eingesetzt werden. Die gewonnenen Daten können zur Entwicklung von Fernerkundungsmethoden führen, die zur Abschätzung des Wassergehalts von Schmelzen in einer Magmenkammer vor einem Vulkanausbruch dienen. Ein derartiges Werkzeug wäre für die Risikobewertung von Vulkanen extrem hilfreich. Andere Untersuchungen zielen auf das Verständnis von Redox-Bedingungen in Magmen während des Aufstiegs zur Oberfläche und der damit verbundenen Abkühlung. Spektroskopische Untersuchungen an Silikatgläsern, die durch Abschreckung von Schmelzen bei hohen Drücken und Temperaturen erzeugt wurden, liefern das Bindeglied zwischen Schmelze/Glas-Strukturen und Schmelzeigenschaften. Dagegen sondiert die *in situ*-Infrarot-Spektroskopie unter hohen Drücken und Temperaturen direkt die Temperaturabhängigkeit der Wasserspeziation in Silikatschmelzen. Durch Untersuchungen zum Abscheidungsverhalten von Eisen-Schwefel-Schmelzen in kristalliner Silikatmatrix unter hohen Drücken lassen sich die Bildungsbedingungen des Erd- und Marskerns eingrenzen.

3.7 Materialwissenschaften

Historisch gesehen wurden Hochdruck-/Hochtemperatur-Experimente ursprünglich eingesetzt, um Prozesse in der tieferen Erde zu simulieren. Später setzten Physiker und jetzt auch Materialforscher die von Erdwissenschaftlern entwickelten Methoden ein, um ganz unterschiedliche Komponenten unter extremen Bedingungen zu untersuchen. Das Bayerische Geoinstitut, ein Standort, an dem einzigartige Hochdruck-Ausrüstungen und -Methoden eingesetzt und weiterentwickelt werden, ist an ausgeklügelten und herausfordernden materialwissenschaftlichen Forschungsarbeiten unter extremen Bedingungen beteiligt.

Eine klassische Aufgabe der Materialwissenschaften ist die Untersuchung von P-T-Phasendiagrammen. Es überrascht, dass Phasenbeziehungen z. B. in Blei, einem der uns am längsten bekannten Metalle, noch nicht endgültig geklärt sind. Die Bestimmung der Phasengrenze zwischen *fcc*- und *hcp*-Bleimodifikationen ist ein Schritt in diese Richtung. Die Elemente der Titan-Gruppe finden heute aufgrund ihres geringen Gewichtes, ihrer statischen Festigkeit und Steifheit eine weite Anwendung in der modernen Technik (besonders in der Luftfahrtindustrie). Die Entwicklung neuer Legierungen auf Ti-Basis erfordert umfangreiche Kenntnisse über das Verhalten und mögliche Veränderungen in der Elektronenstruktur von Titan bei erhöhten Drücken und Temperaturen.

Eine neue Form des Kohlenstoffs stellen Fullerene dar, die in den letzten Jahren aufgrund ihrer ungewöhnlichen kugelförmigen Käfigstruktur und einzigartiger Eigenschaften eine enorme Aufmerksamkeit erfahren haben. Unter Hochdruck-/Hochtemperatur-Bedingungen durchlaufen Fullerene und ihre Komponenten Übergänge zu verschiedenen Polymerphasen; von einigen wird berichtet, dass ihre Härte die des Diamant übersteigt, andere sollen magnetisch oder elektrisch leitfähig sein. Details zum Polymerisationsprozess von C_{60} sind nicht geklärt; die Kombination von *in situ*-Untersuchungen in Diamantstempelzellen mit der Synthese von „größeren“ Materialmengen in Multianvil-Pressen führt zu neuen Möglichkeiten der Erzeugung neuer Materialien auf Fullerit-Basis.

Bekannte und technisch realisierbare Anwendungen von nanokristallinem Titanoxid (TiO_2) liegen in der Pigment-, Kunststoff-, Kosmetik-, Elektronik- und Katalysator-Industrie. Multianvil-Experimente führen zu neuen Erkenntnissen über elastische Eigenschaften und Phasenbeziehungen dieses Stoffes. Trotz erfolgreicher Hochdruck-Studien zu elektronischen/magnetischen Besonderheiten des sogenannten Mott-Übergangs bleiben deren strukturelle Phänomene immer noch verschwommen. Durch eine Kombination der Diamantstempelzellen-Technik mit der Synchrotron-Pulverdiffraktometrie wird eine Reihe struktureller Einzelheiten des Mott-Übergangs in der Modellverbindung FeI_2 enthüllt.

Am Beispiel von Materie mit Perowskit-Struktur kann vielleicht am besten das gemeinsame Interesse von Geo- und Materialwissenschaftlern erläutert werden. In der Materialwissenschaft haben Substanzen mit Perowskitstruktur große Bedeutung als Hochtemperatur-Supraleiter, als Keramik für Brennstoffzellen, für Gassensoren und Membranen für die Sauerstoffextraktion oder für die Wasserstoffproduktion. Bildungs- und Verteilungsmechanismen von Fehlstellen sind gleichermaßen für die Material- als auch Geowissenschaften interessant. Die Methodik der Perowskit-Synthese bei hohem Gasdruck, besonders bei hohem Sauerstoffdruck, wurde von Geowissenschaftlern erarbeitet und wird im Geoinstitut routinemäßig eingesetzt. Es hat sich als sehr erfolgreich für die Herstellung von Mischkristallen aus elektrochemisch aktivem $LiNiO_3$ und $LiGaO_3$ über einen weiten Konzentrationsbereich gezeigt. So werden Möglichkeiten eröffnet, das allgemein als Kathodenmaterial gebräuchliche $LiCoO_3$ gegen ein neues auf Ni-Basis auszutauschen. Das „*spin-crossover*“-Phänomen (SCO), das thermo-, foto-, magneto- und piezochromatische Eigenschaften einer Gruppe von Übergangsmetallen, besonders von Eisenkomplexen, betrifft, ist von wachsender Bedeutung auf dem Gebiet multifunktionaler molekularer Materie. Das

gilt besonders in Hinsicht auf mögliche Anwendungen auf dem Gebiet der Speicher-, Anzeige- und Schalt-Baugruppen im molekularen Maßstab. Sowohl die Mechanismen als auch viele andere Details des SCO sind bisher kaum verstanden. Die Feinabstimmung des Volumens durch Änderung des Drucks in *in situ*-Hochdruckexperimenten mit Diamantstempelpressen eröffnet Möglichkeiten, Phänomene der Kristallgitterdynamik während der *spin-crossover*-Übergänge und Druck-induzierter Amorphisierung zu untersuchen. Moderne Methoden der Materialmodifizierung, wie z. B. die Oberflächenbehandlung von Keramiken mit Lasern, beeinflussen bisweilen nur sehr kleine Probenareale im Submikrometer-Bereich. Hier können standardmäßig in den Geo- wie auch den Materialwissenschaften eingesetzte analytische Methoden, insbesondere die analytische Transmissionselektronenmikroskopie, helfen, die Umwandlungsmechanismen aufzudecken.

3.8 Methodische Entwicklungen

Innovation und Fortschritte beim Verständnis des tiefen Erdinneren sind von neuen Technologien und Methoden zur Untersuchung von Mineralvergesellschaftungen bei erhöhten Drücken und Temperaturen abhängig. Eine exakte Interpretation geophysikalischer, geochemischer und petrologischer Beobachtungen erfordert eine akkurate und komplexe physikalische, chemische und strukturelle Charakterisierung der Materie sowohl bei Umgebungsdruck als auch unter extremen Bedingungen, vorzugsweise *in situ*. In dem Berichtsjahr lag der Schwerpunkt auf zwei neuen Methoden: der Gigahertz-Ultraschall-Interferometrie und den Experimenten zur akustischen Emission in der Multianvil-Presse. Die neuen Techniken erlauben bei hohen Drücken und Temperaturen direkten Einblick in Eigenschaften und Prozesse von Materie, die unter geophysikalischen Aspekten von Bedeutung sind. Weiterhin haben wir unsere Bemühungen fortgesetzt, die Hochdruck- und Hochtemperatur-Ausrüstung zu verbessern und damit bestehende experimentelle Grenzen zu überwinden. Mit der neuen Multianvil-Presse mit gegenständigen Stempeln vom Typ „Drickamer“ lassen sich höhere Drücke einstellen, als mit den herkömmlichen Multianvil-Pressen. Dabei stehen Probenvolumina zur Verfügung, die um eine Größenordnung größer sind als die konventioneller Diamantstempelzellen. Ein im Geoinstitut neu konstruiertes System einer außen beheizten Diamantstempelzelle ermöglicht uns, mit Drücken oberhalb 130 GPa und Temperaturen oberhalb 1200 K zu experimentieren. Stempelzylinder-Pressen bieten neue und elegante Möglichkeiten, natürliche Proben unter hohen Drücken zu tempern, um den Wassergehalt von nominell wasserfreien Mineralen unter Drücken und Temperaturen des oberen Erdmantels zu studieren. Fortschritte in der Analysetechnik werden anhand von neuen Untersuchungen Al-führender Silikat-Perowskite mit ALCHEMI (atom location by channeling-enhanced microanalysis) in der Transmissionselektronenmikroskopie und anhand neuer Entwicklungen in der Festkörper-NMR vorgestellt.

3. Research Projects

In this section an overview of the most important on-going projects is given. Information concerning recently-completed projects can be obtained from the publication lists of sections 4.1 and 4.2. Please note that the following contributions should not be cited.

3.1 Physical and Chemical Properties of Minerals and Rocks

Geological surface or near surface phenomena such as volcanic eruptions or earthquakes are evidence of the dynamic nature of the planet Earth. The understanding of the forces that drive these dynamic processes is one of the main goals in the geosciences. Since the Earth's deep interior is generally inaccessible to direct sampling, indirect methods such as geophysical or geochemical techniques are being applied to probe the Earth's interior. Interpretation of the results from these measurement is often quite dependant on physical and chemical data from experiments conducted (possibly) at conditions that mimic those of the deep Earth. This experimental approach is one of the main focuses of the research within the Geoinstitut.

Seismological studies of the Earth yield data about the distribution of seismic wave speeds and densities in the Earth's interior; these data have to be compared with laboratory measurements of elastic properties of the minerals that occur at various depths in the Earth. During the last year this experimental approach has been extended to the direct measurement of the travel times of acoustic waves in single crystals at high pressure yielding the complete elastic tensor. Besides the elastic behaviour also the plastic deformation of the minerals in the mantle is of great interest since it may be responsible for the formation of anisotropic structures and hence seismic anisotropy. The rheology of the different components of the Earth's mantle is therefore of great importance and is being studied in deformation experiments. However, performing well constrained deformation experiments at mantle conditions remains a challenge. Apart from the understanding of the mechanical behaviour of the constituent phases additional factors such as enhanced fluid content or changes in the crystallographic structure (phase transitions) have to be considered. The distribution of electrical conductivity in the Earth's mantle has been basically understood with the help of conductivity measurements at high pressure in the laboratory. For a more complete interpretation it is however necessary to take into account the effect of varying iron contents in the phases of the upper and lower mantle as well as the transition zone.

Physical and chemical parameters of minerals and rocks also represent important input parameters in calculations that attempt to model various aspects of the deep Earth such as mantle convection or the behaviour of subducting plates. The distribution of earthquakes down to depths of more than 600 km in subducting slabs remains an especially puzzling phenomenon since all materials should show plastic deformation behaviour at these temperature and pressure conditions. Metastable olivine in subducting slabs may at least partly explain the presence of deep earthquakes, but its presence is dependent on a number of physical parameters such as thermal conductivity, the latent heat and the kinetics of the phase transitions as well as the distribution of stresses in the descending plate.

The conditions of formation of natural rocks are reflected in their physical and chemical properties. Microstructures and crystallographic preferred orientations represent a memory of metamorphosis and deformation at high temperature and/or pressure and allow an estimation of these conditions. Magnetic properties of rocks are the result of a complex formation history and may cause large anomalies in the present day magnetic field. Optical properties of minerals and rocks play an important role for their use as gemstones and can also be the result of a formation under changing chemical conditions.

a. *High-pressure elasticity of (Mg,Fe)O (S.D. Jacobsen)*

Periclase-MgO is one of the most widely studied phases in mineral physics as well as an important standard material for testing new experimental techniques and pressure scales. However, the oxide coexisting with (Mg,Fe,Al)SiO_3-perovskite in Earth's lower mantle (660-2900 km depth) is likely to contain anywhere from 5-25 mol.% FeO in its rock-salt structure. The effects of iron, pressure, and temperature on the anisotropic elastic properties of (Mg,Fe)O are not yet known. A new combined X-ray/ultrasonic diamond cell is being used for the first time to measure the effects of iron substitution and pressure on the c_{ij} elastic constants of (Mg,Fe)O single crystals by gigahertz ultrasonic interferometry.

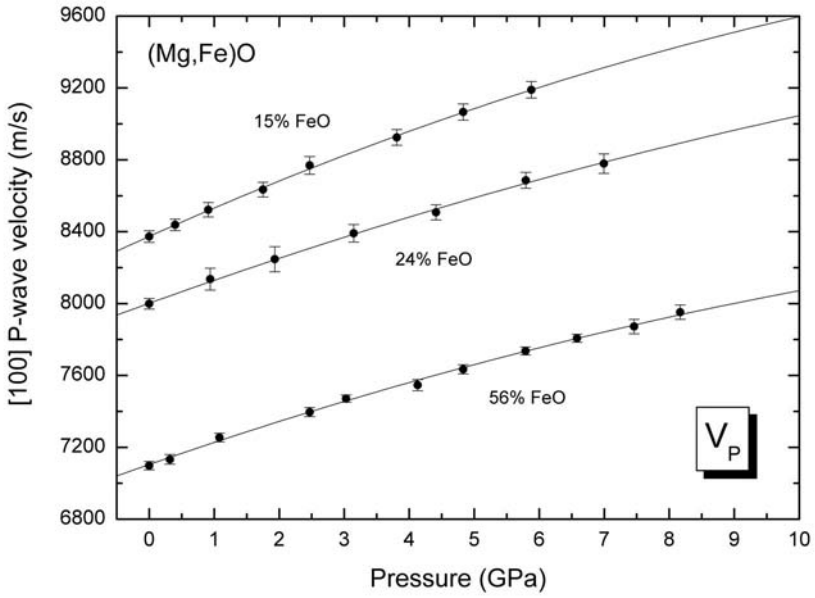

Fig. 3.1-1: [100] P-wave velocities in (Mg,Fe)O as a function of composition and pressure.

Round-trip compression-wave travel times were measured through 40 μm thick (100) plates of (Mg,Fe)O containing 15, 24, and 56 mol.% FeO to a maximum pressure of about 9 GPa. P-wave velocities (Fig. 3.1-1) were calculated from the measured travel times and length changes calculated from pressure-volume equations of state, measured either *in situ* with X-

rays or during earlier isothermal compression experiments. Using these velocities, the elastic constant $c_{11} = \rho(V_P^{[100]})^2$ was calculated as a function of iron-content and pressure, and is compared to pure MgO (from Brillouin scattering measurements) in Fig. 3.1-2.

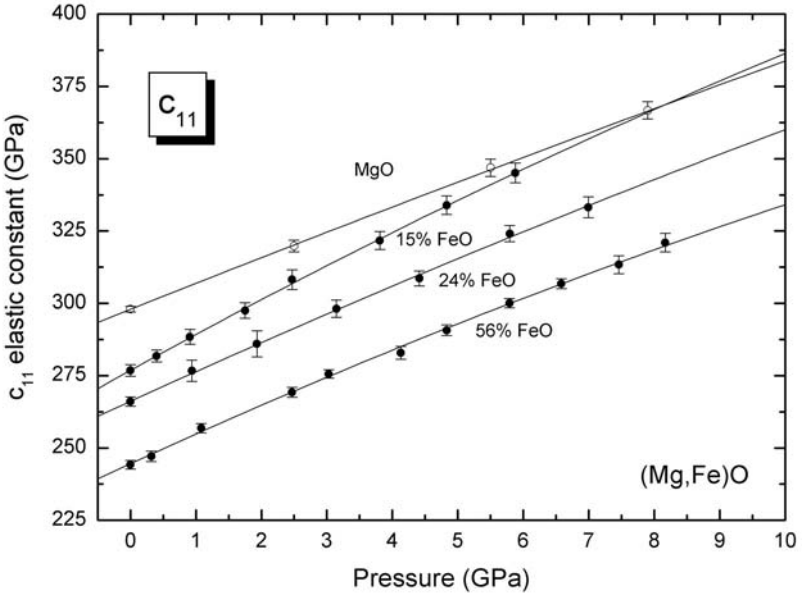

Fig. 3.1-2: The c_{11} elastic constant of (Mg,Fe)O as a function of composition and pressure. Values for MgO are published data from Brillouin scattering. Upon adding just 15 mol.% FeO to periclase, the derivative $\partial c_{11}/\partial P$ increases such that $(Mg_{0.85}Fe_{0.15})O$ is expected to be elastically stiffer in [100] dynamic compression than even MgO above about 8 GPa.

It appears that adding as much as 25 % iron to MgO increases the pressure derivative of the dynamic compressibility in the [100] direction. The derivative $\partial c_{11}/\partial P$ increases 40 % in adding just 15 mol.% FeO (1 % ferric) such that $(Mg_{0.85}Fe_{0.15})O$ is expected to have a higher c_{11} than even MgO above 8 GPa. The rather non-stoichiometric sample containing 56 mol.% FeO (13 % ferric) has about the same derivative $\partial c_{11}/\partial P$ as MgO, but a much lower initial value of c_{11}, so (Mg,Fe)O with higher FeO contents are expected to remain elastically softer than MgO at much higher pressures. In the coming year, [100] shear wave velocities, as well as [111] direction experiments will be carried out in order to determine the complete set of elastic constants and aggregate elastic properties of (Mg,Fe)O as a function of pressure to at least 10 GPa.

b. *Structure and elasticity of natural magnetite (S.D. Jacobsen, T. Boffa Ballaran, L.S. Dubrovinsky, N.A. Dubrovinskaia, in collaboration with H.-J. Reichmann/Potsdam)*

Magnetite (Fe_3O_4) is ubiquitous in the oxidized portion of Earth's crust and upper mantle, where it commonly forms solid solutions with ulvöspinel (Fe_2TiO_4) and magnesioferrite

($MgFe_2O_4$). Magnetite forms during secondary alteration and diagenesis, as well as in primary igneous genesis, so it occurs in nearly all rock types as well as the stony meteorites. It is stable to at least 10 GPa at 1000 ºC.

We measured the structure, compressibility and elastic constants of a natural single-crystal of magnetite from the Ural Mountains of Russia. Magnetite has the inverse-spinel structure (*Fd*3*m*) with structural formula $^{VI}(Fe^{2+},Fe^{3+})_2{}^{IV}Fe^{3+}O_4$. The only general atom-position parameter is the (*x/a*) fractional coordinate x = 0.25462(16) for oxygen, determined for this material from a single-crystal X-ray structure refinement. At room pressure, the cubic cell parameter is a = 8.39639(14) Å, resulting in a calculated density of 5.196(1) g/cm^3. The cell volume was measured under isothermal compression in a hydrostatic alcohol mixture to ~ 8.5 GPa at room temperature, using quartz for internal pressure calibration. Third-order Birch Murnaghan equation of state (EoS) parameters are provided in the following table, and plotted as density versus pressure in Fig. 3.1-3.

Equation of state parameters for natural magnetite

V_0 (Å^3)	ρ_{calc} (kg/m^3)	c_{11} (GPa)	c_{44} (GPa)	c_{12} (GPa)	K_{0S} (GPa)	G (GPa)	K_{0T} (GPa)	K_T'
592.19 ± 0.03	5.196 ± 0.001	261 ± 1	61 ± 3	158 ± 3	192 ± 2	57 ± 3	180 ± 1	5.2 ± 0.4

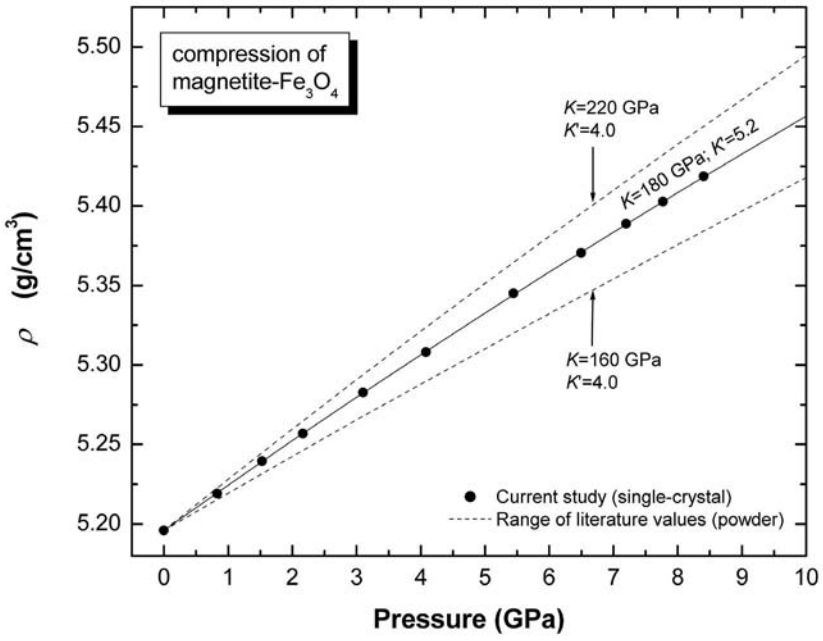

Fig. 3.1-3: Equation of state of magnetite plotted as density versus pressure from the current single-crystal study (solid line with filled circles), as well as the range of values existing in the recent literature from the static compression of powdered samples.

Adiabatic bulk and shear moduli were calculated from the single-crystal elastic constants, measured using gigahertz ultrasonic interferometry. The high-frequency elastic shear waves were produced using a new YAG P-to-S shear wave conversion buffer rod (see contribution of Jacobsen *et al.* in Chapter 3.8). Compressional (P) and shear (S) velocities for the following pure-mode propagation directions are (in m/s); $V_P^{[100]} = 7081 \pm 11$, $V_P^{[111]} = 7214 \pm 17$, $V_S^{[100]} = 3511 \pm 70$, and $V_S^{[111]} = 3153 \pm 68$. Thus, in dynamic compression the oxygen close-packing direction [111] is slightly faster than in [100], exhibiting about 2 % P-wave anisotropy, whereas the [100] direction is about 10 % faster for shear than [111].

To date, there is an unusually large range in reported values of the isothermal bulk modulus (K_{0T}) for magnetite. Extreme minimum and maximum values come consistently from compression of powdered samples, ranging from about 160 to 220 GPa. The behaviour of a strain field in magnetite powder pressurized in diamond cells can be responsible for the apparent inconsistency in elastic properties obtained from single crystal and powder X-ray diffraction experiments.

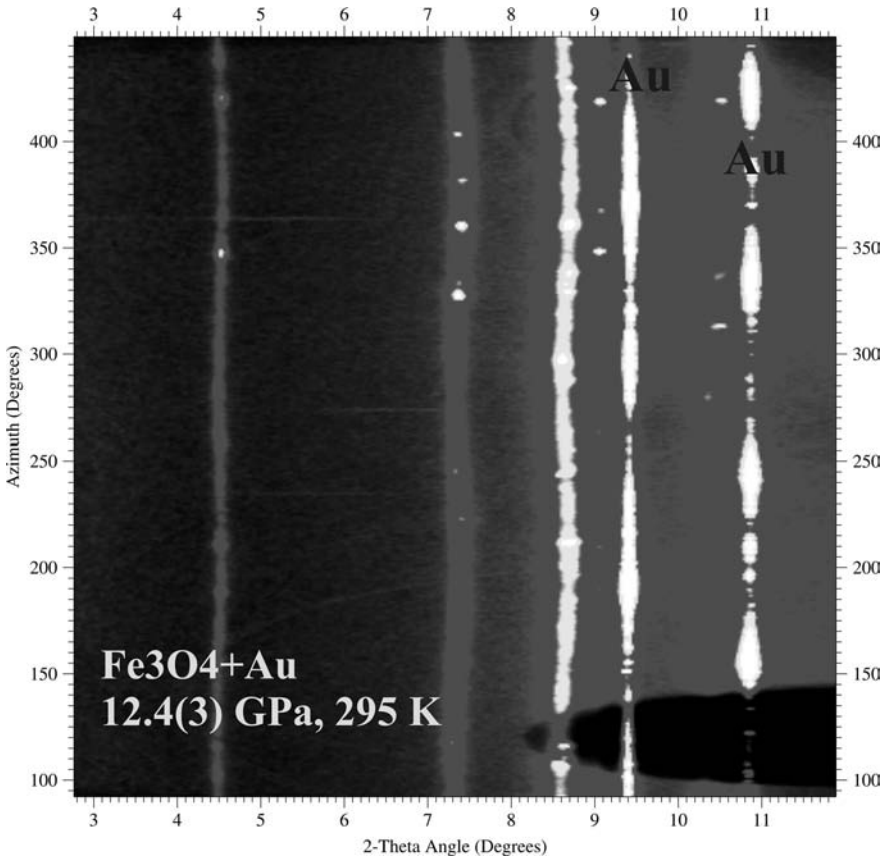

Fig. 3.1-4: An unrolled projection of the Debye-Scherrer lines recorded at the ESRF in parallel geometry from a mixture of magnetite and gold, compressed in a DAC using methanol-ethanol. The gold (Au) diffraction lines are straight, while the lines from magnetite are wavy. The resulting Debye-Scherrer ellipses, if observed only with a line detector, would result in a large range of possible values for K_{0T}, consistent with those reported in the literature.

Figure 3.1-4 shows an unrolled projection of the Debye-Scherrer lines recorded in a parallel geometry (X-ray beam is parallel to the loading direction of the DAC) from a mixture of powdered magnetite and gold, compressed in a methanol-ethanol pressure medium. The experiment was conducted at ESRF (beam line ID30). The gold diffraction lines are straight, while the lines from magnetite are wavy and correspond to the Debye-Scherrer ellipses, instead of the usual Debye-Scherrer rings expected for a material hydrostatically compressed or deviatorically stressed in a DAC. The minimal and maximal *d*-spacings along the Debye-Scherrer ellipses were used to estimate minimum and maximum molar volumes of differently strained crystallites in the compressed powder of magnetite. With a fixed value $K' = 4$ we found K_{T0} could vary from 165 to 224 GPa, corresponding to the range in reported literature values, and also plotted in Fig. 3.1-3.

c. *Sound velocities and elastic constants of Fo_{89} hydrous ringwoodite (S.D. Jacobsen and D.J. Frost, in collaboration with J.R. Smyth, H.A. Spetzler and C.M. Holl/Boulder)*

The bulk hydrogen content of Earth's interior is one of the most poorly constrained compositional variables, and the total water content of the planet is unknown to within an order of magnitude. Interpretation of seismic tomographic imagery using mineral physical data is potentially a powerful approach to constraining how much, if any, hydrogen exists in the high-pressure polymorphs of $(Mg,Fe)_2SiO_4$, wadsleyite (β) and ringwoodite (γ).

Sound velocities and single-crystal elastic constants of Fo_{89} hydrous ringwoodite ($Mg_{1.7}Fe_{0.22}H_{0.16}SiO_4$) containing approximately 10,000 wt ppm H_2O have been determined using gigahertz ultrasonic interferometry. Single-crystal samples measuring up to 800 μm in size were synthesised at 20 GPa and 1400 ºC in the 5000 ton press from starting materials of San Carlos olivine, En_{90} orthopyroxene, brucite, hematite and quartz for a calculated bulk water content of 3 weight perent. Three crystals were oriented to ± 1º on a precession camera from which (100), (110) and (111) double-polished plates were made. FTIR spectrocopy indicates the three samples contain the same amount hydrogen. Unit-cell volumes were measured on the four-circle diffractometer, indicating a very large volume of hydration, about 4.5 $Å^3$ or 0.8 % compared to dry Fo_{90} ringwoodite. Seven separate pure-mode ultrasonic experiments were made: V_P and V_S propagating along [100] and [111], and in the [110] plate we measured V_P and V_S polarized [001] and [-110].

Single-crystal and aggregate elastic properties of Fo_{89} hydrous ringwoodite

V_0 ($Å^3$)	ρ_{calc} (kg/m^3)	c_{11} (GPa)	c_{44} (GPa)	c_{12} (GPa)	K_{0S} (GPa)	G (GPa)	$V_{P\ bulk}$ (km/s)	$V_{S\ bulk}$ (km/s)
530.80 ± 0.07	3.65 ± 0.01	300 ± 6	112 ± 3	113 ± 3	175 ± 4	105 ± 3	9.3 ± 0.2	5.3 ± 0.1

Hydration of iron-bearing ringwoodite is observed to significantly decrease the single-crystal elastic constants and aggregate elastic properties, provided in the table above. Adiabatic bulk and shear moduli are reduced by 7 and 12 percent, respectively, compared to nominally anhydrous Fo_{91} ringwoodite (Fig. 3.1-5). Thus at room pressure, hydration of Fo_{89} ringwoodite to 1 wt.% H_2O has the same effect on aggregate P and S-wave velocities as raising the temperature by about 600 ºC and 900 ºC, respectively. The experiments mark the first time that a high-pressure phase synthesised in a multianvil press has been studied by single-crystal ultrasonic methods.

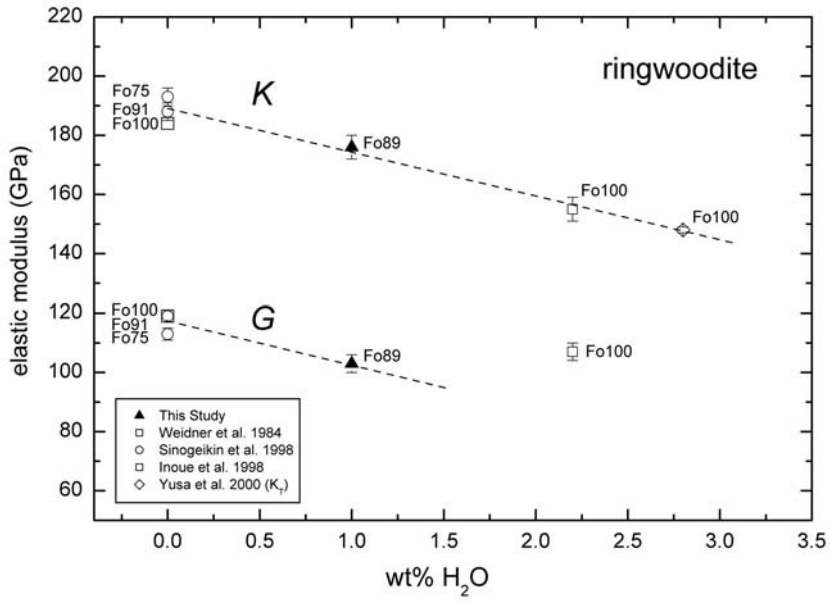

Fig. 3.1-5: Adiabatic bulk and shear moduli of ringwoodite as a function of water content.

d. *Rheology of (Ca,Sr)TiO_3 perovskite (J. Mecklenburgh, F. Heidelbach, S.J. Mackwell and F. Seifert)*

(Mg,Fe)SiO_3 perovskite is considered to be the most abundant phase in the Earth's lower mantle, along with magnesiowüstite and other minor high-pressure phases. Therefore knowledge of the rheological properties of (Mg,Fe)SiO_3 is crucial to the understanding of the rheology of the lower mantle. Presently, deformation experiments, yielding reliable rheological data, cannot be performed within the stability field of (Mg,Fe)SiO_3 perovskite. Fortunately, many elements can combine to form the perovskite structure and hence an analogue for (Mg,Fe)SiO_3 perovskite that is stable at experimentally tractable conditions can be found. (Ca,Sr)TiO_3 is one such material, which is stable at atmospheric pressure, and undergoes two structural phase transitions between 100 and 1600 K depending on the Ca:Sr ratio. By studying the deformation behaviour of (Ca,Sr)TiO_3 some insight can be gained into the rheological properties of (Mg,Fe)SiO_3 perovskite.

Polycrystalline samples of $(Ca_{0.9},Sr_{0.1})TiO_3$ have been synthesized from high purity oxides yielding samples with < 3 % porosity and a grain size of ca. 100 µm. These samples have been used to study the rheological properties of the tetragonal and cubic phases. Data from compression experiments performed over a temperature range spanning the orthorhombic to cubic phase transition show a power-law rheology with a stress exponent of ~ 4 and an activation energy of ~ 700 $kJmol^{-1}$ (Fig. 3.1-6). Crystallographic preferred orientation develops in the compression experiments that are consistent with [110] slip. $(Ca_{0.9},Sr_{0.1})TiO_3$ samples deformed in the cubic stability field to high strain in torsion show a comparable strength to compression tests under the same conditions. In these high-strain torsion experiments there is no shape-preferred orientation of the grains consistent with the shear strain. Despite this lack of a shape fabric a crystallographic preferred orientation develops that is consistent with [100] slip. Lattice rotations towards the rims of grains are observed to be about an axis perpendicular to the shear direction. It is inferred that these samples are deforming by grain boundary sliding, probably accommodated by components of both diffusion and dislocation creep.

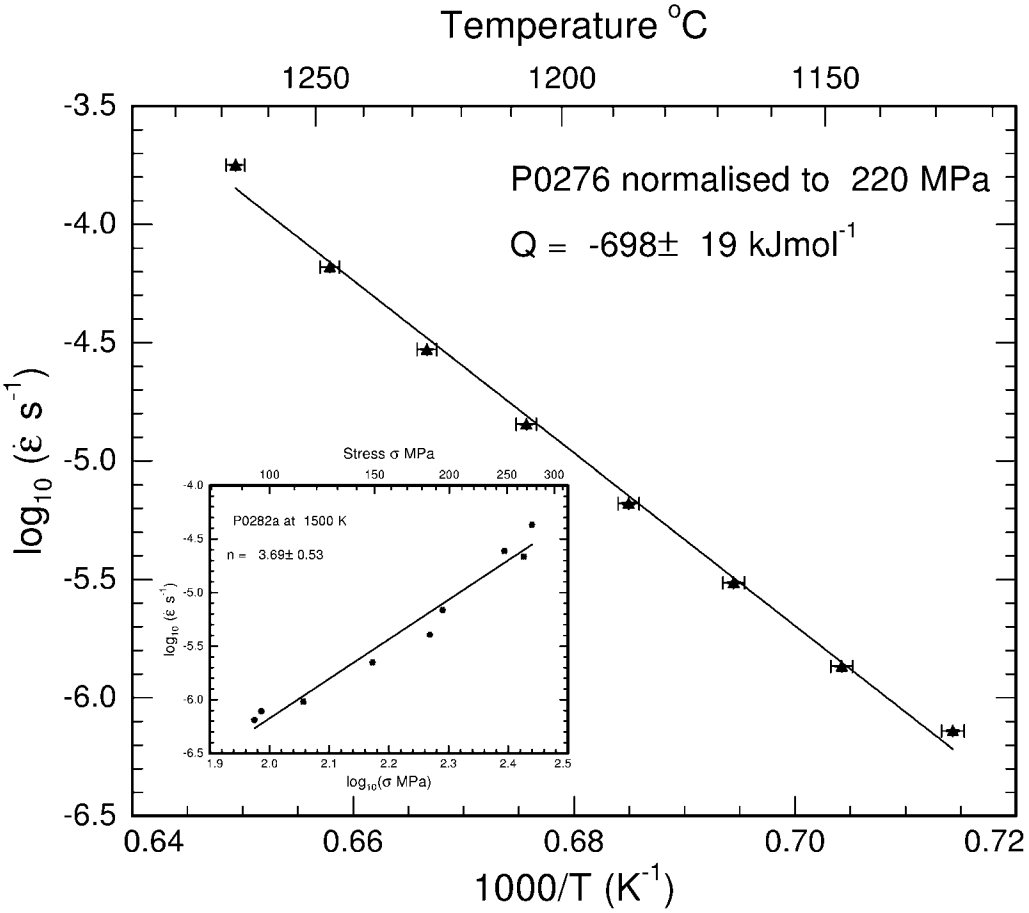

Fig. 3.1-6: Plot of log strain rate ($\dot{\varepsilon}$) against inverse temperature for a temperature stepping constant force experiment. The activation energy (Q) is shown for the linear regression shown. Inset graph is a log strain rate ($\dot{\varepsilon}$) against log stress (σ) for a force stepping experiment at 1500 K. The stress exponent (n) is shown.

e. *Mechanical behaviour and fabric development in experimentally deformed magnesiowüstite (Mg,Fe)O as a function of Fe-content (F. Heidelbach, I.C. Stretton and S.J. Mackwell)*

In a series of tests in a HT-HP deformation apparatus ('Paterson rig') we investigated the deformation behaviour of magnesiowüstite (Mg,Fe)O in torsion at 1400 K, 300 MPa confining pressure and a strain rate of 2 x 10^{-3} s^{-1}. The Fe-content was varied from 10 to 50 at.% in steps of 10 at.%. The samples were deformed to shear strains (γ) up to 15 in order to achieve steady state microstructures and textures. The shear stress – shear strain curves showed little to no weakening after the initial yield and the strength of the samples decreased slightly with increasing Fe. Analysis with electron backscattering diffraction (EBSD) in the SEM revealed that a crystallographic preferred orientation (texture) developed in all the samples indicating that dislocation creep contributed significantly to the deformation process. In all samples deformation was accompanied by recrystallization and grain size reduction. At low Fe-content (low homologous temperature) the recrystallization mechanism is progressive subgrain rotation; with higher Fe content (and increasing homologous temperatures) grain boundary mobility increases resulting in a larger recrystallized grain size at comparable shear strains.

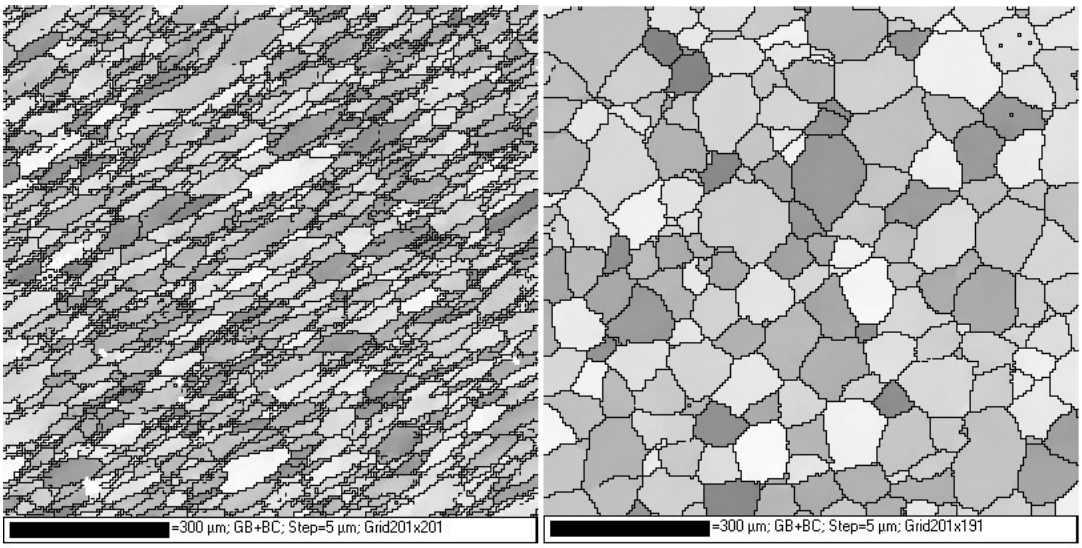

Fig. 3.1-7: Maps of the grain structure generated with SEM-EBSD; shear is dextral and black lines indicate grain boundaries with misorientation angles > 10°; gray shading of grains is arbitrary.

The development of the crystallographic preferred orientation is characterized by the transition from a deformation texture (γ = 1-6) to a recrystallization texture at γ > 6. The recrystallization texture remains constant to the highest strains. The deformation texture at lower strains is consistent with dislocation glide predominant on the {111}<110> and

{100}<110> slip systems, whereas the recrystallization texture cannot be modelled by dislocation glide alone. This texture evolution was observed in all the samples except those with 50 at.% Fe, where a deformation texture develops only at high shear strains and a recrystallization texture was not found. The effect of the high Fe content is illustrated in Fig. 3.1-7 comparing the microstructures of two samples with different Fe content deformed to about the same shear strain: the sample with high Fe content does not develop any shape preferred orientation indicating that grain boundary mobility is high. The lattice preferred orientations (LPO) confirm the increased importance of grain boundary migration (Fig. 3.1-8). The sample with high Fe content does not develop any LPO whereas the sample with low Fe content displays a typical deformation texture. The results suggest that with increased homologous temperature grain boundary migration and grain growth become more important in the deformation process reducing the share of dislocation creep and the formation of a texture. This development could be assisted by a higher content of Fe^{3+} and the associated increase in point defects (vacancies) with higher overall Fe-content.

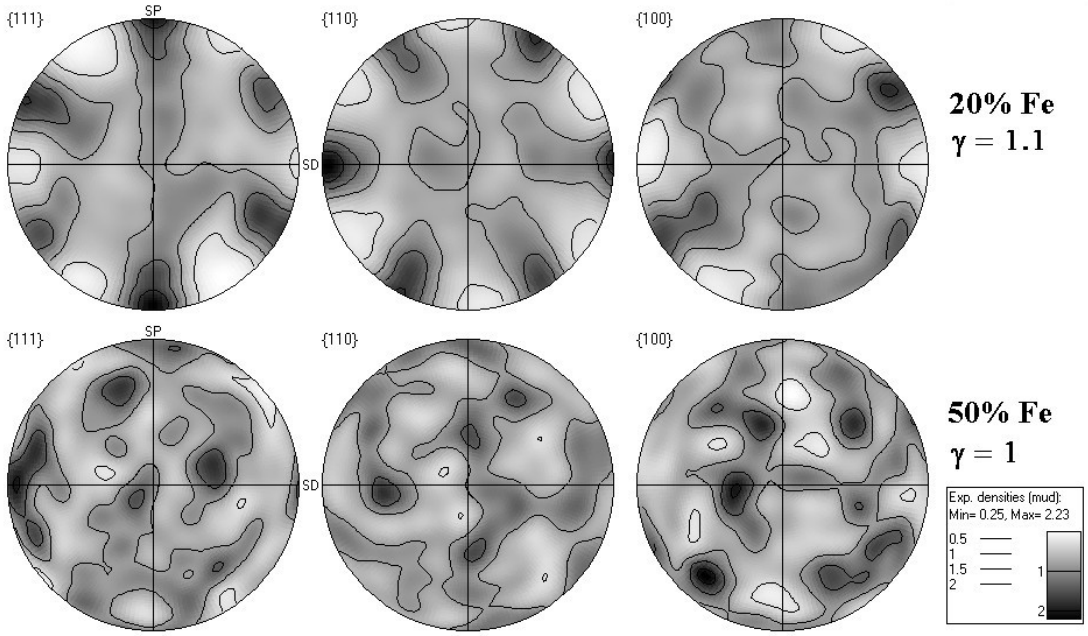

Fig. 3.1-8: Pole figures for the two samples of Figure 1; SD indicates shear direction, SP the pole of the shear plane; shear is dextral.

f. *Plastic deformation of forsterite under high pressure and high temperature: An experimental study in the multianvil apparatus (H. Couvy, S.J. Mackwell, P. Cordier/Lille, D.J. Frost and F. Heidelbach)*

At present, the rheological properties of many major mantle minerals are not well known. However, these properties are crucial for the understanding of a wide range of processes in the Earth's mantle (convection, lithospheric flexure, development of seismic anisotropy,

strength of subducting lithosphere). Experimental deformation of mantle minerals provides much needed constraints which can be used to model many of these processes.

Experiments have been performed in the 6-8 multianvil apparatus using a shear assembly developed in Bayreuth by Karato and Rubie. In this special assembly, a thin slice of the pre-synthesised forsterite $(Mg_2SiO)_4$ with a strain marker (platinum coating) is sandwiched between two hard alumina pistons, cut at 45°, which produce a relatively large strain in the polycrystalline material. The stresses accumulated during compression lead, at high temperature, to plastic shear strain of the sample. The pressure and temperature conditions are the same for all experiments (11 GPa and 1400 °C), with only the duration of the run being varied (1 min, 1h and 8 h). In order to ascertain the reproducibility of the results, several runs are performed at each run duration. Therefore, we can study the evolution of the mineral deformation with time and gain a better understanding of the evolution of deviatoric stress in this sample configuration.

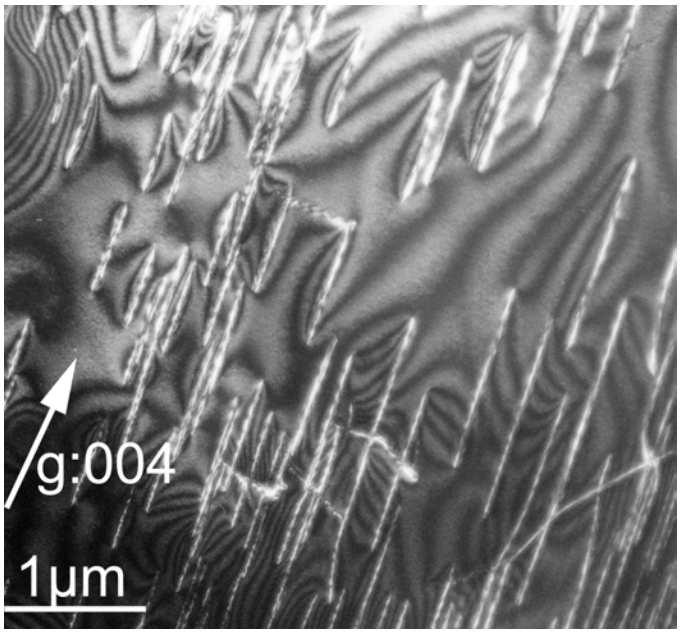

Fig 3.1-9: Dark-field TEM image of [001] screw dislocations (11 GPa, 1400 °C, 1h).

In the absence of direct determination of mechanical stress and strain data, most of the information gained from deformation in the multianvil apparatus is microstructural. Scanning Electron Microscopy (SEM) observations allow us to measure the strain marker rotation. The rotation of the strain marker shows that, even after 8 hours at 1400 °C, the shear strain is less than 10 %. Electron backscattering diffraction (EBSD) shows no texture in the starting material (hot-pressed) or after cold compression. A weak texture appears after 1 hour, with the *c* axis parallel to the shear direction and the *a* axis perpendicular to the shear plane. After 8 hours of heating, grain growth is observed and the textures appear to be weaker. Transmission Electron Microscopy (TEM) gives access to the dislocation microstructure and

hence to the elementary mechanisms responsible for plastic strain. After compression and only 1 minute of heating, we observe [001] dislocations with a density around 10^{14} m^{-2}. Both screw and edge dislocations can be found. After 1 hour of heating, the microstructure consists of [001] screws mostly with a density of 10^{13} m^{-2} (Fig. 3.1-9). After 8 hours of heating, only a few grains show some dislocation activity compared to observations after 1 hour. As a conclusion, our study shows that only limited (< 10 %) plastic strain can be achieved at 11 GPa, 1400 °C on forsterite using the shear deformation assembly. The maximum strain is observed after 1 hour of heating. Further annealing leads to recovery and erases deformation microstructures.

g. *Lattice preferred orientation in wet dunite (S. Majumder and D.L. Kohlstedt/Minneapolis, in collaboration with F. Heidelbach)*

The mechanical behaviour of minerals may be greatly influenced by water that is dissolved within their structure. In the upper mantle water is supplied by subducting slabs and possibly affects the rheology of the rocks in this area of the Earth. In order to investigate the effect of water on the mechanical behaviour of olivine we performed direct shear deformation experiments on water bearing dunite. The experiments were carried out to different amounts of shear strain at well constrained stress levels. The microstructures and lattice preferred orientation (LPO) in the samples were afterwards analyzed with electron backscattering diffraction (EBSD) in the SEM and compared with dry samples deformed under the same conditions.

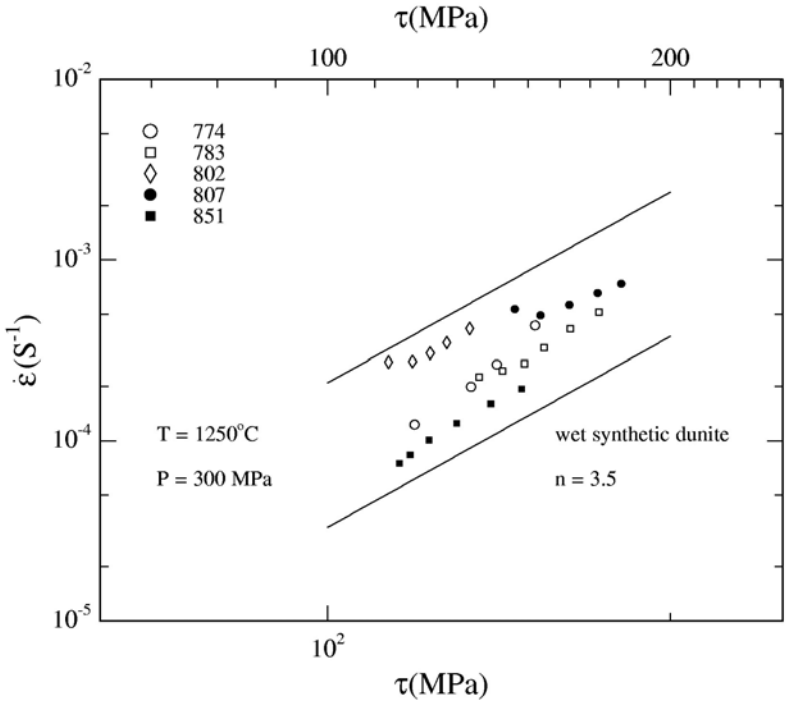

Fig. 3.1-10: Shear strain rate $\dot{\varepsilon}$ versus shear stress τ for all the samples investigated; straight lines give the best overall envelope to the data.

The starting material for the wet samples were prepared by hot pressing powders of San Carlos olivine with free water at 1523 K and 300 MPa. The average duration of the hot press runs were 4-6 hours and the samples had < 1 vol.% porosity after hot press. The deformation samples in form of 600-800 μm thick discs were cut from a cylindrical shaped hot pressed sample. The discs were then shaped to ellipses with 6.3 mm minor radius and 8.4 mm major radius. One disc was used for each deformation experiment. Each disc was cut into two halves along the minor axis and a thin Ni foil strain marker was placed between the halves. The disc and the strain marker were placed between two cylindrical thoriated W pistons cut at an angle of 45 degrees to the axis of the cylinder. The dry sample for observation PI-284 has been provided by Mark Zimmerman (University of Minnesota). Constant load deformation experiments were done on these samples using the same apparatus at 1523 K and 300 MPa. The internal load was calculated so that shear stress in the sample ranges between 100 - 180 MPa. The shear stress vs. shear strain rate plot for these experiments has a slope of 3 (Fig. 3.1-10) indicating deformation in the dislocation creep regime. The shear strains in the samples ranged 1.3 to 4.6. They were calculated both from the offset of the strain marker and the total displacement of the pistons during the deformation.

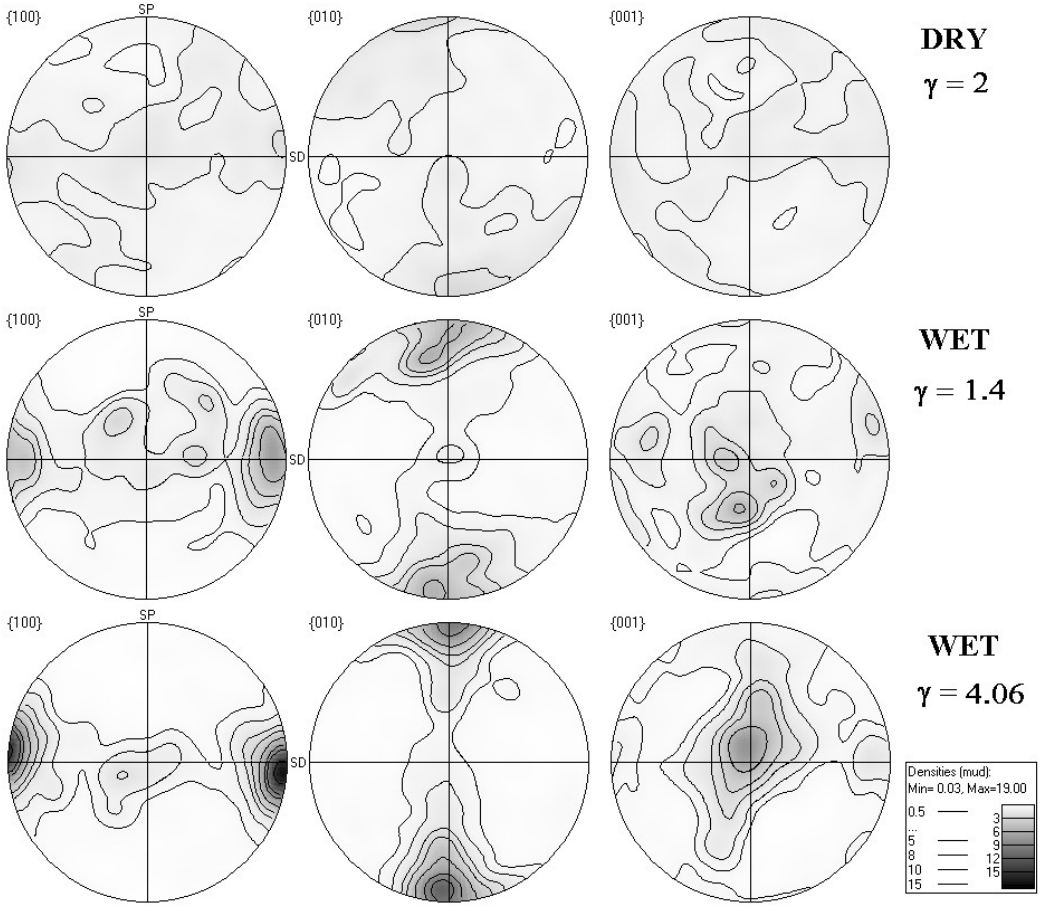

Fig. 3.1-11: LPO of three samples deformed in simple shear; shear plane is horizontal and shear sense is dextral.

The LPO in the samples were measured with EBSD over small areas of 200 μm by 200 μm using small steps of 1 μm and across the whole sample area using 10 μm steps. This was done to observe any possible difference in orientation between the fine grained aggregate and the bulk. Both measurements for each sample showed a strong alignment of {010} with the shear plane and of <100> along the shear direction. A small sub-maximum of {001} in the shear direction is also discernible. The strength of the preferred orientation shows a steady increase with increasing shear strain (Fig. 3.1-11). The dry sample displays a similar LPO with the alignment of {010} in the shear plane, but {100} and {001} are distributed in girdles in the shear plane. Most strikingly, the strengths of the CPOs in the wet samples are much higher compared to the dry sample at similar shear strain (Fig. 3.1.-11).

We interpret the LPOs as an result of dislocation creep on the {010}<100> slip system with a minor component of slip on {010}<001>. In the wet samples slip on {010}<100> seems to increase dramatically indicating that water may especially soften this system resulting in a very strong alignment of this slip system with the shear plane and shear direction. This strong alignment causes also a stronger anisotropy of physical properties such as seismic wave speeds. From our observations, we suggest that the anisotropy will be stronger in water rich regions of the flowing mantle than in the dry regions. The mantle wedge beneath volcanic arcs is probably a good example of such a wet region. The mantle deforms by the corner flow and water is released from the nominally hydrous minerals in the subducted oceanic crust beneath. Spatial variations of degree of anisotropy in this environment can therefore be at least partially due to spatial variations in water content.

h. *Electrical conductivity of garnets: The effect of Fe-Mg substitution in the system pyrope ($Mg_3Al_2Si_3O_8$) – almandine ($Fe_3Al_2Si_3O_8$) (B.T. Poe, C. Romano and N. Kreidie/Rome, in collaboration with C.A. McCammon)*

Previous experimental work has indicated that using experimentally determined electrical conductivities (ECs) of mantle minerals, there is good agreement between a laboratory derived EC profile and the most recent geophysical EC profiles of the mantle. Since the laboratory model takes into account only the two most abundant minerals at any depth, this good agreement suggests that the minor mineral constituents of the mantle have little effect on bulk electrical conductivity. The level of agreement between laboratory and geophysical profiles is poorest at transition zone depths, hinting that the influence of potential hydrous phases might be important. In addition, it has been demonstrated that if the two major components for any given depth have significantly different conductivities, then the bulk conductivity becomes very dependent on the mixing model used (*e.g.* Hashin-Shtrikman bounds, Effective Medium, etc.). Obviously, the two components can differ in their conductivities if their compositions are different, stressing the importance of well constrained partition coefficients at deep mantle conditions. Particularly important in this respect is the effect of iron on mineral conductivities.

We show in this study how electrical conductivity increases as a function of increasing iron substitution along the garnet solid solution between pyrope ($Mg_3Al_2Si_3O_8$) and almandine ($Fe_3Al_2Si_3O_8$). Samples were first synthesized at 10 GPa at temperatures ranging from 1650 to 1800 °C, then recovered for subsequent *in situ* electrical measurements. Complex impedance spectroscopy was carried out at 10 GPa and also at 19 GPa for selected compositions to determine electrical conductivity. Mössbauer spectroscopy was also performed on samples both before and after the electrical measurements in order to evaluate $Fe^{3+}/\Sigma Fe$. Our results indicate that the electrical conductivity is very sensitive to composition along this join, spanning several orders of magnitude at any particular temperature (Fig. 3.1-12). It appears that this strong variation is controlled more by the total iron content of the garnet rather than the ferric to ferrous ratio, as Mössbauer analyses show very little and a nonsystematic variation in $Fe^{3+}/\Sigma Fe$ across the entire join. Since we employed a solid-state buffer consisting of $Mo+MoO_2$ in both the syntheses and electrical measurements, the oxygen fugacity was kept close to that of the iron-wüstite buffer. Finally, we observe that the activation energy for electrical conduction increases smoothly as a function of increasing magnesium content along this join, in a manner similar to that found for pyroxenes in the system ferrosilite-enstatite. However, the endmember pyrope shows an activation energy of about 2.6 eV, much higher in comparison to the 1.6 eV activation energy for enstatite. As pressure is increased to 19 GPa, we observe a significant decrease in the activation energy. These findings demonstrate the strong sensitivity of electrical properties to changes in composition in silicate minerals, even among solid solutions as shown here. The composition, temperature and pressure correlations to conductivity determined for these garnets, particularly at pyrope-rich compositions, provide new constraints on the bulk conductivity of the mantle.

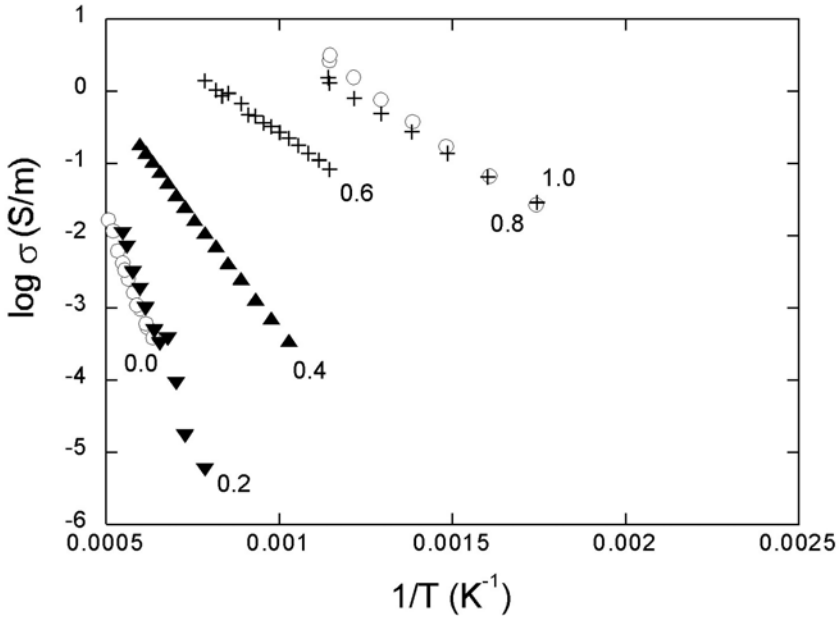

Fig. 3.1-12: Electrical conductivities of garnets in the system pyrope-almandine, determined *in situ* at 10 GPa using complex impedance spectroscopy in the multianvil apparatus. Numbers accompanying the data refer to Fe/(Fe+Mg).

i. *Temperature and mineralogy of subducting slabs: The effects of variable thermal conductivity (F.C. Marton and D.C. Rubie, in collaboration with T.J. Shankland/Los Alamos)*

The temperature and hence mineralogy of slabs of subducting lithosphere are, in part, functions of the thermodynamics, kinetics, and heat transport properties of the polymorphs of $(Mg,Fe)_2SiO_4$. Whereas experimental data on the first two factors have been available for some time, accurate experimental data on heat transport properties, have, until recently, been lacking. Subduction zone models have generally used constant values of thermal conductivity (k) of the lithosphere, along with constant values of isobaric heat capacity (C_P) and density (ρ), in solving the heat flow equation. Recent high P and T measurements of the thermal diffusivities (κ) of San Carlos olivine and its high-pressure polymorphs allow us to use more realistic lattice ks ($k = \kappa \rho C_P$) in our thermo-kinetic subduction models.

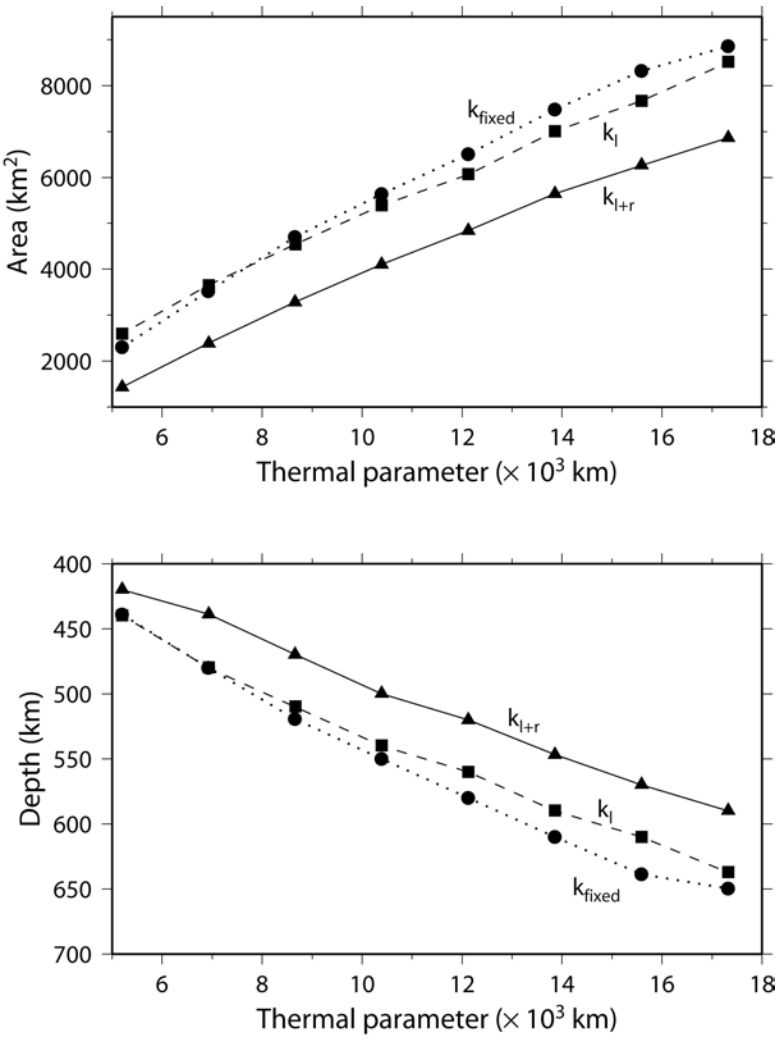

Fig. 3.1-13: Cross-sectional areas (top) and maximum depths (bottom) of metastable wedges of olivine in subducting slabs with φ = 5200-17000; dip angle 60°, age 100 My, velocity 6-20 cm/yr). Dotted lines: k_{fixed}; dashed lines: variable lattice k only; solid lines: variable lattice plus radiative transfer k.

Results on a variety of slabs with thermal parameters (φ = vertical subduction rate × age of lithosphere at the trench) varying from 3500-17000 km show that variable k, along with C_Ps and ρs that are also functions of P, T, and mineralogy (X), warms the slabs considerably, reducing the sizes of metastable olivine wedges by 20-30 % when radiative transfer (k_{rad}) is also included and the maximum depths of the wedges are 20-70 km shallower (Fig. 3.1-13). The metastable wedges are within 10 % in size compared with model slabs run with constant k when only the lattice ks are used. This is important for testing the hypothesis that deep earthquakes are caused by shear instabilities resulting from the transformations of metastable olivine. Olivine must extend to at least the depths of the deepest earthquakes if this mechanism is responsible for them. Thermal erosion of the metastable wedges in our models indicates that the olivine should be completely transformed before it reaches the regions of deepest seismicity, suggesting that other mechanisms should be considered for deep earthquakes.

j. *Effects of the phase transformation on the stress state of deep subducted slabs (J.-Y. Ning, F.C. Marton and D.C. Rubie)*

The presence of metastable olivine in descending slabs and its transformation to high-pressure phases at greater depths than in the average mantle may be responsible for deep seismicity in subduction zones. However, recent laboratory data, as well as precise computations on the phase-transformation kinetics of olivine to its high-pressure polymorphs, suggest less metastability in subducting slabs and significantly smaller wedges of metastable olivine than previously proposed. Mechanisms of transformational faulting therefore have difficulty in explaining the deep seismicity of subducting slabs. We thus need to find other possible mechanisms for explaining the deep seismicity, on which numerical simulations of the stress distributions could shed some light.

Elastic and viscoelastic linear numerical simulations show that the stresses produced by volume changes in the phase transformations from olivine to its polymorphs dominate the stress field. However, these stresses cannot serve as a direct explanation for the deep seismicity in the transition zone, since the main directions of the stresses are not consistent with the observed fault plane solutions. Also, linear numerical simulations exclude the influence of stress on the rheology, and deviate from the real stress states.

We compiled a 2-D viscoelastic model including material non-linearity to study the stress states of four classical subduction zones that already have results of thermal structures and dynamic phase boundaries, examining the roles of phase transformations. The computed stresses will be the results of thermal expansion, gravity, volume changes produced by phase transformations and the drag on boundaries. The model includes the volume changes from olivine to wadsleyite or ringwoodite as well as ringwoodite to perovskite plus magnesiowüstite and the influence of stress on rheology through iterative computation.

The constitutive relation is:

$$\sigma_{ij} = A^{-1}\varepsilon_{ij} + (K - \frac{A^{-1}}{3})\theta\delta_{ij} - K[\alpha_V \Delta T + (\frac{\Delta V}{V})^{ph}]\delta_{ij} A^{-1}B\sigma_{ij}^{(0)} - A^{-1}B\sigma_0^{(0)}\delta_{ij} - A^{-1}\varepsilon_{ij}^{(0)} + \frac{A^{-1}}{3}\theta^{(0)}\delta_{ij}$$

where $A=1/(2G)+\Delta t/(4\eta)$, $B=1/(2G)-\Delta t/(4\eta)$, σ_{ij} is stress, ε_{ij} is strain, K is the bulk modulus, θ is volume strain, α_V is thermal expansion coefficient, ΔT is temperature variation, $\Delta V/V$ is relative variation of volume; η is the viscosity, G the shear modulus, and δ_{ij} is the Kronecker delta. The density, thermal expansion coefficient, and bulk modulus are computed from the molar volume of olivine and its polymorphs as functions of temperature *T* and pressure *P*.

These new computations will show the relative importance of thermal expansion, gravity, and volume changes produced by phase transformations and the drag on boundaries in the stress state of a deep subducted slab. In addition, we will compare different stress features in the transition zone and the top of the lower mantle. Finally, we will compare the different stress states of some typical subduction zones. We will use these results to examine the relationship between the stress states of deep subducted slabs and deep seismicity in the transition zone and to examine the roles of phase transformations on deep seismicity.

k. *Effects of latent heat and kinetics of phase transformations on the topography of phase boundaries and dynamic surface topography (B. Steinberger, D.C. Rubie and F.C. Marton)*

Seismic velocity anomalies seen in mantle tomographic models are frequently assumed to be of thermal origin. Under this assumption they can be converted to temperature anomalies and hence be used to predict equilibrium phase boundary topography. However, the prediction correlates rather poorly with seismologically observed phase boundary topography. Furthermore, mantle flow models based on the thermal density anomalies inferred from seismic tomography can be used to predict dynamic surface topography. This prediction depends on a variety of further assumptions, such as viscosity structure. However, regardless of these assumptions, there is no good global agreement with "observed" dynamic surface topography (*i.e.*, observed topography, minus effect of crustal isostasy, minus thermal effect of ocean floor cooling). Thus, further effects need to be considered in order to better understand surface and phase boundary topography.

Here we study how the effects of latent heat of transformation and kinetics change the predictions of phase boundary and dynamic surface topography. The model will also include the latent heat effects, which are expected to play a role at both the 410 and 660 km discontinuities. Implementing this approach in global flow models requires an iterative procedure. For the effects of kinetics, which are expected to be important at the 410 km discontinuity, we will devise a model based on the solutions to the finite diffusion-controlled

two-phase moving-interface problem, which takes into account material transport as well as thermal diffusion and latent heat effects, and use new experimental data on the $(Mg,Fe)_2SiO_4$ system. The combination of these with mantle temperature and flow models will then allow us to derive a model of the phase boundary deflection and its deviation from equilibrium. In particular, it will be tested whether the advection of phase boundaries due to latent heat and kinetic effects significantly reduces the amplitude of predicted dynamic surface topography and whether this improves agreement with observations.

l. *Ultrahigh-temperature deformation textures in the contact aureole of the Chilka Lake anorthosite, India (C. Dobmeier/Berlin, in collaboration with F. Heidelbach)*

The effects of high temperature metamorphism on the fabrics of a sillimanite gneiss were studied with the SEM-EBSD (electron backscattering diffraction) system. In complex multiphase rocks this method is the only possibility to separate the microstructures and textures of the different phases, since it has no symmetry restrictions (such as U-stage microscopy) and allows for parallel observation of the sample (as opposed to X-ray or neutron goniometry). We analyzed the garnet and quartz textures in a sillimanite – garnet – spinel (hercynitic) – quartz gneiss, situated at the immediate contact of the Chilka Lake anorthosite, India.

Fig. 3.1-14: Three-dimensional view of the studied sillimanite – garnet – spinel (hercynitic) – quartz gneiss. Sample height is 12 cm.

The ultrahigh temperatures of anorthositic plutons at the time of emplacement are reflected in the paragenesis quartz + spinel, which indicates temperatures above c. 900 °C. The studied sample provides the rare possibility to determine the temperature at which the observed glide

system in garnet was active as garnet is part of a mineral assemblage (grt + sil + qtz + spl) suitable for geothermobarometry. The minerals form tightly to isoclinally folded near-monomineralic layers (Fig. 3.1-14). Quartz in fold limbs is strongly recrystallized and the c-axes form a strong maximum close to the projection point of the lineation, indicative of prism <c> slip at high temperatures and non-coaxial progressive deformation. Noteably, prism <c> slip is active in a fluid-absent regime. The a-axes show a great circle distribution normal to the c-axis maximum.

Garnets within the quartz layers form flat discs elongated parallel to the stretching lineation/ fold axis, but do not show subdomains in orientation contrast images. However, the lattice-preferred orientation (LPO) clearly indicates plastic deformation. The presence of six maxima for {111}, arranged on two small circle girdles, and {100} maxima near X and Y (Fig. 3.1-15) suggest dominant <100> [010] slip. However, in comparison to "easy slip" patterns, all maxima are rotated by c. 20°. Although the orientation of sillimanite c-axes shows that the thin section orientation is not exactly perpendicular to the fold axis and parallel to the fold axial plane, this imprecision cannot be held responsible for the considerable obliquity of the garnet texture. Most likely, the observed LPO pattern formed during folding of the rock.

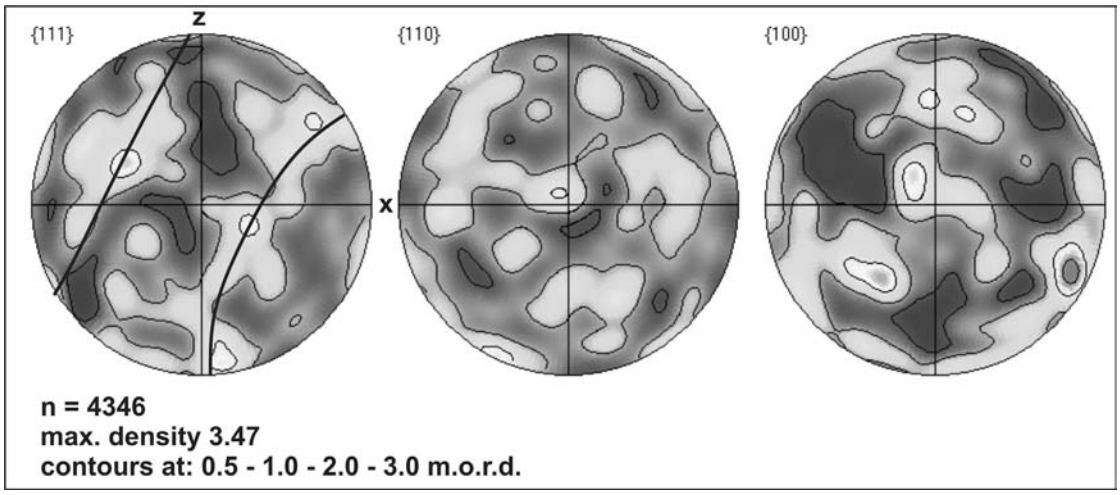

Fig. 3.1-15: Preferred orientation of garnet in sillimanite – garnet – spinel (hercynitic) – quartz gneiss, shown in XZ-sections, Schmidt net, lower hemisphere.

m. *Orientation of exsolution rods in antiperthite from a shear zone within the Bolangir anorthosite, India (C. Dobmeier/Berlin, in collaboration with F. Heidelbach)*

The exsolution texture of antiperthite grains with approximate bulk composition $An_{33}Or_{20}$ from a mylonite situated within meta-leuconoritic rocks of the Bolangir anorthosite complex, India, was studied by electron backscattering diffraction (EBSD). The overall aim of the project is the investigation of possible mechanisms for the formation of shear zones in the

lower crust. Interlocking of exsolution structures in ternary feldspar and dynamic recrystallization may ultimately create fine grained mineral aggregates of alkali feldspar and plagioclase which lead to strain localization in the lower crust. Previous determinations of the orientation of alkali feldspar epipedes by optical methods were incriminated with severe restrictions as the elaborate analytical procedure involves the observability of the (010) twin axis and the (001) cleavage plane, and requires mineral chemical data as the lattice orientation has to be determined indirectly by extrapolation of the measured optical indicatrix axes, which depend on mineral composition in triclinic feldspars.

The analysed antiperthite grains occur as mantled porhyroclasts embedded in a fine grained matrix of alkali feldspar, plagioclase, quartz and biotite (Fig. 3.1-16). The presence of biotite, which probably results from decomposition of pyroxenes, attests to hydrous conditions during deformation. Two-feldspar thermometry suggests that the exsolution process stopped at temperatures of ca. 620 °C. The rod-shaped alkali feldspar epipedes are evenly distributed and show a strong shape-preferred orientation with the long axes oriented subparallel to {010} of the host andesine (Fig. 3.1-16).

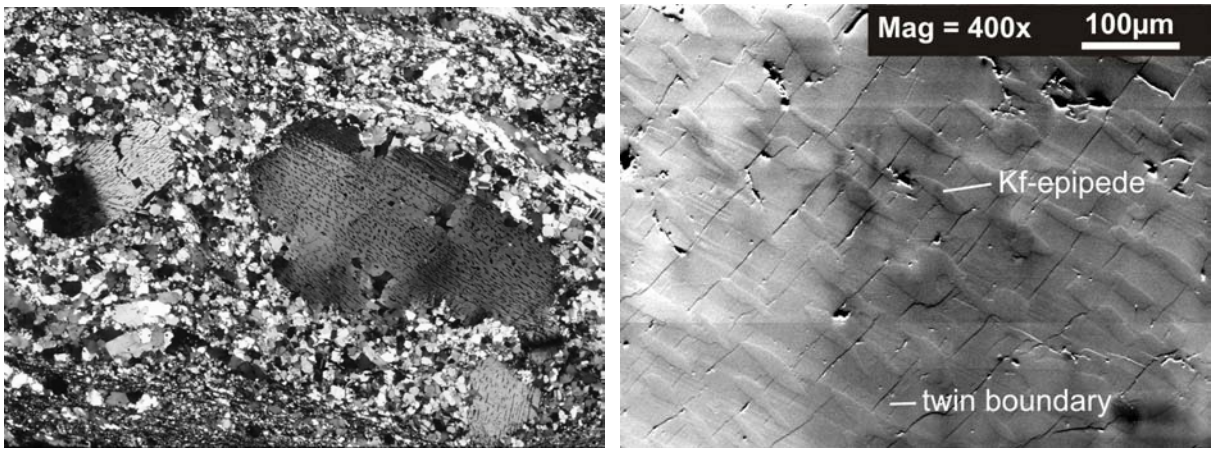

Fig. 3.1-16: Optical micrograph of antiperthite grain (left), and SEM orientation contrast image of exsolution lamellae in antiperthite grain (right).

The EBSD analyses establish, that a small but consistent misorientation of ca. 2° exists between {010} and <010> of the host andesine and the alkali feldspar epipedes, whereas <100> and <001> are strictly parallel. Obviously, the orientation of the epipedes is controlled by (010) of the host plagioclase, which is also the albite-twin boundary. However, the occurrence of rods is not restricted to twin boundaries and a causative relation between twinning and exsolution, or vice versa, is not evident. The presence of subgrains in some epipedes implies that exsolution took place during deformation. This is supported by the observation that the fine grained mantles of the clasts, which consist of two feldpars, form by progressive misorientation of subgrains.

n. *Micrometer- and nanometer-scale mineral chemistry of hemo-ilmenite in relation to magnetism (S.A. McEnroe and P. Robinson/Trondheim, in collaboration with F. Langenhorst and G.D. Bromiley)*

The source of the strong and stable magnetic remanence of members of the ilmenite-hematite series has been investigated for several years. Through this research has come the concept of "lamellar magnetism", in which a special ferrimagnetism is developed at the coherent interfaces of fine 001 exsolution lamellae of hematite in an ilmenite host (hemo-ilmenite) or of ilmenite in a hematite host (ilmeno-hematite). To gain a more thorough understanding of magnetic properties, special advantage was taken of unusual rocks containing nearly 100 % hemo-ilmenite and known to contain hematite exsolution lamellae ranging in thicknesses from 2-3 micrometers down to 1-2 nanometers. In lamellar magnetism, magnetization is acquired at the moment that new exsolution lamellae are formed, either antiferromagnetic hematite in an ilmenite host or ilmenite in an antiferromagnetic hematite host. The actual details of exsolution are governed by the ilmenite-hematite phase diagram and the phase compositions produced, either stable or metastable, and this was the reason for this research.

The hemo-ilmenite sample selected for detailed study has a bulk composition about 84 % ilmenite (Ilm 84). TEM-EDS analyses of ilmenite hosts (Ilm 98) containing fine hematite lamellae down to 1-2 nm thick, also hematite hosts in coarse lamellae (Ilm 15-13) containing fine lamellae of ilmenite (Fig. 3.1-17) yielded compositions of 97.9 and 14.4 % ilmenite respectively (see table below). These compositions were produced under temperature conditions where the hematite had antiferromagnetic ordering.

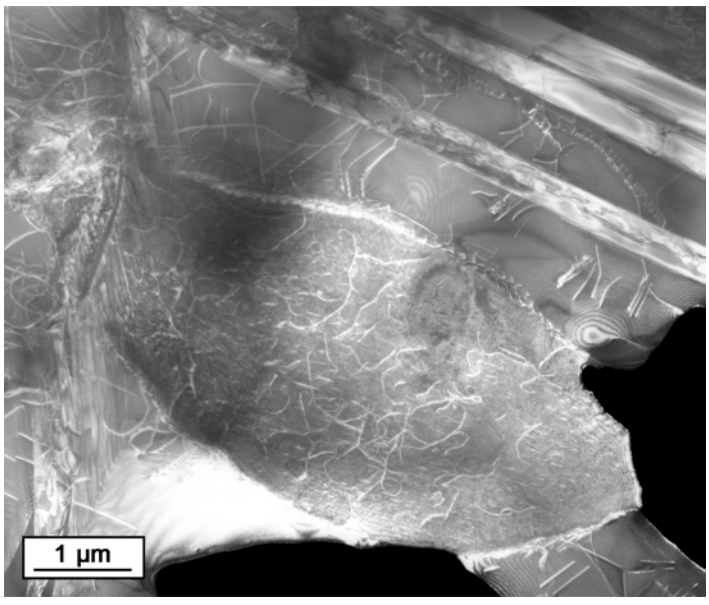

Fig. 3.1-17: Dark-field TEM image of the Frøytlog hemo-ilmenite sample heated at 580 °C. The image shows lens-shaped hematite exsolution in an ilmenite host. Due to deformation in the piston cylinder experiment, both hematite and ilmenite are pervaded by numerous dislocations. Additionally, ilmenite developed deformation twins.

All available phase diagrams suggest that substantial resorption of fine exsolution lamellae should take place above 520 °C. To test this and to acquire information on behaviour of such

materials in the deep crust, small fragments of the Frøytlog hemo-ilmenite were run at 580 °C, 10 kbar for a period of 10 days. To prevent damage to the sample by oxidation/reduction, mineral grains were encased in a powdered sample of the same rock against an enclosing graphite pressure vessel and quenched from high temperature. In reflected light there was evidence of reduction of ilmenite to magnetite by a graphite reaction in the outer parts of the runs, but this appeared not to have penetrated into inside fragments that were prepared for TEM observation and analyses.

Abundant fine exsolution lamellae were well preserved after the heating. However, there was a subtle change of texture in which abundant twinning had developed in place of the coherent strain shadows around lamellae in the original material, presumably as a result of thermal strain. As in the original material, a series of TEM-EDS analyses (see table above) was possible within the host regions of fine lamellae, but again analyses of the fine lamellae themselves was not possible. In regions of hematite host there seemed to be no changes, indicating there had been no resorption of ilmenite lamellae during the run (Ilm 14.4). By contrast, in regions of ilmenite host, two kinds of changes were recorded. In some regions the ilmenite has a higher hematite content (Ilm 95.9), indicating there was some resorption of hematite lamellae. In addition there is a notably lower geikielite component consistent with ion exchange with hematite lamella at a temperature higher than the original exsolution. In other regions, the ilmenite has a lower hematite content (Ilm 98.8), which we suspect is caused by local reduction by a graphite reaction near the edge of the sample to produce minor magnetite.

	Before Heating		**After Heating**	
			Resorption	No Resorption
	Ilm 97.9	Ilm 14.4	Ilm 95.9	Ilm 14.4
$MgTiO_3$	19.6	1.6	18.9	1.5
$FeTiO_3$	77.6	12.4	76.3	12.9
$MnTiO_3$	0.7	0.1	0.7	0
Fe_2O_3	1.3	83.8	3.9	84.3

The heating experiments suggest that fine-exsolution lamellae, once formed, are not easily resorbed into the host, particularly where the host is hematite. Rock-magnetic results, rather than showing a sharp decrease in remanence, that might be expected with resorption of lamellae, show a strong increase. Thus we have two grounds for believing this increase is inherent in the rhombohedral oxide itself. A tentative explanation is that during resorption of hematite lamellae in an ilmenite host, which is indicated by the analyses, the bulk composition of some of the finest hematite has been changed to a composition close to Ilm 45 which would lie on the hematite-rich *R3c* limb of the *R3c*-*R3* two-phase field at about 580 °C. Upon rapid cooling to about 550 °C, this composition could undergo rapid but metastable chemical ordering to an *R3* phase, and that, in turn, would pass through a metastable Curie temperature at about 290 °C to produce thin blades of a metastable strongly ferrimagnetic

titano-hematite. These heating results, still needing much further exploration, provide an unusual insight into magnetic and chemical processes in minerals, even though the quench conditions of the experiments may deviate substantially from conditions in nature.

o. *Magnetic remanence, oxide-silicate mineralogy, and lattice-preferred orientation in ilmenite norite of the Heskestad anomaly, Bjerkreim-Sokndal layered intrusion, Rogaland, Norway (S.A. McEnroe and P. Robinson/Trondheim, in collaboration with F. Langenhorst and F. Heidelbach)*

Layered ilmenite-magnetite norite of Megacyclic Unit IV of the Mid-Proterozoic Bjerkreim-Sokndal Layered Intrusion at Heskestad is the location of a very large negative magnetic anomaly controlled by remanent magnetism. Locally, reversed NRMs reduce magnetic measurements of the present normal Earth field at 50,000 nT down to 20,000 nT. By contrast adjacent layers of the intrusion and much of the country rock yield weak positive anomalies related to induced magnetization controlled by a small amount of magnetite. The Heskestad norites contain only a few percent of oxide minerals, unlike cumulates very rich in hemo-ilmenite elsewhere in the district, yet they have a much stronger remanence.

The oxides consist of multidomain near end-member magnetite that contributes only a small normal induced component of magnetization, and finely exsolved hemo-ilmenite that may contribute an important component of reversed remanent magnetization, particularly if it contains the newly discovered “lamellar magnetism” and has a strong lattice preferred orientation parallel to the magnetizing field at the time of mid-Proterozoic fine-scale exsolution. In addition, there is fine oxide exsolution in the pyroxenes. The orthopyroxenes contain plates and rods parallel to 100 of the pyroxene host. The plates are elongated along the b and c crystallographic axes of the host whereas the rods are elongated along the c-axis. In reflected light the plates and rods appear to consist mainly of ilmenite with very fine exsolution lamellae of hematite. Some of the plates are thin enough to be observed in transmitted light, and appear to consist of reddish brown ilmenite with scattered orange-red elongate blebs that are probably hematite. The much less abundant calcic pyroxenes contain blades and rods of ilmenite, but they also contain a few blades of magnetite.

TEM observations and EDS analyses were carried out on oxides and pyroxenes, to gain a better understanding of composition relations and relative orientations of crystallographic axes that could influence magnetic properties. The hematite lamellae in the ilmenite inside the orthopyroxene are too fine-grained to obtain meaningful analyses, though that in no way precludes their participation in lamellar magnetism. Lattice imaging demonstrated conclusively that the ilmenite shares its 001 plane with 100 of the pyroxene host, and further that the <a> direction of the ilmenite is parallel to <c> direction of the pyroxene (Fig. 3.1-18). Comparison of the lattice dimensions of ilmenite <a> and orthopyroxene <c> indicate that coherent ilmenite plates should be severely elongated along <a> and this could have some

influence on magnetic properties, particularly if there is a bulk lattice preferred orientation of the pyroxene.

Through measurements of the crystallographic orientation with EBSD in several samples, it was demonstrated that these norites contain a very strong lattice preferred orientation of pyroxenes with the {100} planes parallel to the dominant foliation and the <c> axes parallel to a dominant lineation. It appears that this preferred orientation was induced during solid state movements along the layering after igneous crystallization, but probably well above the temperature of oxide and silicate exsolution. Furthermore {100} and <c> are within a few degrees of being parallel to the postulated mid-Proterozoic magnetizing field, an ideal orientation for maximal strength “lamellar magnetism”, provided the ilmenites contained in the pyroxenes are sufficiently exsolved. There is also a lattice-preferred orientation of ilmenite in the matrix, though probably considerably weaker than in the orthopyroxene.

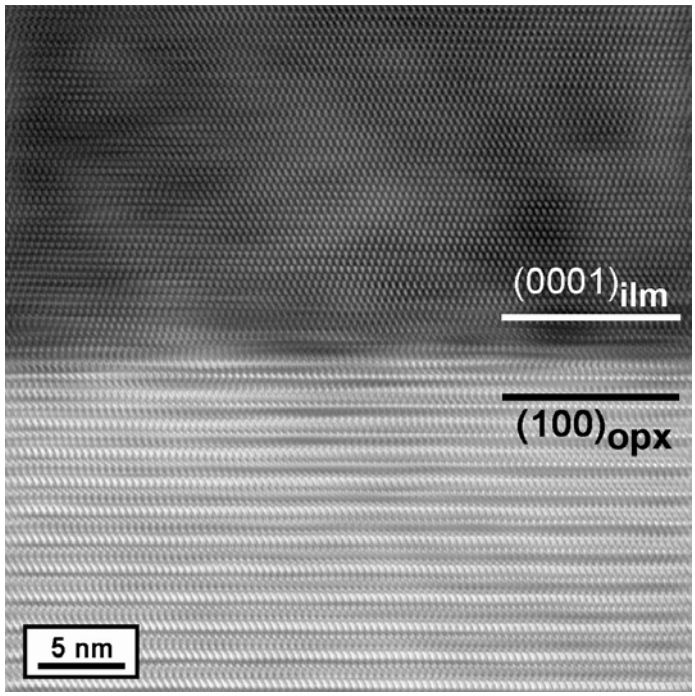

Fig. 3.1-18. High-resolution TEM image of an ilmenite-orthopyroxene interface in the Heskestad norite. The image reveals the following epitaxial relationship between phases: (0001)ilm // (100)opx.

One of the challenges of the Heskestad rocks is that the magnetism appears to be contained within a diverse mineralogy which is not particularly coarse-grained, and it is not easy to isolate the various effects and properties of the different minerals using bulk magnetic experiments. It thus stands out in contrast to the massive hemo-ilmenite at Frøytlog previously studied. By attacking the problem using a combination of approaches, we hope eventually to gain an exact explanation for this anomaly based on sound mineralogical and magnetic principles.

p. *The colouring and constitution of New Zealand jade (C.A. McCammon, in collaboration with C.J. Wilkins†, W.C. Tennant and B.E. Williamson/Christchurch)*

† *deceased*

Nephrite jade, as distinct from jadeite jade, has a long and ancient history, with artefacts dating back to Neolithic times. Nephrite occurrences are widespread around the world, usually associated with ultramafic exposures close to tectonic boundaries, although the lenses are characteristically localised and small. The properties of nephrite arise from its felted mass of microscopic randomly oriented fibres of tremolite-actinolite, where colours extend through shades of green to black or white, and occasionally pink or lavender. Over the last approximately 30 years there has been much work on the formation and properties of nephrite (especially of Siberian, Chinese and Canadian origin) but none on the New Zealand mineral, despite its rich colouring and often attractive flecking. In this study we investigated a range of New Zealand jades, with a particular focus on their colouring and formation. A suite of New Zealand jade samples chosen to represent a range of colour variations were characterised using optical microscopy, the electron microprobe, and infrared, optical absorption and Mössbauer spectroscopies.

Chemical analysis showed that the gem quality nephrites fell within a narrow range of composition close to the tremolite-actinolite join, and that colour variations cannot be accounted for by variations in minor element (Cr, Mn, Fe and Ni) concentrations only. Infrared spectroscopy confirmed their nephritic constitution, although did not provide reliable evidence for hydroxylation due to weathering. Absorption bands observed in optical absorption spectra gave information regarding the origin of different colours, such as due to Fe^{2+}-Fe^{3+} intervalence charge transfer, while Mössbauer spectroscopy provided evidence for oxidative weathering, as well as identification of the black flecks (see Fig. 3.1-19).

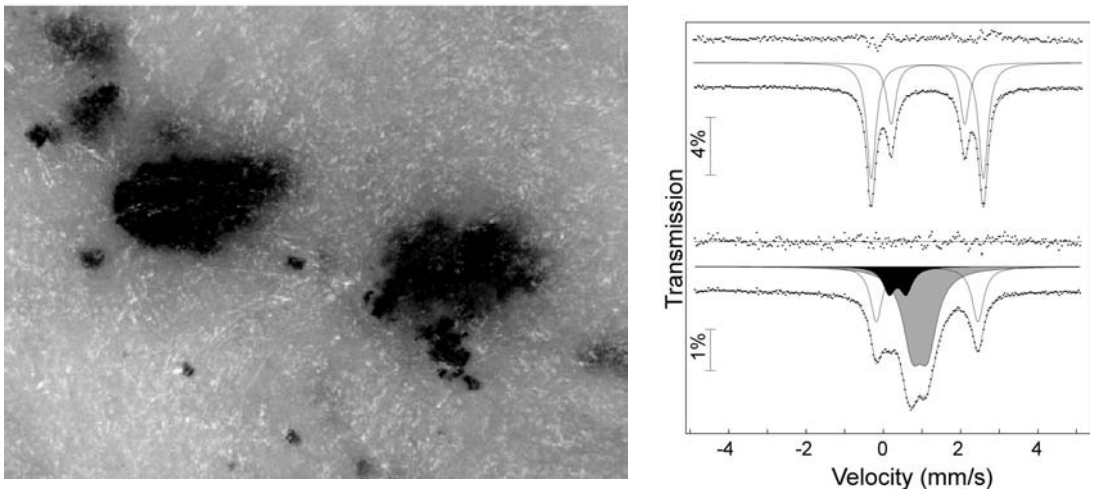

Fig. 3.1-19: (left) Optical photomicrograph of a New Zealand jade showing typical black flecks (field of view ca. 4 mm); (right) Mössbauer spectrum of a reference jade nephrite (top) and a black fleck in the same jade (bottom), demonstrating that the black spots are due to chromite. Peaks are assigned as follows: amphibole Fe^{2+} (unshaded); spinel Fe^{2+} (grey) and Fe^{3+} (black).

We suggest that the black-spotted nephrite, arising from finely-dispersed chromite or magnetite, occurs when redox conditions stabilise Fe^{3+} to an extent that charge-balance considerations inhibit its accommodation in the amphibole lattice. Changing conditions could promote the agglomeration of these particles towards the formation of black spots or the attractively flecked and slightly darkened bands within the highest gem-quality New Zealand nephrites, implying that these distinctive features could arise from climatic and environmental factors within the region.

3.2 Mineralogy, Crystal Chemistry and Phase Transformations

Mineralogy is a vital part of geosciences, since its primary goal is to determine the physical and chemical properties of materials that underlie and control the structural and thermal state, processes and evolution of the Earth. As a result of the continuous developments in high-pressure and high-temperature techniques, the domain of mineralogy is now no less than the whole Earth, from the crust to the inner core. The effort in understanding and quantifying the mineral properties as a function of temperature, pressure, cation substitution and ordering has also given to the word "mineralogy" an extended meaning as a part of an interdisciplinary area which comprises crystallography, solid-state physics and chemistry and material sciences.

It is not surprising, therefore, that the studies outlined in this section cover a broad range of materials and properties.

The nature of iron (in terms of charge, minor substitution or major compound) plays an important role in determining the properties of mantle minerals or of the metal core. For this reason there are a number of ongoing projects dealing with this element, from its substitution as a trivalent cation in major mantle phases, such as majorite garnet or perovskite, to the high-pressure high-temperature transformations of its alloys important for understanding the Earth's deep interior.

Most natural minerals are not pure phases, but show wide compositional variations due to atomic substitutions on different crystallographic sites. Such cation substitutions may have a great effect on the structure – property relations of such minerals. For example a "dolomite-type" structure resulting from ordering of Mg and Cd in the carbonate layers is stable at intermediate compositions between $MgCO_3$ and $CdCO_3$. New different structures have been found at high pressure, depending on the concentration of K into the Na disilicate compounds. Critical temperature and pressure (*i.e.* temperature and pressure values at which phase transitions occur) are also affected by cation substitution as in the case of clinoenstatite which will transform to its high-pressure polymorph at much lower pressure when a small amount of Ca is introduced in its structure.

Other studies deal with the compressibility of materials. The unit-cell volume variation as a function of pressure can be determined at present with great accuracy by *in situ* high-pressure X-ray diffraction. Given the high pressures and temperatures of the Earth's interior it is important not only to know what are the stable phases at such conditions but also their response to changes of the external variables.

a. *Crystal chemistry of Fe^{3+} in Al-containing majorite and implications for the transition zone (C.A. McCammon, in collaboration with N.L. Ross/Blacksburg, USA)*

An ongoing project at Bayerisches Geoinstitut has been to characterise the nature of iron in transition zone and lower mantle phases, particularly with regard to the effect on physical and chemical properties. Garnet occurs in the upper mantle predominantly with composition $(Mg,Fe,Ca)_3Al_2Si_3O_{12}$, where silicon is exclusively in tetrahedral co-ordination. With increasing pressure, however, $(Mg,Ca,Fe)SiO_3$ pyroxenes become increasingly soluble in the garnet phase, introducing the majorite component $(Mg,Fe)_3(Mg,Fe,Si)_2Si_3O_{12}$. In a previous study at Bayerisches Geoinstitut, we studied the crystal chemistry of $(Mg,Fe)SiO_3$ majorite as a function of iron concentration and redox conditions using a variety of spectroscopic techniques (BGI Annual Report 1998). Results showed that the amount of Fe^{3+} increases with increasing iron concentration and oxygen fugacity, reaching a maximum of ca. 22 % $Fe^{3+}/\Sigma Fe$ for $Mg_{0.85}Fe_{0.15}SiO_3$ majorite synthesised under oxidising conditions. Previous studies at Bayerisches Geoinstitut have shown that addition of Al to $(Mg,Fe)SiO_3$ perovskite stabilises Fe^{3+} due to the favourable energetics of coupled substitution, and since the garnet structure has many similarities to the perovskite structure, this raises the possibility that similar behaviour might occur in majorite.

We synthesised a sample of $(Mg,Fe)(Si,Al)O_3$ majorite using the multianvil press at the same conditions as previous $(Mg,Fe)SiO_3$ majorite experiments (19 GPa, 1900 °C, 30 min, Re capsule with ReO_2 added). X-ray diffraction data from the run product showed the sample to be cubic, and electron microprobe analysis yielded the composition $Mg_{0.84}Fe_{0.14}Si_{0.93}Al_{0.09}O_3$. From Mössbauer spectroscopy we determined the value for $Fe^{3+}/\Sigma Fe$ to be only 14 %, which is less than the amount determined for the Al-free sample. The addition of Al to $(Mg,Fe)SiO_3$ majorite does not stabilise Fe^{3+} in the garnet structure, therefore, in contrast to the behaviour of $(Mg,Fe)(Si,Al)O_3$ perovskite (Fig. 3.2-1). In $(Mg,Fe)(Si,Al)O_3$ majorite, both Al and Fe^{3+} compete for the same octahedral site, which likely inhibits the oxidation of Fe^{2+} to Fe^{3+}. Thus, the concentration of Fe^{3+} in $(Mg,Fe)(Si,Al)O_3$ majorite is dependent on oxygen fugacity and not crystal chemistry of the garnet structure, while the concentration of Fe^{3+} in $(Mg,Fe)(Si,Al)O_3$ perovskite is independent of oxygen fugacity, and is related to the favourable energetics of Fe^{3+} substitution in the presence of Al in the perovskite structure.

Current studies suggest that the oxygen fugacity in the bulk transition zone is relatively low, which would imply a relatively low concentration of Fe^{3+} in $(Mg,Fe)(Si,Al)O_3$ majorite within the transition zone. Combined with previous studies at Bayerisches Geoinstitut that show similar concentrations of Fe^{3+} in wadsleyite and ringwoodite, this would indicate that the bulk Fe^{3+} concentration in the transition zone is small. Since the value of $Fe^{3+}/\Sigma Fe$ determined for the upper mantle is also low, an isochemical bulk upper mantle and transition zone with respect to iron oxidation state would be consistent with the present results.

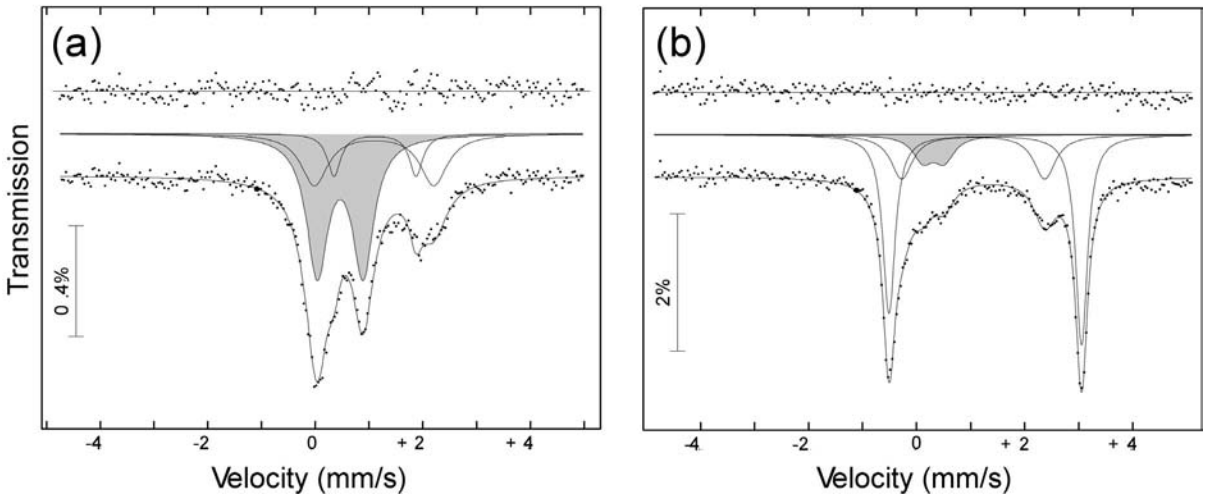

Fig. 3.2-1: Room temperature Mössbauer spectra of single-phase (a) $(Mg,Fe)(Si,Al)O_3$ perovskite; (b) $(Mg,Fe)(Si,Al)O_3$ majorite with similar composition (Mg# ~ 0.9 and ~ 3.5 wt.% Al_2O_3). The subspectra shaded grey are assigned to Fe^{3+}, and their relative areas indicate (to a first approximation) the relative abundance of Fe^{3+}. The presence of Al stabilises Fe^{3+} in the perovskite structure; whereas it destabilises Fe^{3+} in the garnet structure due to competition for the octahedral site.

There is a significant increase in the concentration of Fe^{3+} below the transition zone-lower mantle boundary, however. Even in the absence of Al, $(Mg,Fe)SiO_3$ perovskite contains approximately twice the concentration of Fe^{3+} than $(Mg,Fe)SiO_3$ majorite at comparable conditions. When $(Mg,Fe)(Si,Al)O_3$ majorite transforms to $(Mg,Fe)(Si,Al)O_3$ perovskite, thereby increasing the Al concentration in the perovskite phase, $Fe^{3+}/\Sigma Fe$ is predicted to reach approximately 50 %, based on a pyrolite bulk composition. This high concentration of Fe^{3+} is independent of oxygen fugacity, and has been observed even for samples synthesised in equilibrium with metallic Fe. If the lower mantle were relatively reduced, oxidation of Fe^{2+} to Fe^{3+} could occur through disproportionation ($Fe^{2+} \rightarrow Fe^{3+} + Fe^0$), as observed in experiments, or through interaction with volatiles. Another possibility is through subducted material, where oxygen fugacity may be higher. Based on the results of the present study, majorite within an oxidised subducted slab would incorporate more Fe^{3+} than the surrounding bulk mantle, and provide a mechanism for the transport of oxygen into the deep mantle.

b. *Incorporation of the trivalent cations Fe^{3+} and Al^{3+} into $CaSiO_3$-perovskite at transition zone conditions (U.W. Bläß, T. Boffa Ballaran, D.J. Frost, F. Langenhorst, C.A. McCammon and F. Seifert, in collaboration with P.A. van Aken/Darmstadt)*

Based on experimental studies it is widely accepted that $CaSiO_3$ - perovskite is the most important calcium-bearing constituent in the Earth's lower mantle and the lower parts of the Earth's transition zone. In peridotitic compositions $CaSiO_3$ - perovskite might reach an

abundance of up to 10 % and probably over 20 % in subducted slabs with MORB composition. Trivalent cations can be incorporated into the $CaSiO_3$-perovskite structure most likely by the defect mechanism, in which the replacement of $2Si^{4+}$ by $2R^{3+}$ is charge balanced by the creation of one oxygen vacancy. In the model system $CaTiO_3$-$CaFeO_{2.5}$ high vacancy concentrations lead to ordered oxygen deficient layers perpendicular to the pseudocubic <100> directions, whereas no ordering occurs at low vacancy concentrations. The example of $MgSiO_3$-perovskite has shown, however, that even a few percent oxygen vacancies could cause appreciable changes in physical properties such as elastic or transport properties, which possibly has significant implications for the interpretation of geophysical and geochemical data.

Experiments with different starting compositions on the join $CaSiO_3$-$CaFeO_{2.5}$ run in a multianvil press at several P - T conditions and a buffered oxygen fugacity of Re-ReO_2 have shown that the maximum exchange of silicon for trivalent iron in pure $CaSiO_3$-perovskite is limited to 4 % at 16 GPa. In analogy to the $CaTiO_3$-$CaFeO_{2.5}$ system we expect that at such low concentrations the incorporation of Fe^{3+} and oxygen vacancies occurs in a disordered fashion. This low iron phase is clearly separated by a large solvus from an ordered oxygen deficient perovskite phase with the composition $Ca(Fe_{0.4}Si_{0.6})O_{2.8}$, which is stable over a large P - T range, overlapping the conditions of the Earth's transition zone. However, experiments conducted at low oxygen fugacity in a molybdenum capsule cause the breakdown of this phase into FeO, Ca_2SiO_4 and $CaSiO_3$ (amorphised former perovskite structure). No further oxygen deficient perovskite phases were found on more iron-rich compositions, except the well known end-member $CaFeO_{2.5}$, which we observed to be stable at less than 5 Gpa, only. Due to the stability of the new $Ca(Fe_{0.4}Si_{0.6})O_{2.8}$ phase during quenching to ambient conditions, we could examine it in detail by optical microscopy, X-ray diffraction, Mössbauer spectroscopy, electron microprobe, transmission electron microscopy (TEM) and electron energy loss spectroscopy (EELS). For example the Si *K* edge ELNES spectra demonstrate the existence of octahedral and tetrahedral coordinated silicon (cf. Fig. 3.2-2), generated by the introduction of oxygen vacancies. All observations indicate that the structure can be characterised by oxygen deficient tetrahedral double layers perpendicular to the pseudocubic <111> directions, alternating with eight octahedral perovskite layers, which are one half each occupied by silicon and iron (cf. Annual Report 2001).

TEM observations on the $Ca(Fe_{0.4}Si_{0.6})O_{2.8}$ phase indicate similarities to the rhombohedral perovskite phase $Ca_2AlSiO_{5.5}$ reported by Fitz Gerald and Ringwood (Phys. Chem. Minerals 18, 40, 1991), except that we observed a ten layer superstructure instead of five layers and a slightly different stoichiometry. In order to explore the differences between these two phases, we performed experiments on the system $CaSiO_3$-$CaAlO_{2.5}$. Our results indicate the existence of a phase with a stoichiometry of $Ca(Al_{0.4}Si_{0.6})O_{2.8}$. The powder diffraction pattern as well as the electron diffraction images of this $Ca(Al_{0.4}Si_{0.6})O_{2.8}$ phase are quite similar to the iron-bearing phase, confirming similar structural properties. In addition, we have synthesised an oxygen-deficient perovskite with the stoichiometry of $Ca(Al_{0.5}Si_{0.5})O_{2.75}$, where the observed

lattice constants indicate the existence of an 8-fold superstructure. This might be similar to the phase with a 4-fold superstructure observed by Fitz Gerald and Ringwood during preliminary experiments. Further investigations will clarify the equilibrated phase assemblages in the system $CaSiO_3$-$CaAlO_{2.5}$.

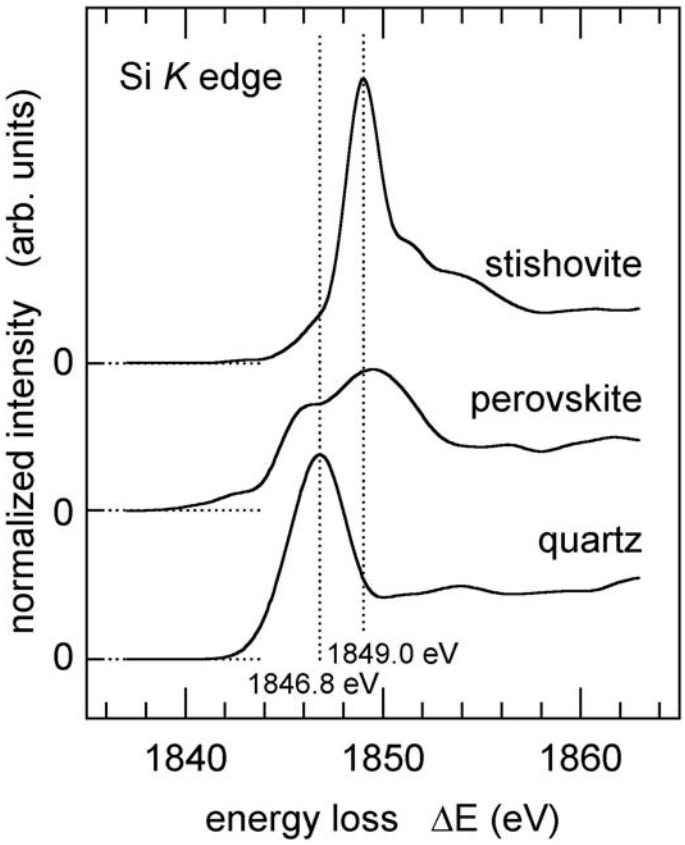

Fig. 3.2-2: Si *K* edge ELNES spectra of the $Ca(Fe_{0.4}Si_{0.6})O_{2.8}$ perovskite phase in comparison with octahedrally coordinated silicon in stishovite and tetrahedrally coordinated silicon in quartz.

c. *High-pressure structural phase transition in hematite (Fe_2O_3) (L.S. Dubrovinsky, in collaboration with G.K. Rozenberg/Tel Aviv and R. Ahuja/Uppsala)*

The majority of the trivalent transition metal oxides crystallize in the corundum-type structure. Due to the importance of these oxides in Earth sciences, technology and material sciences, extensive high-pressure (HP) studies have been carried out in recent years to elucidate their electronic, structural, and mechanical properties. The HP characteristics of α-Fe_2O_3 (hematite) were of particular interest due to its geophysical impact regarding the general role of ferric/ferrous oxides in the dynamics and composition of the Earth's lower mantle.

At ambient pressure the trigonal α-Fe_2O_3 (space group $R\bar{3}c$) is a wide-gap antiferromagnetic insulator and can be regarded as a typical *Mott*-insulator. Its equation of state has been studied up to 50 GPa, using synchrotron XRD, above which it undergoes a sluggish structural phase transition. However, comprehensive studies of the cell geometry variation with pressure was done only to ~ 10 GPa and results and conclusions were ambiguous. For a long time the structure and other properties of the HP Fe_2O_3 phase at P > 50 GPa, designated as HP2, was not clear. The first shock-wave experiments carried out in the late sixties gave sufficient evidence for the existence of a denser phase at P > 60 GPa. Later on, static compression experiments with diamond anvil cells (DACs) not only confirmed the existence of a new phase of Fe_2O_3 above ~ 50 GPa, but also of a considerable smaller volume. On the basis of the relatively poor X-ray data recorded from rotating anode sources, two possible structures of the HP2 have been proposed, namely, an *orthorhombic perovskite* which by its virtue must exhibit two different cation sites or a *distorted corundum* of the Rh_2O_3(II)-type, a single-cation-site structure. At the same time Mössbauer spectroscopy (MS) studies done at 300 K up to 70 GPa reported the onset of a non-magnetic component at ~ 50 GPa coexisting with a magnetic component characterized by a relatively smaller hyperfine field. It was concluded and since then accepted that the HP2 phase of Fe_2O_3 contained two iron sites with different charges ($Fe^{3+} \rightarrow Fe^{2+} + Fe^{4+}$), geometries, and coordination numbers coexisting in the same crystal structure. This compelled the authors to prefer the perovskite option for the HP2 phase with the ABO_3 formula in which *A* and *B* stand for the different iron charge states. The first-order decrease in volume was then qualitatively explained as due to increase in coordination number of the cation. Recent synchrotron XRD, MS, and electrical resistance studies to ~ 80 GPa by Pasternak *et al.* (Phys. Rev. Letters, 82, 4663, 1999) elucidated the nature of the metallic HP2 phase as consisting of a single nonmagnetic Fe^{3+} component. The explanation of this phenomenon was justified on the basis of the pressure-induced breakdown of the electronic d-d correlation (the *Mott* transition), which leads to metallic and nonmagnetic Fe^{3+} states. Thus, according to these data the distorted A_2O_3 corundum structure (Rh_2O_3(II)-type) is the only one accepted for the HP2 Fe_2O_3 polymorph. However, this assignment of the structure still should be tested by X-ray diffraction structural analysis.

Structural studies and full-profile refinement of hematite and its high-pressure polymorph were carried out to 76 GPa using X-ray synchrotron powder diffraction. It was found that pressure induces a progressive distortion of the corundum-like hematite structure (HP1) culminating into a structural phase transition (HP2) at ~ 50 GPa (Fig. 3.2-3). At first sight the powder diffraction data obtained for HP2 could be equally explained in terms of either an orthorhombic perovskite or a Rh_2O_3(II)-type structure and only the recent Mössbauer spectroscopy results, the comparative analysis of the O-O bond length for both structures, and *ab initio* calculations allowed for the definitive assignment of the HP2 phase to the latter structure. As a result of the phase transition the following changes occur: *i*) a substantial decrease in the Fe-O distances with a slight increase in Fe-Fe distances which lead to a reduced cell-volume, *ii*) a diminution of the Fe-O-Fe bond distortion, and, *iii*) a reduction of the distortion of the FeO_6 octahedron. The structural transition coincides with a previously

reported insulator-metal transition due to a *Mott* transition. It is suggested that the unusual volume reduction of 10 % is accounted for by the combined crystallographic *and* electronic (*Mott*) phase transition, the latter resulting in a substantial reduction in the ionic radii due to electron delocalisation.

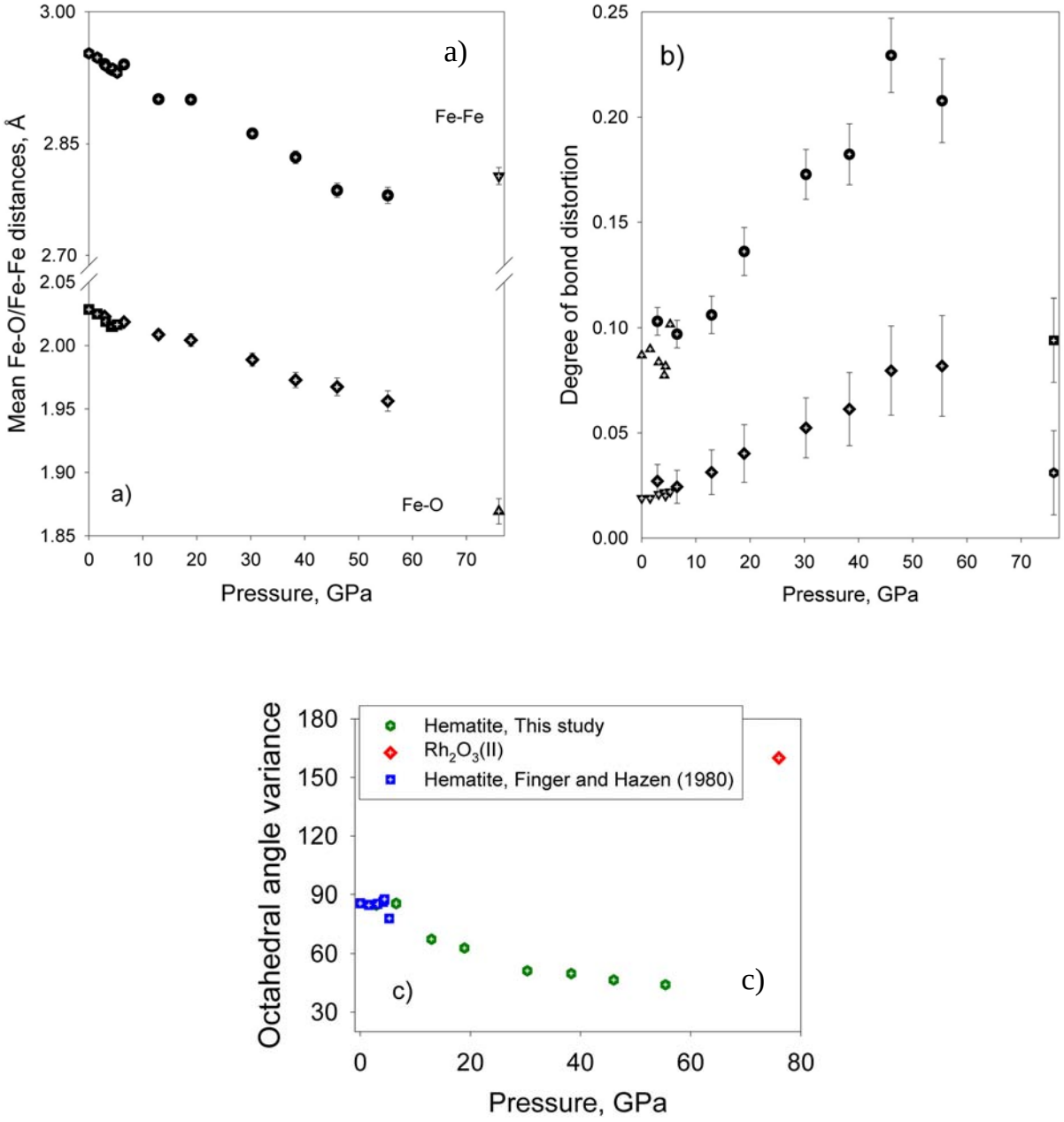

Fig. 3.2-3: Pressure dependencies of various structural features of HP1: (a) the mean Fe-O distances and the mean second-neighbour Fe-Fe distances; (b) the degree of distortion of FeO_6-octahedra (diamonds) and the degree of Fe-Fe bond distortion (circles); and (c) the octahedral angle variance.

d. *New high-pressure Fe-Si phases (D.P. Dobson, L.S. Dubrovinsky, N.A. Dubrovinskaia, F. Langenhorst and C.A. McCammon, in collaboration with L. Vocadlo and I.G. Wood/ London)*

Phases containing reduced iron and silicon are important for our understanding of the Earth's deep interior, and as semiconducting/magnetic materials with tuneable properties. Recent laser-heated diamond-cell experiments suggest that high-pressure iron silicide phases exsolve from dilute Fe-Si alloys under core *P-T* conditions (see Dubrovinsky *et al.*, section 3.3.b). In addition, FeSi takes on the CsCl (B2)-structure in epitaxial thin films on Si and Fe substrates with an estimated stabilisation pressure in excess of 15 GPa. We are performing a combined experimental and *ab initio* simulation study of this important class of potential high-pressure materials and have identified two new FeSi phases.

B2-FeSi was predicted to be the stable high-pressure form and subsequently synthesised in the bulk at 24 GPa and 1950 K. B2-FeSi is metallic, unlike the low-pressure ε-FeSi-structured phase which is a narrow band-gap semiconductor. High-resolution TEM observations of recovered samples suggest a defect-rich structure (Fig. 3.2-4). This is confirmed by electron probe analyses which show a small Si deficit. A silicon-deficient B2-structure is also stabilised over the FeSi-structure in RuSi at atmospheric pressure. Mössbauer spectra of B2-FeSi show a singlet, or narrow doublet with an isomer shift of 0.24 mms^{-1}. This is consistent with the calculated Mössbauer spectrum for defective B2-FeSi (M. Fanciulli et. al., Phys. Rev. B, 59, 3675-3687, 1999), but does not distinguish between Si-vacancies or Fe-substitutional defects. The *P-V* equation-of-state of B2-FeSi was measured to 40 GPa in collaboration with W. Crichton at the ESRF. Unlike ε-FeSi, the elastic properties of B2-FeSi are consistent with silicon being the major light element in the core. B2-FeSi has been identified in equilibrium studies at core-mantle-boundary pressures and temperatures.

We have synthesized a second new high-pressure phase, stoichiometric Fe_3Si_2, which is stable above 15 GPa. The properties of Fe_3Si_2 and the high-pressure Fe-Si phase diagram are the subject of current experimental and theoretical investigation.

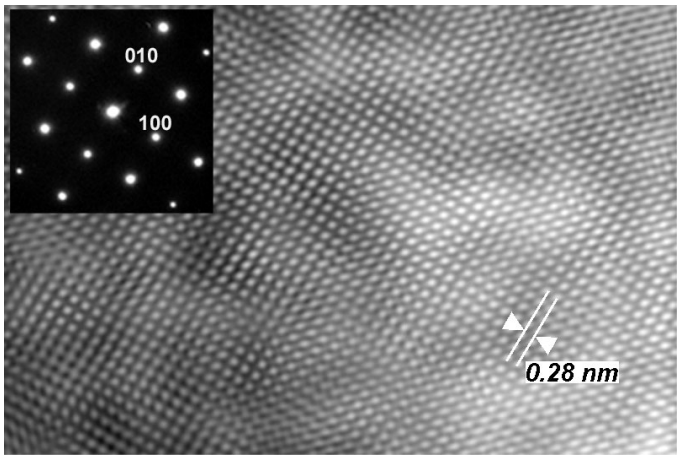

Figure 3.2-4: High-resolution TEM image and electron diffraction pattern of B2-FeSi. The mottled appearance of the HRTEM image may indicate lattice strain induced by point defects.

e. *Structure of iron-nickel alloys at conditions of Earth's core (L.S. Dubrovinsky, N.A. Dubrovinskaia, F. Langenhorst and F. Seifert)*

Cosmochemical data and studies of iron meteorites provide evidence that the Earth's core contains significant (5 to 15 %) amounts of nickel. While studies of pure iron at extreme conditions draw considerable attention, knowledge of the behaviour and properties of Fe-Ni alloys in the multimegabar pressure range and high temperatures are limited. Even relatively small amounts of additional components could significantly affect phase relations and thermophysical properties of iron alloys. Therefore, the understanding and interpretation of properties of the Earth's core (such as seismic anisotropy, fine-scale heterogeneity, super-rotation) requires detailed studies of the Fe-Ni system at high pressures and temperatures.

At ambient pressure iron-nickel alloys with up to 25 at.% of Ni have body-centred cubic (*bcc*) structure, while higher nickel contents promote crystallisation of the *fcc*-structured phase. Compression of *bcc*-structured alloys at ambient temperature results in the transformation to the *hcp*-phase at pressures between 7 and 14 GPa (depending on composition and conditions of experiments). No further transformations of $Fe_{0.8}Ni_{0.2}$ alloy were observed on compression up to 260 GPa. The density of $Fe_{0.8}Ni_{0.2}$ extrapolated to the Earth's centre pressure (360 GPa) is 14.35 g/cm^3 and close to the density of pure ε-Fe (14.08 g/cm^3). However, the nickel content significantly affects phase relations in the Fe-Ni system at high temperature. While the slope of the *hcp-fcc* phase boundary for pure iron is 35-40 K/GPa, there are indications that the phase boundaries of Fe-Ni alloys with 10 to 30 % Ni could have much lower slopes (15 to 25 K/GPa). Moreover, Huang *et al.* (J. Geophys. Res., 93, 7741-7745, 1988; J. Geophys. Res., 97, 4497-4502, 1992) and Lin *et al.* (Science, 295, 313-315, 2002) report the co-existence of *hcp*- and *fcc*-structured phases in rather wide pressure-temperature ranges (between 20 and 80 GPa and up to 2000 K). Taking into account the geophysical importance of the Fe-Ni system it is essential to investigate systematically how the nickel content could influence the *P-T-X* phase diagram.

Figure 3.2-5 shows X-ray diffraction patterns collected in an experiment on Fe-19%Ni alloy. On compression to ~ 9 GPa at ambient temperature initially *bcc*-structured alloy starts to transform into *hcp*-phase. However, at pressure above 11 GPa, even without heating, new reflections from the *fcc*-structured phase appear. Heating at just ~ 500 K significantly enhances the intensity of *fcc*-phase reflections. On further compression to over 80 GPa the intensities of the reflections of the *hcp*-phase increase, but even after 5 hours of heating at 79.4(7) GPa and 1180(10) K there are still clear reflections of the *fcc*-phase. Upon quenching the *hcp*-phase transforms to *bcc*, while the *fcc*-phase remains (Fig. 3.2-5). Studies of quenched products by electron microprobe do not reveal any sign of inhomogeneity. This is confirmed by nanoscale ATEM measurements which do not show any difference between the composition of starting materials and that of recovered iron-nickel phases. The homogeneous composition indicates that the formation of *fcc*- and *hcp*-structured phases at high pressures is not the result of a chemical decomposition of the initial alloys, as proposed by Lin *et al.* (2002).

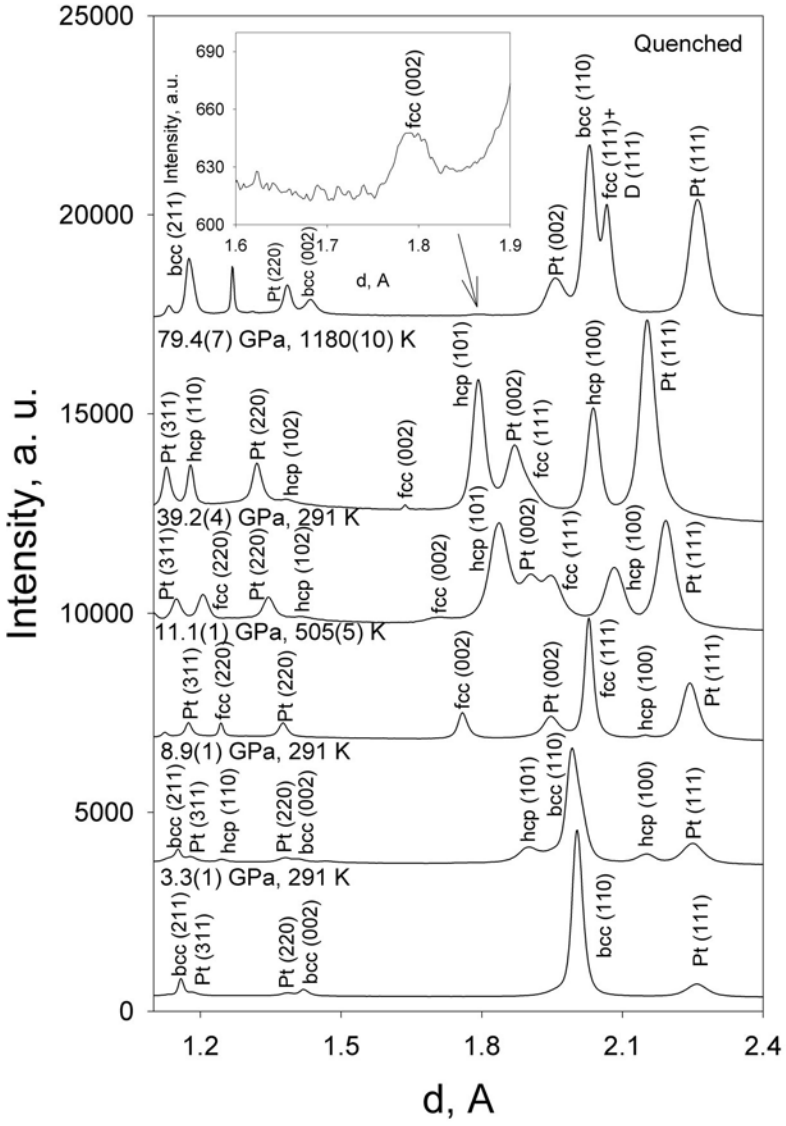

Fig. 3.2-5: A series of X-ray diffraction patterns collected in experiments with Fe-19%Ni alloy (platinum (Pt) used as internal pressure standard; line D is due to diamond from an anvil broken on quenching.

Figure 3.2-6 summarises the results of all our experiments on Fe-10%Ni alloy. The *bcc-fcc* and *bcc-hcp* phase boundaries, as well as the position of *bcc-fcc-hcp* triple point are in good agreement with literature data. However, the slope (15(2) K/GPa) of the "*fcc-in*" phase boundary (defining the appearance of the *fcc*-phase on heating of pure *hcp*-phase) is lower than that reported by Lin *et al.* (2002) and Huang *et al.* (1992) (23(4) K/GPa). It is worth to note that the duration of heating in our experiments was an order of magnitude longer than in the work by Lin *et al.* (2002). We also did not observe decomposition of alloys that could be caused by thermal gradients and/or thermal stresses in laser-heated DACs. We observed *fcc*-structured Fe-7.6%Ni at 138 GPa and Fe-10%Ni alloy at Earth's core pressure of 210 GPa. Extrapolation of the data collected for Fe-10%Ni to outer core conditions (pressures above

330 GPa and temperatures between 5000 and 7000 K) suggests that the Earth's inner core could contain coexisting *fcc*- and *hcp*-structured iron-nickel alloys. The densities of *fcc*-structured Fe-Ni alloys at ambient temperature are slightly lower than the density of *hcp*-structured phases of corresponding compositions, although the difference decreases with pressure and at 330 GPa the molar volume of *fcc*-Fe-10%Ni alloy is expected to be ~ 0.5 % higher than the molar volume of the *hcp*-phase. Such a difference could be important for the dynamics of the Earth's core and could contribute to its fine- or large-scale heterogeneity. Moreover, thermoelastic properties of cubic *fcc*- and hexagonal *hcp*-phases are expected to be rather different, and mechanical and texturing properties of two-phase (*fcc* and *hcp*) mixture could be quite different from the properties of the pure *hcp*-phase. Modelling of the seismic anisotropy of the Earth's inner core in the future will require explicit consideration of phase heterogeneity of the constituent material.

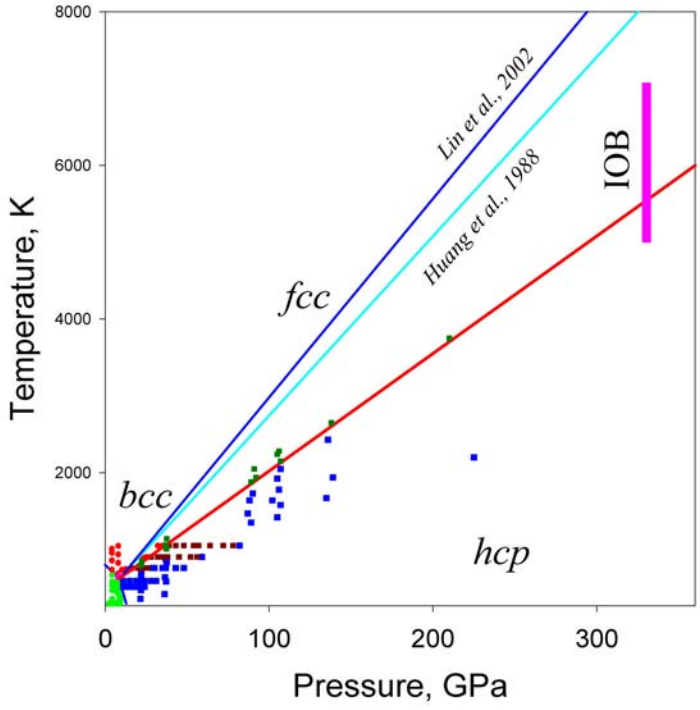

Fig. 3.2-6: Phase relations of *bcc*, *hcp*, and *fcc* phases in Fe-10%Ni alloy. Circles – *bcc*, hexagons – *fcc*, triangles – *bcc+fcc+hcp*, squares – *fcc+hcp*; two datapoints at pressures 225 GPa and 210 GPa are for Fe-7.6%Ni alloy; interval of temperatures expected for inner-outer core (IOB) boundary shown by long rectangle.

f. *A class of new high-pressure silica polymorphs (L.S. Dubrovinsky, N.A. Dubrovinskaia, F. Seifert and F. Langenhorst, in collobaration with V. Prakapenka/Chicago, V. Dmitriev and H.-P. Weber/Grenoble)*

The structures, properties and high-pressure behaviour of silicon dioxide SiO_2 has been extensively investigated because of its importance in Earth and material sciences and

technology. The last decade studies revealed a number of enigmatic phenomena associated with high-pressure silica polymorphs, *e.g.* formation of yet unidentified phases on the compression of α-cristobalite and quartz, controversial theoretical and experimental results on the possible post-stishovite phases, and discovery of new dense natural silica polymorphs in the Martian Shergotty meteorite. Despite its simple chemical composition, silica shows rich polymorphism at elevated pressures and temperatures. It is well known that depending on the conditions of experiments (hydrostaticity of the pressure medium, speed of compression, duration time of high-pressure treatment, starting material, etc.) different silica phases appear on compression and this behaviour is still poorly understood.

We conducted a series of experiments in electrically heated diamond anvil cells (DACs) in order to study silica at pressures above 100 GPa and temperatures above 1000 K. Figure 3.2-7 shows a typical sequence of diffraction patterns obtained in high-pressure high-temperature experiments with α-cristobalite as a starting material. On compression in Ar pressure medium above 10-12 GPa a new phase, first described by Tsuchida and Yagi (Nature 340, p. 217, 1989) as Cristobalite XI, appeared and persisted on compression at room temperature to 37-40 GPa. If at pressures between 30 and 40 GPa temperature increases to 700-900 K, Cristobalite XI reflections could be observed on the compression at high temperature to at least 65 GPa. However, upon heating at pressures above 35 GPa the diffraction pattern of Cristobalite XI slowly evolved – the reflections at about 1.24 Å, 1.45 Å, and 1.85 Å are growing, while other reflections diminish (Fig. 3.2-7). At the same time, long heating at pressures above 75-80 GPa results in crystallization of the α-PbO_2-structured phase (Fig. 3.2-7). However, long heating at pressures above 90 GPa and temperatures above 850 K results in appearance of new reflections, which cannot belong to α-PbO_2-type SiO_2 (Fig. 3.2-7). Moreover, the diffraction pattern from a quenched sample treated at pressures above 110 GPa and 1050 K during 8 hours is quite different from the diffraction patterns of quenched α-PbO_2-type silica.

We interpret our observations as evidence for the existence of a new class of silica phases with different degree of ordering of silicon atoms. Silica polymorphs with octahedrally coordinated silicon known so far (stishovite, fully disordered phase with niccolite-type structure (Liu *et al.*, J. Geophys. Res., 83, 2301-2305, 1978), α-PbO_2-type, and monoclinic ($P2_1/c$ space group) post-quartz phase (Haines *et al.*, Phys. Rev. Letters, 87, 155503, 2001) are members of this class.

The details of the silicon distribution among free positions in the oxygen network strongly depend on the starting material and the conditions of high-P,T treatment of silica, but the general trend is that at pressures above 40-45 GPa most of the silicon atoms are placed in octahedral positions. Our structural model provides a key for an explanation of the mysterious behaviour of silica, known for more than 30 years, when at the same pressure and temperature range different phases were synthesized. At low pressure the variety of silica polymorphs is

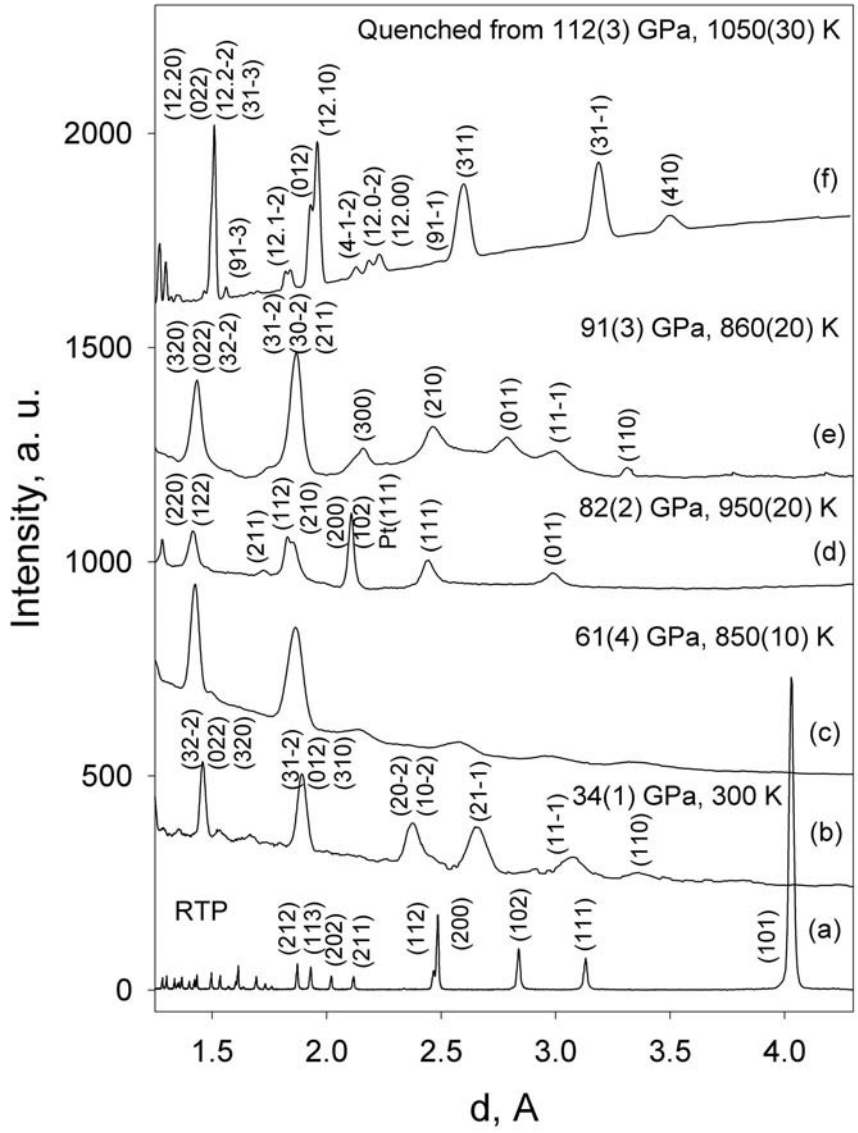

Fig. 3.2-7: Examples of diffraction patterns collected in high-pressure high-temperature experiments with α-cristobalite as a starting material. (a) All observed reflections of the initial material belong to the low-cristobalite tetragonal structure with lattice parameters a=4.9733(3) Å and c=6.9234(4) Å; (b) on compression in Ar pressure medium to 34(1) GPa at ambient temperature the so-called Cristobalite XI phase is formed (indices for monoclinic unit cell with lattice parameters a=7.473(3) Å, b=3.961(1) Å, c=4.993(2) Å, β=120.08(2)°); (c) heating at 850(1) K and 61(4) GPa for two hours produces a disordered phase; (d) the disordered phase crystallizes to the α-PbO_2-structured phase on heating for 4 hours at 82(2) GPa and 950(20) K (indices for orthorhombic cell a=4.232(5) Å, b=3.848(4) Å, c=4.756(9) Å); (e) heating at 91(4) GPa and 860(20) K for about 3 hours results in appearance of new reflections which can be indexed with a monoclinic cell a=7.294(5) Å, b=3.868(3) Å, c=4.841(7) Å, β=118.8(1)°; (f) the top spectrum was obtained from the initial cristobalite sample treated at 112(3) GPa and 1050(30) K for 8 hours and subsequently quenched (indices for monoclinic unit cell with a=30.553(4) Å, b=4.1037(4) Å, c=5.0753(9) Å, β=118.61(1)°).

related to the flexibility of the Si-O-Si bonding angle between corner-shearing SiO_4 tetrahedra. At high pressure the diversity of silica modifications is associated with the ability of silicon atoms to occupy different interstices in the monoclinically distorted *hcp* oxygen lattice. Silica phases with tetrahedrally coordinated silicon demonstrate a significant diversity in densities – from 1.77 g/cm^3 in open framework zeolite-like structures to 2.90 g/cm^3 of coesite, while high-pressure modifications of silicon dioxide with hexagonal close packing of oxygen and octahedrally coordinated silicon have practically the same densities (~ 4.28 g/cm^3) at ambient conditions (quenched metastable phases), and very close densities at a megabar pressure range (the difference in density is only 1-1.5 % between $CaCl_2$-, α-PbO_2-type and disordered SiO_2 phases).

g. *Mixing behaviour of the magnesite-otavite ($MgCO_3$-$CdCO_3$) solid solution (F.A. Bromiley, T. Boffa-Ballaran and F. Langenhorst)*

Knowledge of the calcite-magnesite system is fundamental to the understanding of the carbon cycle in the Earth's crust and mantle. In natural rocks, the calcite end-member $CaCO_3$ and the intermediate ordered dolomite phase $CaMg(CO_3)_2$ are the most important minerals belonging to this system, and the solvus between the two phases is an important proxy for paleotemperatures. With increasing temperature, the two-phase region closes and simultaneously the intermediate phase (dolomite) disorders - a similar situation as in some pyroxene systems. The detailed configuration of the phase diagram is dependent on the nature of the order-disorder phase transition, but required experimental conditions make a precise analysis of this transition difficult. The binary join within the magnesite ($MgCO_3$)-otavite ($CdCO_3$) system has therefore been investigated as an analogue for the magnesite-calcite system as experiments can be carried out at significantly lower temperatures.

Solid-state syntheses were carried out at 600 °C and 1 GPa in the piston cylinder press, and silver oxalate was used as a CO_2 source. An ordered structure of cadmium dolomite [$CdMg(CO_3)_2$] was observed by X-ray powder diffraction and Transmission Electron Microscopy (TEM) in the central region of the system. Towards Mg-rich compositions, two-phase run products confirmed the presence of a miscibility gap between magnesite and cadmium dolomite. Run products at the cadmium-rich end of the system consisted of only one carbonate phase, suggesting that a miscibility gap between otavite and cadmium dolomite, if it exists, has a critical temperature below 600 °C.

The miscibility gap between the "cadmium dolomite" and magnesite structures is also clearly seen in the lattice constants (Fig. 3.2-8), and ordering within samples of intermediate compositions was confirmed by the presence of reflections that are absent in the X-ray diffraction patterns for the disordered structure.

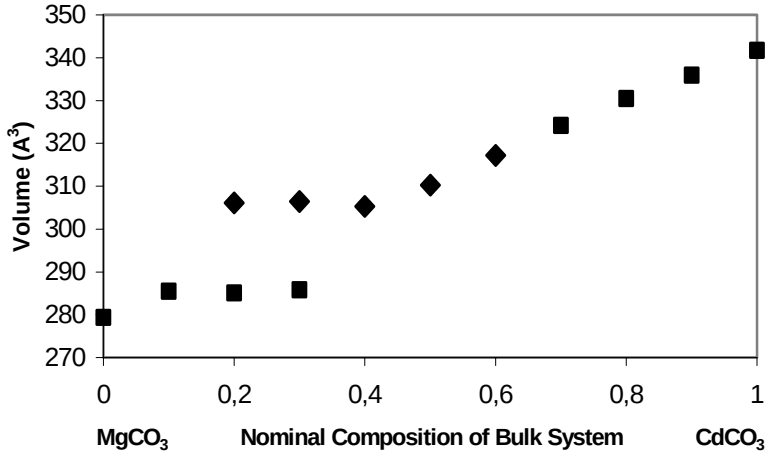

Fig. 3.2-8: Increase of unit-cell volume with composition across the magnesite-otavite system for samples synthesised at 600 °C and 1 GPa. Diamonds = $R\bar{3}c$ samples; squares = $R\bar{3}$ samples.

TEM was used for compositional micro-analysis, electron diffraction and bright-field imaging of samples that lay within the magnesium-rich miscibility gap. Within the $Cd_{0.2}Mg_{0.8}(CO_3)$ sample, two phases exist with two distinct compositions which, according to X-ray data for the 600 °C series, are approximately $Cd_{0.4}Mg_{0.6}(CO_3)$ and $Cd_{0.1}Mg_{0.9}(CO_3)$. The results obtained from TEM micro-analysis are so far fully consistent with these data.

It was noted that grains of the ordered cadmium rich composition were seen to be ten times bigger than those of the disordered phase, hence showing a grain size dependence on composition (Figure 3.2-9). The two phases were analysed by means of Selected Area Electron Diffraction (SAED), and indexation of the patterns. With this procedure it was possible to image reflections, such as the (101) and (003), that are normally absent in the disordered phase, hence showing the presence of an ordered phase.

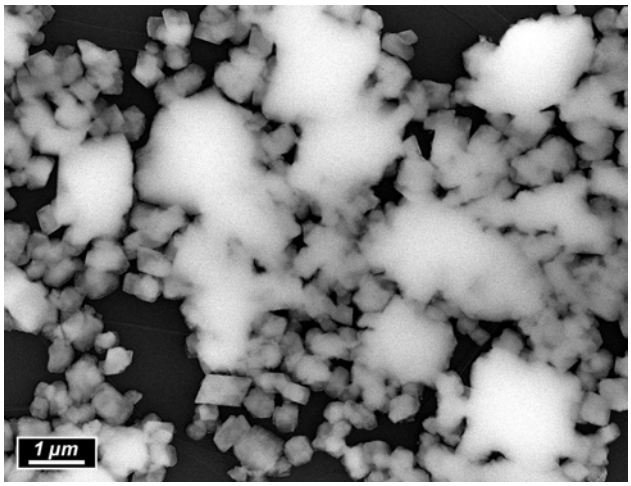

Fig. 3.2-9: Bright field TEM image of ordered (large grain) and disordered (small grains) phases within the $Cd_{0.2}Mg_{0.8}(CO_3)$ sample synthesised at 600 °C at 1 GPa for 3 hours.

h. *Investigations on the stability of Na-K-disilicates at elevated pressures (V. Kahlenberg and S. Rakic/Bremen, in collaboration with B.C. Schmidt)*

Alkali disilicates have been investigated frequently because of their complex polymorphism as well as for their interesting material properties in applications as ion exchangers and builders in washing powders. Furthermore, melts with composition $(Na_{1-x}K_x)_2Si_2O_5$ have been used by geoscientists as models for silicate melt phases which are the essential component of nearly all igneous processes. Although the sodium end member has been studied in great detail, there is only limited crystal chemical information on the formation and the stability of potassium exchanged samples. A more detailed knowledge about the possible ring conformations in the crystalline materials can help to improve the understanding and interpretation of the absorption spectra of the corresponding glasses and melts.

In order to study the formation of mixed alkali disilicates at elevated pressures, hydrothermal crystallization experiments have been performed at two different pressures (1 and 3 kbar) and temperatures between 500 °C and 700 °C. Starting material for the experiments were glasses prepared for x = 0, 0.25, 0.5, 0.75 and 1.0. The characterization of the synthesis products by powder and single crystal diffraction proofed the existence of the following four new alkali disilicates :

- κ- $Na_2Si_2O_5$ (orthorhombic, *Pn*2$_1$*a*, *a* = 8.128(1) Å, *b* = 4.8322(8) Å, *c* = 11.977(3) Å, single layer silicate containing six-membered rings of tetrahedra in *UDUDUD* conformation within the sheets perpendicular to [001]) (Fig. 3.2-10).
- $Na_{1.84}K_{0.16}Si_2O_5$ (isotypic with κ-$Na_2Si_2O_5$, *a* = 8.172(2) Å, *b* = 4.849(1) Å, *c* = 12.078(3) Å).
- $NaKSi_2O_5$-II (monoclinic, *P*2$_1$/*c*, *a* = 4.852(1) Å, *b* = 13.594(2) Å, *c* = 7.463(1) Å, β= 91.20(2)°, double chain silicate containing four-membered rings within the chains running along [100]) (Fig. 3.2-11).
- $Na_{0.5}K_{1.5}Si_2O_5$ (monoclinic, *I2/a*, *a* = 12.731(2) Å, *b* = 7.321(1) Å, *c* = 17.827(3) Å, β = 100.85(2)°, single layer silicate containing four-, six- and eight-membered rings within the layers parallel to (100)) (Fig. 3.2-12).

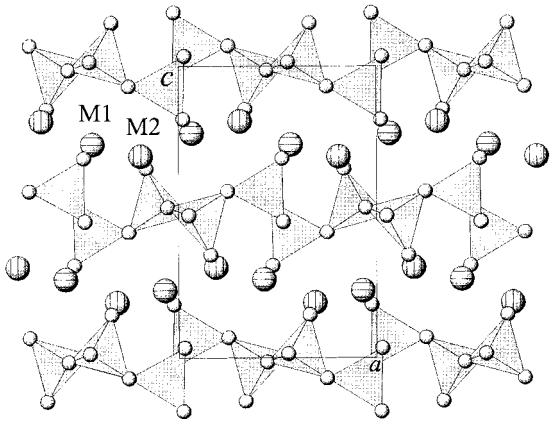

Fig. 3.2-10: Projection of the structure of κ- $Na_2Si_2O_5$ parallel to [010]. Hatched spheres represent the two independent sodium sites.

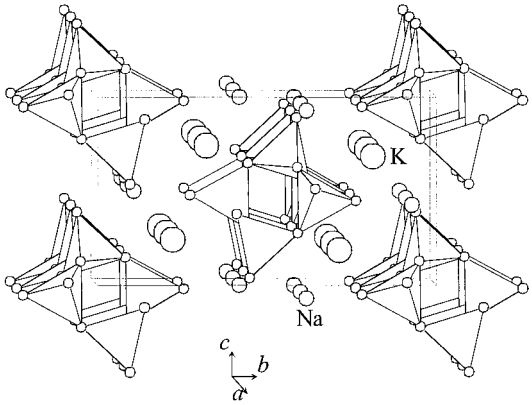

Fig. 3.2-11: Side view of the double chain silicate

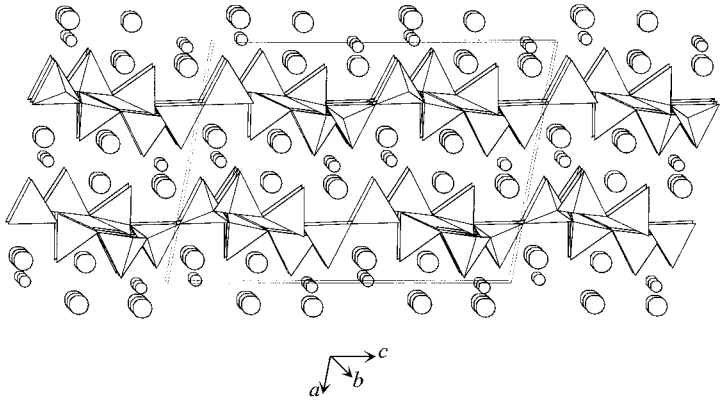

Fig. 3.2-12: Side view of the structure of $Na_{0.5}K_{1.5}Si_2O_5$

i. *Spontaneous strain at the C2/m ↔ $P2_1/m$ transition in cummingtonite (T. Boffa Ballaran, in collaboration with M.A. Carpenter/Cambridge and K. Knight/Chilton)*

Structural phase transitions in minerals are almost invariably accompanied by spontaneous strain. Because strains typically arise by coupling with the driving order parameter, they are frequently used to determine the pattern of evolution of the order parameter as a function of temperature, pressure or composition. Spontaneous strains associated with ferroelastic phase transitions are commonly up to a few % in magnitude. The strains accompanying co-elastic transitions can be on a comparable scale but are usually in the range of up to a few ‰. With high-resolution neutron powder diffraction methods, it is often possible to measure lattice parameters to a precision of ~ 1 in 10^5, and, hence, to determine strains of a few % to a precision of at least 1 in 100.

The objective of the present study was to characterise the spontaneous strains associated with the $P2_1/m \rightarrow C2/m$ phase transition which occurs with increasing temperature in

cummingtonite, $(Mg,Fe^{2+})_7Si_8O_{22}(OH)_2$. To this end, neutron powder diffraction data have been collected at the HRPD beam line of ISIS, Rutherford Appleton Laboratory, in the temperature range 4-500 K. Lattice parameters were determined at each temperature by Rietveld refinements using the GSAS package. In Fig. 3.2-13 is reported the evolution of the unit-cell volume. A clear change in slope is visible at around 300 K. The spontaneous strain parameters and the volume strain have been calculated using as extrapolation of the high-symmetry data a function which takes into account the saturation of the lattice parameter at low temperatures. This function has the form: $y = y_0 + y_1\Theta_s \coth(\Theta_s/T)$ where Θ_s is the saturation temperature. The small curvature of the high-symmetry data is sufficient for constraining the saturation behaviour of the *C*2/*c* phase at low temperature. The resulting parameters from the fit are: y_0 = 884.6(1) Å^3, y_1 = 0.0224(1) and Θ_s = 171(8) K. The transition is continuous and can be modelled with a 2-4-6 Landau potential. Further experiments with longer exposition time have been undertaken in order to obtain high quality data for a complete structural analysis to determine accurate atomic positions as they vary through the phase transition in order to constrain the structural mechanism associated with this transformation.

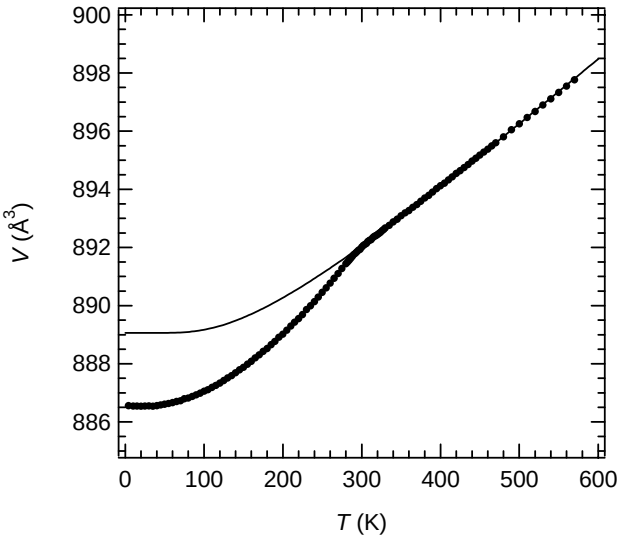

Fig. 3.2-13: Variation as a function of temperature of the unit-cell volume of cummingtonite. Note the change in slope at about 300 K due to the structural phase transition. The solid line is the fit to the high-symmetry data using a function which takes into account the volume saturation at low temperatures.

j. *The high-pressure $P2_1/c$-$C2/c$ phase transition in $Ca_{0.15}Mg_{1.85}Si_2O_6$ clinopyroxene (F. Nestola/Torino and T. Boffa Ballaran, in collaboration with M. Tribaudino/Torino)*

Ca-poor clinopyroxenes are among the major constituents of the upper mantle. At room conditions they display $P2_1/c$ space group; previous investigation on Ca-free enstatite has shown a first order non quenchable phase transition to a *C*2/*c* structure at pressures in excess

of 7 GPa. This transition occurs with large hysteresis. However, in natural mantle clinopyroxenes, a significant Ca-content may be present with consequent effect on the phase transition.

In order to determine such effect a high-pressure study was undertaken on a synthetic sample with composition $Ca_{0.15}Mg_{1.85}Si_2O_6$ and $P2_1/c$ symmetry. A single-crystal was loaded in a DAC cell and compressed up to 7.3 GPa. The $P2_1/c$-$C2/c$ phase transition was detected at 5.1 GPa. This transformation is first order in character, with the same volume discontinuity reported for clinoenstatite. The fit of the unit-cell volume data of the $P2_1/c$ clinopyroxene with a third-order Birch-Murnaghan equation of state (EoS) gives: V_0 = 421.68(8) Å^3, K_{T0} = 102(2) GPa and K' = 8(1). Given the few data points collected for the high-symmetry phase, the EoS fit to the $C2/c$ data was done fixing the value of K' to 8 as obtained for the low-symmetry phase. The resulting EoS parameters for the $C2/c$ structure are: V_0 = 411.06(3) Å^3 and K_{T0} = 108(2) GPa. A comparison with the clinoenstatite behaviour shows a significant decrease in the transition pressure, slightly smaller stiffness of the $P2_1/c$ phase and absence of hysteresis. This suggests that substitution of a small amount of Ca into the clinoenstatite structure might facilitate the nucleation of one structure from the other during the first-order transition process.

Structure refinements based on a full data collection of intensities were performed at room pressure, at 4.5 GPa ($P2_1/c$ symmetries) and at 6.15 GPa ($C2/c$ symmetry). Since these pyroxenes undergoe a $P2_1/c \rightarrow C2/c$ transformation also as a function of temperature and it is known that the HT-$C2/c$ phase is different from the HP-$C2/c$ structure, it is interesting to compare the behaviour of the tetrahedral chains approaching the phase transition as a function of pressure with that as a function of temperature. The difference between the O3-O3-O3 kinking angle of the A and B chains of the $P2_1/c$ structure increases with pressure, whilst it decreases with temperature. The O3 oxygens of opposite chains become closer and closer as the pressure increases (Fig. 3.2-14) therefore suggesting that the phase transition is driven by the repulsion of such oxygens.

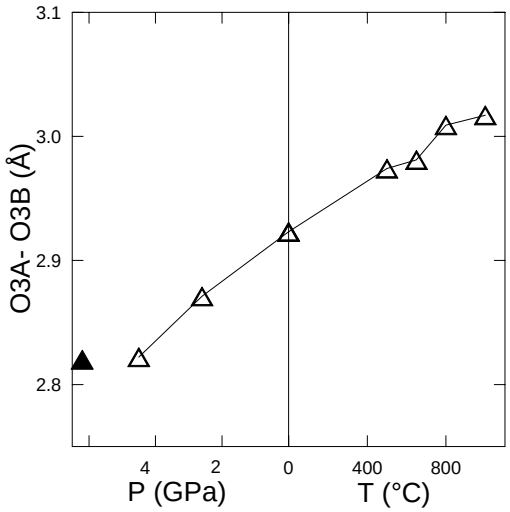

Fig. 3.2-14: Distance between the O3 oxygens belonging to opposite tetrahedral chains (open triangles $P2_1/c$, full triangle $C2/c$).

k. *The compressibility of $CaNiSi_2O_6$ (F. Nestola/Torino and T. Boffa Ballaran, in collaboration with M. Tribaudino/Torino)*

In the framework of a systematic investigation on the compressional behaviour of different end-members of pyroxenes, the cell parameters and equation of state were determined for $CaNiSi_2O_6$ clinopyroxene by single crystal *in situ* X-ray diffraction up to 7.8 GPa. These results were compared with previous investigations of other $CaM1Si_2O_6$ pyroxenes, namely diopside and hedenbergite. Previous works indicate significant changes in compressibility related to cation substitution at the M1 site.

In this study a third order Birch-Murnaghan equation of state has been used to fit the unit-cell volume variation of $CaNiSi_2O_6$. The resulting EoS parameters are: V_0 = 435.21(1), K_0 = 117.7(4) and K'=6.4(1). This bulk modulus is similar to that of hedenbergite, but indicates substantially higher stiffness than diopside (Fig. 3.2-15). The axial compressibility follows for $CaNiSi_2O_6$ the scheme $\beta_a>\beta_c>\beta_b$, similar to hedenbergite, whereas for diopside $\beta_a\cong\beta_c>\beta_b$. Moreover, a smaller compressibility along the *a* axis in $CaNiSi_2O_6$ and hedenbergite with respect to diopside is observed. The difference in ionic radius of the cations at the M1 site cannot explain completely this different behaviour, as Mg has an ionic radius intermediate between Fe^{2+} and Ni^{2+}. Possible effect of crystal field stabilisation energy may explain the similar behaviour of the pyroxenes with Fe^{2+} and Ni^{2+} at the M1 site.

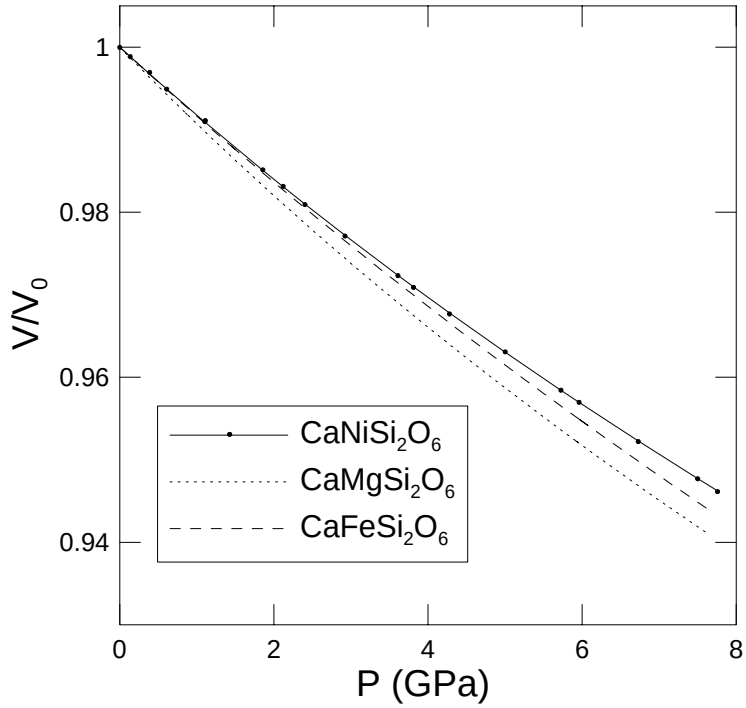

Fig. 3.2-15: Variation of V/V_0 as a function of pressure. The fits are calculated according to the third-order Birch-Murnaghan EoS for $CaNiSi_2O_6$ (this work), and for $CaMgSi_2O6$ and $CaFeSi_2O_6$ (Zhang *et al.*, Am. Min., 82, 245, 1997).

l. *Equation of state of bismuthinite (L. Lundegaard/Copenhagen and T. Boffa Ballaran)*

Bismuth is a group VA element, which in the studied compound bismuthinite (Bi_2S_3) is in a trivalent state and has a lone electron pair with pronounced steric requirements. There are two distinct Bi positions in the structure of bismuthinite, each coordinated to seven S. Each Bi atom is bonded to three S atoms with short bonds (2.65 Å - 2.70 Å) which build strongly bonded rods being the primary building element of the structure. In the *Pnma* setting the rods are parallel to the [010] direction. The space between the rods accommodates the lone electron pairs of Bi. There are only weak interactions between the rods.

For the pressure-volume equation of state a series of high precision unit-cell parameters was collected in the pressure range of 0-5 GPa. A single-crystal was loaded in a BGI type diamond anvil cell, into a 250 μm diameter hole drilled into at steel gasket preindented to a thicknes of 100 μm. A 1:4 ethanole:methanole mixture was used as hydrostatic pressure medium. A Huber diffractometer and the SINGLE99 software were used for data collection. Unit-cell parameters of quartz as an internal standard were used for pressure calibration. The unit-cell lattice parameters obtained are shown in Fig. 3.2-16.

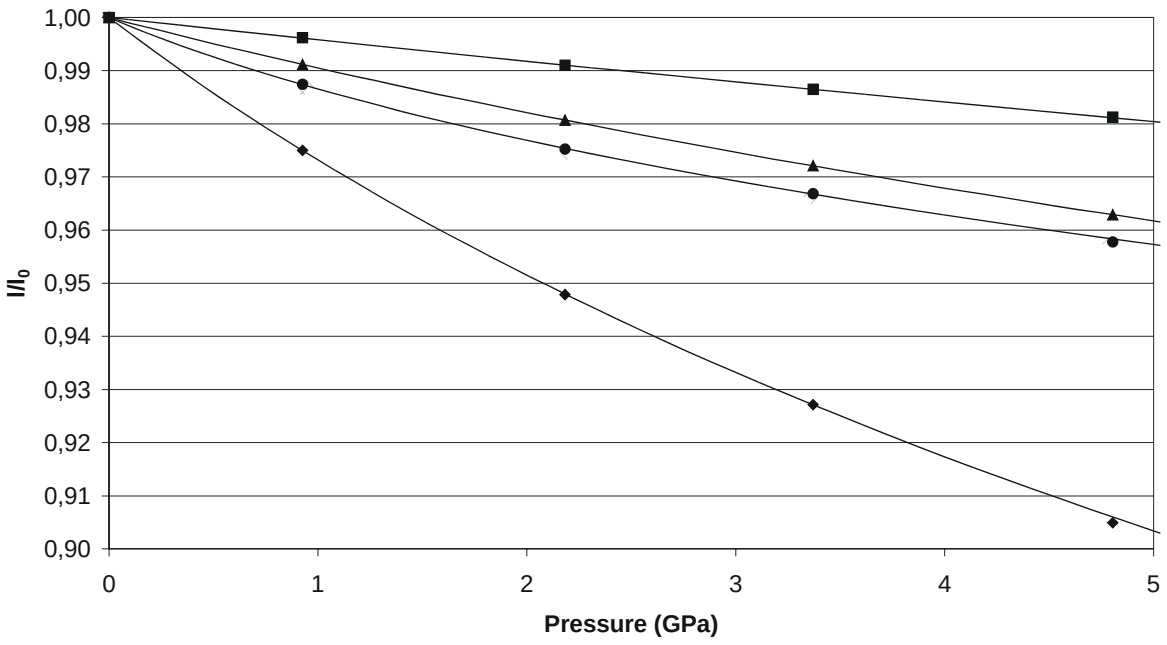

Fig. 3.2-16. Evolution of unit-cell parameters of bismuthinite with increasing pressure. Values are given relative to their zero pressure values. *a*-axis (circles); *b*-axis (squares); *c*-axis (triangles); and volume (diamonds).

The zero pressure volume, bulk modulus and its pressure derivative of bismuthinite were determined from fitting a 3rd order Birch-Murnaghan equation of state (BM3 EoS) to the unit-cell volume data. The resulting EoS parameters are: V_0 = 501.44 Å^3, K_0 = 32.0 GPa and K' = 8.1.

By substituting the cube of the unit cell edge for the volume, a BM3 EoS was also fitted to the unit-cell edge data. The "bulk modulus" of the *a*, *b* and *c* unit cell edges were found to be 19.7 GPa, 78.3 GPa and 32.7 GPa respectively. Due to the strongly bonded rods being oriented along the *b* unit cell edge, bismuthinite is not very compressible in this direction, whereas the lone electron pairs are pointing approximately along the [100] direction which may explain why the compressibility of bismuthinite is greatest along the *a* unit cell edge.

m. *Compressibility of baddeleyite-type TiO_2 from static compression to 40 GPa (N.A. Dubrovinskaia and L.S. Dubrovinsky, in collaboration with V. Swamy/Montreal)*

In the search for potential post-stishovite high-pressure silica (SiO_2) phases in the Earth's mantle, TiO_2 has long served as an analogous system on which to carry out static and dynamic experiments as well as computational studies. Recently, additional interest in the high-pressure phases of TiO_2 and other transitional metal oxides has been generated, because, owing to their high bulk moduli, they are considered as potential superhard oxides.

The present study is concerned with the determination of pressure-volume data of the baddeleyite-type TiO_2 phase from room pressure to 40 GPa in order to obtain a high quality bulk modulus value for this material. The bulk modulus is an important parameter that bears on both thermodynamic stability and hardness of the high-pressure phases. A number of studies have reported rather controversial bulk modulus data on the high-pressure TiO_2 polymorphs. Of the high-pressure forms, only the columbite-type (TiO_2-II) is easily amenable to study under ambient conditions, because it can be synthesised through acid dissolution of Ti_3O_5, and also can be quenched from high pressures. As we have shown in previous studies, cotunnite TiO_2 can be quenched to room pressure through a cryogenic recovery technique. In this way we recovered the room pressure crystal structure of baddeleyite TiO_2 in an effort to obtain the room pressure unit-cell volume, and combine this datum with *in situ* high-pressure measurements to 40 GPa to retrieve the bulk modulus.

Upon compression at pressures above 7 GPa, the X-ray peaks due to anatase used as starting material were broadened (Fig. 3.2-17), and between 9 and 16 GPa, the diffraction spectra contained reflections belonging to TiO_2-II and baddeleyite TiO_2. At pressures above 17 GPa, transformation to the baddeleyite structure was complete, and up to 40 GPa we did not observe any further phase transitions. At pressures above 42 GPa, the diffraction lines due to baddeleyite-type TiO_2 became broader and it was impossible to get accurate data on lattice parameters at these pressures. On decompression at ambient temperature, the baddeleyite-type TiO_2 transformed to TiO_2-II between 8 and 12 GPa. However, rapid decompression (within a second or so) from 37 GPa to ambient pressure in liquid nitrogen at a temperature of 77 K using a cryogenic recovery technique led to the preservation of the baddeleyite structure (Fig. 3.2-17). Lattice parameters of the quenched baddeleyite TiO_2 are: a=4.637(2) Å, b=4.942(2) Å, c=4.884(2) Å, β=99.21(1)°, and V=110.48(5) $Å^3$. These values were used in the

determination of the equation of state of baddeleyite TiO_2 by fitting the pressure-volume data set to a Birch-Murnaghan equation of state. The fit yielded K_T and K' values of 303(5) GPa and 3.9(2), respectively. Figure 3.2-18 shows the experimental data and the isothermal Birch-Murnaghan equation of state for baddeleyite TiO_2.

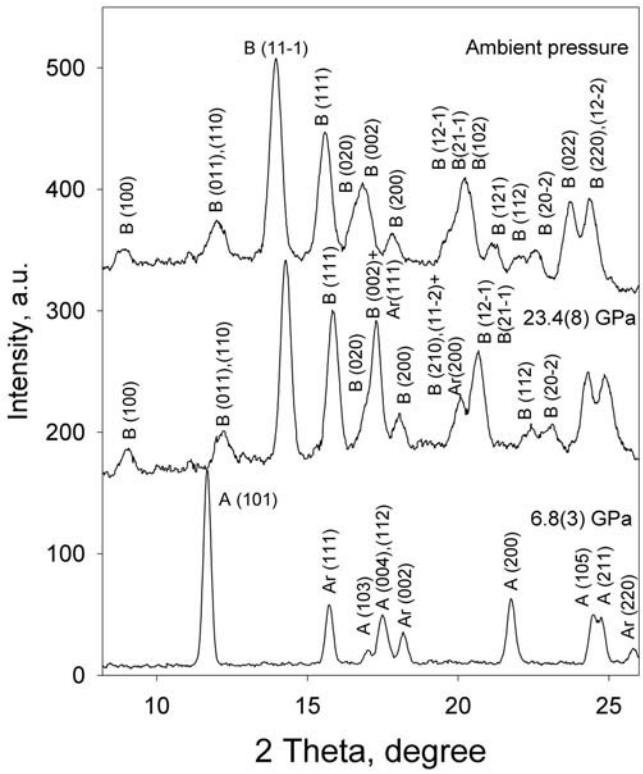

Fig. 3.2-17: Example powder X-ray diffraction spectra obtained from anatase at 6.8(3) GPa, baddeleyite TiO_2 at 23.4(8) GPa, and cryogenically recovered baddeleyite TiO_2 at ambient pressure. A, Ar, and B stand for peaks due to anatase, argon, and baddeleyite TiO_2, respectively.

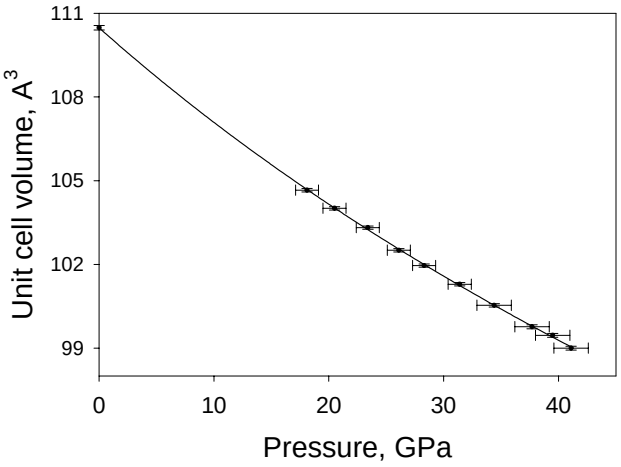

Figure 3.2-18: Experimental pressure-volume data of baddeleyite TiO_2 and a Birch-Murnaghan equation of state fit (curve).

n. *Microstructure of radiation-damaged zircon and its behaviour as a function of pressure (S. Ríos/Cambridge and T. Boffa Ballaran)*

The microstructure found in radiation-damaged minerals such as zircon, $ZrSiO_4$, is relatively complex as a result of the dual origin of the damage mechanism: α-particles and recoil nuclei (see Annual Report 2001). This complexity is evident in single-crystal diffraction experiments performed on highly damaged samples (Fig. 3.2-19). Typical diffraction maxima show several distinct components, difficult to separate otherwise in a standard powder diffractogram. The first contribution, and the weakest one, is the diffuse background (in grey) coming from amorphous regions produced by recoil nuclei. The sharpest contribution (in black), is due to crystalline remnants, which are expanded compared with undamaged zircon as a consequence of defects produced by α-particles. Although no experimental evidence exists so far, oxygen interstitials are believed to be at the origin of the lattice expansion. Additionally, two more contributions are observed at low and high diffraction angles respectively. The first one corresponds to regions with a larger degree of expansion than the average crystallites, whereas the second one corresponds to regions that are under compression. This later contribution has been modelled, for simplicity, with only two Gaussian functions, but it should be interpreted as a continuous distribution of compressed regions. From the peak position of the most expanded/compressed regions a differential strain of approx. 5 % is found. Given the bulk modulus of defective zircon (~ 170 GPa) this means that the most compressed regions are under an internal pressure of ca. 14 GPa. This internal stress must originate from the expansion of crystalline regions - up to 5 % - and the swelling of the amorphous phase itself - up to 18 %. Such a stress is accommodated in the structure by relative twisting (misalignment) of crystalline remnants as shown by transmission electron microscopy images reported in the literature.

As pressure is gradually applied, no significant changes are observed below ~ 3 GPa (see Annual Report 2001), indicating that the major amorphous phase surrounding crystalline islands can reorganize itself to accommodate pressure-induced effects: the external pressure is screened by the amorphous matrix. This effect is more obvious in samples with higher degree of damage where crystalline islands are totally isolated.

For higher pressures, above 5-6 GPa, a large intensity increase is observed (Fig. 3.2-20a). Such an effect was originally believed to be due to a certain degree of defect recovery. Further investigations have shown that, on the contrary, such an intensity increase is primarily a consequence of realignment of crystalline regions, and that only minor defect healing takes place. When pressure is released, the original peak profile is recovered, indicating that pressure-induced effects are totally (or highly) reversible. Realignment of crystalline domains can be observed not only on the intensity increase but also on the sharpening of diffraction peaks at high pressures (Fig. 3.2-20b): the mosaic spread decreases as pressure is applied. At these pressures the amorphous phase also becomes stiffer, so transmitting the external pressure into the embedded crystalline regions better.

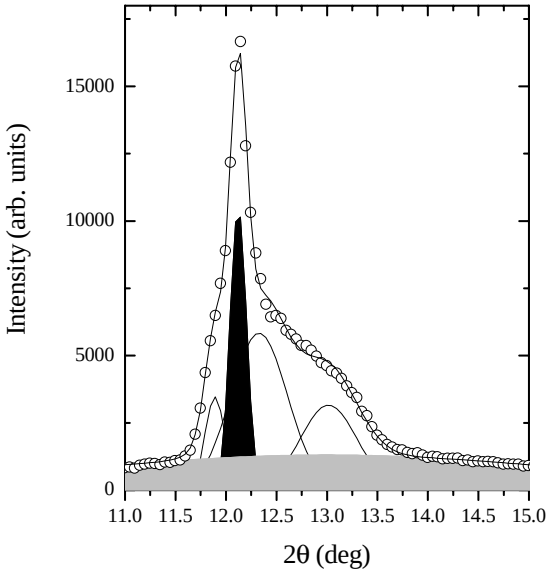

Fig. 3.2-19: (200) reflection in a zircon specimen with approx. 65 % of amorphous regions.

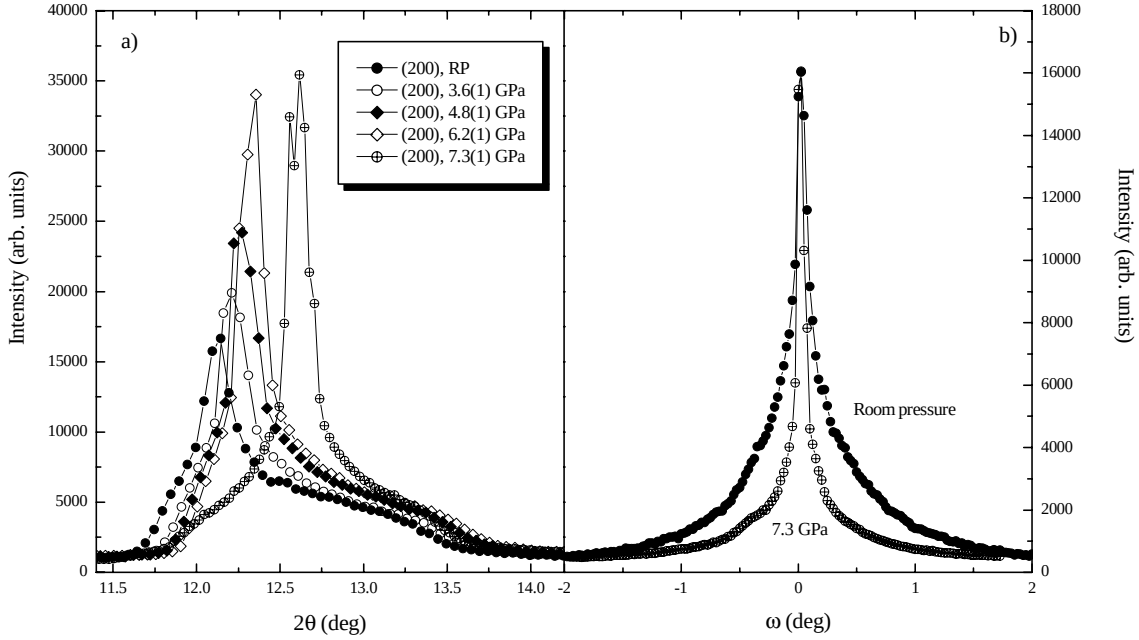

Fig. 3.2-20a,b: (200) reflection as a function of pressure. Note the increase in intensity a) and the decrease of the mosaic spread (full-width at half maximum) b) as crystalline regions realign as a function of pressure. In b) intensities have been normalised to give the same number of counts at the peak maximum.

The *soft* character of the amorphous phase at low pressures is difficult to explain due to the lack of understanding concerning the topology of amorphous zircon. Recent molecular dynamic simulations have shown that the amorphous phase produced during α-decay is constituted by SiO_n densified rims, containing depleted cores of some 20 Å in diameter. Our results might be the first experimental evidence for the existence of these nanovoids. As

pressure is applied, the amorphous phase is pressurised, reducing the volume of the nanovoids. During this stage the amorphous phase behaves as a soft material. Once the nanovoids have totally collapsed, the amorphous phase has lost part of the freedom to deform, so becomes stiffer.

3.3 Geochemistry

Studies of radiogenic isotopes imply that the Earth's metallic core separated from its silicate mantle in the first 30 million years of Earth's history. Such rapid separation may have been aided by the fact that a significant portion of the Earth was molten at this time. This allowed the denser liquid metal to sink to the centre of the Earth leaving a silicate magma ocean, which crystallized into the mantle. Primitive chondritic meteorites probably represent the material that formed the bulk of the Earth. The present day upper mantle in comparison to chondrites is clearly depleted in so-called siderophile elements, which prefer the metallic state over a wide range of conditions. Gold, for example, is a highly siderophile element because it remains in the metallic state even at very high oxygen partial pressures. In the present day upper mantle gold is highly depleted because it was extracted into the core as it formed. Many other elements occur as oxides over wide ranges of conditions and are termed rock forming or lithophile elements. Silicon and calcium, for example, are lithophile elements that only exist in the metallic state at extremely low oxygen partial pressures. A complete range of character exists between lithophile and highly siderophile elements and this is reflected in the degree to which each element is depleted in the Earth's mantle as a result of core formation. This simple explanation for the distribution of elements between the mantle and the core seems initially quite adequate, however, many problems arise from a more detailed examination. Concentrations of many elements in the mantle are far higher than metal-silicate partition coefficients predict and conversely some elements such as silicon are over depleted. One likely reason for this is that our perception of siderophile or lithophile character is generally based on quite low pressure partitioning data. From a thermodynamic standpoint the effect of pressure on partitioning is determined by the volume change between the oxide and metal phases. This volume change is also dependent on pressure as a result of both elastic compression and phase transformations, so the character of element partitioning has the potential to change significantly at high pressure. Many of the studies in this section were performed to improve our understanding of the details of core formation and mantle crystallisation through experiments performed at the high pressures and temperatures at which these processes took place.

Discontinuities in the mantle's elastic properties cause seismic waves to be refracted at 410, 520 and 660 km depth. It is widely accepted that phase transformations in mantle minerals cause these discontinuities. While the 660 km discontinuity is observed to be sharp, occurring over a depth interval of ~ 6 km, observations of the 410 km discontinuity imply it may vary in thickness from 4 to over 10 km. Phase transformations in simple one component systems are sharp because they occur at a single temperature at a given pressure. The simplest common example of this is pure H_2O, which melts exclusively at 0 °C at 1 bar. The mantle is a complex mixture of elements, however, where the main phases are solid solutions involving Fe and Mg. Just as H_2O-NaCl mixtures melt over a temperature range as opposed to pure H_2O, so phase transformations in mantle minerals will occur over pressure ranges corresponding to depth intervals. Experimental studies to determine the width of mantle phase

transformations under various conditions can be compared with seismic observations to give vital information on the nature of the mantle at these depths.

a. *Fractionation of siderophile elements resulting from metal-silicate separation during core formation: The role of magma ocean convection dynamics (D.C. Rubie, in collaboration with H.J. Melosh and K. Righter/Tucson)*

Formation of the Earth's core most likely involved the separation of liquid metal from liquid silicate in a deep magma ocean. The segregating metal sunk to form the Earth's core and was responsible for extracting siderophile elements, such as Ni and Co, from the silicate mantle. It has been shown that metal-silicate partition coefficients for at least some of the moderately siderophile elements reach values that are consistent with core-mantle concentrations at high pressure and temperature (*e.g.* 30 GPa and 2500 K). These conditions have been interpreted to represent the base of the magma ocean, in which case the pressure would be indicative of its depth. This interpretation is based on the idea that liquid metal accumulates to form a layer at the base of the magma ocean and eventually equilibrates there with the overlying convecting silicate liquid.

We have recently shown (*e.g.* 2001 Annual Report) that the concept of a segregated layer of liquid metal equilibrating with the overlying silicate magma ocean is not realistic. This is because equilibration times are 2-3 orders of magnitude larger than the time scale of magma ocean crystallization. Instead, chemical equilibration between metal and silicate must have occurred between small, dispersed metal droplets as they sank through the magma ocean. In this case, the interpretation of apparent pressures and temperatures of equilibration is more complex than for the unrealistic "metal layer" model. It is clear from our earlier results that the final equilibration between metal droplets and silicate liquid will take place at the base of the magma ocean immediately prior to segregation. However, because of fractionation effects, the resulting siderophile element contents of the core and mantle are unlikely to record the partition coefficients at that depth. We demonstrate this point through two simple end-member equilibrium metal-silicate fractionation models. The starting point for both models is a magma ocean that contains uniformly dispersed metal droplets. We calculate a magma ocean adiabat and metal-silicate distribution coefficients for Ni, D_{Ni}^{ms}, as a function of depth. Oxygen fugacity and other variables are adjusted to give D_{Ni}^{ms} =28 (as required for core-mantle equilibration) at a depth of ~ 800 km (Fig. 3.3-1).

Fractionation model 1: In the first model we assume that metal droplets sink and segregate on a timescale that is very rapid compared with the time scale of convective flow and mixing of the magma ocean. The magma ocean is divided into *n* depth increments each initially consisting of 32 wt.% metal and 68 wt.% silicate liquid (*i.e.* core-mantle proportions). Assuming an initially chondritic bulk composition, the equilibrium metal composition in each depth increment is calculated from

$$C_m(i) = \frac{C_B(i)}{0.32 + 0.68 / D_{Ni}^{ms}(i)}$$

where $C_B(i)$ is the bulk composition of the i^{th} depth increment. After calculating the metal composition in each increment, the metal is moved down by one depth increment and new values of $C_B(i)$, $C_m(i)$ and the corresponding silicate composition ($C_S(i)$) are calculated. This procedure is repeated until all metal has segregated at the base of the magma ocean. The final bulk composition of the segregated metal and the average composition of the remaining silicate magma are calculated and a core-mantle partition coefficient is thus obtained. The results show that a magma ocean with a depth of ~ 1350 km (*i.e.* much deeper than 800 km) is required to give a core-mantle partition coefficient of 28 for Ni (Fig. 3.3-1). This is because metal-silicate equilibration at low pressures contributes significantly to the final composition of the silicate (and consequently also that of the metal). This model is only fully realistic if the metal sinks and segregates extremely rapidly because it is assumed that there is no mixing or convective transport of the silicate magma.

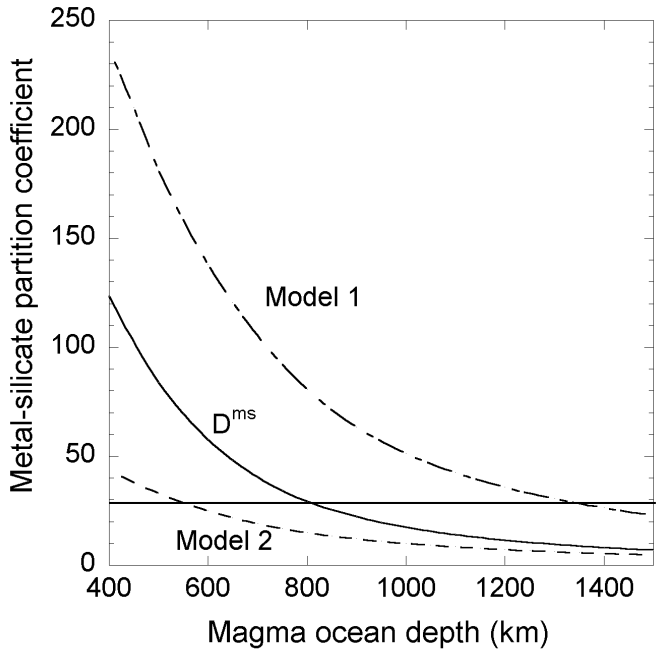

Fig. 3.3-1: Results of equilibrium metal-silicate fractionation models. D^{ms} is the metal-silicate partition coefficient for Ni at the base of the magma ocean, calculated as a function of magma ocean depth from published data. The two dashed lines show the results of the fractionation models and show the effective partition coefficient (Ni concentration in metal/Ni concentration in silicate) after metal-silicate segregation is complete. The horizontal line indicates the core-mantle Ni partition coefficient value of ~ 28.

Fractionation model 2: In this model, we assume that vigorous convection keeps the silicate magma ocean fully mixed and chemically homogeneous and that metal droplets are suspended in the magma ocean and only segregate gradually as they enter the boundary layer at its base. The segregation of metal fractions, that equilibrate finally with silicate at the base of the magma ocean, cause the bulk composition of the magma ocean, the mass fraction of remaining dispersed metal and thus the composition of the segregating metal to change continuously. A numerical simulation of this fractionation process shows that a magma ocean depth of ~ 550 km results in a core-mantle partition coefficient of 28 (Fig. 3.3-1).

From these results, it is clear that the compositions of metal and silicate that result from the segregation of metal droplets in a magma ocean depend strongly on the dynamics of segregation, convection and chemical mixing. Based on criteria for the suspension of particles in a magma ocean, model 1 may be more realistic than model 2. However, a more detailed analysis will be required to obtain a definitive solution to this problem.

b. *Iron-silicon alloy at extreme conditions (L.S. Dubrovinsky, N.A. Dubrovinskaia, F. Langenhorst, D.P. Dobson, D.C. Rubie, in collaboration with I. Abrikosov and B. Johansson/ Uppsala)*

The boundary between the Earth's metallic core and its silicate mantle is characterized by sharp changes of density, seismic wave velocities, electrical conductivity, chemical composition, and lateral heterogeneity. Although iron (with ~ 5 wt.% Ni) is a dominant component of the Earth's core, Fe-Ni alloy is too dense by ~ 10 % for the outer liquid core and by 2-5 % for solid inner core, to satisfy the observed density along any reasonable geotherm. Thus, on the basis of cosmochemistry, it has been proposed that the core also contains one or more light elements, such as H, C, O, S, and/or Si. It is likely that such light elements were dissolved into the liquid metal during core formation in a magma ocean during the early history of the Earth. At the likely temperature of the magma ocean (~ 2800 K), 2-6 wt.% Si can dissolved in liquid Fe at 25 GPa and an appropriate oxygen fugacity. On the basis of a simple thermodynamic model, Gessmann *et al.* (2001) proposed that the solubility of Si at core conditions is close to zero. Thus, following core formation, Si should be expelled from liquid Fe as the metallic core evolves towards chemical equilibrium.

But, what happens to the Fe-Si liquid, formed during core segregation in a magma ocean at 20-30 GPa, that could contain up to 6 wt.% Si? Theory predicts that, as pressure increases, an alloy of this composition would dissociate into a mixture of silicon-poor *hcp* Fe and the Si-rich *B2* structured phase. Note that these theoretical calculations were done at T=0 K, while at high temperature entropic contribution may be important. Therefore, theoretical predictions have been tested through a series of high-P,T DAC experiments on Fe-Si alloys containing 9.6(1), 5.1(1), and 4.3(4) wt.% Si (the latter produced by equilibrating Fe with SiO_2 at 22 GPa and 2473 K in multianvil apparatus). We found that all alloys behave similarly and Fig. 3.3-2 shows representative X-ray patterns obtained *in situ* at high-P,T using the 5.1 wt.% Si alloy as the starting material. At 300 K and pressures below 14-18 GPa all studied alloys have the *bcc* structure (Fig. 3.3-2a). At higher pressures the alloys start to transform to the *hcp* phase and above 20-22 GPa the transformation is completed (Fig. 3.3-2b). No further phase transformations were observed on compression to over 100 GPa at ambient temperature, but heating promoted a transformation. Figure 3.3-2d (see also left inset in Fig. 3.3-2) shows an example of a diffraction pattern collected after 5 hours of external electrical heating of the Fe 5.1 wt.% Si alloy at 140(10) GPa and 1380(25) K. Two new lines at 2.494 Å and 1.762 Å are present belonging to the *B2* structured alloy (a=2.493(1) Å) as predicted by *ab initio*

calculations. When the same sample was heated for 8 hours at 30(2) GPa and 1100(10) K, the extra lines disappeared indicating that the reaction was reversed and only the *hcp* phase remained (Fig. 3.3-2e).

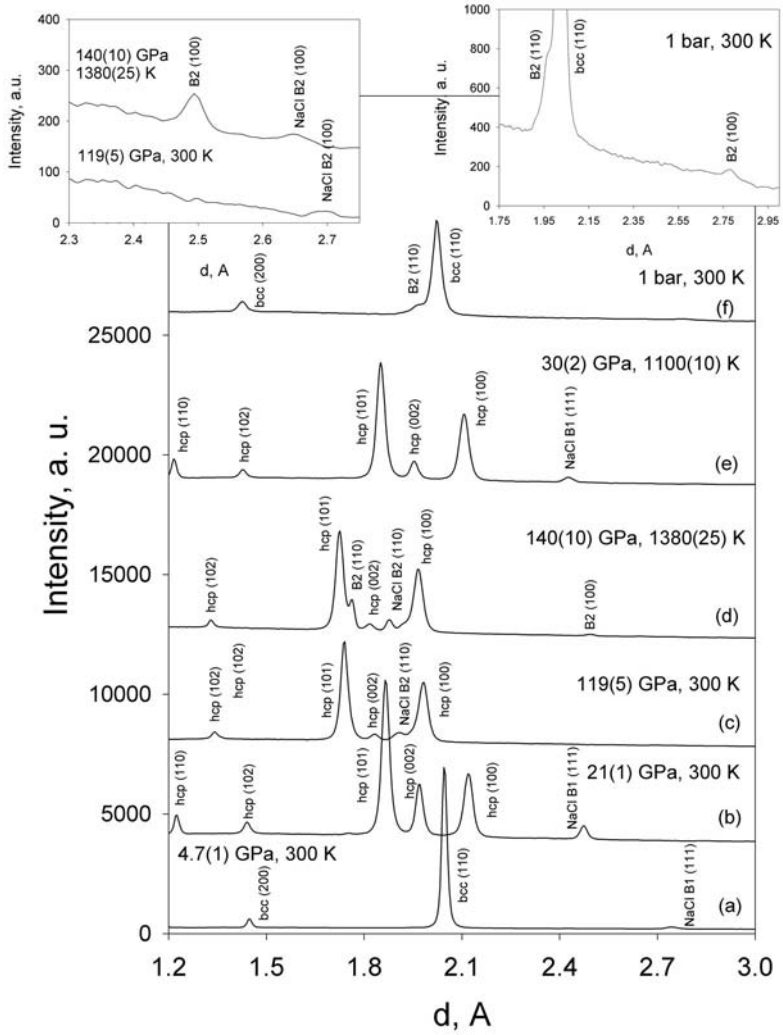

Fig. 3.3-2: Examples of X-ray diffraction patterns collected in experiments with Fe – 5.1 Si wt.%.

One of the samples of Fe-10 wt.% Si alloy was compressed to 105(5) GPa in a NaCl pressure medium, and then laser-heated from both sides at 2500(100) K. After decompression, the NaCl was carefully dissolved in water. The diffraction pattern of the recovered foil is shown in Fig. 3.3-2f (and right inset in the same figure). The extra reflections at 1.969 Å and 2.781 Å correspond to the (110) and (100) peaks of the quenched *B2* FeSi phase. The lattice parameter of this phase (2.783(2) Å) is slightly lower than the lattice parameter of *B2*-structured FeSi (2.7917(1) Å) synthesized in multianvil experiments, indicating that the composition of the *B2* phase obtained in our experiments may be close to 1:1 Fe:Si molar ratio.

Our results on the behaviour of the Fe-Si alloys in solid and liquid states with different Si concentrations are summarized in Fig. 3.3-3. We found that at pressures above 60 GPa and

high temperatures the alloys dissociate into a mixture of *hcp*-structured Si-poor and *B2*-structured Si-rich phases.

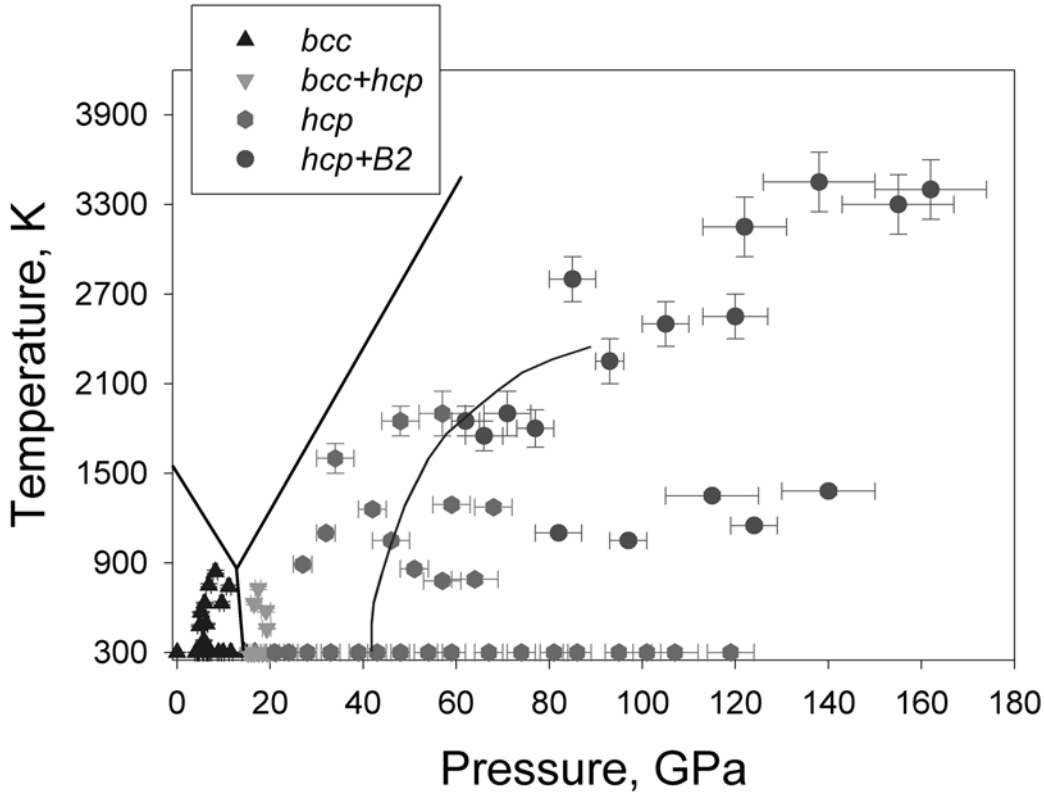

Fig. 3.3-3: Phases observed in electrically- (below 1500 K) and laser- (above 1500 K) heated DAC experiments with iron-silicon alloys (9.6(1), 5.1(1), 4.3(4) wt.% Si). We found that all alloys behave similarly and the symbols show these combined phase relations. Continuous black lines show the phase relations of pure iron. The solid curve originating at around 40 GPa is the phase boundary between *hcp* and *hcp+bcc* regions in Fe – 7.9 Si wt.% alloy from a previous study.

At the CMB pressure (140 GPa), the density of *B2* FeSi (~ 9.0 g/cm^3) is significantly lower than the density of the core (~ 10.0 g/cm^3) immediately below the CMB but significantly higher than the density of the overlying mantle (~ 5.6 g/cm^3). *B2* FeSi does not react with silicate perovskite, periclase or ferropericlase at conditions of Earth's lower mantle. This means that the silicon-rich alloy produced either by re-equilibration of proto-core metal in a magma ocean, or by reaction between iron and silicate at the CMB could accumulate at the boundary between the lower mantle and core. *Ab initio* simulations and measurements on *B2* FeSi recovered from multianvil experiments show that this compound is an electric conductor (conductivity of 6(1) 10^5 S/m measured at ambient conditions). The presence of *B2* FeSi at the base of Earth's mantle could thus explain its anomalously high electrical conductivity and provide a key for understanding why the amplitude the Earth's oscillation is out-of-phase with tidal forces.

c. *The behaviour of sulphur in metal-silicate core segregation experiments under reducing conditions (J. Siebert, V. Malavergne, R. Combes/Marne La Vallée and F. Guyot/Paris, in collaboration with D.J. Frost)*

Many geochemical mass balance calculations for the Earth imply a core composition with significant amounts of Si. This is, however, not consistent with the average oxygen fugacity of the silicate Earth as deduced from the bulk Fe^{2+} content of the upper mantle. Large amounts of Si in the core seem to be precluded because the equilibrium:

$$SiO_{2\ \text{in silicates}} + 2\ Fe_{\ \text{in metal}} \quad <=> \quad 2\ FeO_{\ \text{in silicates}} + Si_{\ \text{in metal}}$$

is displaced strongly to the left at ambient conditions and at moderate pressures and temperatures. This inconsistency could be resolved, however, if this equilibrium were found to proceed to some extent towards the right at some conditions compatible with core formation *i.e.* very high temperatures or pressures. Several previous high-pressure studies have been performed to test this possibility but only very few studies have examined the role of sulphur on this equilibrium. The main goal of this study was to determine if the presence of sulphur could affect the solubility of Si in liquid metal. The starting materials used were FeS, Si, natural enstatite $(Mg_{0.88}\ Fe_{0.12})SiO_3$ and synthetic enstatite ($MgSiO_3$). High-pressure high-temperature experiments were performed using a 1200-tonne multianvil apparatus. Samples were studied and analysed by optical microscopy, by SEM (equipped with an energy-dispersive X-ray analyzer (EDX) able to analyse oxygen quantitatively), and Raman spectroscopy.

Results show that during the experiments FeS and Si were combined into single large metallic blobs (Fig. 3.3-4). SEM images revealed that these blobs are composed of two phases; an Fe-S rich, Si-poor phase and an Fe-Si rich, S poor phase (Fig. 3.3-4). The textures indicate, however, that the liquid metal was a single phase at high pressure and temperature. At 1 bar there is a liquid miscibility gap in the Fe-S-Si system. Our observations thus suggest that, at 2000 °C and 20-25 GPa, this miscibility gap is closed or is at least considerably reduced, since our metal compositions would fall well within the gap existing at 1 bar.

The silicate material recovered in the experiments was mainly majorite, but stishovite was also observed at the contact between the metal and majorite. This suggests that some silicon was oxidized to stishovite. Abundant metal droplets observed within the majorite also imply that Fe^{2+} in the silicate phase was reduced, in accordance with the previously described equilibrium reaction. The Si content of the metal, however, is not very different from that which has been measured in the sulphur-free system at the same conditions. This means that the presence of sulphur in the liquid metal does not have a significant effect on the Si content at comparable redox conditions.

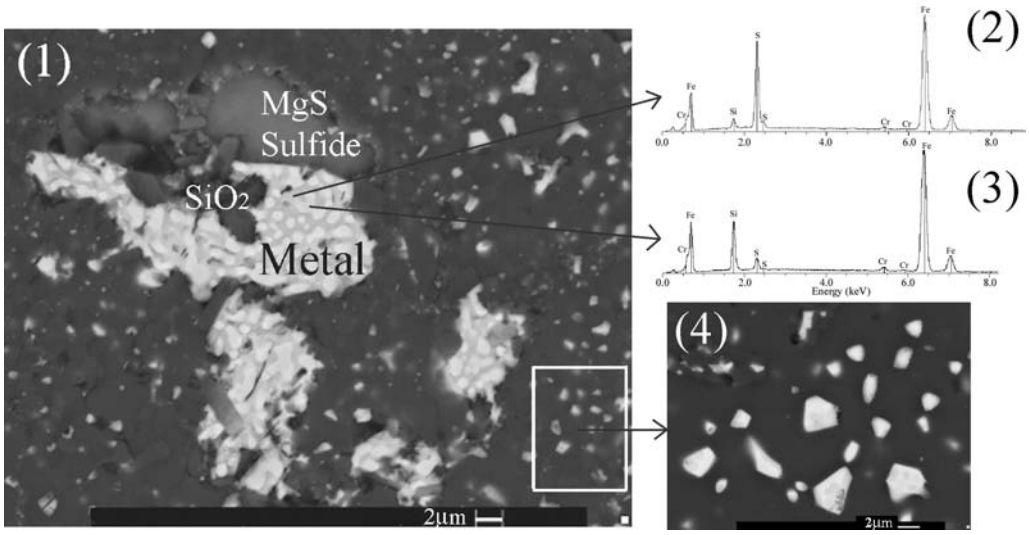

Fig. 3.3-4: (1) backscattered electron image of sample S2861. The Fe-Si rich, S poor phase (white) and Fe-S rich, Si poor phases (light grey) can be seen. SiO_2 and MgS-sulphide are observed in contact with the metal. (2) EDX spectrum of the Fe-S rich, Si poor metal phase (light grey). (3) EDX spectrum of the Fe-Si rich, S poor metal phase (white). (4) Enlargement of the region enclosed by the white frame in (1) showing small metal droplets formed by reduction of FeO in majorite. These metallic particles also show exsolution.

A MgS phase containing minor amounts of Fe and Ca, was also observed in contact with the liquid metal (Fig. 3.3-5). Cubic monosulfides with the general formula (Mg, Fe, Ca, Mn)S have been found in enstatite chondrites and in enstatite achondrites. These phases have no first order Raman spectra, however, in contrast to the MgS phase found in our samples.

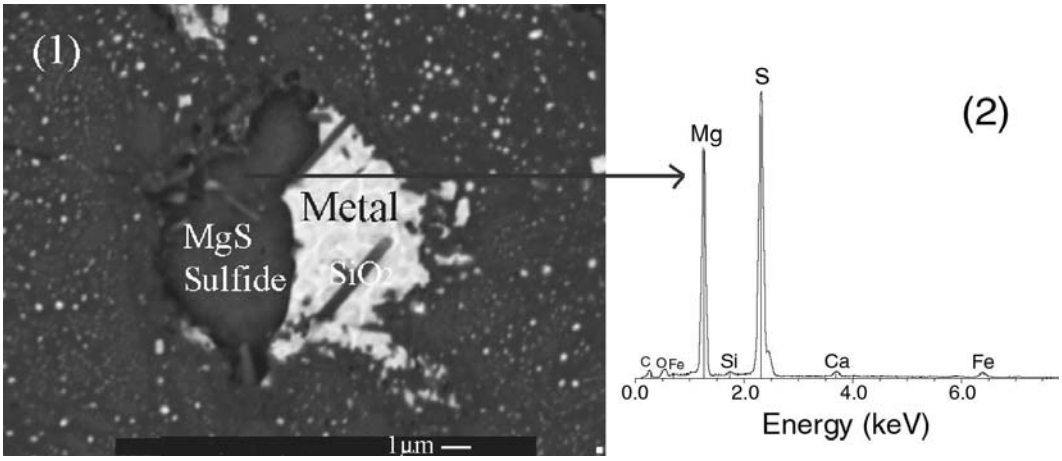

Fig. 3.3-5. (1) backscattered electron image of sample S2853. (2) EDX spectrum of the MgS sulfide (with small amounts of Ca and Fe) showing that stochiometry is close to MgS.

This magnesium sulphide phase is thus likely to be a high-pressure polymorph, the structure of which awaits determination. The formation of these sulphides requires exceptionally low oxygen fugacities. In our experiments, the formation of MgS most likely occurred by the reaction:

$2\ FeS + 2\ MgSiO_3 + Si_{\text{ in metal}} \Rightarrow 2\ MgS + 3\ SiO_2 + 2Fe_{\text{ in metal}}$

Our results imply that this reaction forms MgS between 20-25 GPa and 2000-2200 °C.

d. *Effect of high pressure on Fe-Mg interdiffusion in ferropericlase (C. Holzapfel, D.C. Rubie, S.J. Mackwell and D.J. Frost)*

Ferropericlase (Mg,Fe)O is one of the main constituent phases of the Earth's lower mantle. It forms by the breakdown of $(Mg,Fe)_2SiO_4$ ringwoodite, the stable high-pressure form of olivine, into silicate perovskite and ferropericlase at pressures corresponding to the 660 km discontinuity. Experimental investigations show that ferropericlase remains a stable phase over the whole range of the lower mantle between 660 km and 2900 km. Processes such as the chemical exchange between subducting slabs and the surrounding mantle and the interaction between the mantle and core forming metal all depend on the diffusional properties of the phases involved. In this study Fe-Mg interdiffusion experiments at high pressure were performed employing diffusion couples of ferropericlase with varying Fe-Mg compositions. These experiments were performed using a multianvil apparatus at pressures of 8-23 GPa, temperatures of 1653-2073 K and at oxygen fugacities corresponding to the Ni-NiO buffer.

Crystals of ferropericlase with different X_{FeO} contents, where X_{FeO} denotes mole fraction of FeO were synthesized by annealing them in oxide powders at 1 bar. The compositions used as diffusion couples were either $X_{FeO} = 0.07$ or pure MgO on one side and $X_{FeO} = 0.37$ on the other side. To buffer the oxygen fugacity the diffusion couples were embedded in a Ni capsule together with NiO powder. These capsules were run in a multianvil apparatus at the previously described conditions.

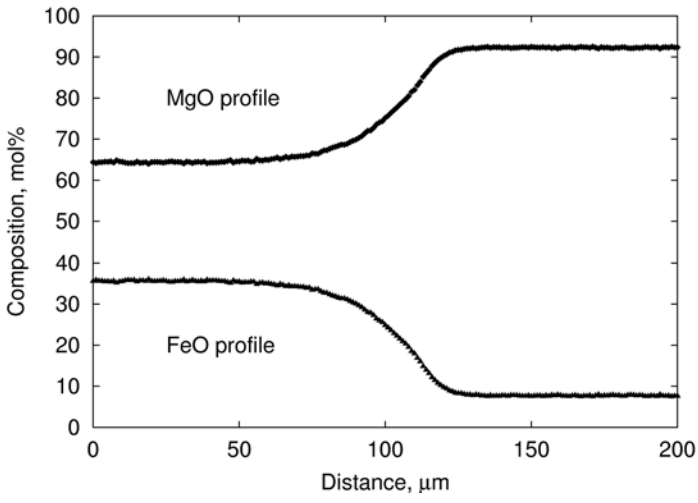

Fig. 3.3-6: Diffusion profile measured across the interface of a ferropericlase diffusion couple. The high-temperature, high-pressure anneal was performed at 23 GPa and 1656 K for 961 minutes. Asymmetry of the profile is clearly visible with a steeper concentration gradient at the MgO-rich side.

Diffusion profiles were analysed after the high-pressure, high-temperature anneals with an electron microprobe (Fig. 3.3-6). The profiles were approximately 75-200 µm in length. Due to the compositional dependence of diffusion the profiles are clearly asymmetric. Therefore, a numerical simulation using finite differences was performed. For compositions $X_{FeO} > 0.07$ a pure exponential dependence of the Fe-Mg interdiffusion coefficient was observed. For one experiment employing pure MgO as one end-member of the diffusion couple, Fe-Mg interdiffusion coefficients were overestimated by a pure exponential compositional dependence. The profile could only be properly simulated over the entire range of compositions by adding a power law term in the numerical algorithm. This is consistent with results of Fe-Mg interdiffusion experiments at 1 bar.

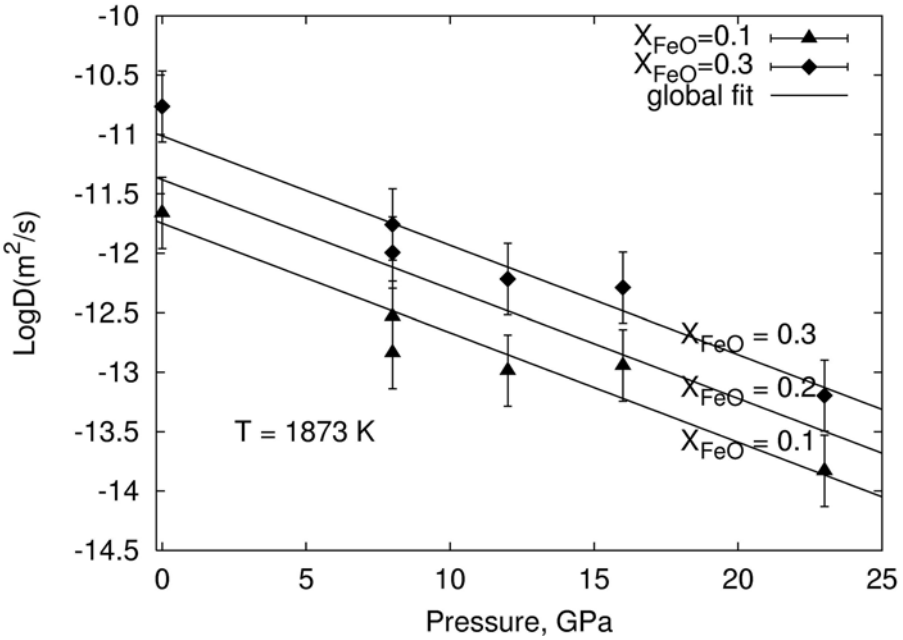

Fig. 3.3-7: LogD as function of pressure at a constant temperature of 1873 K. The data points have been recalculated to X_{FeO} = 0.1 and X_{FeO} = 0.3. Also shown are lines calculated by the global fit with values stated in the text.

The dependence of Fe-Mg interdiffusion on pressure is shown in Fig. 3.3-7. The data can be reproduced well with a global model employing a single activation energy (E_A = 255 ± 16 kJ/mole), activation volume (V_A = 3.3 ± 0.1 cm³/mole), preexponential factor (D_0 = (9.8 ± 0.7) x 10^{-6} m^2/sec), and composition term (α = 132 ± 13 kJ/mole) using the equation:

$$D_{Fe-Mg} = D_0 \cdot \exp\left(\frac{\alpha \cdot X_{FeO}}{R \cdot T}\right) \cdot \exp\left(-\frac{H_A + V_A \cdot P}{R \cdot T}\right)$$

Using this model for Fe-Mg interdiffusion at high pressures it is possible to calculate the diffusivity at different depths in the Earth. At the top of the lower mantle, diffusivity will be on the order of 0.5-1.1 $\times 10^{-13}$ m²/sec for compositions X_{FeO} = 0.1-0.2.

e. *Melting of Mg_2SiO_4 between 10-24 GPa (C. Liebske, D.J. Frost and D.C. Rubie, in collaboration with R.G. Trønnes/Reykjavik)*

Knowledge of the melting relations of mantle peridotite at high pressures is important for constraining models for the evolution of a crystallizing deep magma ocean, which may have formed during the accretion of the Earth. Melting experiments on mantle compositions can be performed up to 26 GPa using a multianvil apparatus, however, strong thermal gradients (up to 200-300 °C/mm), which are difficult to avoid due to the small samples sizes, complicate the interpretation of experimental results at very high pressures. One potentially complicating aspect resulting from the high thermal gradient is that minerals and partial melt tend to completely separate during a high-pressure experiment leaving a layer of melt and a layer of minerals. It seems impossible at high pressures (> 10 GPa) to produce a partially molten assemblage with interstitial liquid.

We are performing melting experiments on a simple Mg_2SiO_4 composition in order to investigate the effects of thermal gradients on mineral-melt separation. A technique to minimize these effects is presented. Studying this simple system also allows a treatment of the melting relations using simple thermodynamic formalisms. Experiments are being performed in a multianvil apparatus using a 10/4 (octahedral edge length/anvil truncation length in mm) pressure cell configuration with a $LaCrO_3$ heater and axially inserted W-Re thermocouples. The recovered phases are analysed by micro-Raman spectroscopy and electron microscopy.

Mg_2SiO_4 melts incongruently at pressures above 10 GPa. The determined melting curve (liquidus) of Mg_2SiO_4 (Fig. 3.3-8) appears to be slightly lower in temperature than determined in previous studies although the difference is still within the experimental uncertainties. Incongruent melting of forsterite and wadsleyite to produce liquid plus anhydrous phase B is observed between 15 and 17 GPa at ~ 2230 °C. At higher temperatures the melting reaction changes to periclase plus liquid. Between 18 to 23 GPa wadsleyite melts incongruently to periclase and liquid with an estimated Clapeyron slope of about + 5 °C/GPa. Melting of magnesium-silicate perovskite plus periclase was observed at 24 GPa. It is interesting to note that the determined melting curve of Mg_2SiO_4 is, within the uncertainties, almost identical to that of natural peridotite over the range of pressures examined.

The presence of a thermal gradient within the sample leads to a strong separation of crystals and melt. In some experiments where anhydrous phase B was observed a phase assemblage consisting of wadsleyite and majorite was also present at apparently lower temperature. This

observation is inconsistent with the bulk composition. It is therefore likely that the thermal gradient also causes a compositional gradient within the samples, which may lead to significant misinterpretation of experimental results. However, thermal gradients have the advantage that isobaric phase relations over a broad temperature range can be observed in a single experiment. In multi-chamber experiments (Fig. 3.3-9) several thin (~ 20-125 µm) sample chambers are stacked on top of each other in order to exploit the thermal gradient. The aim was to provide information about phase relations over a temperature range but to avoid any compositional gradient and separation between the hottest and coldest part of the assembly. However, as shown in Fig. 3.3-9 each of the capsules has an identical assemblage of liquid and crystals, which seems to suggest an identical thermal regime in each chamber.

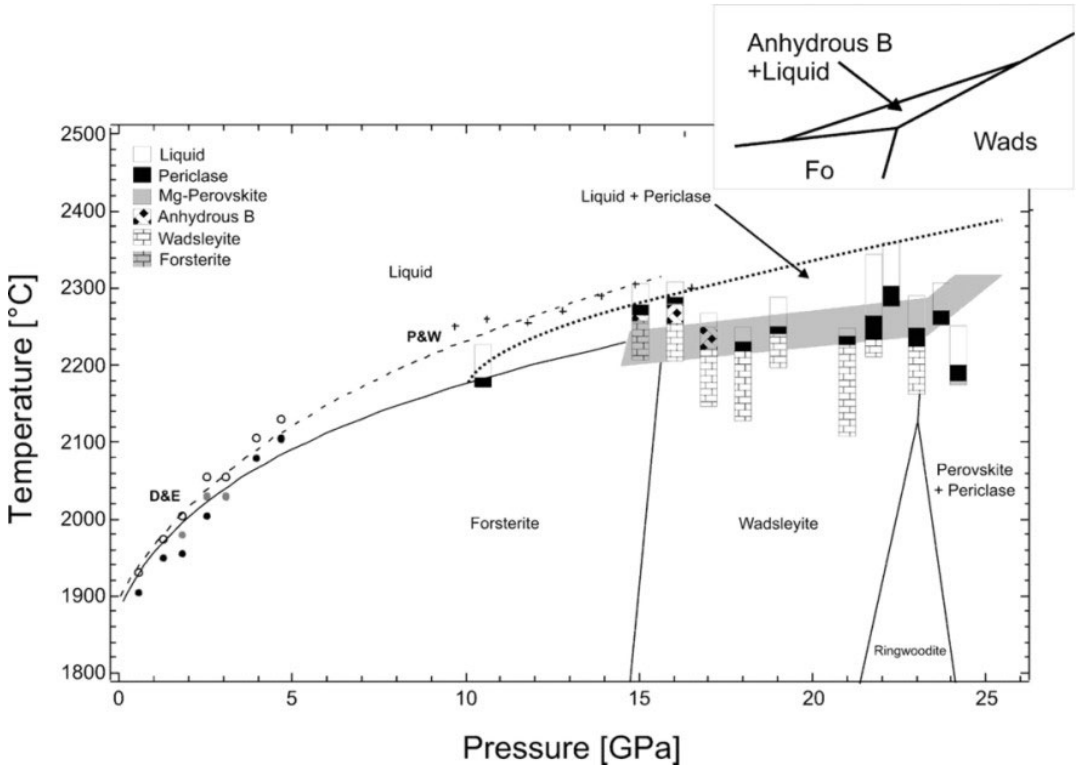

Fig. 3.3-8: Phase relations of Mg_2SiO_4. Previously published data shown as circles and crosses are included. The dashed line is a fit of a Simon equation to these previously published data. Our data are shown as bars with the length being an indication of the thermal gradient and the internal shading representing the various phases identified along this gradient. The change in slope of the melting curves of forsterite and wadsleyite cannot be resolved, although it must take place.

The difference in the thermal regime between capsules must, therefore, be relatively small and the thermal gradient within each capsule must be extremely small. Even so, separation of crystals and melt has occurred effectively. This effect seems to be unrelated to settling. The liquid is always separated to the thermocouple side of the experiment, whether this is inserted from the top or the bottom of the assembly. We conclude that the separation is most likely a

response to a thermal gradient, but an extremely minor one. Further study is required, but we believe that the reason why this separation takes place at high pressure probably has less to do with the larger thermal gradients but more to do with changes in silicate melt properties and melting phase relations at high pressure.

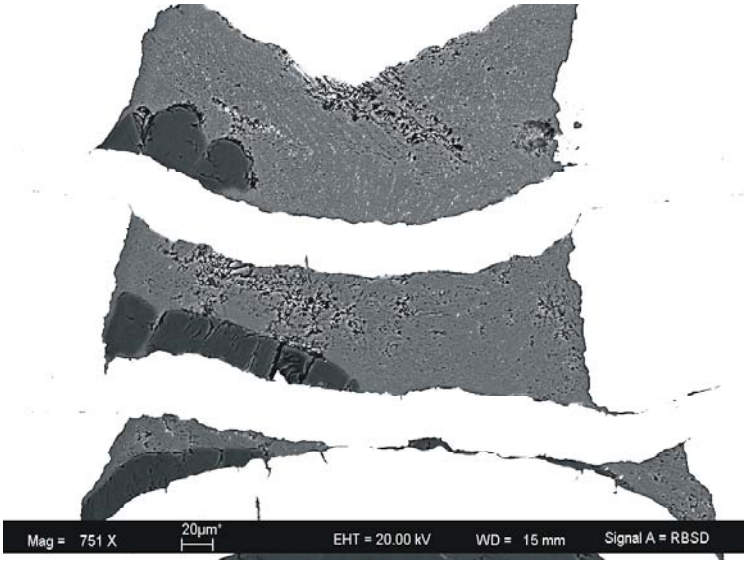

Fig. 3.3-9: Melting of Mg_2SiO_4 at 16 GPa and 2300 °C. All sample chambers consist of periclase and liquid. Separation of phases was thought to occur due to the presence of a strong thermal gradient but all sample chambers show the same assemblage and must therefore be at approximately the same temperature. The total length is 250 micons.

f. *Oxygen fugacity profile of the Slave cratonic mantle (C.A. McCammon, in collaboration with M. Kopylova/Vancouver)*

Oxygen fugacity is an important, although often neglected, parameter of the mantle. It can affect subsolidus and supersolidus phase relations as well as determine the presence and speciation of a fluid phase, and is hence relevant to diamond formation. A direct determination of oxygen fugacity can be made from equilibrium mineral assemblages, and investigations over the past decade have provided constraints on the oxygen fugacity of the lithosphere at depths within the spinel facies. Currently, however, there are only limited data from samples deeper than the spinel-garnet transition (120-150 km), since a reliable olivine-orthopyroxene-garnet oxybarometer has only recently been calibrated. Existing data include results from the Eastern Finland Kimberlite Province and the Kaapvaal craton, which show a decrease in oxygen fugacity with increasing depth. To extend our knowledge to other regions of the mantle, particularly with reference to diamond formation and mantle dynamics, we have commenced a study of mantle xenoliths from the Slave Province (northwestern Canada).

The sample set comprised single grains of garnet and spinel chosen from suites of peridotites, harzburgites, pyroxenites and megacrysts. Major element analysis was performed using the electron microprobe and the relative Fe^{3+} concentration was determined using the Mössbauer milliprobe. Pressures and temperatures were determined using various mineral

thermobarometers, and oxygen fugacities were calculated using the olivine-orthopyroxene-spinel and olivine-orthopyroxene-garnet oxybarometers.

Preliminary results show a significant decrease in oxygen fugacity with depth through the cratonic mantle, reaching values at 200 km depth that lie predominantly between the wüstite-magnetite (WM) and iron-wüstite (IW) buffers. The decrease is fully consistent with the reduced volume of ferric iron in garnet; hence upper mantle mineral assemblages containing garnet require no additional component to buffer the system. At greater depths, laboratory experiments have shown that the increased affinity of high-pressure phases for ferric iron should lower oxygen fugacity further, and so the general picture is of a relatively reduced deep upper mantle and transition zone. In contrast, highly oxidised xenoliths have been reported from regions of the lithosphere that experienced recent or active subduction, consistent with the infiltration of fluids derived from dehydration and decarbonation. Work is underway to correlate these observations with data from diamonds and their inclusions with a view to constructing a model for diamond genesis within the framework of mantle oxygen fugacity.

g. *Fe-Mg partitioning between magnesiowüstite, olivine and wadsleyite (D.J. Frost)*

The seismic discontinuity at 410 km depth in the Earth is believed to result from the phase transformation of $(Mg,Fe)_2SiO_4$ olivine to the high-pressure polymorph wadsleyite. The depth interval over which the discontinuity occurs appears in some regions of the Earth to be as sharp as 4 km, while in other regions it seems considerably broader, with estimates up to 35 km. While some of this variation may be an artefact of the range of different seismic methods employed, it is also possible that variations in width are caused by local changes in the mantle environment. If the physical and chemical properties that cause such variations in width could be experimentally calibrated then seismic observations could be inverted to give precise information on, for example, the local temperature or H_2O content of the mantle.

In the Fe_2SiO_4-Mg_2SiO_4 system the olivine to wadsleyite transformation occurs over a pressure interval as a result of the system being divariant. Previous studies have implied that this interval would be equivalent to a depth of at least 10 km in the Earth. Published phase equilibria determinations of this pressure interval may have lacked the required precision, however, and may have been influenced by the presence of H_2O or Fe^{3+}, which will act to broaden the transition. This pressure interval can be accurately calculated, however, from a detailed knowledge of the non-ideality of Fe-Mg mixing in the olivine and wadsleyite solid solutions. In order to constrain the activity-composition relations that describe non-ideal mixing, Fe-Mg partitioning experiments have been performed between magnesiowüstite and the three $(Mg,Fe)_2SiO_4$ polymorphs as a function of pressure at 1400 °C. Because the activity-composition relations in the magnesiowüstite solid solution are well known activities in the other phases can be determined through such partitioning experiments. In addition because

there is only weak pressure dependence to this Fe-Mg partitioning these experiments do not require high precision pressure determinations. In the experiments performed the presence of metallic Fe ensured redox conditions compatible with the transition zone and the H_2O contents of these samples were also found to be very low.

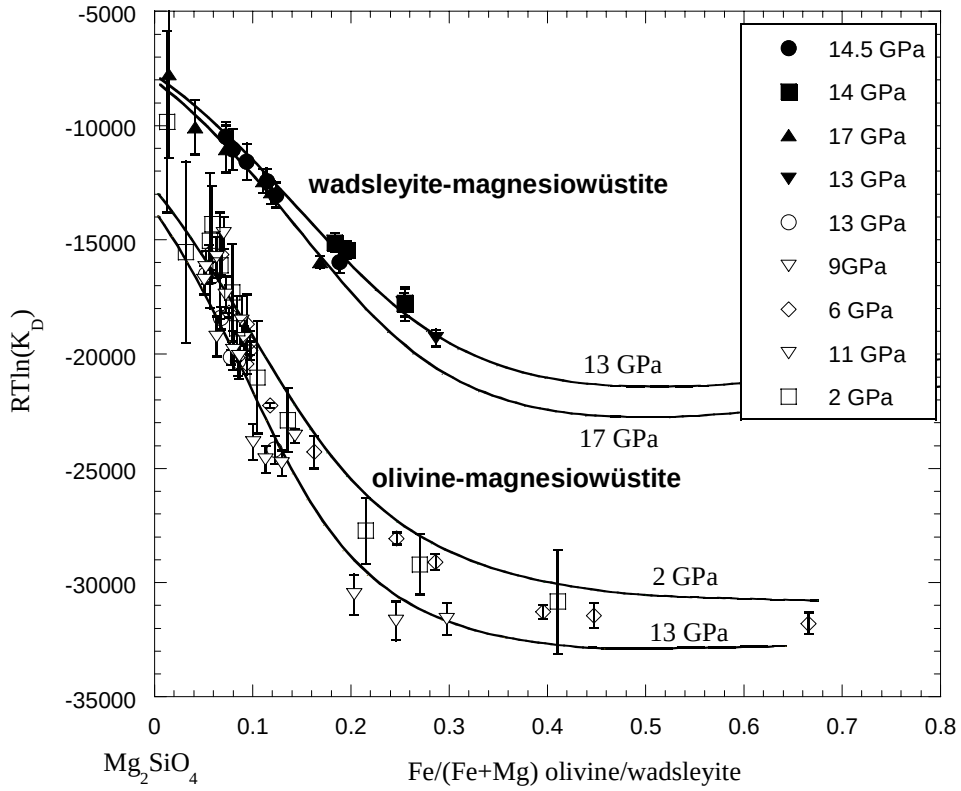

Fig 3.3-10: Fe-Mg partitioning between olivine and magnesiowüstite and wadsleyite and magnesiowüstite between 2 and 17 GPa at 1400 °C. The variation of $RTln(K_D)$ is a function of the non-ideality of Fe-Mg mixing in magnesiowüstite and the olivine polymorph solid solutions. $K_D=[XFe_{(ol)}.XMg_{(mw)}]/[XMg_{(ol)}.XFe_{(mw)}]$. As the activity-composition relations of magnesiowüstite are known those for wadsleyite and olivine can be determined from the fitted curves.

The Fe-Mg partitioning between magnesiowüstite and the two polymorphs olivine and wadsleyite can be described in terms of K_D the Fe-Mg distribution coefficient. Fig. 3.3-10 shows the variation of $RTln(K_D)$ with the Fe/(Mg+Fe) ratio of olivine and wadsleyite for partitioning between magnesiowüstite and these polymorphs. By fitting these data with isobaric curves the activity-composition relations for wadsleyite and olivine can be determined from those of magnesiowüstite. Combining these data with previously reported results on ringwoodite shows the degree of non-ideality of Fe-Mg mixing to decrease in the order wadsleyite>>ringwoodite>olivine. These partitioning data were used, along with published phase equilibria measurements for Mg_2SiO_4 and Fe_2SiO_4 end-member transformations, to refine thermodynamic data for the Mg_2SiO_4-Fe_2SiO_4 system at 1400 °C.

An internally consistent thermodynamic model was derived that reproduced the partitioning data and the end-member phase transformations in this system.

The Fe_2SiO_4-Mg_2SiO_4 phase diagram calculated from the refined thermodynamic data is shown in Fig. 3.3-11. The two-phase transformation region is much narrower than previous phase equilibria determinations. Peridotite mantle at a depth of 410 km would be comprised of approximately 60 % olivine, 30 % garnet and 10 % clinopyroxene. Fe-Mg partitioning between all these phases will influence the width of the discontinuity, although as clinopyroxene is relatively Fe poor its presence will have a minor effect. In Fig. 3.3-11 the transformation interval in the presence of 40 % garnet is shown to be substantially narrower than a garnet free transformation as a result of changes in the Fe-Mg partitioning between garnet and the $(Mg,Fe)_2SiO_4$ phases. The 410 km discontinuity in dry peridotite mantle at 1400 °C is therefore predicted to be approximately 5 km wide. An increase in temperature of less than 100 °C could explain seismic observations of a 4 km thick "410". Lower temperatures or the presence of H_2O in the mantle, on the other hand, could explain regional observations of a broader "410".

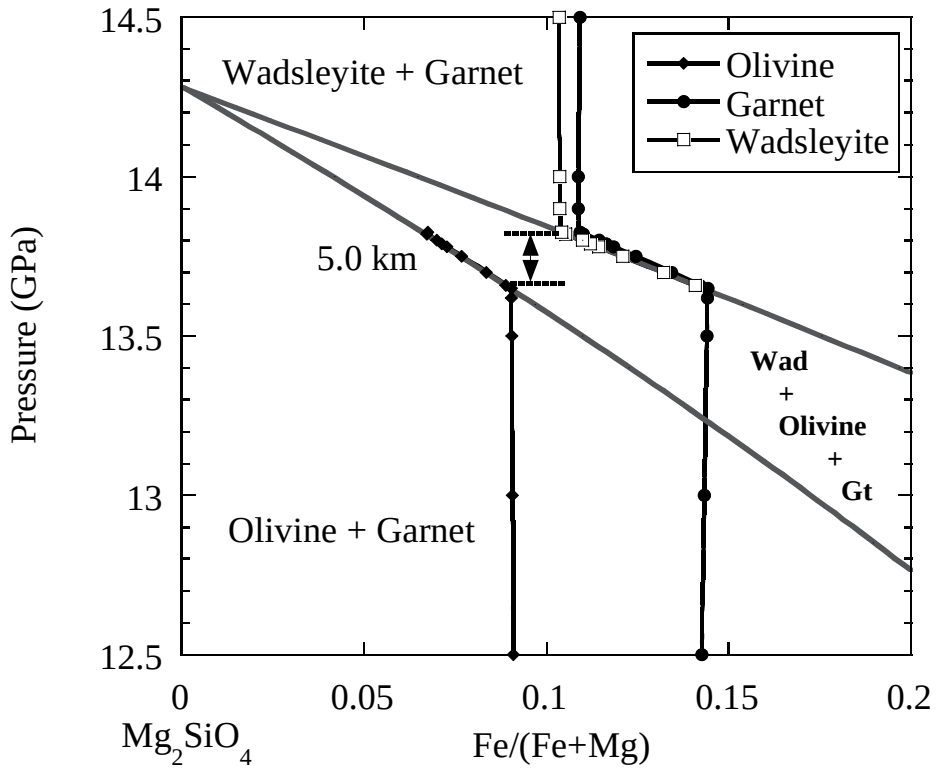

Fig. 3.3-11: A portion of the Mg_2SiO_4-Fe_2SiO_4 phase diagram at 1400 °C calculated from Fe-Mg partitioning between magnesiowüstite and the olivine polymorphs. The Fe contents of olivine, garnet and wadsleyite in a peridotite mantle composition are shown. The transformation interval in a peridotite composition is narrowed to approximately 5 km due to changes in the Fe-Mg partitioning between garnet and the $(Mg,Fe)_2SiO_4$ phases. The garnet Fe-Mg partitioning data were reported in the 2001 annual report.

h. *The stability of anhydrous phase B (J. Ganguly and D.J. Frost)*

Anhydrous B (Anh-B), $Mg_{14}(^{VI}Si)(^{VI}Si)_4O_{24}$, is a potentially important mineral in the Earth's mantle. It can form by the reaction of forsterite (Fo), Mg_2SiO_4, and periclase (Per), MgO, according to (a) Anh-B = 5Fo + 4Per. It can also form, along with stishovite (St), from the breakdown of Mg_2SiO_4 (β or γ high-pressure polymorphs) according to (b) 7 β/γ = Anh-B + 2 St. Thermodynamic considerations suggest that in both reactions, Anh-B should form on the lower temperature side of the phase boundary. It is possible, therefore, that Mg_2SiO_4 might transform to Anh-B + St in the interior of a cold subducting oceanic slab, which will have interesting consequences on slab density and buoyancy. Reaction (a) could also lead to stabilization of Anh-B in portions of the mantle which are silica deficient. Anh-B also appears on the peridotite solidus at pressures of approximately 15 GPa and would therefore have crystallized from a magma ocean at transition zone conditions. Since the equilibrium temperature of reaction (b) is likely to be too low to be amenable to laboratory investigation within a practical time scale, we undertook an investigation of reaction (a) with the objective of retrieving thermodynamic properties of Anh-B that would permit calculation of reaction (b).

We have determined the position of equilibrium (a) in a multianvil apparatus in the temperature range 900-1600 °C, using crystalline starting mixtures. The equilibrium boundary was bracketed by converting Anh-B to For + Per and also by the reverse reaction at different temperatures. The results, which are illustrated in Fig. 3.3-12, put very tight constraint on the equilibrium boundary.

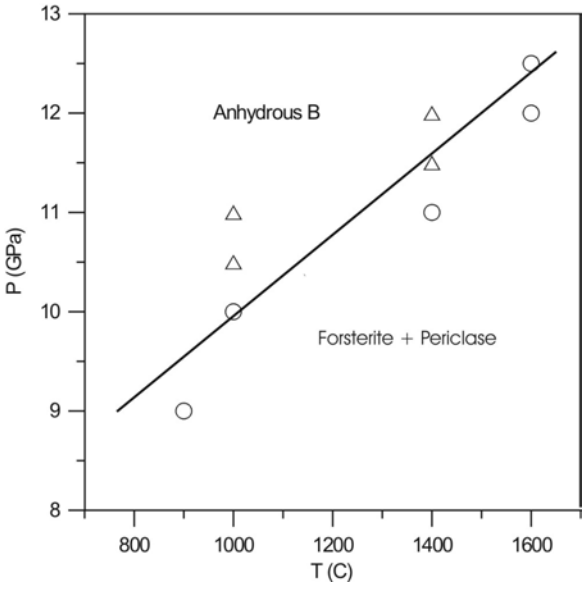

Fig. 3.3-12: Equilibrium boundary of the reaction For + Per = Anh-B, as determined in the multianvil press, by noting the direction of reaction in a crystalline starting mixture. Triangles indicate P-T conditions in the field of Anh-B, whereas circles indicate those in the field of For + Per. The uncertainty in the calibrated pressure is approximately 0.5 GPa.

Using a recent thermochemical database we retrieved the Gibbs energy of formation, $\Delta G_f°$, from the elements of Anh-B at the P-T conditions of equilibrium (a), and used these data to calculate equilibrium (b). The results show that the assemblage Anh-B + St will be stable only below 600 °C at 15 GPa, which is probably too low a temperature to be attained in the interior

of a subducting slab. However, decreasing $\Delta G_f°$ of Anh-B by only 0.1 % causes a sufficient expansion of its field of stability to make the assemblage Anh-B + St stable relative to either β or γ spinels within the interior of a cold subducting slab. Depending on whether we are dealing with β (wadsleyite) or γ (ringwoodite) phases, the equilibrium boundary of reaction (b) has a slope of ~ 18 bar/K or – 50 bar/K, respectively. These observations open the intriguing possibility that in the interior of a cold slab, the sequence of phase transformation of Mg_2SiO_4 with increasing depth may be: olivine→ β → Anh-B + St → γ.

i. *Preparation and investigation of solid Xe compounds relevant to the Earth (C. Sanloup/Paris, in collaboration with B.C. Schmidt*)

Xe is apparently depleted in the atmospheres of Earth and Mars in comparison to other gases. The aim of this project is to investigate if there are Xe-compounds that form at high pressure, which could exist in the Earth's interior and explain the missing Xe in the atmosphere. The stability of both xenon silicate and xenon clathrate phases at deep crustal pressures and temperatures has indeed been shown recently in diamond anvil cell experiments.

For the study presented here, Xe was loaded as a gas along with silica polymorphs or FeS into platinum capsules, which were then pressurized and heated using a piston-cylinder apparatus or a multianvil press. Samples quenched from 0.5-1.5 GPa and T > 1500 °C have a mean Xe concentration of 2.2 wt.% and up to 17 wt.% locally and a new, but minor phase was identified by X-ray diffraction. This new phase does not account for all the Xe trapped in the sample as there is still an important porosity on the sub-micron level. The much larger quantity of recovered material compared to DAC experiments combined with the high quality of the X-ray data acquired at the ESRF/Grenoble (Fig 3.3-13), allowed to further characterise the structure of this new phase, which was found to have hexagonal symmetry with the cell parameters: a=14.7 Å, c=16.2 Å. We propose that this phase is a SiO_2-Xe compound, probably a clathrasil with Xe hosted inside SiO_2 cages.

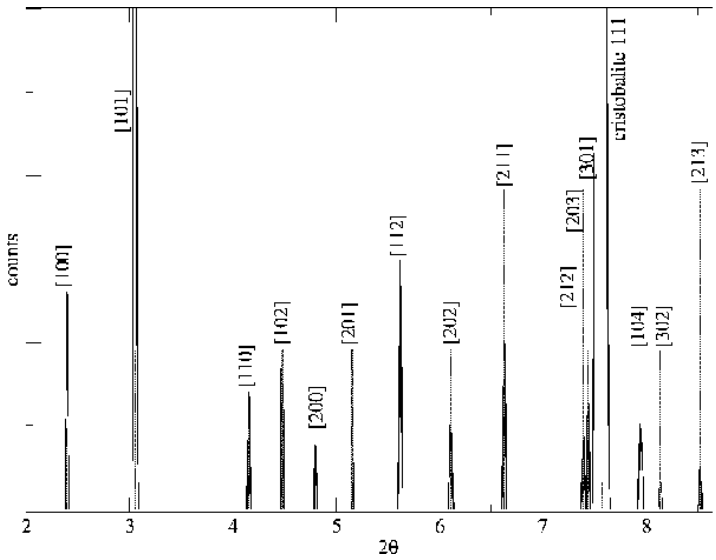

Fig 3.3-13: X-ray diffraction pattern collected at the ESRF Grenoble of a new SiO_2-Xe compound, most likely a Clathrasil where Xe is accommodated in SiO_2 cages.

Besides cristobalite, hydrated glass, quartz and silicate were used as the starting material for the high-pressure experiments. In all cases, the new phase was observed although in quite different proportions, which may be linked to different transport properties of Xe in the various silica polymorphs.

In the case of Xe-FeS experiments, the Fe-20wt.%S sample was separated from the Pt capsule by using an inner MgO single crystal capsule since Fe dissolves into platinum at high temperature. Two experiments were conducted at 10 GPa in the liquid field of Fe-20wt.%S and for both recovered samples no xenon was detected in the Fe-S zone by microprobe analysis. Xenon therefore does not dissolve (within EMPA detection limits) in Fe-S liquids, at least in the P-T conditions of this study. It is worth noting that contents of up to 0.3wt.% of Xe were measured in the MgO capsule, which was partially transformed to (Mg,Fe)O. However, due to the potential presence of microcracks in the single crystal capsule and in the absence of X-ray/TEM analysis, no firm conclusion can be reached so far.

j. *Supersilicic clinopyroxenes at high P and T in simplified and natural bulk compositions (J. Konzett/Innsbruck, in collaboration with D.J. Frost)*

In recent years an increasing number of ultra high pressure (UHP) rocks have been reported in the literature that contain clinopyroxene with oriented inclusions of quartz-rods or needles. These are interpreted as exsolution products from a pre-existing SiO_2-rich clinopyroxene which contained excess silica under peak metamorphic conditions. Two mechanisms have been proposed to account for excess silica in clinopyroxene:

1) The presence in solid solution of the Ca-Eskola component $Ca_{0.5}\square_{0.5}AlSi_2O_6$.
   Quartz exsolutions may form during uplift and exhumation due to the reaction $2Ca_{0.5}\square_{0.5}AlSi_2O_6 \Rightarrow CaAl_2SiO_6 + 3\ SiO_2$

2) The presence in solid solution of a clinopyroxene-component containing 6-coordinated silicon. The stability of a Na-rich clinopyroxene synthesized at 15 GPa and 1600 °C with a composition $Na(Mg_{0.5}Si_{0.5})Si_2O_6$ and Si in both tetrahedral and octahedral coordination, for example, has been previously confirmed.

The present study was initiated in an attempt to explore both these possibilities for the formation of quartz-exsolutions from UHP clinopyroxenes. To study the compositional evolution of clinopyroxene, especially with respect to its $Ca_{0.5}\square_{0.5}AlSi_2O_6$ content, a natural bulk composition from the North Dabie ultrahigh-pressure metamorphic complex in central-eastern China was used. This rock is a typical eclogitic assemblage, *i.e.* garnet + clinopyroxene + Ti-phase. In the field observations the clinoproxene contained quartz-rods. Experiments were performed with a multianvil apparatus in the P-T range 5-10 GPa and 800

to 1200 °C (relevant for a subduction P-T path) using graphite-lined Pt-capsules to keep fO_2 within reasonable limits and run durations between 12 hours and 3 days.

The lower P-stability limit of $^{[6]}$Si-clinopyroxene was studied using two simplified bulk compositions in the systems Na_2O-MgO-SiO_2 and Na_2O-CaO-MgO-SiO_2. Two potential reactions were examined:

$$2\ NaAlSi_2O_6 + 0.5\ Mg_2Si_2O_6 \Leftrightarrow 2\ Na(Mg_{0.5}Si_{0.5})Si_2O_6 + Al_2O_3$$

and

$$2\ NaAlSi_2O_6 + CaMgSi_2O_6 \Leftrightarrow 2\ Na(Mg_{0.5}Si_{0.5})Si_2O_6 + CaSiO_3 + Al_2O_3$$

These reactions are analogous to the majorite-forming reaction from pyrope + enstatite which also commences at similar conditions. Experiments were performed in the P-T range 5-10 GPa and 1200 °C with run durations of 12 to 14 hours. Preliminary results indicate that $Na(Mg_{0.5}Si_{0.5})Si_2O_6$ does not appear in solid solution at pressures $\leq$ 8 GPa in the bulk compositions used.

3.4 Metamorphism at different Time-Scales

Metamorphism occurs in the context of two basically different geological processes: (a) orogeny/plate tectonics and (b) impact cratering. Both geological processes differ particularly in terms of the time scale of metamorphic overprint. Orogeny is an endogenic process, which may last up to millions of years and is driven by slow mantle convection. This slow process results in severe changes in rock textures and in metamorphic reactions that produce new mineral assemblages. In contrast, impact metamorphism is an exogenic process, which results from bolide meteorite impacts and takes place in less than a few seconds. Minerals respond by specific transformation and deformation effects, diagnostic of the short-lived process. Typical rocks are impact breccias, which represent chaotic mixtures of melt lumps, mineral and rock clasts of different origin and degree of shock damage.

In recent years, important discoveries and advances have been achieved in both fields of metamorphism. In the field of regional metamorphism, the most spectacular rocks are possibly high and ultra-high-pressure metamorphic rocks (gneisses and eclogites) that are now increasingly recognised world-wide in metamorphic belts of various age. These rocks attract metamorphic petrologists because they contain spectacular high-pressure mineral assemblages with *e.g.* diamond and coesite. The metamorphic rocks underwent deep subduction followed by rapid exhumation and provide now unique insights in processes taking place at great depth in continent-continent collision zones. For example, the fine-scale study of rock fabrics and the characterization of defect microstructures in metamorphic minerals with SEM and TEM techniques provide important information on the deformation behaviour of deeply subducted rocks.

Research in the field of shock metamorphism focused recently on the formation of new high-pressure polymorphs in impact breccias and the decomposition behaviour of shocked volatile-rich minerals. Controlled shock experiments have largely contributed to a better understanding of the formation mechanism of high-pressure minerals and the degassing behaviour of carbonates and sulfates. The latter is important for understanding the evolution of Earth's climate and the role of shock-released toxic gases in the mass extinction pattern at the Cretaceous-Tertiary boundary.

a. *Insight into deformation mechanisms in garnet from high-pressure granulite shear zones (M.P. Terry and F. Heidelbach)*

Garnet is one of the most important metamorphic minerals in the crust and mantle. Its strength and unique internal structure gives it the ability to diffuse elements slowly, to include and protect inclusions from the early part of its growth history, and armour early deformation fabrics. Study of these aspects has made enormous contributions to petrology, structural geology, and tectonics. Here, we link petrologic, microstructural, and textural observations in

naturally deformed gabbro at conditions of 780 °C and 1.8 GPa to determine the metamorphic reactions producing garnet, the timing of garnet growth relative to deformation, and provide insight into deformation mechanisms.

The Haram Gabbro was metamorphosed to conditions approaching the high-pressure stability limit of plagioclase. In the absence of strong deformation, gabbros commonly show the development of corona textures around pre-existing mafic minerals (Fig. 3.4-1A) controlled by diffusion of elements. These textures are well developed in the Haram Gabbro away from shear zones. Strongly deformed areas show alternating layers that are typically dominated by plagioclase, garnet, omphacite, and ilmenite with original igneous pyroxene occurring as porphyroclasts. The assemblage varies slightly based on bulk composition but textural relations among the minerals present indicate that the development of the coronas and the gneissic layers were produced by the same general reactions:

1) Ca plagioclase + Orthopyroxene = Garnet + Omphacite + Kyanite + Na plagioclase + Qtz.
2) Ca plagioclase + Orthopyroxene + Spinel = Omphacite + Garnet + Na plagioclase.

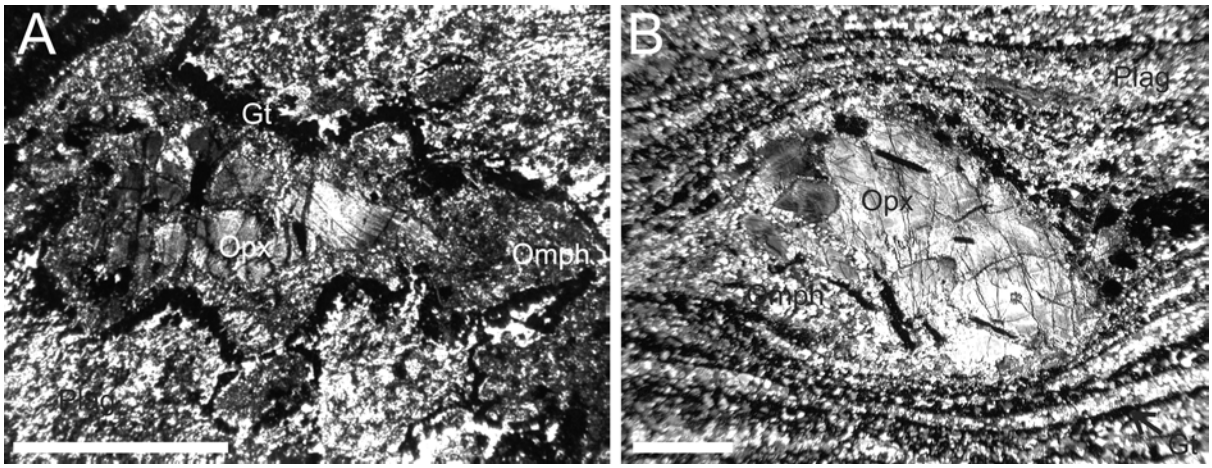

Fig. 3.4-1. Photomicrographs of garnet corona gabbro from sample 1630 outside (A) and sample 453 within (B) mylonite zone showing evidence for the reactions described above (scale bars = 2 mm).

Reaction products, plagioclase and kyanite, show a strong preferred grain shape orientation related to deformation in the shear zones. Garnet occurs in layers up to a few hundred microns in width and isolated grains down to just a few microns in diameter. Omphacite occurs as polycrystalline layers in strain shadows around orthopyroxene porphyroclasts (Fig. 3.4-1B).

Mapping of garnet, plagioclase, omphacite, and ilmenite using EBSD to determine lattice orientation was completed on samples that represent a range of strains inside and outside shear zones. Plagioclase, ilmenite, and omphacite all show texture related to the deformation

in the shear zone. Orientation data for garnet shows a weak local texture but overall there is no clear texture related to the deformation.

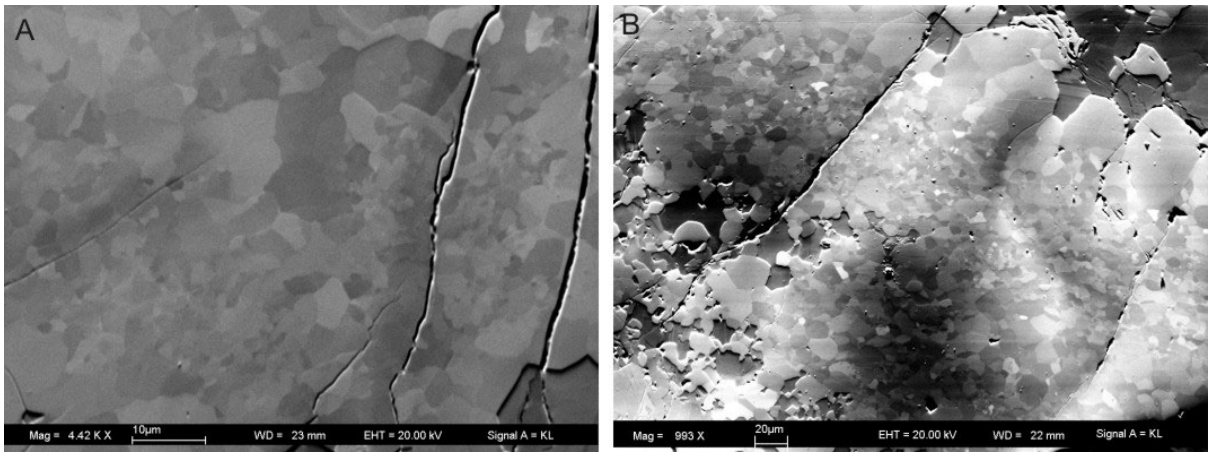

Fig. 3.4-2. Orientation contrast images of garnet in layers corona from sample 1630 outside the mylonite zone (A) and sample 453 in a mylonite zone (B).

Garnet layers viewed in orientation contrast images of deformed and undeformed samples have similar grain size ranges from ~ 1-150 µm (Fig. 3.4-2). The different grain sizes of garnet in the deformed samples are much more organized, with fine grain sizes (~ 1-15) in the interior of the layer toward ilmenite or omphacite with coarse grain sizes (~ 50-100) adjacent to plagioclase rich zones (Fig. 3.4-1B). The fine grained areas in the deformed samples appear often to have a preferred grain shape orientation. Other important structures seen in garnet layers are in pinning structure, local development of granoblastic structure, and grain boundary bulging.

Microstructures and textures indicate that all reaction products in deformed areas were growing at the time of deformation with the exception of garnet. However, the metamorphic reactions described above could not have proceeded in the absence of garnet. Thus, garnet must have been present during deformation. The very fine grain size of garnet in layers from deformed and undeformed samples is interpreted to result from metamorphic overstepping of reaction. The coarse grain size of garnet on the outer part of the layer is attributed to reduction in strain rate and in the shear zones during continued growth of garnet.

The absence or local development of a weak texture in garnet indicates that fine grain size is compatible with boundary sliding as the dominant deformation mechanism for garnet. The development of subgrains and local evidence for a texture in garnet indicate that intra-crystalline deformation mechanisms were operating but were not the dominant deformation mechanism, probably due to the relatively high strength of garnet. Other features including bulging, pinning and local granoblastic textures indicate that grain boundary migration occurred and garnet experienced local recrystallization and recovery within the layers.

b. *UHP metamorphism of a kyanite-garnet gneiss from Fjørtoft, Western Norway (P. Robinson/Trondheim, F. Langenhorst and M.P. Terry)*

Nearly a decade ago microdiamonds were discovered in kyanite-garnet-graphite gneiss, at Fjørtoft, using a total rock digestion process. More recently the island was mapped and geothermometry on a kyanite eclogite, containing polycrystalline pseudomorphs of coesite, yielded T = 820 °C and P = 34-39 kbar on the edge of the diamond stability field. Nevertheless there has been no record of microdiamonds *in situ* in a mineral host. We used a special rock polishing techniques to test a number of specimens for the occurrence of microdiamonds. This permits location of microdiamonds over relative large areas on specially polished surfaces. At the same time attention was focused on some samples with garnets up to 5 cm in diameter, in the hopes that these would contain mineralogical relics from the UHP conditions under which these rocks were presumed to have equilibrated, despite a strong amphibolite-facies metamorphic overprint. Based on the present assemblage of quartz-kyanite-garnet-biotite-plagioclase-K-feldspar-rutile-graphite, it was postulated that under UHP conditions the rocks would have consisted of coesite-kyanite-garnet-phengite-jadeite-rutile ± diamond.

Despite careful work on 6-8 polished surfaces, covering both large garnets and fine-grained matrix, no traces of microdiamonds were found. Transmitted- and reflected-light examination of polished thin sections including both large and small garnets, and qualitative SEM analyses, showed the following: 1) Numerous monocrystalline quartz grains inside garnet, but no recognizable polycrystalline quartz aggregates after coesite as found in the nearby kyanite eclogite; 2) Abundant inclusions of graphite plates; 3) Inclusions of colorless mica, commonly associated with kyanite and coarse rutile; 4) Fine colorless, low birefringent needles of kyanite; 5) Rounded high-relief, high-birefringent inclusions with white internal reflections are Nb-rich rutile (Fig. 3.4-3). This is distinct from coarse polycrystalline rutile as inclusions in garnet and in matrix, and monocrystalline rutile rods apparently exsolved from outer parts of garnet.

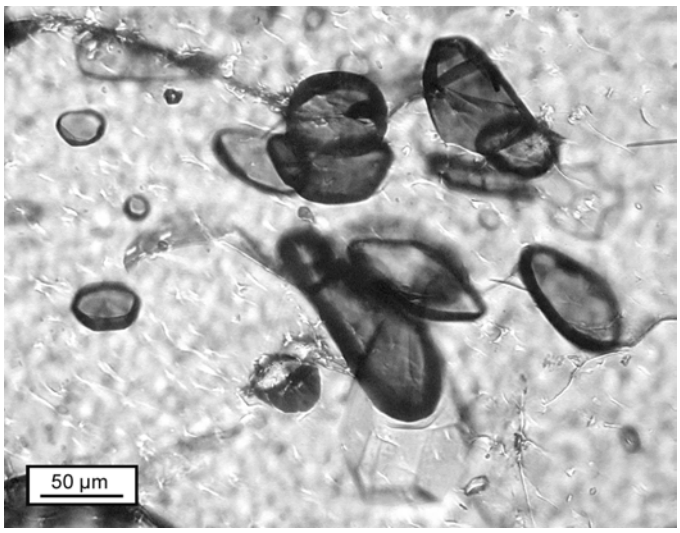

Fig. 3.4-3. Optical micrograph of Nb-rich rutile crystals occurring as inclusions in garnet.

Accepting the correctness of earlier reports of scarce microdiamond in these outcrops, we now would interpret the large garnets as having grown and included monocrystalline quartz, graphite, kyanite, white mica, and rutile in an amphibolite-facies prograde path well before reaching UHP conditions. If correct, then the postulated UHP mineralogy would have appeared late and in the matrix where most susceptible to later amphibolite facies retrograding. This has important implications for interpreting previously reported U-Th-Pb ages of monazite in these rocks: 407 Ma as the maximum age of inclusions of monazite in garnet and 395 Ma as the time of retrograde equilibration. We are currently examining the pattern of chemical zoning in the garnets with respect to the distribution of the three types of rutile, to learn more about metamorphic evolution.

c. *Microstructure of metamorphic coesite from Dora Maira, Alps (F. Langenhorst and J.-P. Poirier, in collaboration with H.-P. Schertl/Bochum)*

In 1981, Chopin reported the first discovery of metamorphic coesite in a pyrope-quarzite from the Dora Maira Massif, Alps. The presence of relic coesite indicates that the metamorphic host rock was subducted to depths greater than 100 km, at peak metamorphic conditions of 3.7 GPa and 800 °C. The coesite occurs as inclusions in garnets and is surrounded by a rim of retrograde quartz, displaying usually a palisade structure.

The knowledge of the mechanical properties of coesite is important for understanding the rheology and deformation behaviour of lower crustal rocks and deeply subducted crustal slabs. Almost nothing is known however about the rheological laws and slip systems of coesite. Therefore, we conducted a transmission electron microscopy (TEM) study and characterized the dislocations in Dora Maira coesite. Furthermore, the TEM study was aimed to gather structural information on the back-transformation to quartz.

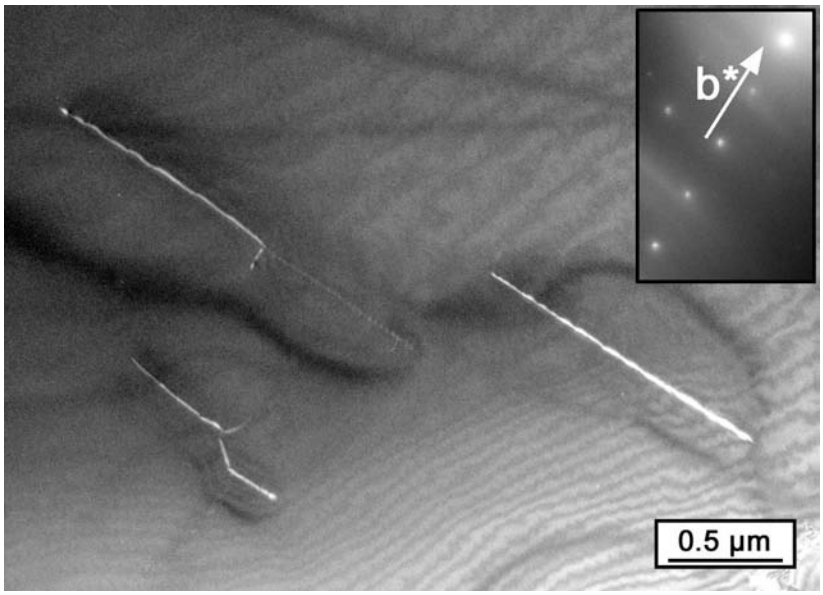

Fig. 3.4-4: Dark-field TEM image of dislocation nodes in Dora Maira coesite. Analysis of the node configuration reveals the reaction between ***a*** and ***a***+***b*** dislocations.

Coesite from Dora Maira exhibits very few signs of plastic deformation; dislocation densities are always less than 10^{11} m^{-2}. Most dislocations are straight and presumably sessile but there are also few examples of dislocation loops, nodes and dipoles (Fig. 3.4-4). The Burgers vectors of dislocations in monoclinic coesite are [100], [001], [110] (*i.e.*, ***a***, ***c***, and ***a***+***b***) and other symmetrically almost identical vectors. In the hexagonal setting, these Burgers vectors correspond to ***a*** and ***a***+***c***, just as in quartz. The (110) plane could be identified as a slip plane. Small prismatic dislocation loops with Burgers vector [010] (***c*** in the hexagonal setting) are also observed and are possibly formed by water-related defects.

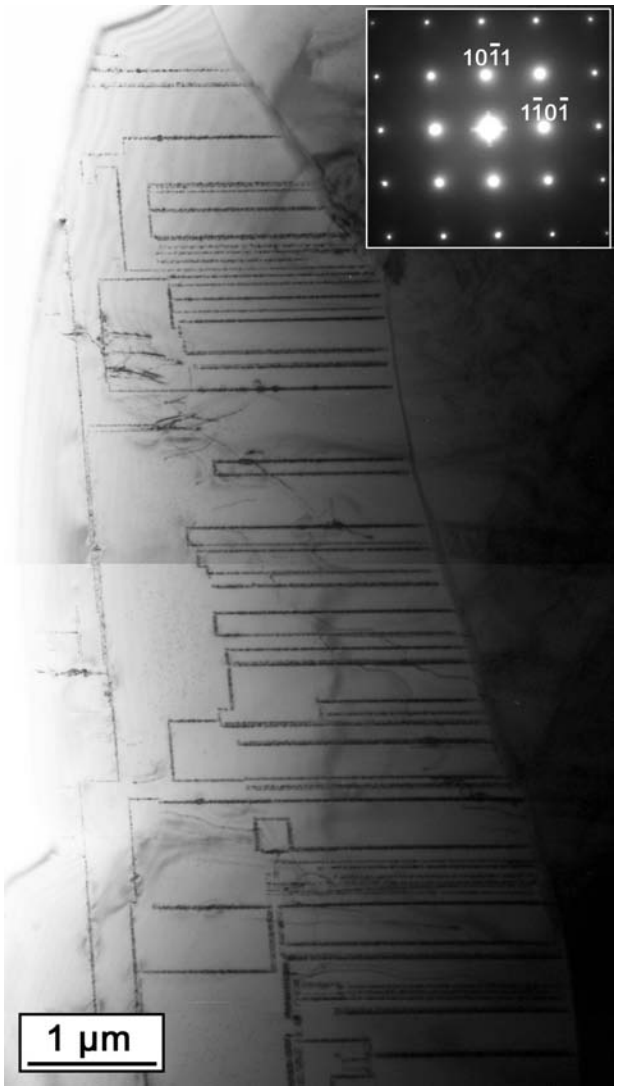

Fig. 3.4-5. Bright-field TEM image of Brazil twins parallel to $\{10\bar{1}1\}$ planes in palisade quartz.

Retrograde quartz occurs at the margin of coesite with the palisade texture and as discrete veins within coesite. Palisade quartz exhibits a high dislocation density of dislocations pinned on bubbles and Brazil twins parallel to $\{10\bar{1}1\}$ planes (Fig. 3.4-5). The twin planes are

decorated with a large number of water-related bubbles. The quartz veins are aligned parallel to (100) and (021) composition planes of rotation twins in coesite. These observations indicate that back-transformation starts at grain and twin boundaries, and that coesite loses water to quartz during transformation. Altogether, the results show that water plays an important role in both formation of dislocations and back transformation to quartz.

d. *A transparent, very hard and dense form of carbon in heavily shocked gneisses from Popigai, Russia (A. El Goresy/Mainz, L.S. Dubrovinsky, P. Gillet/Lyon, V.L. Masaitis/St. Petersburg)*

Diamonds encountered in heavily shocked gneisses of impact craters were produced by shock-induced solid-state phase transformation of graphite to diamond. The diamond is polycrystalline with crystallite sizes in the range from a few to hundreds nanometers. Shocked Lappajärvi and Popigai gneisses contain, in addition to diamond and graphite, a coating of amorphous carbon. Recently, we reported transparent hard very dense carbon platelets in shocked gneisses from the Ries crater that are "Raman inactive". We have conducted *in situ* investigations on polished thin sections (PTS) of shocked gneisses from Popigai, Russia, using reflected-light microscopy, laser micro Raman spectroscopy, and X-ray synchrotron powder diffraction. Of special interest is to scrutinize the nature of the transparent, hard and very dense carbon species we discovered both in Ries and Popigai shocked rocks.

Two distinct types of very hard dense carbon phases were encountered in the PTS: (a) large (30-200 μm) transparent flat platelets with very high relief. They display uneven surfaces due to high resistance to polishing, (b) small grains (1-12 μm) with high relief. Phase (a) is distinctly harder than phase (b) as deduced from the magnitude of their relief. Both types display radiating scratches characteristic of diamond and are abundantly intergrown with graphite. EDX analysis at low voltage using a Field Emission SEM (FESEM) indicated that both materials are pure carbon. Laser micro Raman studies of several grains of the two objects revealed two distinct Raman spectra. The large transparent grains (a) depict high fluorescence background and broad Raman bands with values different than those of graphite and diamond. In contrast, the small grains (b) display a sharp Raman band at 1331 cm^{-1} characteristic of cubic diamond. X-ray diffraction (Fig. 3.4-6) shows in grain (b) that both diamond and lonsdaleite regions are present.

Apparently, the shock events in Popigai and the Ries induced phase transition of graphite to two different transparent, hard and dense species: (a) very dense transparent platelets that display broad Raman bands with different values than those of graphite and diamond, and (b) cubic diamond. The Raman spectrum of (a) is not necesssarily the pristine signature of the phase. The present phase could not have formed by phase transition of diamond to this species at high post-shock temperatures, since the host Ries rocks experienced very low post-shock temperatures. We also suspect that the original phase is very sensitive to laser or electron

irradiation, is highly metastable and looses its structural nature during the Raman measurement. The original phase was definitely much harder than diamond and surprisingly retained its transparent and super-hard nature despite the laser irradiation. The relatively harder nature and the lack of the characteristic Raman bands of diamond argue against diamond or lonsdaleite as the possible parental phase. The lack of intimate intergrowth between (a) and (b) is another evidence against a genetic link between the two. One plausible explanation for the high fluorescence is the presence of pending bonds related to structural disorder. X-ray investigations to characterize the nature of this phase using synchrotron radiation are under way.

Our findings have several important consequences: (1) Dense carbon phases occurring in naturally shocked gneisses consist of two distinct very dense species formed by different mechanisms: transparent constituent (a) and diamond (b). The exact nature of (a) or its parental phase is not known for the time being. (2) The shock events in Popigai and Ries produced the different dense carbon constituents in different grain-size ranges. (3) Shocked gneisses in Popigai contain considerable amounts of secondary highly ordered graphite, along with the shocked highly disordered primary graphite. Both graphites abundantly occur attached to constituent (a) or to diamond (b). Mechanical separation of the two graphites in residues obtained by chemical demineralization processes is difficult to achieve, if not impossible. Carbon isotopic measurements conducted on graphite in residues represent the average of the isotopic signatures of two genetically different graphites. In addition, carbon isotopic composition of transparent grains obtained from the same residues reflect the average of constituents (a) and (b).

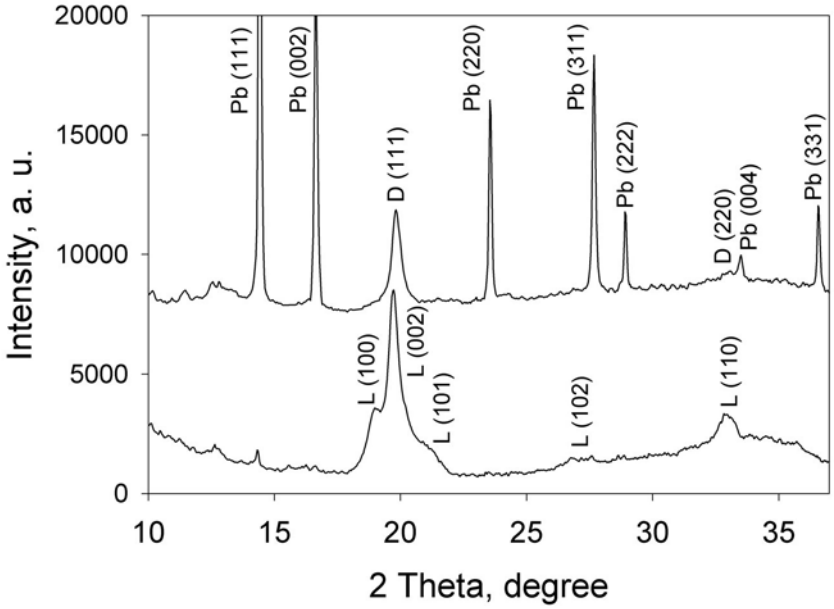

Fig. 3.4-6. X-ray powder diffractions of two regions of the carbon grain from Popigai shocked rock (wavelength 0.7 Å, data collected at SNBL/ESRF).

e. *Formation of ringwoodite in high-explosive experiments on muscovite-biotite-quartz slates (E. Kozlov/Snezhinsk, L. Sazonova and V. Feldman/Moscow, N.A. Dubrovinskaia and L.S. Dubrovinsky)*

In order to study the formation of impactites in the astrobleme Janisjarvi (Karelia, Russia), a series of shock compression experiments has been conducted. The experiments were performed in the Research Institute of Technical Physics, Snezhinsk, Chelyabinsk Region, Russia. A shocked mineral aggregate was obtained in high-explosive experiments on muscovite-biotite-quartz slates, using a setup with a spherically converging shock wave geometry. These slates contain garnet and staurolite porphyroblasts and dominate among the target rocks of Janisjarvi astrobleme impactites formation.

The sample of the laminated rock had the form of a sphere with its initial diameter equal to 49 mm and an average volume density ρ_0=2.803 g/cm^3. The sphere was welded up into the hermetic jackets of austenite steel. It was then subjected to spherical explosive compression by detonating an outer layer of high-explosive with a thickness of 10 mm. Shock pressure on the outer surface of the sample was 25 GPa and increased to 300 GPa at a distance of 1 mm from the center of the sphere. High quenching rates of 10^8-10^9 °C/s may favour the preservation of high-PT phases in the shocked samples.

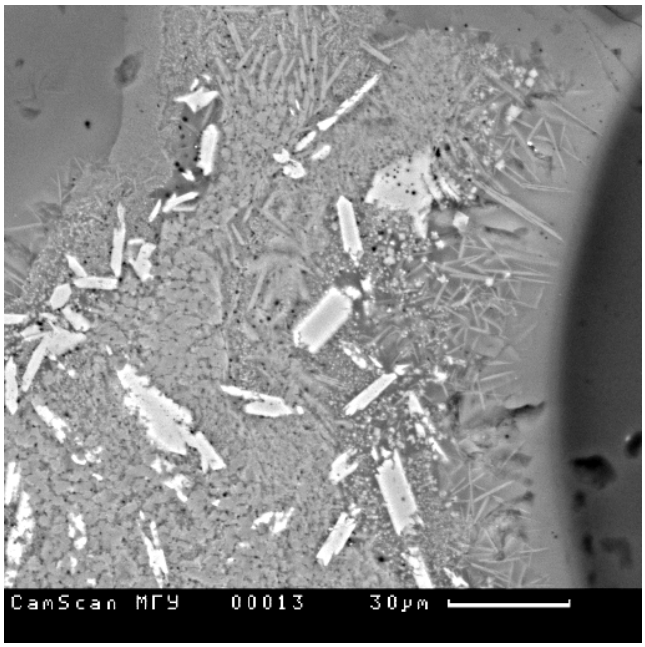

Fig. 3.4-7. The mineral aggregate obtained on decomposition of biotite. Grey mass - an amorphous matrix with residual nontransformed biotite, very small white grains- hercynite, white elongated crystals- ringwoodite. The pressure of formation of ringwoodite may be estimated from the distance from the centre of the sphere and it is about 22 GPa for the composition SiO_2 – 32.84, TiO_2 – 0.43, Al_2O_3 – 8.53, FeO – 28.78, MgO – 28.97, K_2O – 0.12 and 28 GPa for the composition SiO_2 – 30.54, TiO_2 – 0.27, Al_2O_3 – 8.92, FeO – 35.54, MgO – 24.29, K_2O – 0.09.

The mineral aggregate obtained on decomposition of biotite (Fig. 3.4-7) consists of an amorphous matrix, hercynite, and a substance with a chemical composition allowing to propose that it is ringwoodite. The analyses show a high Al content (0.94-14.17 wt.%), which is unusual for ringwoodite. The Raman spectrum of ringwoodite is known quite well at ambient conditions. It has a characteristic doublet between 780 and 900 cm^{-1}. To analyze the sample a LabRam spectrometer with a 632 nm laser was used. Raman spectra were recorded using a ×50 objective and a confocal hole of 1.1 mm. In such a configuration the studied area is approximately 7 μm in the focal plane and the depth of the focus is less than 10 μm. The resolution was 2 cm^{-1}. Figure 3.4-8 shows the three Raman spectra in the interval 500-900 cm^{-1}: a) synthetic ringwoodite, b) and c) the spectra from white elongated crystals (see Fig. 3.4-7). Clear similarities in the spectra allowed us to identify the unknown white mineral as ringwoodite. In natural impactites ringwoodite has been found just in impact rocks Extremadura, Spain, where its skeleton crystals were formed from a rapidly cooled melt. The ringwoodite we studied was formed from the target rocks due to a solid-state transformation (no morphological signs of melting were observed). In nature, such ringwoodite could potentially be found only in rocks originated from astroblemes, because these rocks are subjected to the high-parameter shock metamorphism without melting and may become a source of quenched high PT mineral phases.

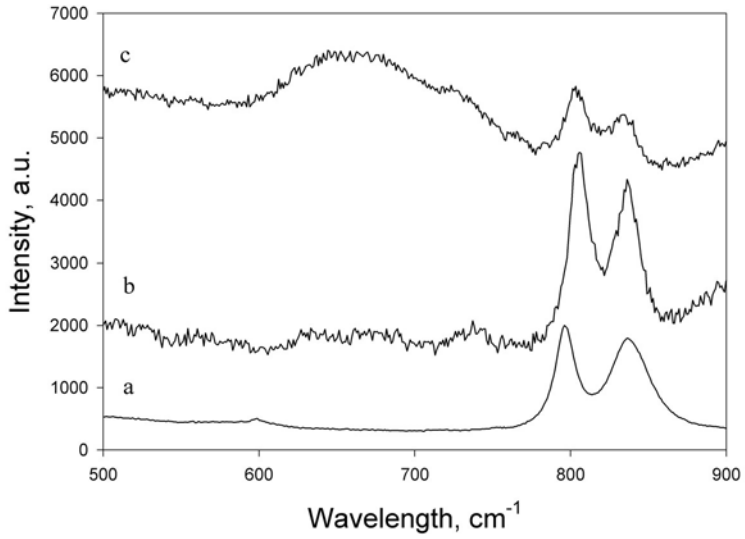

Fig. 3.4-8. Raman spectra from synthetic ringwoodite (a), and from white elongated crystals (b,c) (see Fig. 3.4-7).

f. *Experimental study of shock deformation and decomposition of anhydrite (F. Langenhorst, in collaboration with A. Deutsch/Münster and U. Hornemann/Efringen-Kirchen)*

Bolide impacts into carbonate and sulfate-rich target rocks liberate large amounts of the greenhouse gases CO_2 and SO_x and hence may have significantly influenced the evolution of

Earth's atmosphere. In case of the 65 Ma old Chicxulub impact and the related Cretaceous/Tertiary (K/T) boundary, it has been argued that the perturbation of the atmosphere with these gases was sufficient to considerably modify its radiative balance and to increase rain acidity. To assess the effects on the climate and biosphere, it is however important to quantify the amounts of these gases, which in turn requires the knowledge of the threshold pressures and temperatures for devolatilization.

Recent theoretical assessments indicate that in the context of the Chicxulub event, global warming due to CO_2 input was minor compared to cooling due to SO_x gases. Despite this potential importance of impact-released SO_x gases, the shock-metamorphic behaviour of sulfates is much less studied than that of carbonates. We therefore conducted a series of conventional high-explosive shock experiments in the pressure range from 12.5 to 85 GPa. Samples were embedded into iron containers to allow complete recovery of material for post-mortem studies. Samples shocked to pressures < 46.5 GPa are highly fragmented powders, whereas above this pressure limit samples are compact.

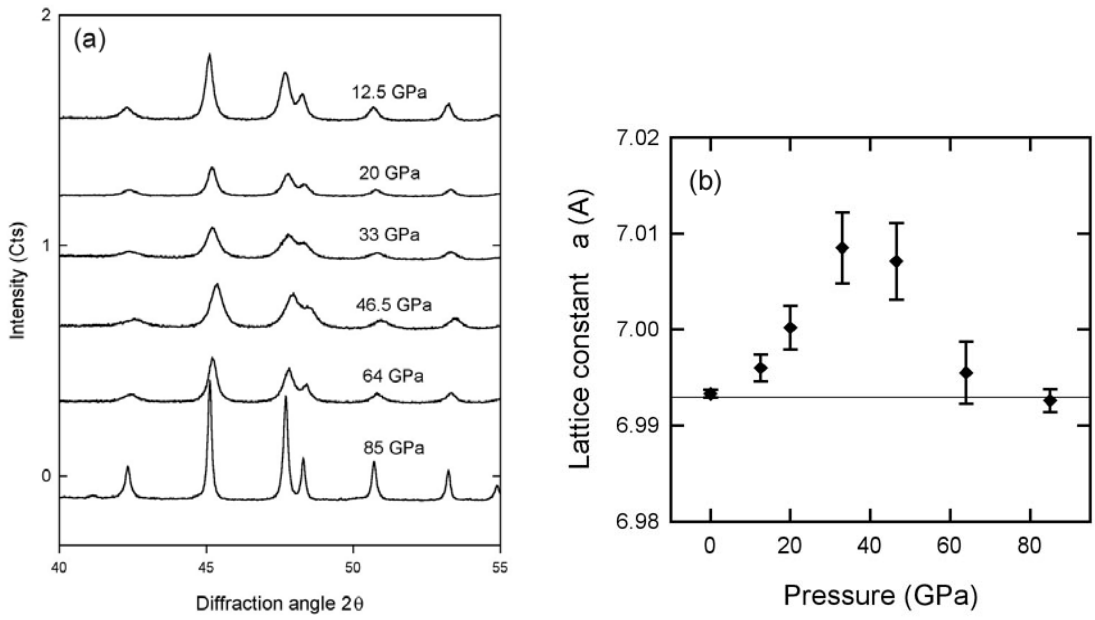

Fig. 3.4-9. (a) X-ray diffraction patterns of anhydrite experimentally shocked to 12.5-85 GPa and (b) lattice constant ***a*** as function of shock pressure.

So far, X-ray experiments have been performed on the recovered anhydrite specimens. All X-ray diffraction patterns recorded are compatible with the anhydrite structure; extra-peaks have not been observed. Peak intensities decrease and peak broadening increases progressively in the pressure range from 0 to 46.5 GPa (Fig. 3.4-9a). At higher pressures the peak broadening diminishes again and the X-ray diffraction pattern of the 85 GPa sample resembles that of unshocked, well-crystallized anhydrite. The quantitative evaluation of X-ray patterns reveals no change in the lattice constants ***b*** and ***c***, but for the intermediate pressures of 33 and 46.5

GPa we note a marked increase in the lattice constant ***a*** (Fig. 3.4-9b). This change is coupled with an increase in the cell volume ***V*** from 305.6 to 306.2 $Å^3$.

The X-ray results show that anhydrite is very resistant to shock compression and does not decompose up to pressures of 85 GPa. At this uppermost pressure, the post-shock temperature was obviously high enough to allow either solid-state recrystallization or melting with subsequent crystallization of anhydrite. This question and the cause for changes in lattice parameters will be further addressed by SEM and TEM studies.

g. *Evidence for degassing of anhydrite in drill cores from the Chicxulub impact crater, Yucatan, Mexico (F. Langenhorst, in collaboration with A. Deutsch/Münster and E. Lounejeva/Mexico City)*

The Chicxulub Scientific Drilling Program (CSDP), a scientific drilling project within the International Continental Drilling Program (ICDP), was successfully completed in February 2002. The drill site of the 1510 m deep Yaxcopoil-1 well, about 30 km south of Merida on the Yucatan peninsula, is close to the buried rim of the Chicxulub impact crater (Ø=180 km). The previous Y-6 drill site of the PEMEX oil company lies also within the crater but closer to the center. Both cores are stored at the UNAM, Mexico City, and were available to the CSDP science team members during the first sampling meeting in late April 2002.

Chicxulub is one of the few impact sites, where evaporites and carbonates occurred as target lithologies. The evaporites and carbonates at Chicxulub are particularly important because shock-released sulfur oxides and carbon dioxide eventually played a major, yet unconstrained role in the faunal crisis at the K/T boundary. In particular, the behaviour of sulfates during impact metamorphism and cratering is not well studied. To address this problem, we sampled anhydrite-bearing impact breccias from both cores for petrologic study.

The drill cores reveal that the crater fill at Chicxulub consists of impact melt rocks, topped by impact melt breccias and suevites. Textural features and fragment population of these impactites vary strongly. The impact melt rocks mostly lack sulfate and carbonate clasts. Their absence reflects an extremely high formation temperature for this melt lithology, causing thermal dissociation of $CaSO_4$ and $CaCO_3$. Impact melt breccias yield a similar picture: samples from deeper levels contain mineral assemblages with Ca-rich pyroxenes and plagioclases (Fig. 3.4-10), which can be interpreted as evidence for dissociation of $CaSO_4$. Large anhydrite clasts within the melt breccias display corroded margins and consist of equant crystals with 120° triple junctions. These features indicate incomplete dissociation and solid-state recrystallization of the remnant anhydrite rock fragments. Melt breccias from shallower and apparently colder levels contain fragments, still displaying the original fine-grained sedimentary texture of the anhydrite rocks. Annealed anhydrite fragments are also nearly absent in the suevites, which had a still lower formation temperature.

An important feature in the impact rocks are up to 100 µm wide veins with secondary minerals cut the matrix of all lithologies (Fig. 3.4-10). The veins resemble the “degassing vents” in the suevite outcrops at the Ries crater. We interpret the observations as first solid evidence for melting and dissociation of platform sediments in the hot impact melt layer and massive release of toxic sulfur oxides. The proposed process, however, differs obviously from the commonly purported idea that SO_x release occurred instantaneously during and after pressure release.

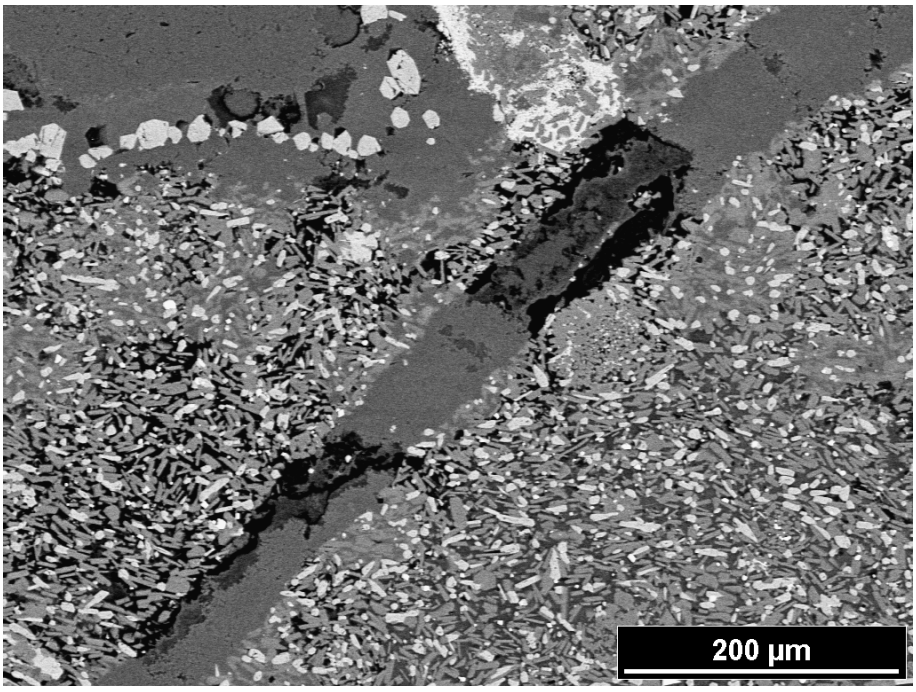

Fig. 3.4-10. Backscattered electron image of a “degassing vent” in Y6 drill core cutting a fine-grained melt matrix, which is composed of Ca-rich pyroxene, plagioclase and quartz.

3.5 Fluids and their Interactions with Melts and Minerals

The creation of the hydrosphere was one of the most profound events in the Earth's history to influence the course of life on Earth. Evolution of the hydrosphere is intimately related to processes involving fluids within the Earth's mantle. Water and other volatile components have been transported to the Earth's surface over geologic time through volcanic activity and other non magmatic processes, and recycled back into the mantle through subduction. While water is a trace component of the upper mantle, there are indications that concentrations may be higher in the transition zone and lower mantle.

One of the first steps in quantifying the effect of hydrogen on physical and chemical properties of the mantle, as well as the effects on mantle processes, is characterising the nature of hydrogen incorporation into mantle phases. Since hydrogen incorporation can be influenced by the presence of point defects and minor concentrations of certain elements, it is important that studies include relevant mantle compositions, and focus on natural as well as synthetic samples. Recently, studies have evolved to include the effects of dehydration on physical properties such as elasticity and rheology, which provide tangible constraints on mantle chemistry based on bulk geophysical measurements. The kinetics of dehydration provide information on the degree of history preserved in natural samples, enabling the use of hydrogen profiles in natural samples to elucidate temporal and thermal histories of xenoliths and magmas. Direct studies of fluids in the laboratory are important to understanding the nature of processes such as diamond growth, and constraining basic physical properties such as melting.

a. *Full characterisation of modes of hydrogen incorporation in synthetic, water-saturated jadeite and jadeite-rich pyroxenes (G.D. Bromiley, in collaboration with H. Keppler/ Tübingen)*

In the last decade, considerable effort has been focused on studying hydroxyl incorporation in the nominally anhydrous minerals thought to constitute the Earth's mantle. Investigations of natural samples from mantle xenoliths and synthetic samples from high-pressure experiments have demonstrated that of all the major upper-mantle phases, pyroxenes can contain the most water. It has been suggested that high water contents in some pyroxene compositions are a result of the presence of cation vacancies at high pressure, as well as the highly-underbonded nature of the O_2 site in the *C*2/*c* structure. The pyroxenes that have been shown to contain the highest water contents are omphacites. Omphacite is a pyroxene characteristic of high-pressure eclogitic rocks, and is likely to be a stable phase during subduction of crustal material to mantle depths. In simple terms, omphacites are a solid solution between jadeite ($NaAlSi_2O_6$) and diopside ($CaMgSi_2O_6$) end-members, although the compositions of natural samples are usually considerably more complex, and can be modelled by the presence of numerous additional components. One of the most important of these is Ca-Eskola component

($Ca_{0.5}\square_{0.5}AlSi_2O_6$), which implies the presence of M_2 vacancies in the pyroxene structure. Investigations of natural omphacites have shown that the highest recorded water contents are for jadeite-rich samples with high Ca-Eskola components. As such, omphacite may provide a good model for understanding the interrelationship between cation vacancies and hydrogen incorporation in pyroxenes at high pressure.

Despite the possible importance of omphacite as a host for water in subducting slabs, only limited work has been performed on characterisation of possible modes of incorporation of hydrogen in the omphacite structure. Considerable work has, however, been performed on hydrogen solubility and speciation in natural and synthetic diopside. To date there has been no experimental investigation of hydrogen solubility in jadeitic or omphacitic compositions.

The purpose of this work is to provide a systematic calibration of the effects of pressure on the incorporation of hydroxyl in synthetic jadeite and jadeite-rich omphacitic compositions. Samples have been synthesised up to 10 GPa using piston-cylinder and multianvil apparatus, and hydrogen incorporation has been studied using FTIR spectroscopy. FTIR spectra for jadeite are characterized by the presence of up to five absorption bands in the wavenumber range corresponding to stretching of the OH dipole (Fig. 3.5-1). Anisostopy of absorption bands in polarised radiation, the effects of pressure on peak height, and frequency shifts of the bands with increasing temperature suggest that there are at least five distinct modes of hydrogen incorporation in the jadeite structure. FTIR spectra for synthetic jadeite also share many similar features with spectra for natural omphacites with more complex compositions (Fig. 3.5-1).

Detailed examination of the jadeite structure reveals that a large number of possible sites for hydrogen incorporation are present. Using the correlation of O-H stretching frequency with oxygen-oxygen distances and information on absorption band anisostropy, an initial assignment of the absorption bands in the jadeite IR spectra has been attempted. In Figure 3.5-2, part of the octahedral sheet in jadeite is shown, with favourable mechanisms for hydrogen incorporation illustrated. Previously it had been suggested that the most favourable mode of incorporation would be hydrogen associated with the highly-underbonded O_2 site, with vibration of the OH dipole in the direction of an M_2 vacancy. However, this mechanism is inconsistent with oxygen-oxygen distances across the M_2 site. Instead, the most favourable mechanisms appear to involve hydroxyl incorporation along the edges of edge- and face-sharing octahedra. Hydrogen incorporation is still likely to be associated with cation vacancies, but OH dipoles would appear to sit on the outside of vacated octahedra, rather than vibrating in the direction of the vacancy. This is perhaps in some ways analogous to the hydrogarnet substitution mechanism, whereby four protons replace one Si on the tetrahedral site. Neutron diffraction work has suggested that all four OH dipoles sit around the outside of the tetrahedron, rather than vibrating in the direction of the Si vacancy, as previously suggested.

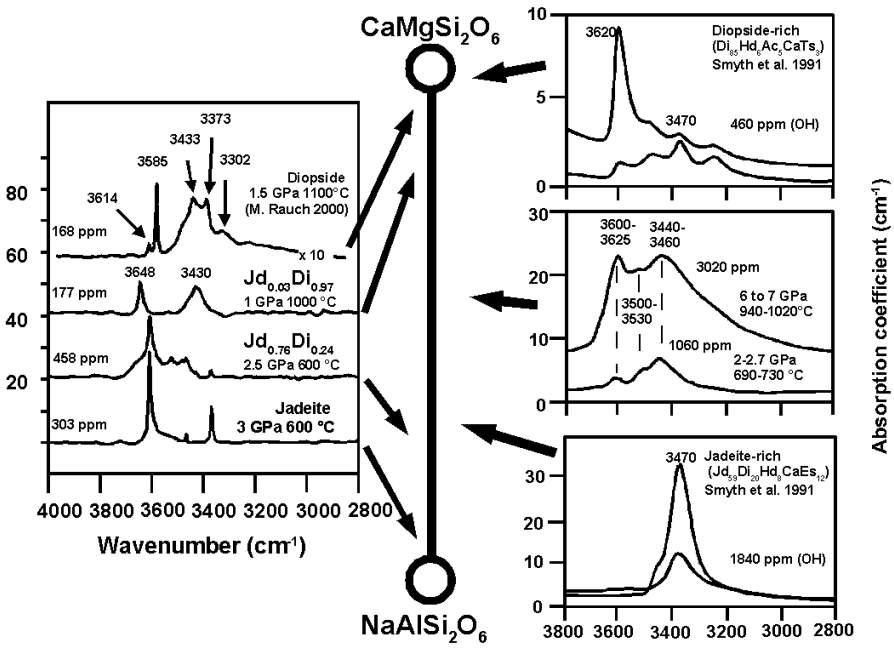

Fig. 3.5-1: Comparison of FTIR spectra for synthetic (left) and natural (right) ompahcites along the jadeite-diopside tie-line.

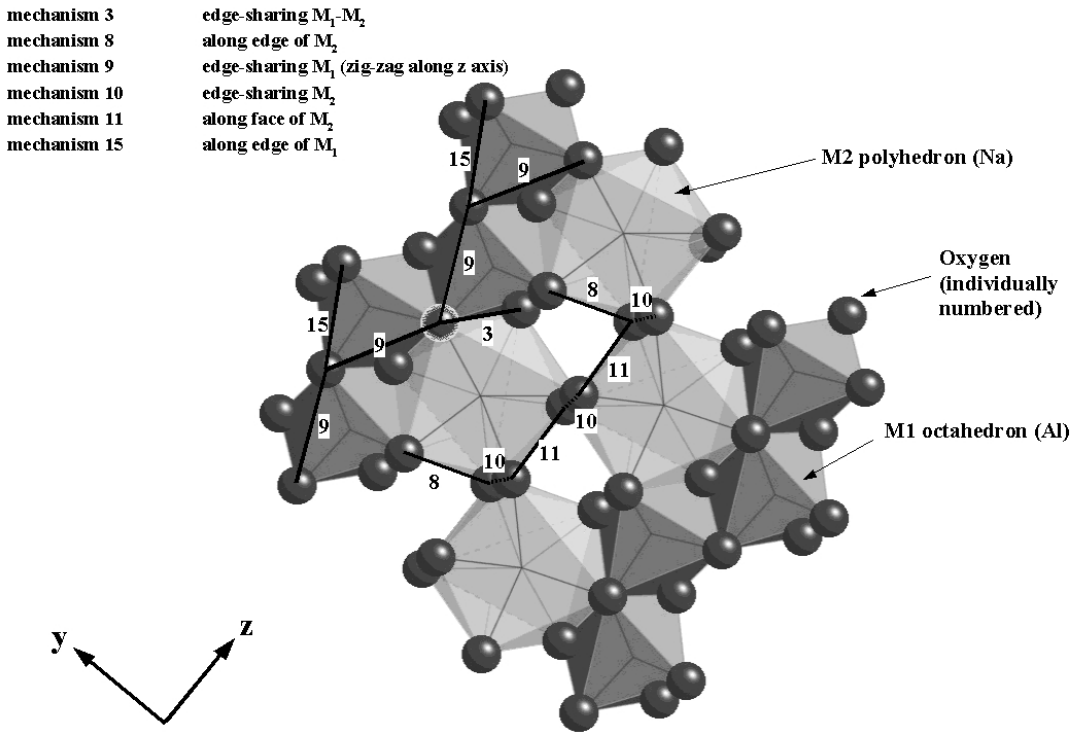

Fig. 3.5-2: Jadeite octahedral layer, viewed just off of the *x* axis, showing possible mechanisms for hydrogen incorporation in the structure.

b. *Structural systematics of hydrous ringwoodite (J.R. Smyth and C.M. Holl/Boulder, in collaboration with D.J. Frost, S.D. Jacobsen, F. Langenhorst and C.A. McCammon)*

The nominally anhydrous silicate minerals of the transition zone in the Earth's mantle are capable of incorporating water as hydroxyl many times the amount in the oceans. Such a large reservoir of water may have acted as a buffer to maintain the volume of the oceans over geologic time. In order to assess whether or not the water is indeed present in the Earth's interior, it is necessary to measure the effects of hydration on seismically observable properties such as velocity, density, and the depth of mineralogical phase transitions. In order to quantify the effects of hydration at the atomic scale, the unit cell parameters and crystal structures of seven hydrous and anhydrous ringwoodite samples synthesised at BGI have been refined at ambient conditions.

Seven separate samples of hydrous ringwoodite with compositions ranging from Fo_{100} to Fo_{89} and hydrogen contents from 0.2 to 1.1 weight percent have been synthesized in the 5000 ton multianvil press. Synthesis conditions range from 18 to 22 GPa and 1400 to 1500 °C. The crystals have been characterised by single-crystal X-ray diffraction, electron microprobe, IR and Mössbauer spectroscopy, and by analytical and high-resolution transmission electron microscopy. The crystals are optically isotropic, and the Fe-bearing samples are deep blue in colour. Mössbauer spectroscopy and ELNES spectroscopy on the Fe-bearing samples indicates that about 10 percent of the iron is in the ferric state. High-resolution TEM examination of one of the Fe-bearing samples indicates that the crystals are homogeneous and free of significant inclusions or exsolution features. Infrared spectra show a broad absorption band extending from about 2500 to 3600 cm^{-1} with maxima ranging from 3105 cm^{-1} for the pure magnesian samples to 3150 cm^{-1} for the Fo_{89} samples. Unit cell parameters at ambient conditions indicate a systematic expansion of the cell with hydration (Fig. 3.5-3). The crystal structures of the seven ringwoodites have been refined by X-ray single-crystal diffraction. Refinement of cation site occupancies indicates full occupancy of the tetrahedral site for all samples, whereas the occupancy of the octahedral site appears to decrease systematically with H content. The principal hydration mechanism involves octahedral cation vacancies. The IR spectra are consistent with protonation of the short O-O approach on the tetrahedral edge, which would imply partial Mg-Si disorder.

The crystal chemistry of Fo_{90} hydrous ringwoodite ($Mg_{1.7}Fe_{0.22}H_{0.15}SiO_4$) containing 0.93 % H_2O by weight has been studied at pressures up to 11.2 GPa by single-crystal X-ray diffraction in the diamond anvil cell. The unit cell edge and volume have been refined at 30 different pressures in this pressure range. The refined bulk modulus for the unit cell is 169.0 ± 3.4 GPa with K' = 7.9 ± 0.9. We observe a systematic decrease of bulk modulus with hydration (Fig. 3.5-4). The oxygen position parameter has been refined from X-ray intensity data at ten pressures over this range. With K' fixed at 4.0, the bulk modulus of the Si tetrahedron is 245 ± 31 GPa and that of the octahedral site is 150 ± 7 GPa. Consistent with previous studies we observe a systematic decrease of bulk modulus with H content. Hydration of ringwoodite has a larger effect on seismic velocity than temperature within the possible ranges of these parameters under upper mantle conditions. This means that in tomographic images of the transition zone in regions distant from subduction zones, seismically fast blue

regions could equally equate to ‘dry’ as to ‘cold’ areas. Observed seismic velocities in the transition zone are consistent with significant hydration of the ringwoodite (γ-Mg_2SiO_4) structure.

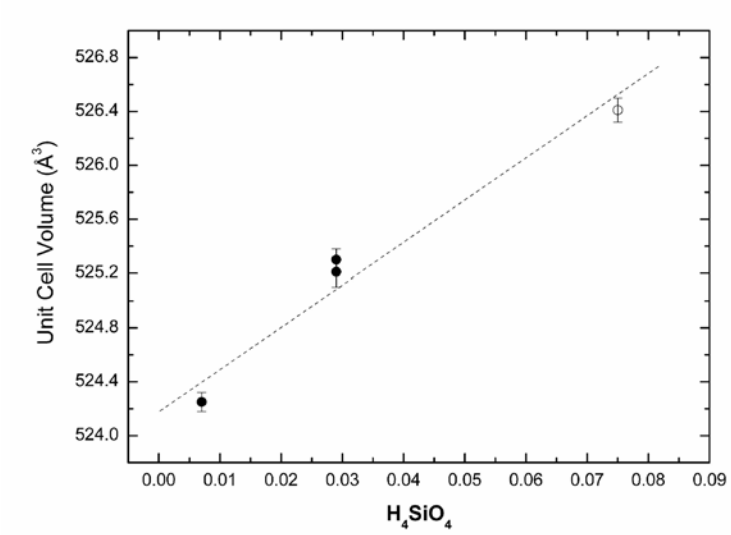

Fig. 3.5-3: Plot of unit cell volume of Fe-free ringwoodite versus mole fraction of H_4SiO_4 from this study (solid symbols) and Kudoh *et al.* (2000) (open symbol).

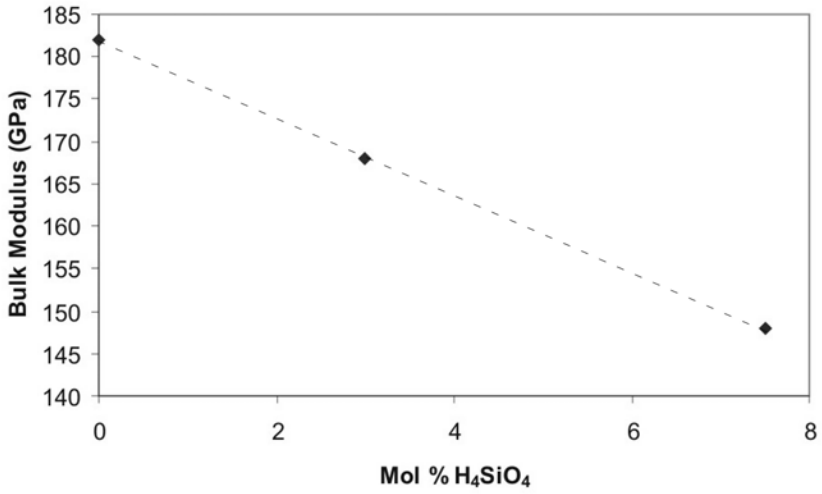

Fig. 3.5-4: Bulk modulus versus H content of ringwoodite. The cell bulk modulus shows a linear trend with H content.

c. *Raman investigations of deuterated ringwoodite (A.P. Jephcoat and A.K. Kleppe/Oxford, in collaboration with J.R. Smyth/Boulder and D.J. Frost)*

Ringwoodite, γ-$(Mg,Fe)_2SiO_4$, the nominally anhydrous highest-pressure polymorph of olivine, is considered to be the most abundant mineral in the transition zone between 520 and

660 km depth. In contrast to olivine, however, ringwoodite can incorporate relatively large amounts of water: up to ~ 2.5 wt.% H_2O as OH^- in its crystal structure. The hydration mechanism of ringwoodite is still poorly understood and results from different laboratories vary considerably. In particular, reported Raman active OH stretching vibrations are contradictory.

OH-stretching vibrations are expected to occur in the range 3100-3700 cm^{-1}. Raman OH modes have been reported for hydrous ringwoodite Mg-end member compositions in several previous studies. In contrast, however, we have been unable to detect any OH Raman activity in Mg and Fe bearing ringwoodite samples that showed clear evidence of significant hydration in IR absorption and SIMS measurements. One possibility is that the OH stretching modes are very weak and therefore evade detection at the modest laser powers that must be employed to avoid back reaction of the samples at 1 bar. No OH modes were observed, however, in diamond anvil cell experiments performed in the stability field of ringwoodite where high laser powers could be used.

To obtain better constraints on the protonation mechanism of ringwoodite and to examine the lack of observed OH Raman signal, we synthesised deuterated Fe-free and Fe-containing ringwoodite samples in the multianvil apparatus. The starting materials were a mixture of magnesiowüstite (MgO), silica (SiO_2), deuterated brucite [$Mg(OD)_2$] for the Mg-endmember ringwoodite, and with additional (natural) siderite ($FeCO_3$) for Fe-bearing ringwoodite. Fe-free and Fe-bearing powders were sealed in Pt and Re capsules, respectively, and held at 20 GPa and 1200 °C for 2 hours. Deuteration provided the advantage of excluding hydrogen due to surface contamination and avoided the instrumental hydrogen background signal of the SIMS analysis method.

The Raman spectrum of deuterated Fe-bearing ringwoodite is shown in Fig. 3.5-5. The ambient pressure Raman spectrum of deuterated Fe-bearing ringwoodite shows two intense bands at 793 and 841 cm^{-1} that correspond to the asymmetric (T_{2g}) and symmetric (A_{1g}) stretching vibrations of isolated SiO_4 tetrahedra, respectively. The three further spinel modes (expected at 302, 372, and 600 cm^{-1}) are not observed. The Raman spectra of the deuterated samples are similar to spectra of hydrated samples. Although the presence of deuterium in the ringwoodite samples was confirmed by SIMS analysis, Raman active OD stretching modes were not observed, allowing for their mass-scaled expected shift in the wavenumber range. The low-frequency Raman signal (100-250 cm^{-1}) might be associated with localised modes (frequencies in ranges forbidden to the normal modes of the perfect host crystal) generated by disorder due to Fe^{2+}, Fe^{3+} and coupled H/D substitution in the ideal magnesium ringwoodite host structure. The modes appear not directly related to vibrational modes of the Fe or H/D species. It is worth noting that there is no report of similar effects in any other silicates relevant to the Earth's transition zone, largely because studies have concentrated on Mg-end member cases. More work on a structural model for the hydration mechanism and

spectroscopic observations are needed to resolve the current uncertainties in the Raman results.

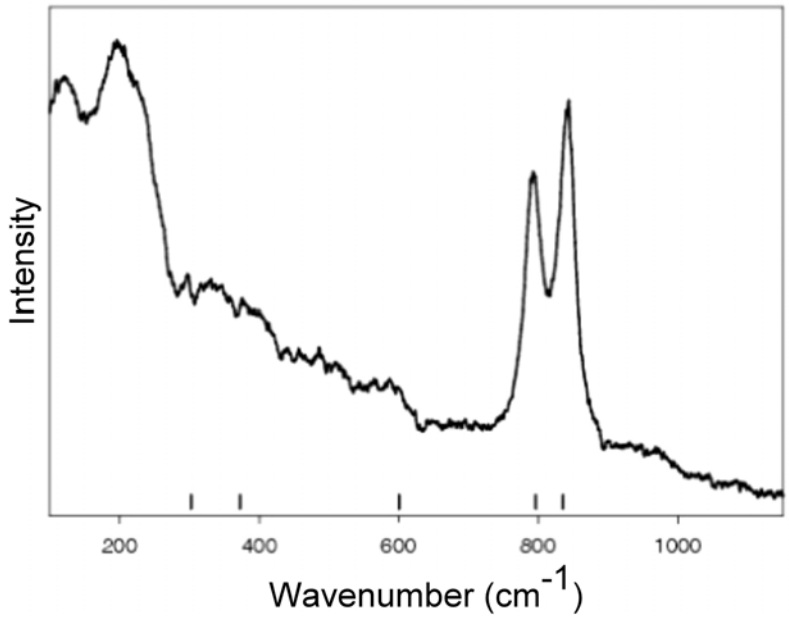

Fig. 3.5-5: Raman spectrum of deuterated, Fe-bearing ringwoodite. The relative intensities of the T_{2g} (793 cm^{-1}) and A_{1g} (841 cm^{-1}) modes vary with changing orientation of the crystal relative to the incident laser beam, while the intensity of the low-frequency features remains nearly constant. For comparison, bars below the spectrum represent the Raman frequencies of iron-free hydrous ringwoodite, and agree with the frequencies of iron-free anhydrous ringwoodite.

d. *Kinetics of hydration into synthetic iron-free forsterite (S. Demouchy and S.J. Mackwell)*

Physical and chemical properties of the Earth's mantle are readily modified by interaction with volatiles such as water. Thus, characterisation of the solubility and kinetics of incorporation of water in nominally anhydrous minerals, such as olivine, clinopyroxene, orthopyroxene and garnet, is important in order to understand the behaviour of the Earth's interior under hydrous conditions. Previous experimental studies on the olivine-water system indicate that significant amounts of OH can dissolve within olivine as point defects. Our study concerns the kinetics of hydrogen transport in the iron-free olivine-water system.

We performed hydration experiments under hydrothermal conditions at high fluid pressures on dry, synthetic, crystallographically oriented crystals of iron-free forsterite. Experiments were performed at 1.5 GPa and 1000 °C for 3 hours in a piston cylinder apparatus, or at 0.2 GPa and 900-1110 °C for 3-20 hours in TZM cold-seal vessels. The oxygen fugacity was buffered using Fe-FeO or Ni-NiO powders. Polarised Fourier Transform Infrared (FTIR) spectroscopy was utilised to quantify the hydroxyl distributions in the samples after the

experiments. Hydrogenation rates were measured parallel to the three crystallographic axes from profiles of hydroxyl content as a function of position in the samples. The chemical diffusion coefficients are marginally slower than in olivine for the same diffusion process, but the anisotropy of diffusion is the same, with the [001] axis the fastest direction of diffusion and [100] the slowest. Using an Arrhenius law (Fig. 3.5-6), we determined activation energies and pre-exponential terms of 214 ± 32 kJ mol^{-1} and $10^{-3.6\pm1.3}$ m^2 s^{-1} for diffusion parallel to [001], 208 ± 50 kJ mol^{-1} and $10^{-4.4\pm1.9}$ m^2 s^{-1} for diffusion parallel to [010], and 233 ± 43 kJ mol^{-1} and $10^{-4.3\pm1.7}$ m^2 s^{-1} for diffusion parallel to [100]. Since the activation energies are, within error, the same for all directions, we performed a global fit to all data for all directions and determined an activation energy of 215 ± 22 kJ mol^{-1} for the diffusion of metal vacancies in forsterite. These results are in reasonable agreement with the previous results for natural olivine. Hydrogenation thus occurs by coupled diffusion of protons and octahedrally coordinated metal vacancies. Hence diffusion rates are sufficiently fast to modify water contents within xenoliths ascending from the mantle, but too slow to permit a total equilibration of forsterite or olivine crystals.

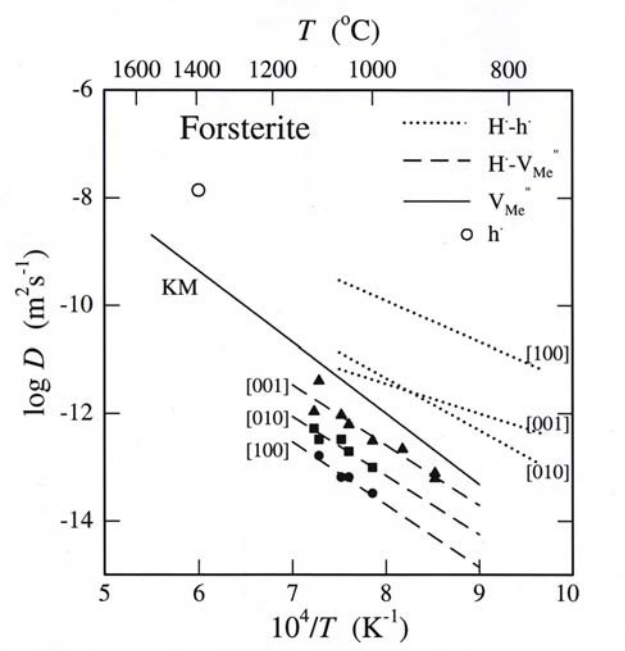

Fig. 3.5-6: Diffusivity for metal vacancy and hydrogen ions in olivine and forsterite. The dashed lines with symbols indicate our results from the hydrogen incorporation process linked to metal vacancy diffusivities for each crystallographic axis. The dotted lines represent the results from Kohlstedt and Mackwell (1998, *Z. Phys. Chem.*, **207**, 147-162) for hydrogen diffusion during redox exchange. The solid line represents the linear fit to the compilation of data for metal vacancy diffusion in iron-bearing olivine from previous publications (Nakamura and Schmalzried 1983, *Phys. Chem. Minerals*, **10**, 27-37; 1984; Mackwell *et al.* 1988, *Philo. Mag. A.*, **57**, 779-789; Kohlstedt and Mackwell 1998, *Z. Phys. Chem.*, **207**, 147-162). The circle represents the polaron diffusivity calculated from Sato (1986, *Earth Planet. Inter*., **41**, 269-282) from electrical conductivity measurements.

e. *Water in nominally anhydrous minerals: First water diffusion profiles in xenolithic olivine (S. Demouchy, S.J. Mackwell, F. Gaillard and S.D. Jacobsen, in collaboration with C. Stern/Boulder)*

Experimental work on the kinetics of hydration/dehydration of olivine indicates that dissolved water would be lost in a few hours on ascent from depths at temperatures over 800 °C. Therefore, the water content in natural olivine is only representative of the last hydration/dehydration event in its geologic history. To date, water diffusion profiles in natural nominally anhydrous minerals have not been studied.

We present preliminary results of water diffusion profiles in natural xenolithic olivine. The sample is a garnet-bearing peridotite xenolith from Quaternary Pali-Aike alkali basalts of southernmost South America (Chilean Patagonia). A previous petrological and geochemical study showed that the sample has a major element composition similar to pyrolite (upper mantle composition proposed by A.E. Ringwood). Also, core compositions of minerals in the garnet peridotite indicate equilibration temperatures of 970 to 1160 °C, and pressures between 1.9 and 2.4 GPa. Observations of spinel-garnet transformations on the garnet rims and chemical zonation of pyroxenes indicate a cooling event, followed by secondary heating before ascent to the surface. According to a more recent isotopic study, the garnet-peridotite xenoliths appear to originate from fertile garnet lherzolithic subcontinental lithosphere.

We are studying water solubility and kinetics in this unusual garnet peridotite using FTIR spectrometry. Unpolarised infrared spectrometry analysis shows that olivine (Fo_{92}-Fo_{85}), chrome diopside and orthopyroxene (En_{90} to En_{82}) contain a significant amount of water (Fig. 3.5-7, A-D), ranging from 0 to 16 wt ppm H_2O for olivine, and up to 410 wt ppm H_2O in the pyroxenes (Paterson's calibration). The garnet crystals are rich in hydrous and brownish glassy inclusions. However, analysis of clear regions of small garnet crystals indicates that the garnets are dry. We also checked for homogeneity of water solubility in the largest olivine grains, and found that those larger than ~ 0.5 mm are heterogeneous, with depleted rims (Fig. 3.5-7 E). The resulting water profiles yield diffusion profiles similar to those obtained by experiment.

We are also conducting related dehydration experiments on natural En_{100} crystals containing ~ 80 wt ppm H_2O. In these oriented samples we are measuring polarised FTIR diffusion profiles, and plan to measure the effects of hydration on elastic wave velocities using gigahertz ultrasonic interferometry. We will investigate further the natural garnet peridotite xenolith using FTIR in order to quantify diffusion rates using a theoretical diffusion law. Such diffusion profiles in natural olivine from a xenolithic peridotite have not previously been observed, permitting us to compare experimental studies on hydrogen diffusion in the water-olivine system for the first time.

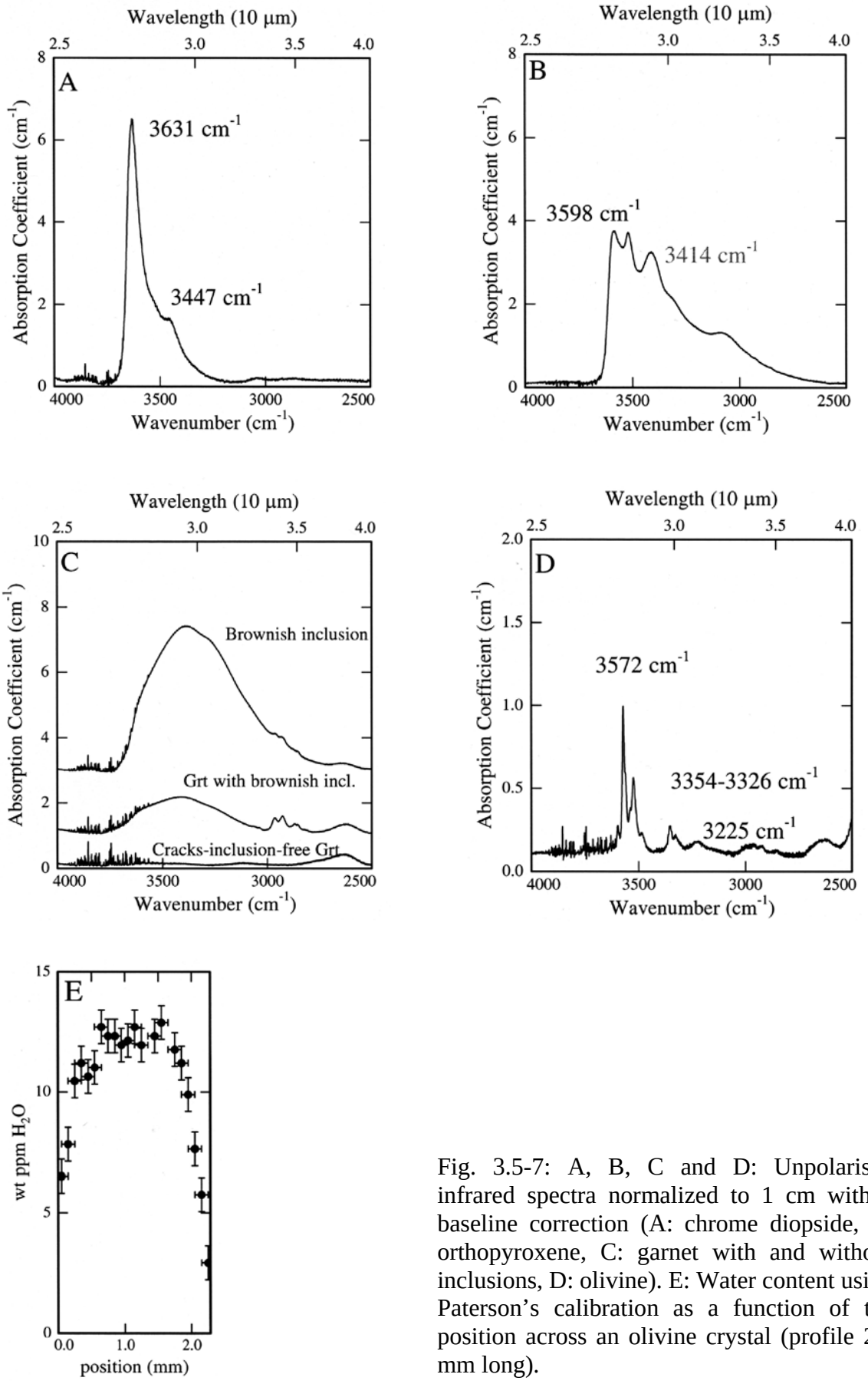

Fig. 3.5-7: A, B, C and D: Unpolarised infrared spectra normalized to 1 cm with a baseline correction (A: chrome diopside, B: orthopyroxene, C: garnet with and without inclusions, D: olivine). E: Water content using Paterson's calibration as a function of the position across an olivine crystal (profile 2.3 mm long).

f. *Hydrogen profiles in olivine as a geospeedometer of magma ascent rate (F. Gaillard, F.A. Bromiley and S. Demouchy, in collaboration with K. Roggensack/Tempe)*

Exsolution of water and other volatiles from magmas upon ascent provides the energy for explosive volcanism. However, evidence exists for eruptions with single vent geometry and similar pre-eruptive volatiles content but with contrasting eruptive styles. Recent scientific reports support the idea that the regime of magma ascent (ascent rate but also temporal storage during ascent) controls the depth of volatile release from the magma. According to these scenarios, explosive magmas have a fast rate of ascent and release their volatiles as they reach the surface; whereas in the case of non-explosive magmas, a slower ascent rate allows discharge to occur in the crust (in the region of several hundred meters to several km depth). In parallel, many experimental and theoretical studies showed evidence of the critical control of melt decompression rate on the kinetics and regime of volatile exsolution, which gives credence to the argument that the rate of magma ascent dominates the depth of volatile release. However, in contrast to methods of evaluation of pre-eruptive conditions, methods for estimating magma ascent rate are not yet fully available. The purpose of this study is to develop such a method.

The basis of this study retains the idea that diffusion-controlled processes in minerals preserve the physical-chemical history of the host rocks. However, the time-scale of the recorded event depends on the diffusion rate of the considered process. For instance, partitioning of Na-Ca between plagioclase and the melt is strongly governed by the water content of the melt. Therefore, one should expect a change in Na-Ca content of plagioclase in response to water degassing from the melt upon ascent. The rate of cation diffusion in plagioclase is, however, much slower than the rate of magma ascent; thus the use of Na-Ca profiles in plagioclase as evidence of magma ascent is not viable. In contrast, recent reports on hydrogen in olivine crystals have shown that (1) the hydrogen content in olivine is a function of the water fugacity (which is buffered by the water content in the melt), and (2) the diffusion rate of hydrogen in olivine corresponds well to the timescale of magma ascent. Therefore, the use of hydrogen profiles in natural olivine is a promising tool for extracting information concerning the rate of volatile exsolution and therefore the timescale of magma ascent.

The successful completion of this project will partly depend on the choice of the magma studied. In particular, it is crucial that the eruption should have been eye-witnessed and the eruptive-style characterised. In addition, the pre-eruptive conditions should have been well documented, and careful characterisation of the olivine (inclusion and crack free) should have been performed. The Cero Negro volcano, Nicaragua, produced two eruptions of basaltic rocks in 1992 and 1995 with two distinct eruptive styles. Although recent studies revealed that the pre-eruptive conditions were similar (400 MPa, 5-6 wt.% water in the melt), in 1992, an explosive eruption produced a 7 km-high sustained ash column; whereas the 1995 eruption was mainly effusive. If the difference in eruptive style is due to different ascent rates, it should be recorded in the hydrogen profiles within olivine crystals. Preliminary results

obtained from FTIR measurements have revealed that the hydrogen content is lower in the rim compared to the centre, which is consistent with an H content profile that has retained evidence of a reduction in water activity within the system. A more specific study is now being carried out, including: (1) orientation of the crystals with respect to the crystallographic axes; and (2) determination of the chemical profiles parallel to the different crystallographic axes. As the diffusion rate of hydrogen is different along the *a*, *b*, and *c* axes, it is expected that three different profiles constraining the duration of ascent will be obtained. Knowing the diffusion rate, inversion of the profile is feasible to extract the duration of the decompression event (ascent rate). In Figure 3.5-8, a simulated decompression-induced hydrogen profile in olivine is shown.

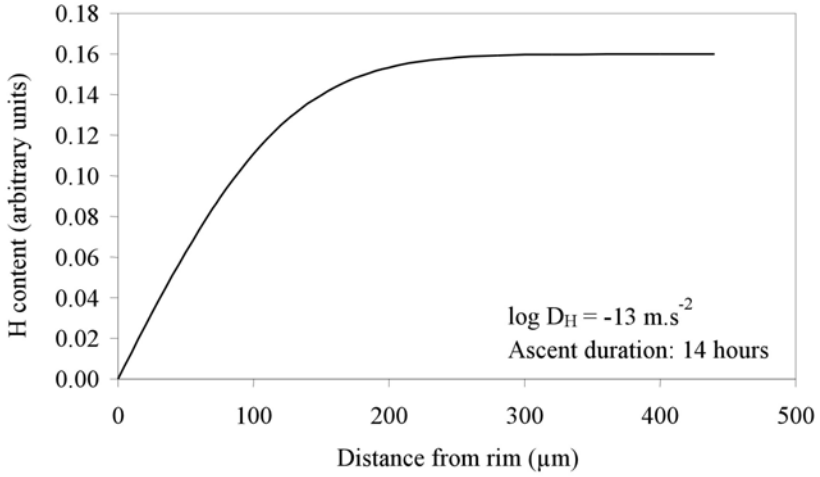

Fig. 3.5-8: Calculated chemical hydrogen profile in olivine induced by a decompression rate of 0.3 MPa/min (~ 1 meter/min). The initial H content is 0.16.

g. *Deformation and dehydration interactions in serpentinite under orogenic conditions (K. Neufeld, I.C. Stretton, S.J. Mackwell and J. Mecklenburgh)*

When rocks undergo diagenetic and metamorphic processes, dehydration is often an important factor that affects the deformation behaviour. It increases the pore pressure inside the rock which can lead to remarkable changes in the mechanical properties of the involved rock masses. This study is focused on deformation and dehydration properties in serpentinite, a rock which is of geological importance in orogenic and subduction environments. In both environments serpentinite rocks undergo deformation processes that interplay with dehydration properties and affect fluid flow inside the rock.

The starting material for this study is an approximately 95 % pure serpentinite from the Bergell area in the Swiss alps. It is a part of the Val Malenco serpentinite complex in which the ultramafic rocks are connected with intrusive bodies of mostly granitic composition. The serpentinite is composed primarily of antigorite with small amounts of chrysotile, spinel and

magnetite. A preliminary deformation experiment was performed at a confining pressure of 300 MPa and temperatures between 720 and 900 K. Even at 920 K and a strain rate of 6 x 10^{-6} s^{-1} deformation occurred by distributed brittle deformation processes (BGI Annual Report 2001). Chemical and structural investigations of the deformed sample showed only minimal dehydration, but a clear influence of deformation fractures on the water distribution inside the rock, suggesting interplay between deformation and dehydration.

In the present study deformation experiments have been performed in a Paterson deformation apparatus at conditions of 300 MPa confining pressure and a temperature range between 700 and 1100 K under drained conditions to determine the onset and development of dehydration and its effect on the deformation properties. A strong dehydration effect was observed at a temperature of 1100 K, where the serpentinite sample was completely dehydrated to forsterite with small amounts of talc. At lower temperatures no dehydration was observed. An experiment with a constant applied stress of 310 MPa showed a very low degree of deformation (5.35 % strain) and a constant reduction of the strain rate to 6 x 10^{-7} s^{-1} at the end of the experiment (Fig. 3.5-9). Further experiments are planned with varying temperatures above 1000 K, constant applied stress conditions and a stepwise reduction of the effective pressure controlled by pore pressure. Hence the pressure dependence of strain and water development will be investigated under contact metamorphic conditions, a field in which only few studies have been conducted so far.

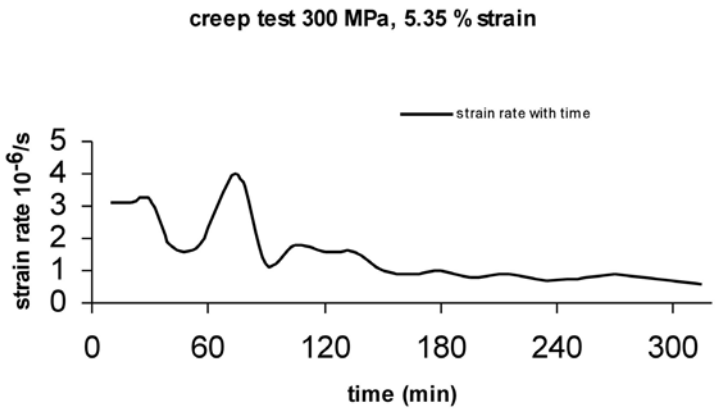

Fig. 3.5-9: Development of the strain rate during an experiment (drained conditions) at 1100 K and a constant applied stress of 310 MPa.

h. *Experimental investigation of diamond growth in high-pressure fluids (H. Bureau/Saclay, F. Langenhorst and D.J. Frost, in collaboration with C. Shaw/Fredricton and J.-P. Gallien/Saclay)*

The origin of “metasomatic” diamonds is still a matter of debate. Some of these mantle diamonds found in kimberlites contain primary fluid and melt inclusions arranged around an

inclusion-free diamond core. The inclusions are volatile-rich and have compositions similar to potassic magmas, but are very different to the melts expected from partial fusion of an olivine-clinopyroxene-garnet assemblage. Since the inclusions are themselves hosted in diamond, they are believed to have formed during diamond growth from an extremely volatile-rich melt. If this is the case, then these inclusions provide evidence for the existence of carbonatitic and hydrous fluids in the diamond stability field, deep in the upper mantle.

The aim of this project is to test the hypothesis that the “metasomatic” diamond parents may be high-pressure fluids, composed of melt (silicate and carbonate) and volatiles (mostly water). Our experimental approach was to show that diamond can grow in such a fluid, possibly with trapping fluid inclusions. Therefore, we have performed 13 multianvil experiments in the range of pressures and temperatures corresponding to diamond formation (7-9 GPa, 1300-1600 °C) for a few hours. Each run was containing a Pt capsule loaded with graphite, and a mixture of ½ water and ½ oxide and carbonate powders from a composition corresponding to the composition of fluid inclusions contained in natural metasomatic diamonds, either with or without diamond seeds (40-60 µm in diameter). In a few experiments, diamond seeds were pre-oxidised by heating in air in order to create possible cavities for inclusions on the surface of the initial cores.

SEM and TEM investigations have shown that the diamond nuclei were overgrown by secondary diamond crystallites in almost all of the experiments (Fig. 3.5-10). New diamonds in the fluid were also nucleated in most of the cases. These experimental results demonstrate that diamonds can grow in a high-pressure fluid containing 50 wt.% of water, silicate melt and carbonates. No inclusions were observed in the local microstructure of the new diamonds, either grown around the cores (pre-oxidised or not), or in the nuclei. However, in one case a nucleus of phengite was observed in epitaxial relationship at the surface of a diamond. This phengite may represent incipient formation of an inclusion in the diamond during its growth in a high pressure fluid.

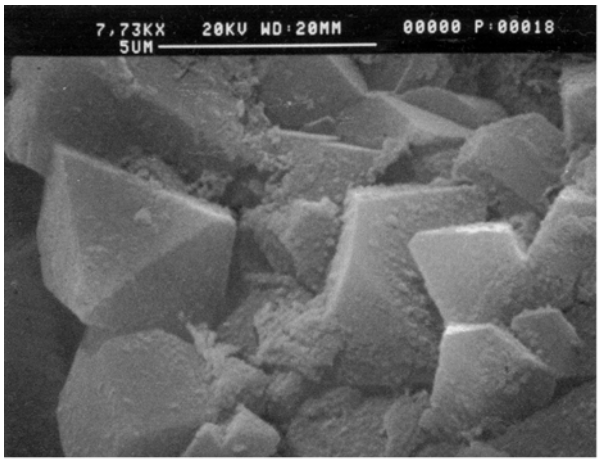

Fig. 3.5-10: SEM photograph of secondary diamonds crystallised in a high-pressure fluid at 9 GPa and 1300 °C.

i. *Melting curve of water studied in an externally heated diamond anvil cell (N.A. Dubrovinskaia and L.S. Dubrovinsky)*

Properties and phase relations of ice and fluid water at high pressures and temperatures are of fundamental interest, and are important to a number of physical, chemical, geophysical, and technological problems. Information on fluid water at very high pressures and temperatures has been obtained largely from shock-wave experiments. Ice VII is a stable water phase at room temperature above 2.3 GPa. The melting curve of ice VII was previously determined to about 10 GPa by resistivity measurements in a multianvil pressure device, and later studied by a different group to about 16 GPa by monitoring the disappearance of the (110) peak in the X-ray diffraction pattern collected with an energy dispersive detector. The three melting points obtained in the study agree well with previous data. A more recent study, however, made visual observations of melting at pressures up to 13 GPa (at temperatures about 750 K) and found large discrepancies with respect to previous determinations at temperatures higher than 550 K. At 700 K the melting pressure differs between different studies by 4 GPa. Resolving such a controversy requires further experimental studies with accurate *in situ* measurements of pressure and temperature in diamond anvil cells.

We performed high *P*,*T* experiments in the stability domain of ice VII utilising the newly developed electrically heated high-pressure diamond anvil cell (this Annual Report). Doubly distilled and deionised H_2O and a small piece of gold wire with 0.005 mm diameter were loaded into an Ir gasket drilled with a 0.09 mm hole. Melting was monitored by the disappearance on heating or appearance on cooling of the reflections of ice VII. We followed the melting curve of ice VII up to 37 GPa (Fig. 3.5-11). The results can be described by the Simon equation:

$$P = 2.2 + 1.31\,[(T/365)^{3.3} - 1].$$

Our data agree well with the results of all previous investigations up to about 4 GPa. Above this pressure, the melting temperature in our studies is higher than that reported by Fei *et al.* (J. Chem. Phys. 99, 5369, 1993), but generally follows the trend reported by Datchi *et al.* (Phys. Rev. B 61, 6535, 2000). Note that Fei *et al.* (1993) studied melting by monitoring the disappearance of the (110) peak in the X-ray diffraction pattern collected with an energy dispersive detector. This way they obtained the minimal melting temperatures at about 7, 9 and 15 GPa. The approximately 100 K difference in the melting temperatures at 35 GPa from our work and that of Datchi *et al.* (2000) could be due to the difference in pressure calibration scales and methods of registration of the melting events (X-ray diffraction versus fluorescence scale and visual observations).

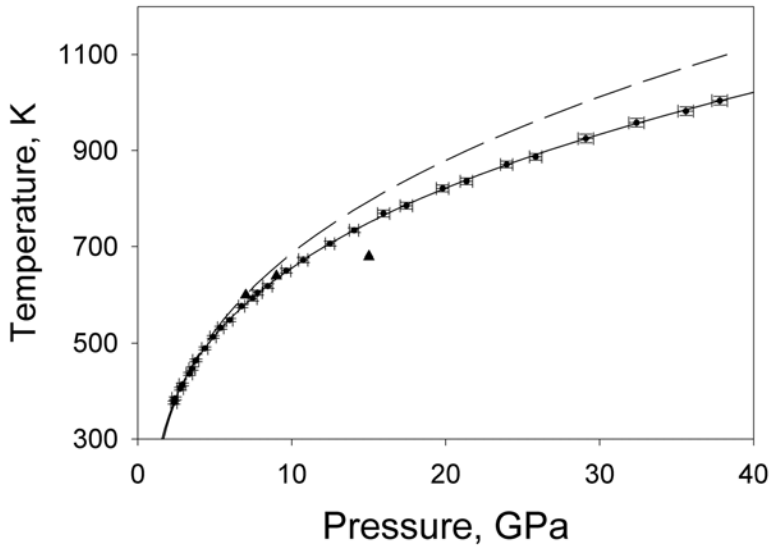

Fig. 3.5-11: Comparison between present and previous melting curves of ice VII: continuous line and dots with error bars – this work; triangles – Fei *et al.* (J. Chem. Phys. 99, 5369, 1993); dashed line – Datchi *et al.* (Phys. Rev. B 61, 6535, 2000).

3.6 Physics and Chemistry of Melts and Magmas

Melt phases are important components throughout the Earth with important consequences for the evolution of our planet. Silicate and metallic melts enabled the differentiation of the Earth into crust, mantle and core, and continue to play a key role in the dynamic behaviour of the Earth. Although near surface melts can be observed during volcanic eruptions, the physical and chemical properties of melts in the Earth's interior can only be studied by laboratory experiments.

The following contributions tackle questions over a wide range of melts relevant to the entire Earth. Studies of melt viscosity and transport properties such as ionic or thermal diffusivity at mantle pressures are experimentally challenging, but are crucial to constraining magma ocean properties in the early Earth, and heat and material transport in planetary interiors. Despite its experimental difficulty, impedance spectroscopy was successfully applied to determine the electrical conductivity of hydrous silicate melts at crustal pressures. The data obtained may help to develop a tool for the remote sensing of the melt water content in a magma chamber before eruption, a method that would be useful for volcanic risk assessment. Other studies focus on the evolution of redox conditions in magmas during ascent and cooling. Spectroscopic studies on silicate glasses quenched from melts at high pressures and temperatures provide important links between melt/glass structure and melt properties; whereas *in situ* infrared spectroscopy at high pressures and temperatures probes directly the temperature dependence of water speciation in silicate melts. Finally, the investigation of the high-pressure segregation behaviour of iron-sulfide liquids in a crystalline silicate matrix provides constraints for the core formation of Earth and Mars.

a. *Determination of peridotite liquid transport properties at high pressure (B. Schmickler, D.C. Rubie, C. Liebske, A. Suzuki, H. Terasaki and B.T. Poe)*

The knowledge of pressure effects on ionic diffusivity and viscosity of peridotite liquid is crucial for the understanding and modeling of magmatic processes in the present Earth mantle and is directly relevant for modeling magma ocean properties during the early history of the Earth. Based upon previous successful studies of diffusivities and viscosities of diopside liquid (Reid *et al.*, Annual Report, 2001), we have extended our research on transport properties to peridotite compositions at high pressure.

The self-diffusion experiments were performed (to 11 GPa and 2400 °C) in a multianvil apparatus at the Bayerisches Geoinstitut using an 18/11 mm octahedral MgO pressure medium with a $LaCrO_3$ heater. Starting materials for the self-diffusion experiments were powdered peridotite with 5 wt.% FeO and naturally abundant O and Si isotope contents which was enriched with 1 wt.% CoO and a peridotite powder enriched in ^{18}O, ^{44}Ca, ^{25}Mg and ^{30}Si isotopes as well as 1 wt.% Ni. Due to the high diffusivity in the low viscosity peridotite

liquids, the diffusion times (for the length scale of the 3mm capsule) must not exceed 10 to 20 seconds in order to avoid the establishment of isotopic equilibrium during the experiment. The self-diffusion profiles of Si, O, Ca and Mg-isotopes were measured with the SIMS at Edinburgh, whereas NiO and CoO diffusion profiles were measured using electron microprobe analysis as well as laser ablation ICP MS.

The present study shows the diffusivity of O, Ca, Mg and Si in peridotite liquid to be an order of magnitude faster than in diopside liquid (Fig. 3.6-1). Furthermore, diffusivity in peridotite liquid appears to be temperature dependent and not pressure dependent. Mg shows the highest diffusion coefficients followed by O, Si, and Ca. Viscosity has been estimated from the self-diffusion data using the Eyring equation. These calculations show the viscosity of peridotite to be an order of magnitude less than that calculated for diopside liquid at these temperatures and pressures.

The Eyring relation has been found to be successful in calculating viscosity from diffusivity data for diopside liquid. We are testing the further applicability of this relation for low viscosity Si-poor peridotite liquid by measuring the viscosity of peridotite melt directly by *in situ* falling sphere experiments. These measurements are performed at the SPring8 synchrotron radiation facility (Hyogo, Japan). Although falling sphere viscometry is an established technique to determine viscosities, measuring peridotite liquid viscosities is complicated due to the rapid rate of fall of the spheres as a consequence of the very low viscosity of the melt at these temperatures. Hence, a sample setup with excellent sphere visibility and stability up to 2200 °C was required and has now been developed.

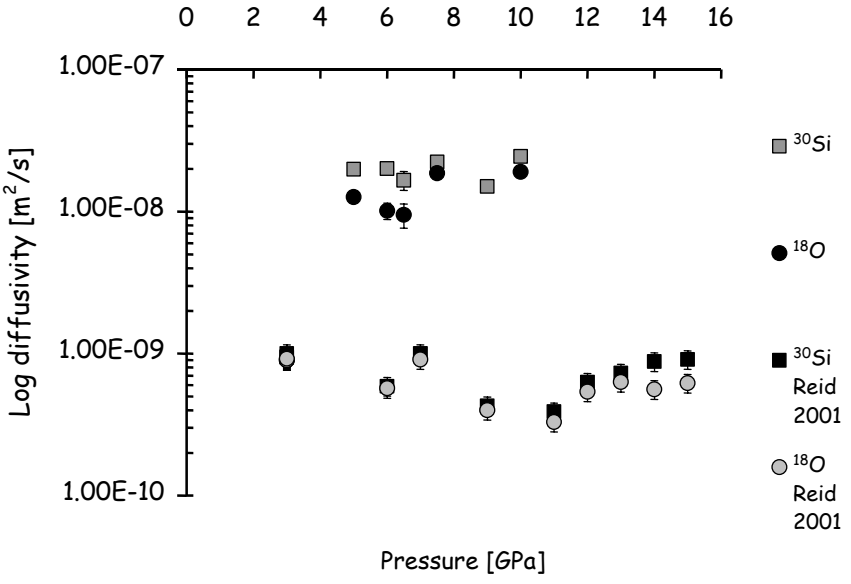

Fig. 3.6-1: Evolution of Si and O diffusivity in silicate melts with pressure. There is no pressure effect on the diffusivity of peridotite liquid at 2150 °C, which is an order of magnitude faster compared to diopside melt (data labelled Reid 2001).

b. *Thermal diffusivity of $CaMgSi_2O_6$ glass at high pressure (A. Suzuki and D.C. Rubie)*

Knowledge of the thermal properties of silicates is very important to discuss the heat and material transport in the planetary interior. Thermal diffusivity of a silicate melt is necessary to consider the convection of magma, because that is one of the terms in Prandtl and Rayleigh numbers. However, the measurement of thermal diffusivity of silicate melt is very rare mainly because of the technical difficulty. In order to investigate the thermal properties of melts, glasses are alternatively used because the glass can be considered as a quenched melt. In the present study we have measured the thermal diffusivity of silicate glass at high pressure.

Thermal diffusivity was measured using the periodic temperature wave method (Ångström method). This method was demonstrated in the past to be very useful for measurements at high pressure. A heating system with a cylindrical geometry was used, as developed for previous thermal diffusivity experiments at the Bayerisches Geoinstitut on silica glass, periclase, olivine, and the high-pressure polymorphs of olivine, wadsleyite and ringwoodite. The cylindrical sample was contained within a cylindrical resistance heater. The electric power supply to the heater was cycled periodically (sine wave function) and temperature was measured at the center and outer part of the sample as a function of time. The distance of the inner and central thermocouples in the recovered sample was measured using a optical microscope and a micrometer.

The measurements of the thermal diffusivity of silicate glasses with the compositions of diopside, jadeite, sodium disilicate and sodium tetrasilicate have been carried out so far. Here in this report the result of diopside glass is shown. Figure 3.6-2 shows the thermal diffusivity of diopside glass as a function of temperature. The experiments were performed from 400 to 800 K at 3, 5, 7 and 9 GPa. No significant change was observed with increasing temperature and pressure.

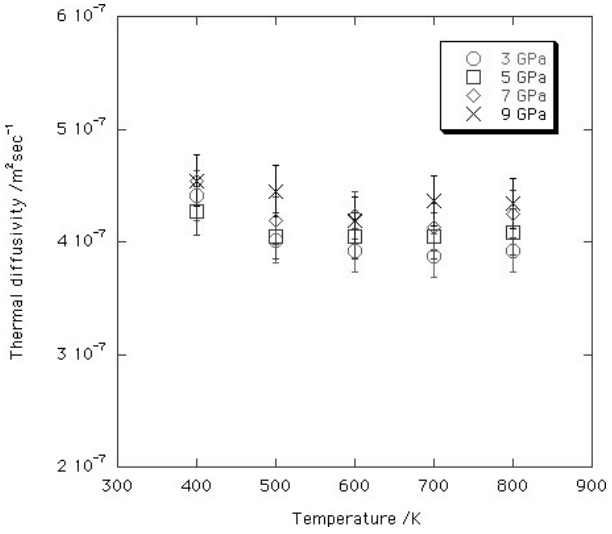

Fig. 3.6-2: Thermal diffusivity of diopside glass at high pressure.

c. *Electrical conductivity of water-bearing magmas as a tool for estimating magmas water content? (F. Gaillard)*

Phase relations for volcanic rocks and chemical analyses of crystals and glasses of erupted lavas tell us that most explosive volcanic eruptions were caused by extremely water-rich pre-eruptive conditions. Eruptions of Mt. Vesuvius, Santorini, Krakatoa, Mt. Pelee or more recently Mount St. Helens and Pinatubo are famous examples of volcanic disasters caused by over-accumulation of water-bearing volatiles in the magma prior to its arrival to the Earth's surface. In addition to their tragic impacts on human activity, most of these explosive eruptions gave rise to vertical ash columns of several kilometers in height transferring some gases to the upper atmosphere, which can have dramatic effects on the Earth's global climate. Therefore, the construction of tools allowing the prediction of where and when such catastrophic eruptions could occur is of major interest.

Currently, volcanologists estimate the potential explosive risk of a volcano mainly by determining the pre-eruptive water contents of lavas erupted in the past and applying the well-known principle of uniformitarianism (the past is the key to the present and vice versa) they hypothesize that future eruptions should show similar features. However, there is some evidence that the eruption styles of several volcanoes can vary greatly making the application of uniformitarianism to such volcanoes unreliable and unsafe. Predicting the explosiveness of upcoming volcanic eruptions requires the development of methods that allow a direct estimation of the water content in the magma prior to eruption. Such an approach would have the obvious and vital advantage of providing direct constraints about upcoming eruptions rather than about past events. Since drilling holes towards magma chambers is not feasible, only remote geophysical methods allow us to probe deep volcanic activity from the surface of the Earth. Such an approach could be promising providing that the measurements and their interpretations are based on relevant laboratory constraints. Of all available geophysical methods, electrical conductivity of silicates is the most sensitive to chemical composition. I have therefore undertaken an experimental program aiming at elucidating the effect of water on the electrical conductivity of natural magmas under crustal conditions. The idea is to correlate the electrical conductivity to the water content of a magma, which can be used as an indicator of its hazardousness and its maturity with respect to eruption. This work should promote and provide a framework for future geoelectrical investigations beneath active volcanoes.

Electrical conductivity measurements (impedance spectroscopy) are performed using a two electrodes set-up in an internally heated pressure vessel. The explored temperature and pressure range, 25-1400 °C and 0.1-400 MPa, allows the water content of the magma to vary between 0 to 10 wt.%. The material used is a natural rhyolitic obsidian cylinder loaded together with distilled water into a Pt-capsule. One end of the capsule is arc-welded whereas the other end is closed with the help of a BN cone through which an inner electrode is introduced (Fig. 3.6-3). Cement is added to ensure the sealing around the BN cone. The capsule is used as an outer electrode. The melt is insulated from the BN cone by a wafer of quartz. An additional wafer of quartz was added on the other side of the melt. This configuration, which sandwiches the melt between two slices of quartz, prevents any

deformation of the electrodes-melt system. Preliminary tests revealed that chemical exchanges between the melt and quartz are negligible even after one week at 1000 °C for melts containing between 2 to 5 wt.% water.

Figure 3.6-4 shows the conductivity of a hydrous rhyolitic melt at different temperatures for a pressure maintained at 50 MPa. The conductivity of anhydrous basalt melt is shown for comparison. For a given temperature, the conductivity of the hydrous rhyolite is much higher. Also the activation energies differ significantly implying that the nature of the charge carriers in both melts is different. Conductivity measurements of melts with different water contents will be performed. The effect of water on electrical conductivity of basaltic compositions will also be determined to help to elucidate the nature of high conductivity zones identified beneath the crust where subduction-related volcanism occurs.

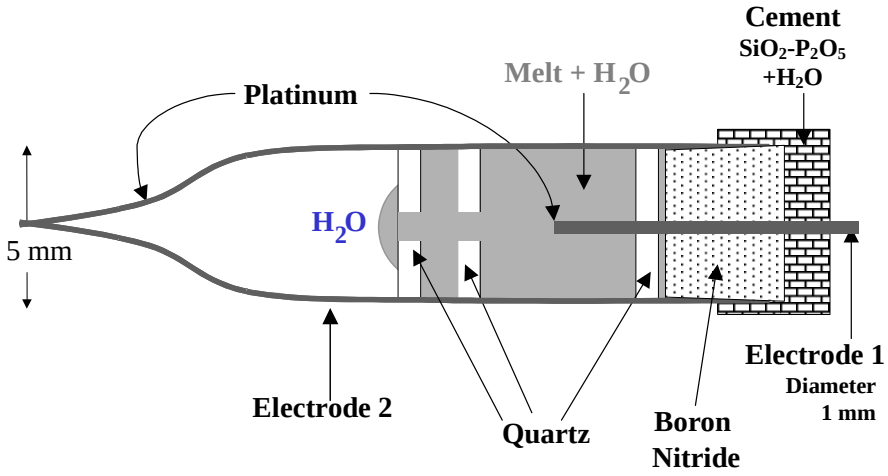

Fig. 3.6-3: Cell geometry for electrical conductivity measurements of silicate melts at high pressure and temperature.

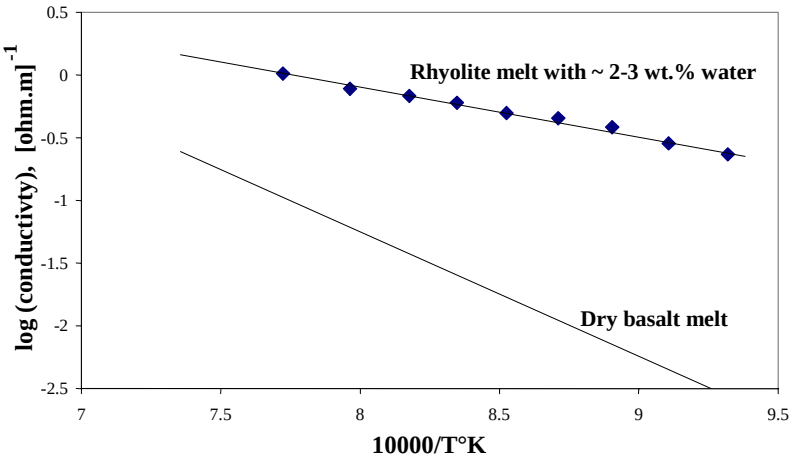

Fig. 3.6-4: The effect of temperature on electrical conductivity of a natural rhyolite melt containing 2-3 wt.% of water at 50 MPa.

d. *Redox history of magma ascent (F. Gaillard, B.C. Schmidt and C.A. McCammon)*

Numerous studies have shown that the redox potential (oxidised or reduced) of a magma affects properties such as viscosity, density and the chemical composition of the derived lavas, as well as controlling a number of magma-related processes. For example, it is now established that reducing conditions prevail during the formation of basaltic oceanic crust, whereas oxidised lavas are involved in the formation of island arcs and probably the continental crust. With respect to magmatic-atmospheric interactions, it has been shown that the amount of sulfur released from an eruption, which has a major impact on climate evolution and rainwater acidity, is partly controlled by redox conditions in the magma. However, in contrast to a solid understanding of its *effect*, the *origin* of the redox potential of magmas is still poorly constrained. The means by which the redox signature of magmas are acquired and how they can be modified is a fundamental issue for understanding the Earth's formation and its subsequent evolution.

The redox state of erupted lavas reflects multistage interactions between volatiles and magmas; hence to a certain extent the magma redox potential can be considered a measure of what and how much they "breathe". The elucidation of these interactions will therefore help to clarify the origin of the magma redox state. Among the different stages of magma-fluid interactions, the ascent of magma toward the Earth's surface prior to eruption occurs last. The magma ascent is accompanied by a progressive pressure reduction, which causes a decrease in solubility of all volatiles in the melt. In response to this solubility reduction, volatiles generally exsolve from the melt in the form of bubbles, and the rate of extraction is primarily limited by the diffusion rate of volatiles in the melt. Since the diffusion rate of volatiles varies significantly, the abundance ratio of different volatiles in the melt is likely to vary during a decompression event. Among the different volatiles to be considered, H_2O and H_2 are critical because their ratio defines the redox potential (oxygen fugacity, fO_2) of the melt through the following equilibrium:

$$H_2 + ½\, O_2 \leftrightarrow H_2O$$

At a given temperature their diffusion coefficients differ by several log units; hence changes in the ratio H_2/H_2O in melts are expected to occur during a decompression event and affect the redox state of the magma. Since H_2 diffuses faster than H_2O, an oxidation of the melt would be expected, and might account for magnetite microlites frequently observed in the glass matrix of erupted rocks as well as around Fe^{2+}-rich minerals such as olivines, biotites or amphiboles. An oxidation event accompanying decompression should be measurable through changes of ferric-ferrous ratio (Fe^{3+}/Fe^{2+}) of the quenched glass. It has often been reported that the fO_2 calculated from glass Fe^{3+}/Fe^{2+} is slightly higher than the fO_2 estimated from mineral assemblages of the same erupted rock. Therefore an oxidation event affecting the Fe^{3+}/Fe^{2+} ratio of the melt during the magma ascent seems likely to occur. Sulfur, which can adopt several redox states in magmas (from -2 to +4), is also likely to undergo oxidation

during magma ascent, which may have significant implications concerning the amount of sulfur release during an eruption.

To study these effects, we plan experiments aimed at characterising the rate of redox changes during decompression of water-saturated Fe- and S-bearing magmas. Experiments will be performed at the Bayerisches Geoinstitut in the internally heated pressure vessel that has recently been equipped with an H_2-loading system. After equilibrating the melt at specific *P*, *T* and fO_2 conditions, the samples will be decompressed at a chosen rate and quenched at different pressures, *e.g.* 150, 100, 50 and 5 MPa from an initial pressure of 200 MPa. Following the experiments the Fe^{3+}/Fe^{2+} ratio will be determined using Mössbauer spectroscopy and the fraction of both H_2 and H_2O will be analysed using Raman and infrared spectroscopy. For S-bearing samples, the sulfur redox state will be measured by electron microprobe. Hence the redox history of ascending magma and its ultimate effect on the glass redox state after eruption will be accessible.

The expected implications of our experiments are a reconsideration of the redox state of erupted lavas as an indicator of pre-eruptive conditions. Elucidation of the redox behaviour of sulfur upon magma ascent will improve the estimation of its release in the atmosphere during eruptions. Also, the extent of iron and sulfur oxidation should be a function of the duration of the decompression event, and hence we anticipate at least a qualitative and perhaps a quantitative indicator for magma ascent rates.

e. *Oxygen fugacity gradients in high-silica rhyolites of the Rattlesnake Tuff, Oregon (C.A. McCammon, in collaboration with M. Streck/Portland)*

The evolution, structure and dynamics of magma chambers have been the focus of many investigations due to their close link with transport of heat and volatiles within the Earth's crust and ultimately into the atmosphere. Oxygen fugacity is an important parameter, since it can influence the structure, composition and properties of magma. The history of magma chambers can be preserved in zoning patterns, where high-silica rhyolite chambers are of particular interest because of the high viscosity of such magmas. The Rattlesnake Tuff of eastern Oregon provides a particularly good example, with five distinct compositional and mineralogic zones. We undertook an investigation to determine the variation of Fe^{3+} within minerals in the different zones, and to correlate results with determinations of oxygen fugacity, with a view towards quantifying the history of the magma chamber.

Mineral separates were obtained from the five representative pumices, where the major iron-containing minerals were clinopyroxene and titanomagnetite (modal abundance < 0.1 %). The relative concentration of Fe^{3+} in clinopyroxene was determined using Mössbauer spectroscopy, and in titanomagnetite using stoichiometry based on electron microprobe analyses. Glass was separated from the pumice samples using heavy liquid methods, and the

relative Fe^{3+} concentration was determined using Mössbauer spectroscopy. Pressures and temperatures were estimated from feldspar and zircon phase relations, and the melts were inferred to be water-undersaturated based on feldspar compositions. To calculate oxygen fugacity we used equations based on the Fe^{3+} concentration in the glass from the literature, as well as the fayalite-magnetite-quartz equilibrium. The preliminary picture shows a progressive increase in oxygen fugacity with the degree of magma evolution. Results are complicated by an apparent increase in oxygen fugacity during cooling, however, which led to the formation of microlite groundmass magnetite. This is reflected in both a higher value of oxygen fugacity recorded by the glass (up to several log units) and the presence of magnetite in Mössbauer spectra of the glass. Further work is planned to investigate different horizons in the outcrop in order to distinguish magmatic from post-magmatic conditions.

f. *On the water solubility mechanisms in hydrous aluminosilicate glasses: Information from ^{27}Al MAS and MQMAS NMR (D. Padro and R. Dupree/Warwick, in collaboration with B.C. Schmidt)*

The question whether or not aluminosilicate melts and glasses depolymerise upon hydration under formation of terminal T-OH groups (T=Si/Al) is a matter of discussion since more than a decade. Recently a quantitative model based on multinuclear NMR spectroscopic data and thermodynamic considerations was brought forward, predicting the extent of different depolymerisation reactions in hydrous alkali aluminosilicate glasses (Zeng *et al.*, Geochim. Cosmochim. Acta 64, 883, 2000). According to this model, formation of Al-OH groups is a major water dissolution mechanism that depends strongly on the Si/Al ratio. For the most favourable compositions the predicted fraction of hydroxyls in Al Q^3-OH could exceed 30 % leading to significant fractions of Al in such depolymerised units.

The aim of this study is to provide further information on the changes at the aluminium environment upon hydration in aluminosilicate glasses with the help of modern NMR spectroscopic techniques such as very high magnetic fields (14.1 and 17.6 T) and multiple quantum magic angle spinning (MQMAS) NMR. These techniques improve the resolution of the ^{27}Al NMR spectra and were shown previously to resolve resonances which in conventional MAS NMR spectra are highly overlapping. Therefore they should be most promising for the detection of the signal of Al Q^3-OH units.

The samples studied here were chosen to favour the probability of formation of Al-OH groups according to the model of Zeng *et al.* (Geochim. Cosmochim. Acta 64, 883, 2000) and have the compositions $NaAlSi_{7.7}O_{17.4}$ (Q52-D) and $Na_{1.03}AlSi_{1.1}O_{4.22}$ (Ne-D). Dry glasses were prepared at 1600 °C and 1 atm from oxide-carbonate mixtures, hydrous glasses were prepared at 5-10 kbar and 1300-1400 °C. The water contents were determined using Karl-Fischer titration and static ^{1}H NMR to be 5.7 (Q52-6H) and 6.0 wt.% (Ne-6H). Within the Zeng

model Ne-6H should contain a fraction of about 10 % of all Al in Q^3-OH, for Q52-6H this fraction should even be higher and should exceed 25 %.

The ^{27}Al NMR data for both compositions give no evidence of network depolymerisation at Al sites, *i.e.* in the ^{27}Al MQMAS NMR spectra of the hydrous glasses is no evidence for an extra resonance (Fig. 3.6-5). The data strongly suggest that aluminium is only present as Al Q^4(4Si) units for the glasses studied unless Al Q^3(3Si)-OH units have a very similar chemical shift and quadrupole parameters so they cannot be resolved, which however seems to be highly unlikely. For the particular case of nepheline glasses consisting predominantly of Al-O-Si units the absence of Al Q^3-OH suggests also the absence of Si Q^3-OH (considering a water dissolution mechanism like Si-O-Al + H_2O → Si-OH +Al-OH), which is consistent with previous ^{29}Si NMR data. Following this line of reasoning, our ^{27}Al NMR data for nepheline glass suggest the absence of any significant depolymerisation of such glasses upon hydration.

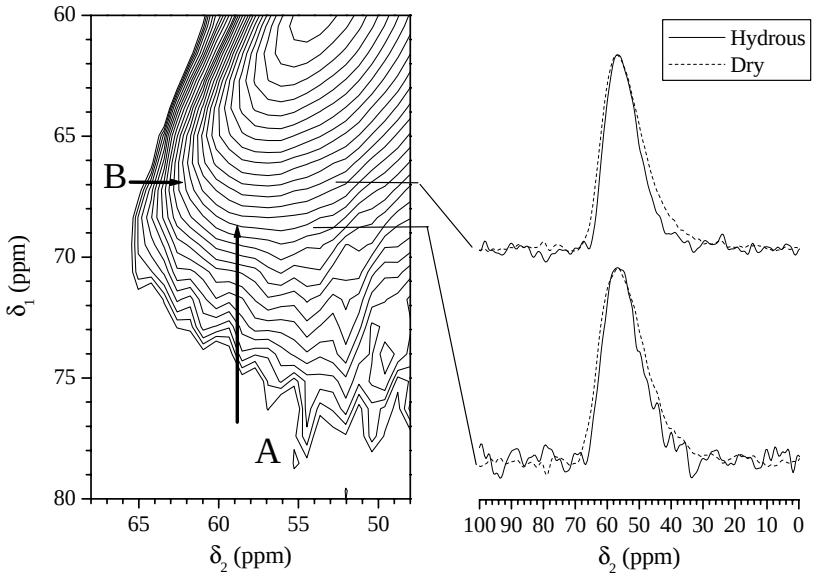

Fig. 3.6-5: An expanded view of the ^{27}Al 3QMAS spectrum from Q52-6H sample at 14.1T. The contour lines are plotted emphasising the low intensity levels by having a multiplication factor of 1.15 starting at 2 % (2.0, 2.3, 2.6, 3.0, 3.5, 4.0, 4.6, 5.3, 6.1… %). The site A and B represent the expected position of the Al Q^3-OH unit using parameters proposed previously. Right plots show the MAS slices at the position of sites A and B. The MAS slices at the same positions of the dry glass are superposed for comparison.

g. *Effect of boron on the water speciation in (alumino)silicate melts and glasses (B.C. Schmidt and F. Gaillard)*

In previous studies we investigated the structures of dry and hydrous boroaluminosilicate glasses (see the Annual Reports of 2000 and 2001). We observed different effects on the glass

structure by adding boron to albite composition or by substituting boron for aluminium. In all cases we observed a strong effect of dissolved water on the framework structure, but also an important effect of boron on the water speciation. In this contribution we focus on near-infrared (NIR) spectroscopic investigations of melts and glasses along the join reedmergnerite-albite ($NaBSi_3O_8$- $NaAlSi_3O_8$) to shed further light on the water incorporation in glassy and molten boro(alumino)silicate systems.

Glasses with five different compositions along the join reedmergnerite-albite (Rd-Ab) were studied (Rd100, Rd75Ab25, Rd50Ab50, Rd25Ab75 and Ab100, in mol.%). Hydrous glasses containing 0.5 to 8 wt.% water were synthesized at 2 kbar and 1000-1100 °C in TZM rapid quench autoclaves. Near infrared spectra show that beside the ”normal” NIR bands at 5200 cm^{-1} (molecular H_2O) and 4500 cm^{-1} (structurally bonded OH groups) a new hydroxyl-related band at 4730 cm^{-1} develops with increasing B-content. Since such band has never been observed in B-free glasses it seems reasonable to assume that it is related to B-OH complexes. The variations in the spectra indicate also that with increasing B-concentration but constant total water content the concentration of structurally bonded hydroxyl groups increases on the expense of molecular H_2O. The quantitative determination of such evolution requires the IR extinction coefficients for the relevant bands to be known. For this purpose, glasses with a range of known water content must be available. So far two glass series of Rd100 and Rd25Ab75 composition with 0.5 to 8 wt.% water have been prepared and studied with NIR spectroscopy. Since the three relevant NIR bands are not well separated, only linear extinction coefficients (peak heights) were determined. Compared to integral intensities (peak areas) they are less affected by the overlapping character of the peaks. In a first attempt we tried to determine the extinction coefficients for each band individually. This is possible with a modified law of Lambert-Beer, which has the form of an equation for a plane in the 3D-space. However, for our glasses the relative intensities of the two OH peaks do not vary sufficiently with total water content. Therefore the data do not plot on a plane but on a straight line (in the 3D-space), making an individual determination of the extinction coefficients for the 4500 and 4730 cm^{-1} bands impossible. In a first approximation the extinction coefficients were then determined in assumption that those of the hydroxyl related bands are identical. The evolution of the water speciation in Rd100 glasses using this assumption is shown in Fig. 3.6-6. It is clear that the hydroxyls represented by the new peak at 4730 cm^{-1} (possibly B-OH groups) make a significant fraction of the of the different water species.

For silicate glasses we know now that the water speciation strongly depends on temperature and that the speciation observed in glasses does not correspond to that in the melt at experimental conditions but rather to that of the glass transition temperature T_g, where the structure is frozen in. In order to learn more about the water speciation in B-bearing (alumino)silicate melts we performed *in situ* NIR spectroscopy at high P and T using a hydrothermal diamond anvil cell. Figure 3.6-7 shows NIR spectra of Rd100 melt between 330 and 800 °C. With increasing temperature the intensity of the H_2O band (5200 cm^{-1}) decreases while the intensity of the OH band at 4500 cm^{-1} increases. At the highest temperatures the OH

band at 4730 cm^{-1} cannot be resolved anymore. However, we cannot decide if this band and thus the related structural unit really disappears at high T or if we cannot observe it anymore as the result of the increasing background below 5000 cm^{-1} caused by the broadening of the 4000 or 3600 cm^{-1} bands. In any case the spectra clearly indicate that the 4730 cm^{-1} peak does not significantly increase with increasing T and thus the related structural unit does not participates in a large extent in the conversion of H_2O to hydroxyls. This conversion produces dominantly OH groups that are represented by the 4500 cm^{-1} NIR band. A more quantitative evaluation of the high temperature NIR spectra is highly desired but the difficulty of choosing the correct baseline makes the quantitative determination of the water speciation with T extremely difficult.

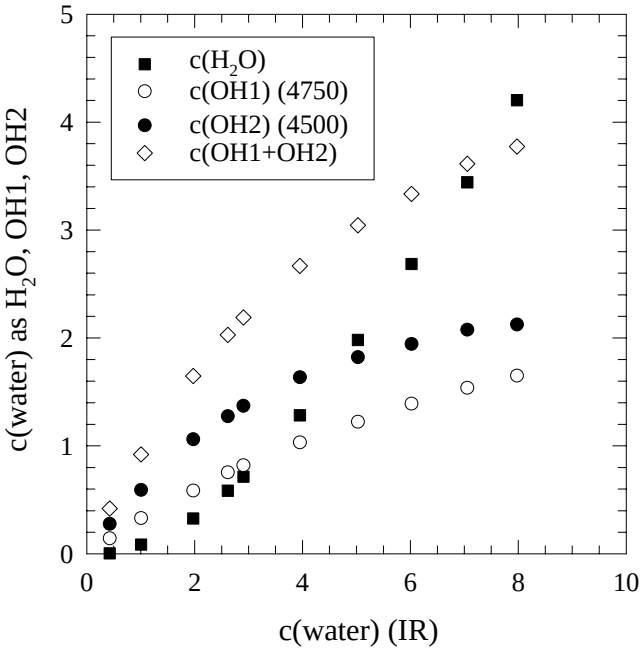

Fig. 3.6-6: Water speciation in RD100 glasses

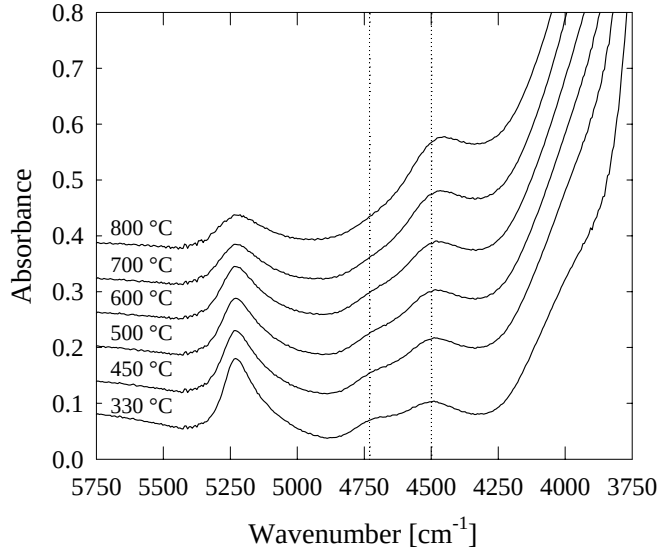

Fig. 3.6-7: NIR spectra of hydrous RD100 melts between 330 and 800 °C. The experiments were performed in an externally heated diamond anvil cell.

h. *The effect of time and melt fraction on connectivity of liquid Fe-S alloy in olivine under high pressure (H. Terasaki, D.C. Rubie and D.J. Frost)*

The determination of whether a liquid iron-alloy can segregate from a solid silicate matrix is a crucial factor in the investigation of terrestrial planet core formation. It is well known that the dihedral angle between liquid iron-alloy and solid silicate controls the connectivity of the liquid iron-alloy. The effects of physical and chemical properties, such as pressure and composition of the liquid, on the dihedral angle have been widely reported in recent years in a range of experimental studies. The timescale for textural equilibrium to occur and the effect of melt fraction on connectivity are not well established, however, especially under high-pressure conditions. In this study, we have determined the dihedral angle between liquid Fe-S alloy and olivine crystals as a function of time and of liquid volume fraction and estimated the time scale of textural equilibrium at 4.6 GPa and 1830-1960 K.

High-pressure experiments were carried out using Kawai- and Walker-type multianvil apparatus with $LaCrO_3$ stepped heaters and graphite capsules. The size of the cell assemblage was 25/15 to obtain a large volume of the sample. Mixtures of powdered iron-sulphide and synthetic olivine (Mg# =77) were used as starting materials. Two iron-sulphide compositions ($Fe_{78}S_{22}$ and FeS) were adopted. All experiments were performed at 4.6 GPa and 1830-1960 K. We changed the experimental durations (0.5-144 hours) and volume fractions of iron-sulphide (1-6 vol.%).

Apparent dihedral angles were measured from backscattered electron images of the recovered samples with magnifications of x1200 and x2000 (Fig. 3.6-8). The true dihedral angle between olivine and sulphide melt was taken to be the median value of the apparent dihedral angle distribution. The apparent angle distribution was close to the theoretical distribution reported by Harker and Parker, Am. Soc. Metal. Trans. 34, 156, 1945. The dihedral angle observed in experiments on 2 vol.% FeS decreased with time but levelled off after 12-15 hours. The dihedral angle of $Fe_{78}S_{22}$ showed similar behaviour (Fig. 3.6-9). On the other hand, in the case where 6 vol.% FeS was employed, an interconnected FeS network texture could be observed after 8 hours duration at which time the dihedral angle apparently took a minimum value. If the melt fraction exceeds the critical value, a melt can form an interconnected network of melt channels in spite of its dihedral angle value. (von Bargen & Waff, J. Geophys. Rev., 91, 9261, 1986). In the case of 2 vol.% FeS an interconnected texture was not observed for any experimental duration. The dihedral angle behaviour of 6 vol.% FeS with time reflects the time scale for textural equilibrium to be achieved and for the development of a melt channel network. Consequently, at least 12 hours are required to establish textural equilibrium for liquid Fe-S if the melt fraction is less than the critical melt fraction.

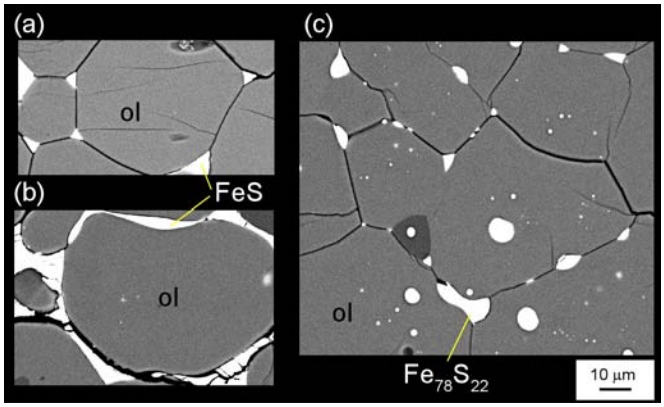

Fig. 3.6-8: Back scattered electron images of run products. (a) texture of FeS with low melt fraction (b) interconnected network of FeS melt (c) texture of $Fe_{78}S_{22}$ with low melt fraction.

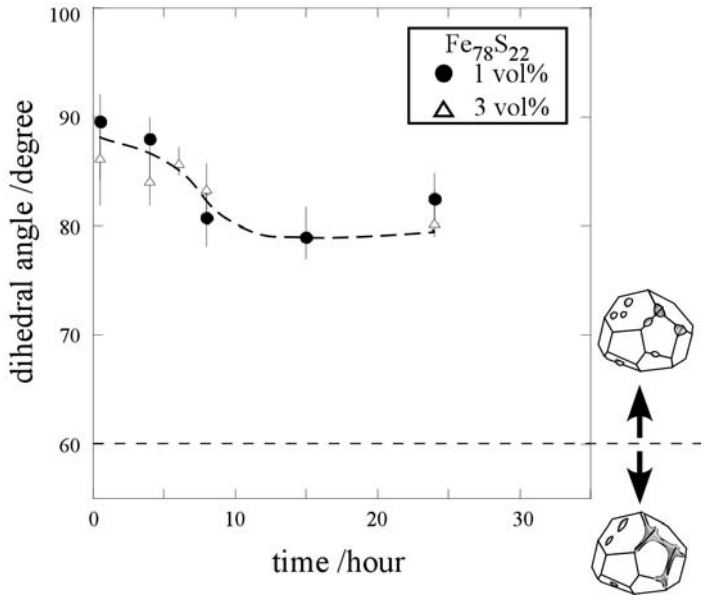

Fig. 3.6-9: Time dependence of dihedral angle of $Fe_{78}S_{22}$. The error of the dihedral angle corresponds to the 95 % confidence interval around the population median.

3.7 Materials Science

The goal to model processes in the deep Earth's interior has stimulated experiments at high pressures and temperatures. Physicists and material scientists also use such methodology to study different classes of compounds at extreme conditions. Bayerisches Geoinstitut incorporates existing and developing high pressure equipment and methods, and is involved in numerous challenging materials science investigations at extreme conditions.

One of the classical tasks of materials science is the study of P-T phase diagrams. It is surprising that phase relations in Pb, one of the oldest metals known to man, are not well established, and determination of the phase boundary between *fcc* and *hcp* Pb polymorphs is a step in this direction. The titanium group elements are widely used in modern technology (particularly in the aerospace industry) due to their light weight, static strength and stiffness. The development of new Ti-based alloys requires fundamental knowledge of the behaviour and possible changes in the electronic structure of titanium at elevated pressures and temperatures.

Fullerenes are a new form of carbon which have attracted enormous interest over the last ten years due to their unusual close cage structure and unique properties. Under high pressure – high temperature treatment, fullerenes and their compounds undergo transitions to different polymeric phases. Some of them have been reported to be harder than diamond, while others are magnetic and electrically conducting. The details of the polymerization process in C_{60} are not clear, and the combination of *in situ* studies in diamond anvil cells and synthesis in multianvil apparatus where relatively large amounts of material are available opens new possibilities for the creation of new fullerite-based materials.

Among known and potential technological applications of nanocrystalline titania (TiO_2) are pigments, plastics, cosmetics, electronics, and catalysts. Experiments in diamond anvil cells provide new insight into elastic properties and phase relations in this material. Although high-pressure studies were successful for investigation of electronic/magnetic features of the Mott transition phenomenon (the fundamental process in which strongly correlated insulating systems transform into a metallic state without magnetic moments), their structural features are still ambiguous. Combination of diamond anvil cell experiments with synchrotron based X-ray powder diffraction studies uncovers a number of structural details of the Mott transition in the model layered compound FeI_2.

Materials with the perovskite structure are probably the best example of compounds with interest to both geo- and material scientists. In materials science, perovskites are important as high-T_c superconductors, ceramics for fuel cells, gas sensors, and membranes for oxygen extraction or hydrogen production. The mechanism of formation and distribution of defects is equally important for both materials science and geoscience. Well developed by geoscientists and routinely used in BGI, methods of synthesis at high gas pressure, particularly at high

oxygen pressure, are effective for the preparation of solid solutions of electrochemically active $LiNiO_2$ and $LiGaO_2$ over the entire concentration range. It opens the possibility to replace $LiCoO_2$, which is commonly used as a cathode material, with a new one based on Ni. The spin-crossover phenomenon (SCO) involving thermo-, photo-, magneto-, and piezo-chromic properties of a class of transition metals, particularly iron complexes, is one of growing importance in the area of multifunctional molecular materials, especially for possible applications in memory, display and switching devices at the molecular scale. The mechanism and numerous details of SCO are still poorly understood. The fine tuning of volume with pressure provided by *in situ* high-pressure experiments in diamond anvil cells opens the possibility for studying lattice dynamics during spin-crossover transitions and pressure-induced amorphization. Modern methods of materials modifications, e.g. laser surface processing of ceramics, often change only a small submicron area. In such cases, the analytical methods that are common to geosciences and material sciences, particularly analytical transmission electron microscopy, can help to uncover the transformation mechanism.

a. *FCC-HCP phase boundary in lead (L.S. Dubrovinsky, in collaboration with A. Kuznetov, V. Dmitriev and H.-P. Weber/Grenoble)*

Elemental lead, one of the oldest metals known to man (mentioned in Exodus!), has many applications. Some are derived from its low tensile strength (shock absorbers in foundations of high-rise buildings), others from its high absorption of electromagnetic radiation (protective shielding), its high resistance to corrosion (economical plumbing), and its easy alloyability (solder material) – to mention just a few key attractive properties. In everyday life, its economically most important use comes from its favorable electrical properties; lead-acid storage batteries, the demise of which has been predicted for decades, are still being continuously improved. In its compounded form, the uses of lead are even more ubiquitous and therefore too numerous to mention here. So lead is clearly, already in its elemental form, a material of strategic importance, and it is therefore surprising that the phase diagram of such an important element has been so cursorily explored until now. Isothermal high-pressure X-ray diffraction experiments first disclosed the transformation of Pb from the face-centered cubic (FCC) form to the hexagonal-close-packed (HCP) structure at 14 GPa and then, at about 120 GPa, to the body-centered cubic (bcc) phase. However, the phase boundaries, phase coexistence regions and their evolution with increasing in temperature were not studied.

In situ high-pressure – high-temperature data were obtained at the ID-30 beam line of the European Synchrotron Radiation Facility (ESRF, Grenoble, France) by angle-dispersive X-ray diffraction techniques employing monochromatic (λ=0.3738 Å) X-radiation. Small pieces of polycrystalline Pb (99.999 % purity, Advent) were studied in an externally heated, gasketed diamond anvil cell. The existence of reliable data on pressure – temperature EOS for

NaCl allowed us to use this material both as a pressure-transmitting medium and the pressure calibrant at high temperature. A K-type thermocouple placed close to the high-pressure sample chamber was used to measure the temperature of the sample. Diffraction measurements were performed up to a maximum pressure of 40 GPa and to a maximal temperature of 800 K; these limits ensured a completion of the fcc-to-hcp transformation.

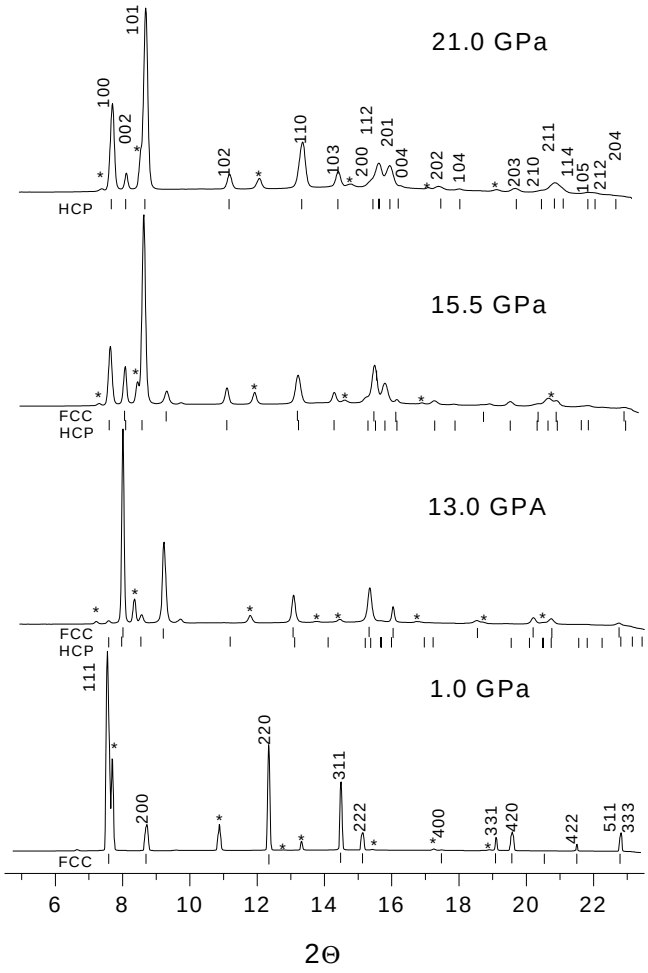

Fig. 3.7-1. Examples of high-pressure synchrotron radiation X-ray powder diffraction patterns of Pb metal in different phases at room temperature. * denotes B1 NaCl peaks.

Figure 3.7-1 shows the selected angle-resolved X-ray diffraction patterns of lead up to 21 GPa at ambient temperature, covering the transition region. All peaks could be indexed with the fcc, hcp structures of Pb and the B1 NaCl structure. At room temperature, the onset of the phase transition from the fcc phase to the hcp phase takes place at a pressure of about 12.0 GPa, where at least two diffraction peaks of the hcp Pb, (100) and (101), which do not overlap with fcc peaks, are observed (Fig. 3.7-1). With increasing pressure, the intensities of the hcp lines increase and the fcc lines disappear. The fcc-to-hcp transition in Pb is very sluggish; both the fcc and hcp phases coexist up to a pressure of 20 GPa.

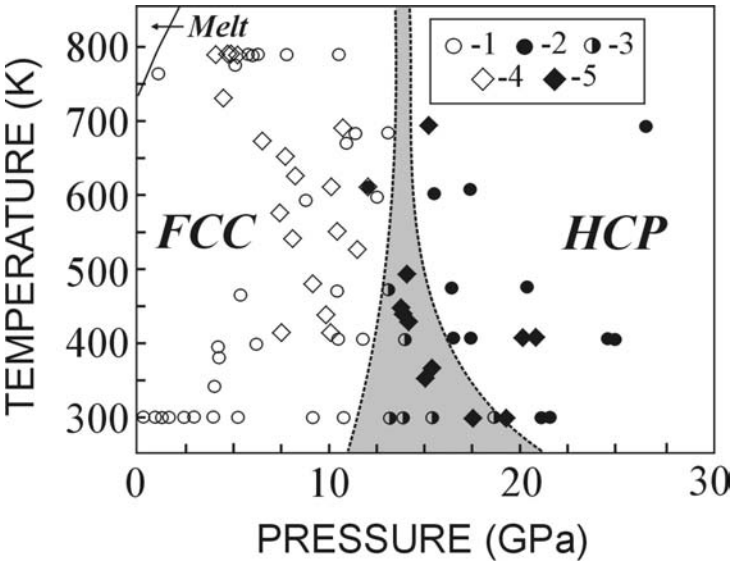

Fig. 3.7-2: P-T phase diagram of lead. Compression: 1, fcc phase; 2, hcp; 3, two-phase mixture. Decompression: 4, fcc; 5, hcp. The two-phase region is shaded grey.

Figure 3.7-2 summarises results of diffraction experiments and shows the phase diagram of lead in the pressure range covering the fcc-to-hcp transformation region. One can see that the two-phase pressure range decreases with temperature increase, in full agreement with the kinetic interpretation of its nature. The progressive decrease of $\Delta V/V$ with increasing temperature is characteristic for this pressure-induced transition.

b. *Titanium metal at high pressure: Synchrotron experiments and ab initio calculations (L.S. Dubrovinsky, N.A. Dubrovinskaia, in collaboration with R. Ahuja, J.M. Osorio Guillen, B. Johansson/Uppsala)*

The titanium group of elements and their alloys are very important materials both from a technological and a scientific point of view. Technologically, these materials have application in the aerospace industry due to their light weight, static strength and stiffness, and they show oxidation resistance and do not degrade rapidly when the temperature is increased. From a fundamental point of view, these elements are situated at the beginning of the transition metals series and have a comparatively narrow *d*-band in comparison to the broad *s* band with regard to electronic structure. The transfer of *s* electrons into the *d* band with pressure in these metals governs both the electronic and structural properties. Conventional ideas about the crystal structure stability of transition metals suggest that the most important parameter controlling the stability of a given structure is the *d*-occupation number. This is related to the fact that the *d* density of states for different structures show characteristic element independent shapes.

The titanium group of elements are all stable in the hcp structure under ambient conditions, but at high temperature they transform to the bcc structure. It is now well established that the two other elements of the titanium group (Zr and Hf) transform to the bcc phase at ambient

temperature and high pressure. Ti, Zr and Hf show a phase transition from hcp to ω phase under pressure. On further compression, the ω phase transforms to the bcc phase in the case of Zr and Hf. The search for a high pressure bcc phase in titanium is still ongoing.

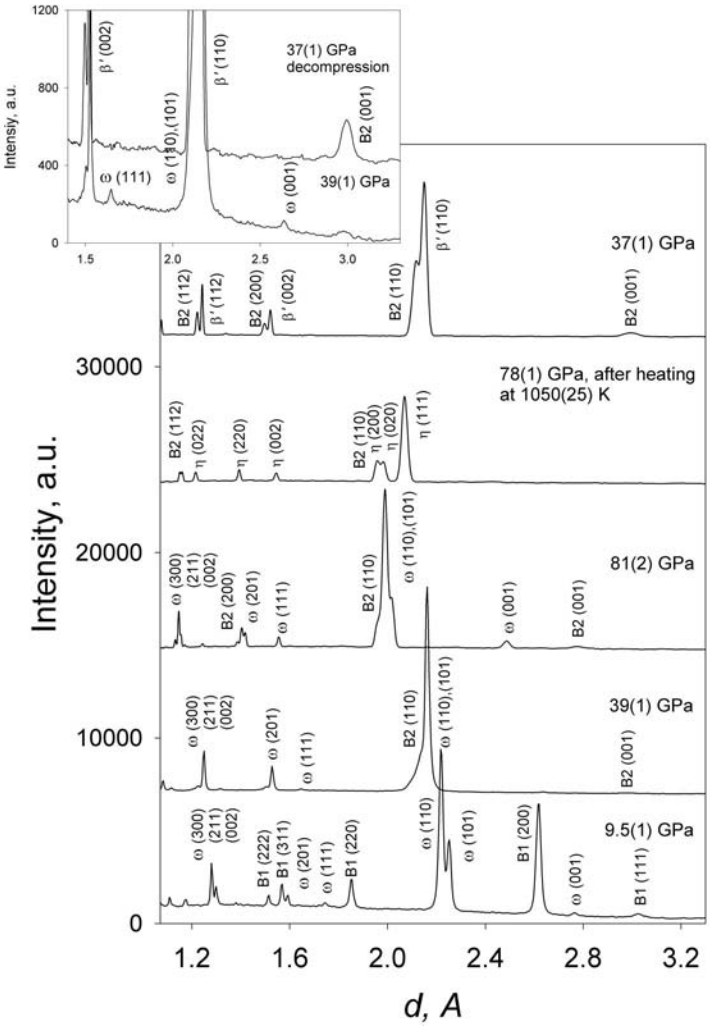

Fig. 3.7-3: Examples of X-ray diffraction patterns obtained in our experiments for titanium metal (B1 and B2 denote the low- and high-pressure NaCl polymorphs, respectively).

In our experiments high purity (99.999 %) Ti was used as a starting material. At applied pressures of about 9 GPa the initial α phase Ti (hcp structure) transforms into the ω-phase (Fig. 3.7-3). Further compression to 39 GPa does not result in any phase transformations. However, at 42 GPa we observed the appearance of new reflections in addition to those of the ω-phase (Fig. 3.7-4). These reflections are nearly indistinguishable on the 1D-integrated ("conventional") diffraction pattern, but could be easily recognised on the on rolled (option "CAKE" in Fit2D program) images (Fig. 3.7-4). A pressure increase to 81 GPa did not result in more pronounced splittings of the reflections of ω-Ti and the new phase, and all the peaks observed on the 1D-integrated pattern could still be indexed as reflections of pure ω-Ti (Fig. 3.7-3). However, the quality of the full-profile refinement decreases with pressure and it is practically impossible to describe the pattern collected at 81 GPa in terms of only two phases – B2-NaCl (pressure medium) and ω-Ti. At the same time, if we assume that bcc-structured

titanium is present in the sample (we call it β' to emphasise its structural similarity with low-pressure bcc-titanium), we are able to quantitatively describe the diffraction patterns at pressures up to 80 GPa.

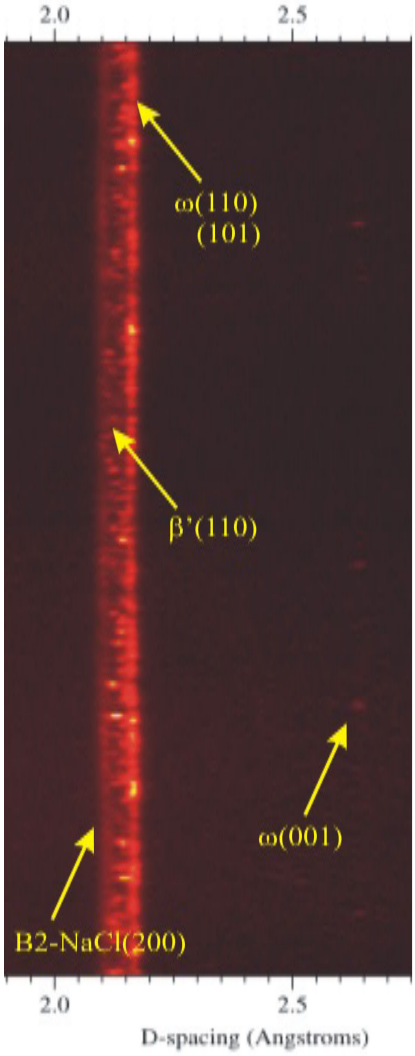

Fig. 3.7-4: Part of the integrated image collected at 42(1) GPa showing diffraction lines of ω-Ti and new bcc-structured β'-Ti

Laser-heating at 1200-1300 K or electrical heating at 1050(25) K during 3 hours at 78-80 GPa results in significant changes of the diffraction pattern (Fig. 3.7-3). Reflections of the new η-phase could be indexed as an orthorhombic lattice and the diffraction pattern could be reproduced by the *Fmmm* space group with Ti in the 4a (0, 0, 0) position. The lattice parameters of η-Ti at 78(1) GPa and ambient temperature are a=3.918(1) Å, b=3.968(1) Å, c=3.092(1) Å. The structure of the η phase could be considered as a monoclinically distorted bcc structure with lattice parameters $a'=b'$=2.788 Å, c=3.092(1) Å, γ=89.3°.

On decompression at room temperature η-Ti transforms into ideal bcc-structured β'-phase at pressures below 40 GPa (Fig. 3.7-3). Note that while on compression (or on decompression of the unheated sample) the characteristic (001) and (111) reflections of ω-Ti are easily detectable, they are absent in the diffraction pattern of the β'-phase obtained by decompression, of η-Ti (Fig. 3.7-3, inset). On further decompression, at pressures below 30 GPa, β'-Ti transforms to the ω-phase, which could be quenched to ambient pressure.

In summary, our experimental and theoretical studies show the existence of the bcc-structured phase in Ti at high pressure. We have found that titanium has the potential to form metastable phases (such as δ, γ, or η) with similar molar volumes. This is also shown by *ab initio* calculations. Our results suggest that stable Ti phases behave similarly to their counterparts Zr and Hf, *i.e.* on compression at room temperature, there is a transformation from the hcp to the ω-phase, and further to the bcc-structured phase.

c. *In situ study of C_{60} polymerisation at high-pressure high-temperature conditions (A. Talyzin/Uppsala and L.S. Dubrovinsky)*

High-pressure high-temperature (HPHT) treatment of C_{60} below 9 GPa and 900 K lead to the formation of several kinds of one and two-dimensional polymers. For these polymers, a ”2+2” cycloaddition reaction mechanism has been proposed where double bonds in neighboring C_{60} molecules are broken under the formation of four-membered rings joining two C_{60} molecules. Reports on the dimeric phase are still controversial. One-dimensional orthorhombic C_{60} polymers (chain-like) are the most widely studied. They have been obtained over a wide range of pressures (up to 8 GPa) and relatively low temperatures (starting already from 370 K). At higher temperatures, two different two-dimensional polymers have been reported which are tetragonal at lower pressures and rhombohedral at higher pressures. Raman spectroscopy is widely used for characterization of the C_{60} polymers. Some of the most typical signatures in Raman spectra for polymerization are: (i) a shift of the $A_g(2)$ mode proportional to the number of square rings connecting neighboring C_{60} molecules around 900-1000 cm^{-1}, (ii) peaks originating from square rings vibrations, and (iii) new peaks below 200 cm^{-1} due to intercage vibrations. Above about 9 GPa a number of different three-dimensional polymers have been reported. At low temperatures the *fcc* structure is maintained but the cell parameter is strongly reduced. Several other three-dimensionally polymerized structures have been claimed to exist at pressures above 12-13 GPa and temperatures above 800 K. Many of these structures have been proposed from single observations using conventional XRD. Recently strongly elliptical Debye-Scherrer lines have been found in 2D images of samples treated at 13 GPa and 830 K. Amorphous phases have also been observed at high pressures. The transition temperature for the formation of a non-crystalline phase is pressure dependent. At about 10 GPa an amorphous phase is formed above 900 K, but X-ray amorphous structures have been observed already at room temperature above 20 GPa. Some of these amorphous phases have been reported to be “superhard” with hardness comparable to or even exceeding that of diamond.

Several groups have recently presented P-T phase diagrams for C_{60}. All results summarized in these diagrams originated from *ex situ* studies where the samples were heated to a certain temperature and rapidly cooled to room temperature and analyzed after a rapid release of pressure (quenching). This means that the P-T diagrams recorded *ex situ* should be considered more as a map showing the conditions under which a certain phase (or mixture of phases) can be produced. A problem with this type of study is that the phase composition of the quenched samples can be different from the phase composition at the HPHT conditions.

The C_{60} polymerisation was studied *in situ* by Raman spectroscopy in the pressure range 10-27 GPa and temperatures up to 830 K utilizing externally heated diamond anvil cells. Quenched samples were studied by XRD using synchrotron radiation. Below 18 GPa only one and two-dimensional polymers were found to form during the heating (Fig. 3.7-5). During slow cooling and quenching only the relative amounts of the different polymerised C_{60} phases

were changing. The structure of the samples quenched after treatment between 10 and 18 GPa is rhombohedral. The observed polymerisation pathway suggests a gradual increase of polymerisation which occurs in the following sequence: monomers-dimers-chains-tetrapolymer-hexapolymer. Above 18 GPa the *in situ* Raman spectra during heating remained almost unchanged. XRD of the quenched samples revealed that they have a cubic structure with cell parameter above 13 Å. The sample heated at 27 GPa showed elliptical Debye-Scherrer diffraction rings due to the strong anisotropic deformation. No super dense phases reported in previous studies (so called "superhard fullerite") were observed.

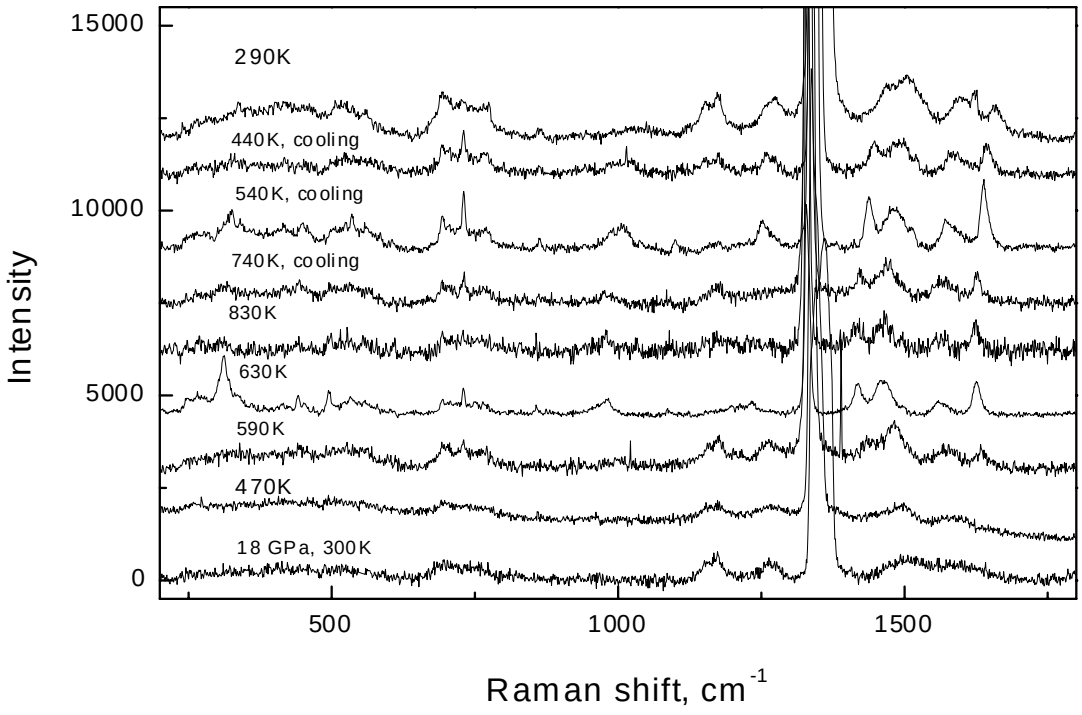

Fig. 3.7-5: *In situ* Raman spectra recorded during the heating of C_{60} at 18 GPa.

d. *High pressure Raman study of $C_{60}S_{16}$ (A. Talyzin/Uppsala and L.S. Dubrovinsky)*

Theoretical calculations have shown that a phase with sulfur atoms connected to two carbon atoms of C_{60} with covalent bonds (similar to the well known $C_{60}O$ phase) may exist and could exhibit unusual optical and electronic properties. So far all attempts to synthesize this compound have failed. Nevertheless, the recent success in the synthesis of a dimeric $C_{120}OS$ compound shows that covalent bonding of sulfur to carbon atoms in the C_{60} cage is possible, although attempts to synthesize $C_{120}S_2$ have been unsuccessful. It is likely that new types of C_{60}-sulfur materials may be obtained by high-pressure high-temperature treatment either in the form of the predicted $C_{60}S$ compound or as some kind of polymer like $C_{120}S_2$.

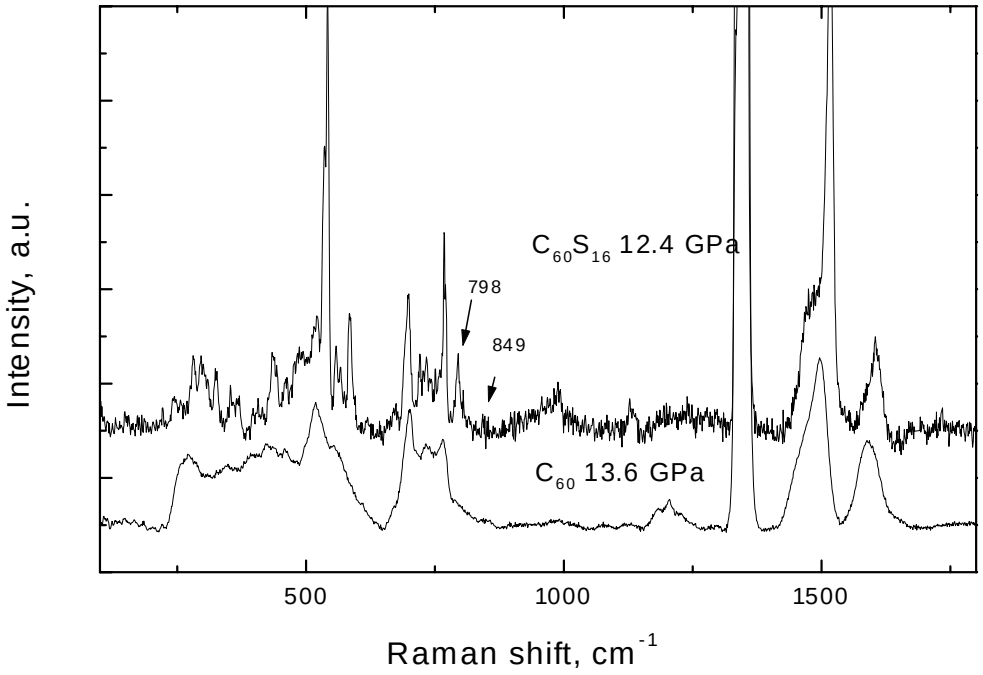

Fig. 3.7-6: Raman spectra of $C_{60}S_{16}$ and pure C_{60} recorded *in situ* at 12.4 and 13.6 GPa, respectively.

We conducted a Raman spectroscopic study of the behaviour of $C_{60}S_{16}$ in diamond anvil cells at pressures up to 13.6 GPa (Fig. 3.7-6). The key point in the analysis of our spectra must be the identification of possible C-S-C vibrations. Since this kind of bridge has longer bonds and a weaker force constant than the C-O-C bridge, this is expected to result in lower vibration frequencies. The epoxy group vibrations are expected near 1265 cm^{-1} and between 800 and 900 cm^{-1}, but were not clearly identified for $C_{60}O$, $C_{120}O$ and other C_{60} oxides. In our recent study it was found that C_{60} at this pressure and room temperature transforms to a mixture of dimeric and chain polymers. The $C_{60}S_{16}$ spectrum at high pressure (Fig. 3.7-6) is very similar, but exhibits much sharper peaks compared to compressed C_{60}. The spectra of $C_{60}S_{16}$ recorded at high pressure (starting from 7.2 GPa) showed peaks at about 798 cm^{-1} and 849 cm^{-1}, which are probable candidates for C-S-C vibrations. These lines are not present in the spectra of pure C_{60} pressurized to similar pressure, and cannot belong to modifications of sulfur rings since all sulfur lines are found below 600 cm^{-1}.

The spectrum of the quenched sample is similar to pristine $C_{60}S_{16}$ in the sense that we observe clear peaks of S_8 rings and lines of C_{60} (Fig. 3.7-7). However, there are some clear differences between the spectra. The state of C_{60} molecules has clearly changed, most probably due to polymerization. The $A_g(2)$ mode is downshifted to 1464 cm^{-1}, the $A_g(1)$ mode is split into two peaks at 489 and 493 cm^{-1}, while the $H_g(1)$ mode shows splitting on three peaks at 257, 260 and 297 cm^{-1}. In general, the spectrum of quenched $C_{60}S_{16}$ is very similar to that of dimeric C_{60}.

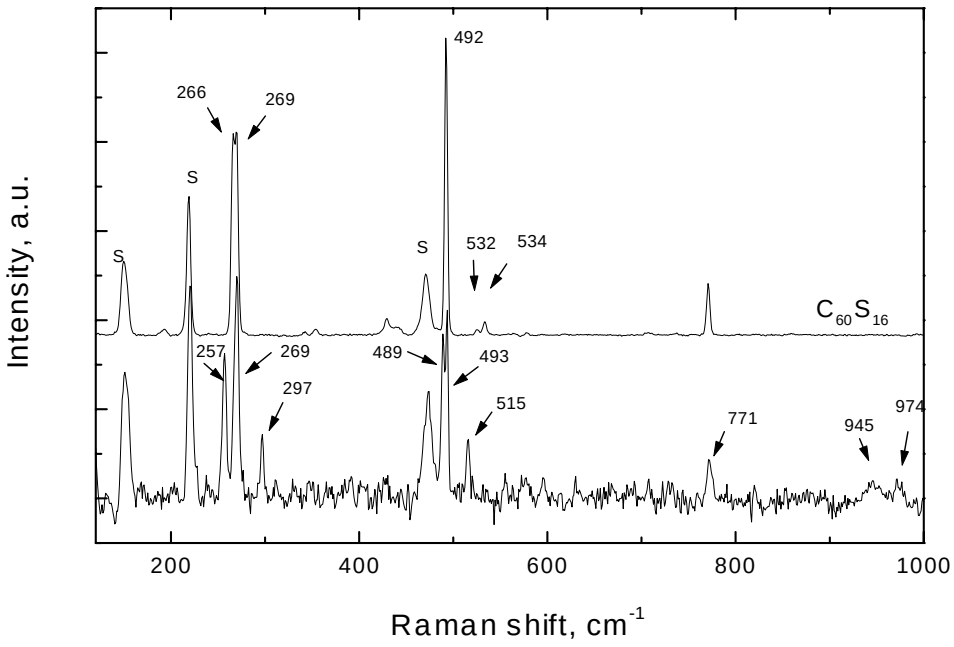

Fig. 3.7-7: Raman spectra of pristine $C_{60}S_{16}$ (top) and the sample quenched from 12.4 GPa (bottom).

The peaks at 945 and 974 cm^{-1} are typically assigned to vibrations of square rings connecting C_{60} molecules. On the other hand, the spectrum of quenched $C_{60}S_{16}$ looks very similar to that of $C_{60}O$. It is interesting that the $C_{60}O$ spectrum also shows the position of the $A_g(2)$ mode at 1464 cm^{-1}, a splitting of the $H_g(1)$ mode with the strongest peaks at 258, 268 and 289 cm^{-1}, and splitting of the $A_g(1)$ mode into two peaks at 475 and 488 cm^{-1}. The $C_{60}O$ spectrum also shows some broad features around 950-1000 cm^{-1}. Finally, it should be noted that specific peaks found for $C_{60}S_{16}$ at high pressure were not observed in the quenched sample.

In conclusion, the *in situ* high pressure studies show some additional peaks, *e.g.* 849 and 798 cm^{-1} (at 12.4 GPa) which cannot be attributed to any known polymeric phase. This could be due to the formation of C-S bonds. After quenching these peaks disappeared, indicating that C-S bonds are broken upon quenching. However, the presence of peak shifts and splitting suggest that the sample consists of either $C_{60}S + S_8$, or that C_{60} in the $C_{60}S_{16}$ become polymeric.

e. *Compression behaviour of nanocrystalline anatase TiO_2 (L.S. Dubrovinsky and N.A. Dubrovinskaia, in collaboration with V. Swamy/Montreal)*

Titanium dioxide (TiO_2) in the macrocrystalline and nanocrystalline forms is an important material with several known and potential industrial applications. Among the major technological applications of this material are pigments, plastics, cosmetics, electronics, and

catalysts. TiO_2 has also served mineral physicists as a model system in the study of pressure-induced structural phase transitions of oxides relevant to the Earth's mantle, in particular that of SiO_2. More recently, nanocrystalline TiO_2 has been used as a model system to investigate the size-dependent phase transition behaviour of nanoscale oxides in terrestrial environments. Because of its technological and fundamental importance, numerous experimental and computational studies have investigated the phase stability and properties of macrocrystalline TiO_2 polymorphs. Only a beginning has been made, however, in the study of the properties and phase stability of nanocrystalline TiO_2 polymorphs. In the case of nanocrystalline anatase, different studies have reported contradictory high-pressure behaviour. In view of the contrasting published data, we undertook a powder X-ray diffraction study of the room-temperature compression behaviour of nanocrystalline anatase to 35 GPa with the diamond anvil cell (DAC) technique and synchrotron radiation.

We collected X-ray diffraction spectra in the pressure range between 0 and 35 GPa at intervals of about 2 GPa to analyze the pressure-induced changes in nanocrystalline anatase and to retrieve an isothermal (room-temperature) bulk modulus. A selection of X-ray diffraction spectra representing the entire pressure range is presented in Fig. 3.7-8. The diffraction spectrum obtained at 18.2(4) GPa showed, in addition to the anatase peaks, the first appearance of the most intense reflections belonging to the baddeleyite-structured TiO_2 (reflections marked as B in Fig. 3.7-8). Distinct reflections due to anatase could be seen in spectra obtained up to 25 GPa. We did not observe diffusion halos or significant increases in the background that could be attributed to amorphization in any of the high-pressure diffraction spectra.

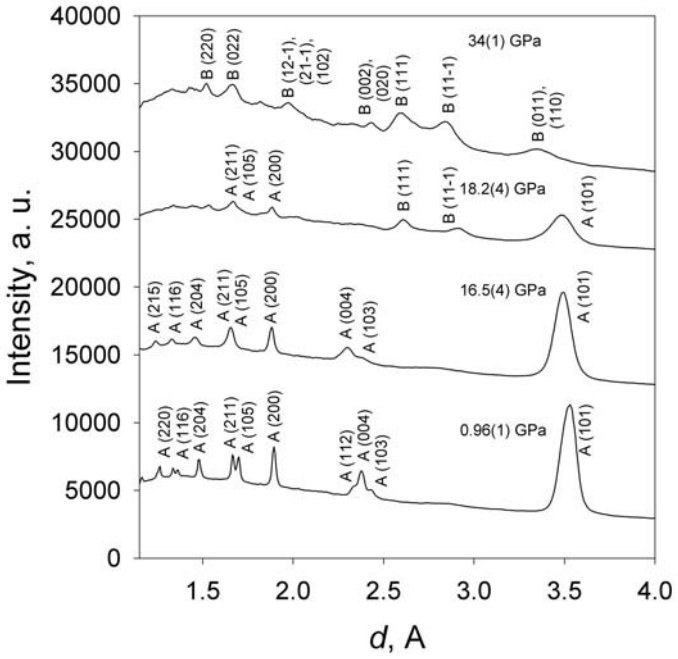

Fig. 3.7-8: Representative powder X-ray diffraction patterns obtained from compressed nanocrystalline anatase. Reflections marked A originate from anatase, and those marked B from baddeleyite-TiO_2.

The size effect on the pressure-induced phase transition of anatase at room temperature is now rather clear. Single crystal anatase transforms to the α-PbO_2-structure at 2.5-7 GPa. Although there have been reports of a phase transition in microparticle (polycrystalline) anatase around this pressure, a recent study seems to suggest that the phase transition is suppressed in microparticle anatase to about 8-13 GPa, where it transforms to the baddeleyite structure. A further increase in stability with pressure is observed for nanocrystalline anatase. The data from this study demonstrate that the smaller the crystallite size of the nanocrystalline anatase, the larger the transition pressure. We observed the preservation of single-phase nanocrystalline anatase to about 16.5 GPa at room temperature, and its coexistence with baddeleyite-TiO_2 to 25 GPa.

The unit cell volume versus pressure data obtained for the nanocrystalline material are compared with that of macrocrystalline anatase in Fig. 3.7-9. A fit of the volume-pressure data to a Birch-Murnaghan equation by assuming the pressure derivative of the bulk modulus, K' = 4, gave the following equation of state parameters: zero-pressure volume, V_o = 136.15 $Å^3$ and bulk modulus, K_T = 243(3) GPa. The bulk modulus obtained for the nano-anatase is about 35 percent larger than the corresponding value of about 180 GPa for the macrocrystalline counterpart.

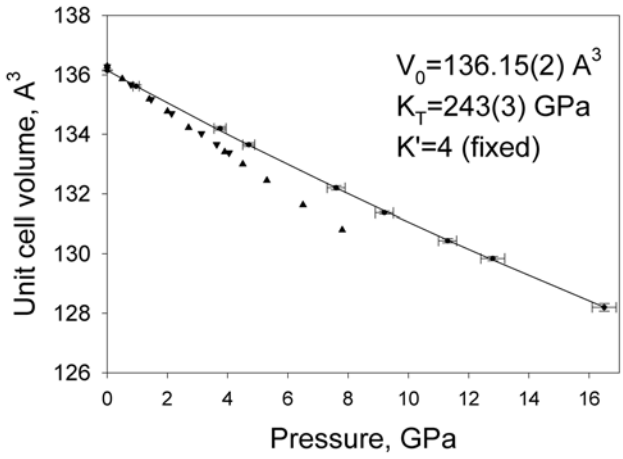

Fig. 3.7-9: Room-temperature pressure-volume data of nano-anatase (circles) compared with data from polycrystalline (triangles, from Swamy and Dubrovinsky, 2001) and single crystal (inverted triangles, from Arlt *et al.*, 2000) anatase.

f. *Pressure-induced structural transformations in the Mott insulator FeI_2 (L.S. Dubrovinsky, in collaboration with G.K. Rozenberg/Tel Aviv and R. Ahuja/Uppsala)*

In the past decade, substantial progress in the study of Mott transition phenomena (the fundamental process in which strongly correlated insulating systems transform into a metallic state without magnetic moments) was achieved owing to a significant improvement of high-pressure apparatus and methods such as development of high-pressure Mössbauer spectroscopy and electrical resistivity for probing of transport properties. In spite of a

succession of high-pressure studies of electronic/magnetic features of the Mott transition, the structural features are still ambiguous. Similar to the view of the origin of the “Coulomb” gap, it was anticipated that a pressure-induced gap-closure and its associated insulator-metal transition should not necessarily involve a structural change, and should be accompanied only by a collapse of the transition metal (TM)-magnetic moment. Meanwhile from the few crystallographic studies following a correlation breakdown in the TM compounds RNiO$_3$ (R = Pr, Nd, Eu, and Sm), V_2O_3 and Cr_2O_3-V_2O_3, it was found that in the case of the *temperature-induced* Mott transition, an appreciable change of the interatomic distances takes place. This may result from a symmetry change due to a strong distortion. Recent studies of *pressure-induced* Mott transitions (in hematite, for example), demonstrated as well that this electronic transition might induce or be a consequence of structural alterations. Hence, a study of structural aspects of the pressure-induced Mott transition may provide insights into the phenomena and allow a more quantitative picture of the transition. A new important electronic feature recently discovered is the quenching of the orbital ordering induced by pressure. In the case of $LaMnO_3$, it was shown that orbital order has been suppressed at P > 18 GPa and the Mott transition occurred only at 32 GPa. A related discovery was the quenching of the orbital term in FeI_2 observed from Mössbauer spectroscopy causing the breakdown of the spin-orbit coupling and the reorientation of the magnetic moment. This result is rather unexpected, and the structural aspects of this phenomenon should also be investigated.

Another important reason for studies of the high-pressure structural evolution of FeI_2 is that FeI_2 represents a very broad class of layered materials that exhibit several important properties. It simulates an anisotropic two-dimensional antifferomagnet, and furthermore is a rather compressible system. Isomorphic $Me(OH)_2$ systems demonstrate a trend to pressure-induced amorphization, which could be attributed to the disorder in both the O-H and in the Me-O layers, or to the (O-H) molecular ion alone. It is possible to propose that a similar phenomenon could be attributed to the FeI_2 system. All the above-mentioned features stimulate a significant interest in a structural study of FeI_2 at a broad pressure range.

A full-profile refinement of FeI_2 structures at pressures up to 70 GPa combined with *ab initio* calculations were performed to particularly elucidate the structural aspects of the pressure-induced Mott transition phenomenon, and clarify the crystallographic features of the orbital order quenching induced by pressure. Synchrotron powder XRD diffraction studies (Fig. 3.7-10) have shown that at 17 GPa a substantial alteration of lattice parameters takes place, which can be attributed to the sudden quench of the orbital term. Starting at P ~ 20 GPa, a sluggish structural phase transition takes place (Fig. 3.7-10) related (according to resistance and MS studies) to the onset of a Mott transition. In accordance with *ab initio* calculations, the doubling of lattice parameters and the formation of a new Fe sublattice of the original CdI_2-type structure could describe this structural transition. The latter alterations in the Fe sublattice may indicate a trend of the Fe sites to disorder in the new HP phase. This phase transition is characterized by a significant change of the unit cell parameters, reduction in

volume and Fe-I distances (Fig. 3.7-11). The transition is completed at ~ 35 GPa. The substantial reduction of Fe-I distances with minimal changes in the Fe-Fe bond lengths at the transition suggests a *Charge-Transfer* gap closure mechanism involving the iodine *p*-bands. At P > 40 GPa the reverse of the structural transition is observed, resulting in the onset of the original atomic arrangement.

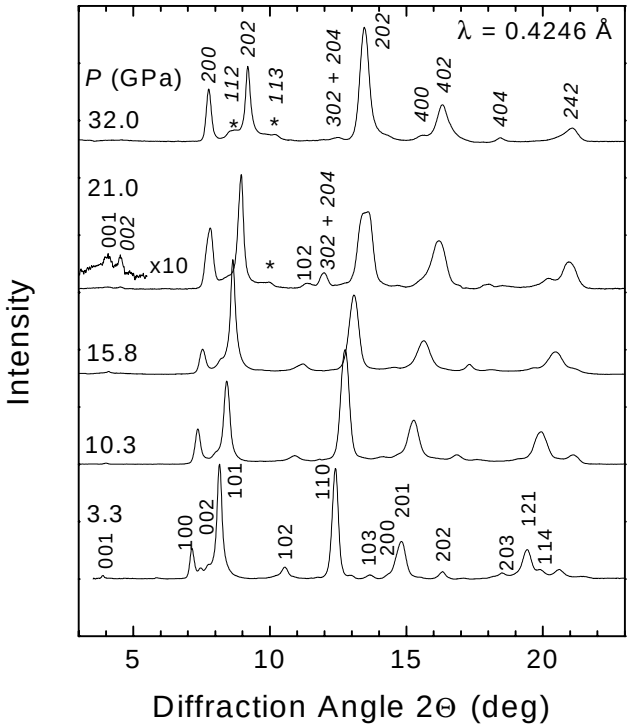

Fig. 3.7-10: X-ray powder diffraction patterns of FeI_2 at T = 298 K and various pressures. Note the distinctive splitting of the diffraction peaks for the pattern at P = 21 GPa, especially the (001), (102) etc. reflections. A part of the spectrum at the 2Θ range of 3º – 5.5º is reproduced with x10 magnification to give emphasis to the (001) splitting. Weak peaks, which appeared at 20 GPa in addition to the original CdI_2 type structure, are marked with (*). Italics indicate the diffraction peaks of the HP phase.

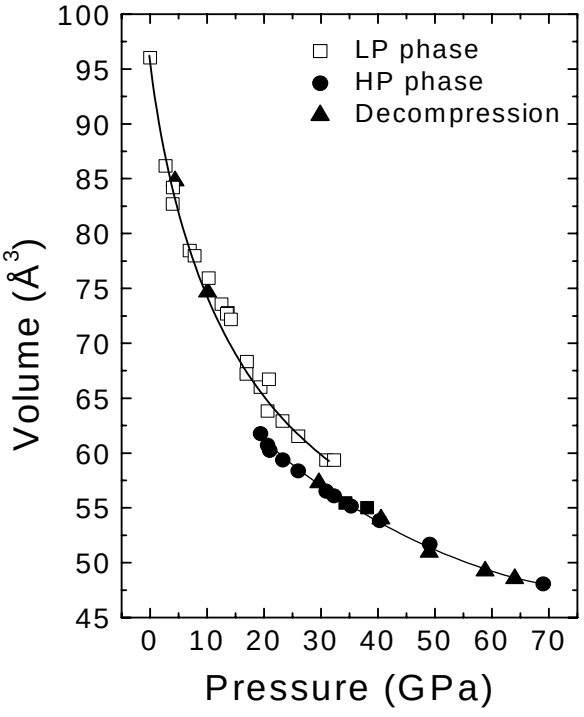

Fig. 3.7-11. Pressure evolution of the FeI_2 unit cell volume. Solid lines are provided as a guide for the eyes. The transition to the HP phase is accompanied by a ~ 5 % volume reduction. No hysteresis is observed on pressure decrease.

g. *Oxygen vacancies in Fe^{3+}-substituted barium titanate (E. Mashkina/Erlangen, in collaboration with F. Seifert and C.A. McCammon)*

Considerable interest has been focused on the defect structure and transport properties of perovskite-type compounds due to their important technological applications, including uses in electrochemical devices such as fuel cells, gas sensors, and membranes for oxygen extraction or hydrogen production. Their thermal and chemical stability is a decisive advantage in these applications; thus it is important to understand the properties that are relevant to fast oxygen transport. $BaTiO_3$-based ceramics are mixed conductors showing both ionic and electronic conductivities (*n*- and *p*-type) at elevated temperatures, where the electrical properties are controlled by doping with aliovalent impurities. One interesting aspect of these compounds is their ability to accommodate anion vacancies in order to maintain electrostatic neutrality when Ti^{4+} is replaced by Fe^{3+}. These vacancies lead to high ionic and electronic conductivities, and thus promote better performance as electrochemical devices. In this study we focused on the vacancy structure of Fe^{3+}-substituted $BaTiO_3$ and its relation to transport properties.

We prepared polycrystalline samples of $BaTi_{1-x}Fe_xO_{3-\delta}$ (x=0.1-0.3,0.6) at elevated temperatures in air using a solid state reaction method, and found all run products to be close to the nominal composition based on electron microprobe analysis. We collected electrical conductivity data at elevated temperatures in the oxygen partial pressure range between 0.21 and 10^{-16} atmospheres, and extracted an ionic conductivity with maximum near x=0.25 that might reflect changes in oxygen vacancy concentration and/or Fe^{4+} concentration. We also found a similar maximum in the system $CaTiO_3$-$CaFeO_{2.5}$, but not in the systems $SrTiO_3$-$SrFeO_{2.5}$ and $Ca_{0.5}Sr_{0.5}TiO_3$-$Ca_{0.5}Sr_{0.5}FeO_{2.5}$.

To investigate this further we heated a separate suite of samples at 1200ºC in open AgPd capsules under controlled atmosphere with CO-CO_2 gas mixtures corresponding to oxygen fugacities of -3 and -11 log bar units. These samples were drop quenched and examined by X-ray diffraction and Mössbauer spectroscopy.

The crystal structure of $BaTi_{1-x}Fe_xO_{3-\delta}$ (x=0.1,0.2,0.3,0.6) was found to be hexagonal with 6H-$BaTiO_3$ type, space group $P6_3/mmc$, which is different to the perovskite structure. The 6H-$BaTiO_3$-type structure contains both perovskite-like corner-shared octahedra and pairs of face-shared octahedra, where oxygen vacancies are predominantly associated with the shared face. Experience from other perovskite systems (see BGI Annual Report 1999) led to a fitting model that showed Fe^{3+} to be distributed between octahedral and pentacoordinated sites (Fig. 3.7-12a). For reduced samples containing Fe^{3+} only, the number of oxygen vacancies is constrained by the chemical composition based on electrostatic neutrality; hence the number of Fe^{3+} and Ti^{4+} cations associated with oxygen vacancies (*i.e.* that occupy pentacoordinated sites) can be determined from the Mössbauer data. These data show that there is a nearly equal distribution of Fe^{3+} and Ti^{4+} on pentacoordinated sites for highly reduced samples (Fig. 3.7-12b). For samples synthesised under more oxidising conditions, Mössbauer spectra showed that the ratio Fe^{3+}/Fe^{4+} is highly sensitive to iron concentration. For example, Fe^{3+} is stable over a large range of oxygen fugacities (including that of air) for samples with x<0.15.

At higher iron concentrations, however, Fe^{4+} becomes more stable under oxidising conditions. This might provide a basis for understanding the maximum in the ionic conductivity data, where the Fe^{3+}/Fe^{4+} equilibrium is critical to determining which transport mechanism would be favoured.

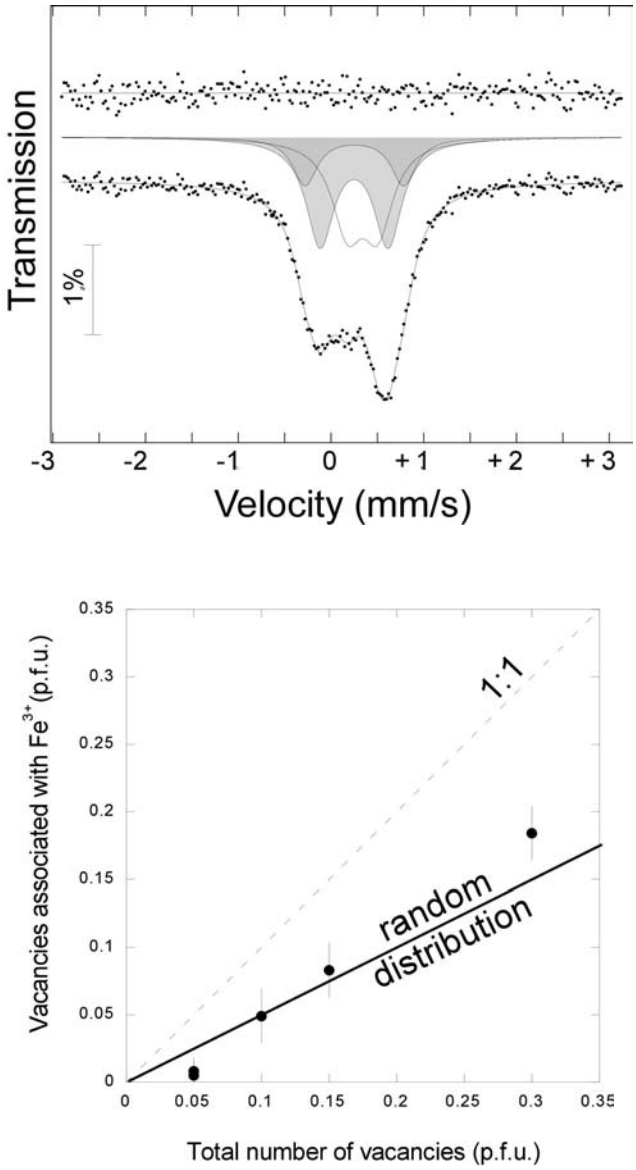

Fig. 3.7-12: (a) Room temperature Mössbauer spectrum of $BaTi_{0.4}Fe_{0.6}O_{2.7}$ quenched from 1200 °C and log fO_2 = -11. Subspectra are shaded as follows: one octahedral Fe^{3+} doublet (unshaded); two pentacoodinated Fe^{3+} doublets (grey); (b) Site distribution of pentacoordinated sites in $BaTi_{1-x}Fe_xO_{3-x/2}$ quenched from 1200 °C and log fO_2 = -11. Data points represent the number of Fe^{3+} cations occupying pentacoordinated sites as determined from the Mössbauer data, where the difference between data points and the 1:1 correlation gives the number of Ti^{4+} cations on pentacoordinated sites. The line marked "random distribution" indicates the trend that would be predicted for the Mössbauer data if Ti^{4+} and Fe^{3+} were distributed equally over the pentacoordinated sites.

h. *Stabilization of Ni-containing layered oxides under high-oxygen pressure (G.D. Bromiley and T. Boffa-Ballaran, in collaboration with R. Stoyanova/Sofia)*

Cathode materials for lithium-ion batteries are based on lithium-transition metal oxides with layered crystal structure that can intercalate large amounts of lithium reversibly at potentials higher than 4V vs. Li. A desire to replace the most commonly used $LiCoO_2$ materials (due to the high costs and toxicity of Co) has encouraged the materials science community to develop new layered cathode materials based on Mn and/or Ni. Here we report high-oxygen pressure synthesis of novel $Li[Li_xNi_{1-x}]\ O_2$ compositions ($0<x<0.2$) with a structure markedly different from that of the well-known $LiNiO_2$, which is a structural analogue of $LiCoO_2$. This synthetic route was shown to be effective for the preparation of solid solutions of electrochemically active $LiNiO_2$ and electrochemically inactive $LiGaO_2$ over the entire concentration range.

The critical parameter that controls the composition of layered nickel based oxides is the oxygen partial pressure. Therefore, in order to use the conventional piston-cylinder type apparatus, lithium nickelates were prepared using a starting mixture of Li_2O_2 and NiO. Synthesis experiments were performed at 700 °C for 2.5 hours with pressures between 2 and 4 GPa. Under these conditions, thermal decomposition of Li_2O_2 produces an oxygen-rich atmosphere inside the sample volume, which is sustained for the duration of the experiment, in addition to providing Li_2O for the solid-state reaction with NiO.

When the Li/Ni-ratio in the initial Li_2O_2-NiO mixture is 1.2, nearly stoichiometric $LiNiO_2$ consisting of LiO_2- and NiO_2-layers is obtained (Fig. 3.7-13). The unit cell dimensions match well those for $LiNiO_2$ prepared under atmospheric pressure. By increasing the Li/Ni-ratio in the Li_2O_2-NiO mixture from 1.2 to 1.5, novel oxides with $Li[Li_xNi_{1-x}]O_2$ composition are formed. The crystal structure of these oxides is composed of nearly pure lithium layers and mixed lithium/nickel layers (*R*-3m space group). Short-range superlattice ordering of Li and Ni is suggested to develop in the $Li_xNi_{1-x}O_2$-layers. The replacement of Ni^{3+} by Li^+ in nickel-rich layers is compensated for by the appearance of the corresponding amount of Ni^{4+} ions. This leads to a strong contraction of the mean Li_xNi_{1-x}-O distance as compared to Ni-O in $LiNiO_2$. The formation of mixed $Li_xNi_{1-x}O_2$-layers causes doubling of the IR modes corresponding to the layer vibrations.

The interplay of the geometric and electronic structure of Ni, Co and Al determines the formation of solid solutions between $LiGaO_2$ and $LiMO_2$ (M=Ni, Co, Al). The aptitude of layered $LiNiO_2$ to dissolve Ga under high-oxygen pressure was found to be unlimited in contrast to that of $LiCoO_2$. According to the structural refinement, Ga substitutes for Ni in NiO_2-layers, and mixed $Ga_yNi_{1-y}O_2$-layers remain free from Li^+ dopants. However, the progressive replacement of the smaller Ni by the larger Ga causes, up to $y<0.50$, a contraction in the intralayer distance between metal ions (*a*, unit cell parameter, Fig. 3.7-14), while above $y>0.50$, both *a* and *c* unit cell parameters obey the Vegard's behaviour. In contrast, the unit cell dimensions for isostructural Ga-substituted $LiCoO_2$ and $LiAlO_2$ display the normal

Vegard's behaviour (Fig. 3.7-14). This structural peculiarity observed for Ni containing oxides can be related to the increased extent of the trigonal distortion of metal layers (Fig. 3.7-14).

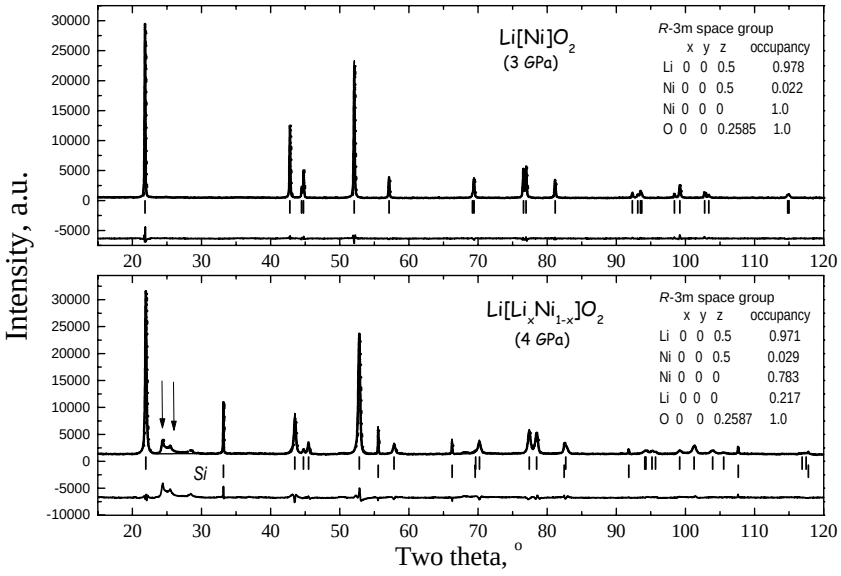

Fig. 3.7-13: XRD patterns of nearly stoichiometric $LiNiO_2$ prepared at 3 GPa and $Li_{1+x}Ni_{1-x}O_2$ composition synthesised at 4 GPa. The difference between observed and calculated proffiles is plotted. Bragg reflections for layered structure and Si standard are indicated. Arrows refer to peaks not filtered by the refinement.

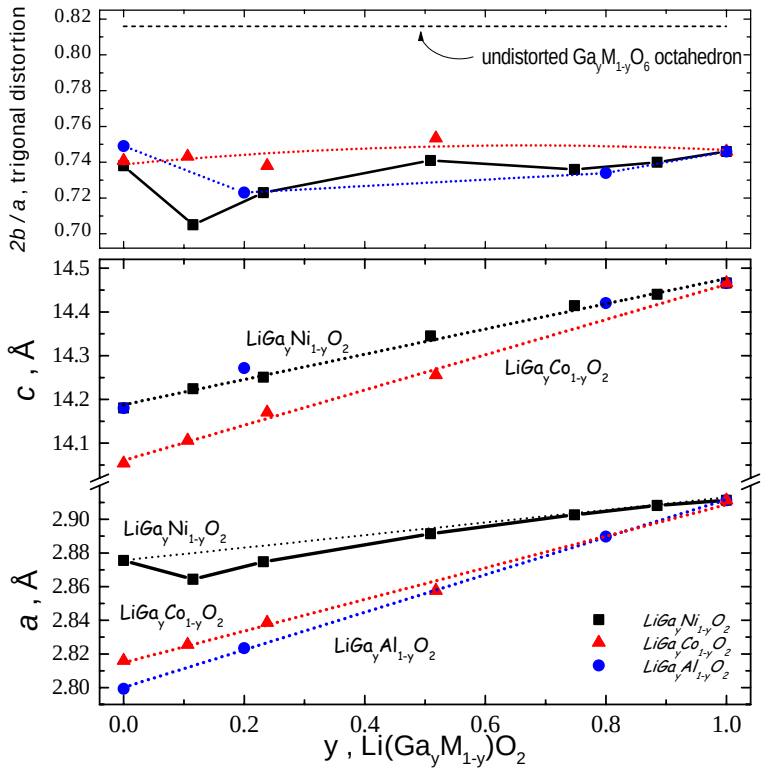

Fig. 3.7-14: Unit cell parameters *vs.* Ga content for $LiGa_yM_{1-y}O_2$ solid solutions (M=Ni, Co and Al) synthesised under high-pressure (3 GPa). For the layered structure, the extent of the local trigonal distortion is given by the ratio between the distance of two opposite faces of the octahedron, *2b*, and the edge of the octahedron, *a* (*2b/a*).

i. *Combined isotope substitution and pressure-tuning Raman study of the spin-crossover complex Fe(pyridine)$_2$[Ni(CN)$_4$] (G. Molnar and A. Boussekso/Toulouse, T. Kitazawa/Toho and L.S. Dubrovinsky)*

The spin-crossover (SCO) phenomenon, involving thermo-, photo-, magneto- and piezo-chromic properties of a class of transition metal complexes, is one of growing importance in the area of multifunctional molecular materials, especially for possible applications in memory, display and switching devices at the molecular scale. The thermodynamic aspects of SCO are well described at the molecular level. However, this molecular phenomenon is highly influenced in the solid state by intermolecular couplings, giving rise – in some cases – to a cooperative spin-transition with a hysteresis loop, conferring a potential memory effect on these systems.

In this context, we have recently started to study a series of novel, highly cooperative, iron(II) spin-crossover polymers using variable temperature Raman and IR spectroscopy as well as the DSC technique. Two observations have turned out to be important. One concerns the vibrational entropy change (ΔS) associated with the spin-transition, which is very high (50-70 $JK^{-1}mol^{-1}$). Secondly, ΔS contains an important contribution from low-frequency ligand and phonon modes. The reason behind this involves either coupling with the metal-ligand vibrations (which are the most influenced by the spin state change) or with the lattice expansion.

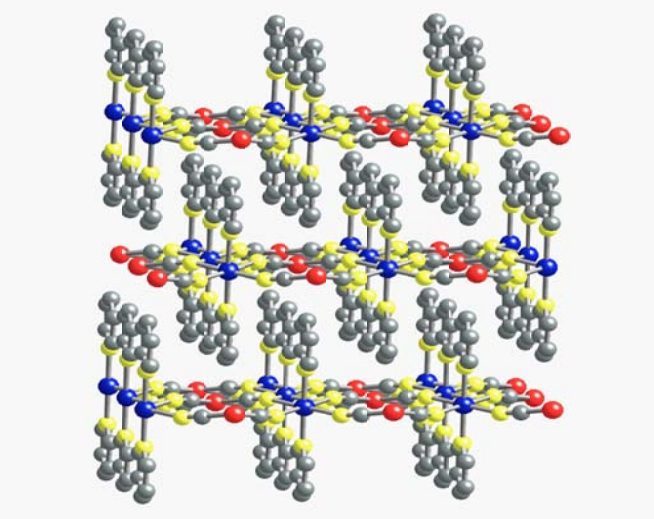

Fig. 3.7-15: Schematic view of the complex Fe(py)$_2$[Ni(CN)$_4$].

To gain further insight into the lattice dynamics of these 2D and 3D systems we have conducted a series of pressure tuning Raman measurements on the compound Fe(pyridine)$_2$[Ni(CN)$_4$] (Fig. 3.7-15) complemented with isotope substitution studies (pyridine-5D). The temperature and pressure dependent Raman spectra revealed similar changes upon SCO. Most importantly, we observed an overall blue shift (up to 160 cm^{-1}) of Raman modes in the low-frequency range when going from the high-spin (HS) to the low-spin (LS) state. The intensity variation of Raman bands revealed that the HS form (stable in

ambient conditions) transforms reversibly to the LS phase either by cooling (T_c = 202 K) or by pressurization ($P_c \cong$ 10 kbar) (Fig. 3.7-16). A small downshift of T_c (to 195 K) was observed due to the isotope effect while the P_c values could not be distinguished within experimental error (±1 kbar).

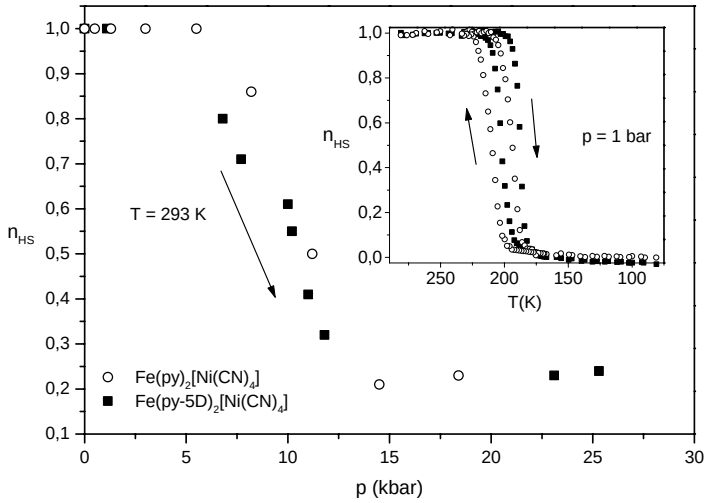

Fig. 3.7-16: Variation of the high-spin (HS) fraction as a function of pressure and temperature in $Fe(py)_2[Ni(CN)_4]$ and in its deuterated analogue.

A closer inspection and the assignment of Raman modes revealed some intriguing features. Firstly, at the onset of the pressurization only the internal pyridine modes and modes involving the displacement of the pyridine ligand as a rigid unit exhibited frequency shifts, while modes assigned to displacements in the 2D polymer sheet remained unaffected. The compressibility is thus highly anisotropic. The pressure shift (dν/dP) of the low-frequency modes was found to be rather small (0.1-0.6 cm^{-1}/kbar) between 0-30 kbar. This implies that the usual assumption $\Delta S(P_{atm}) \cong \Delta S(P > P_{atm})$ is valid at moderate pressures (< 5-10 kbar) and that the internal pressure change which accompanies the spin transition does not lead to a substantial variation in ΔS. On the other hand, the isotope effects revealed that the range of vibrational couplings is significantly higher in the LS state compared to the HS state. This is the first experimental evidence that the surrounding lattice (HS or LS) can affect the vibrational frequencies to a considerable extent and thus the vibrational entropy. Metal dilution experiments are in progress to clarify the magnitude of this latter contribution to ΔS.

j. *In situ Raman study of pressure-induced amorphization in $Eu_2(MoO_4)_3$ single crystal (D. Machon and V. Dmitriev/Grenoble, L.S. Dubrovinsky, F. Langenhorst, V. Sinitsin and E. Ponyatovsky/Chernogolovka)*

The microscopic details of the process of amorphization are not well understood in spite of the effect being documented for more than one hundred inorganic, organic and mineral compounds.

Although the topic is of great interest, the required simultaneous pressure-temperature experiments are still occasional and rare due to experimental difficulties. However we expect these experiments to give decisive information on the existence of the "post amorphous" state, a state which cannot be reached at room temperature simply because of kinetic reasons. We expect also that different mechanisms of amorphization will lead to different "post amorphous" states. The objective of this project was to clarify the mechanism of pressure-induced amorphization, and, possibly, to identify the driving forces behind the amorphization of the rare-earth molybdate crystals.

Raman spectra of $Eu_2(MoO_4)_3$ single crystal samples were studied in the pressure range up to 50 GPa and temperatures from 300 K to 850 K. We observed that different regimes of high temperature – high pressure treatment bring the samples either into different amorphous phases, identified from their different Raman spectra (Fig. 3.7-17 and 3.7-18 c.f. Fig. 3.7-19), or recrystallize them in the crystalline state (Fig. 3.7-20). Thus, surprisingly, two states different in their driving forces of amorphization were discovered as revealed by TEM experiments. We distinguish between: a) an amorphous state driven by a chemical decomposition process, occupying a low-temperature domain of the phase diagram, and b) a high-temperature crystallographically disordered state, without a long-range order and showing no signs of decomposition. We have thus mapped, for the first time, the stability regions of the amorphous states in the P-T phase diagram of $Eu_2(MoO_4)_3$ (Fig. 3.7-21).

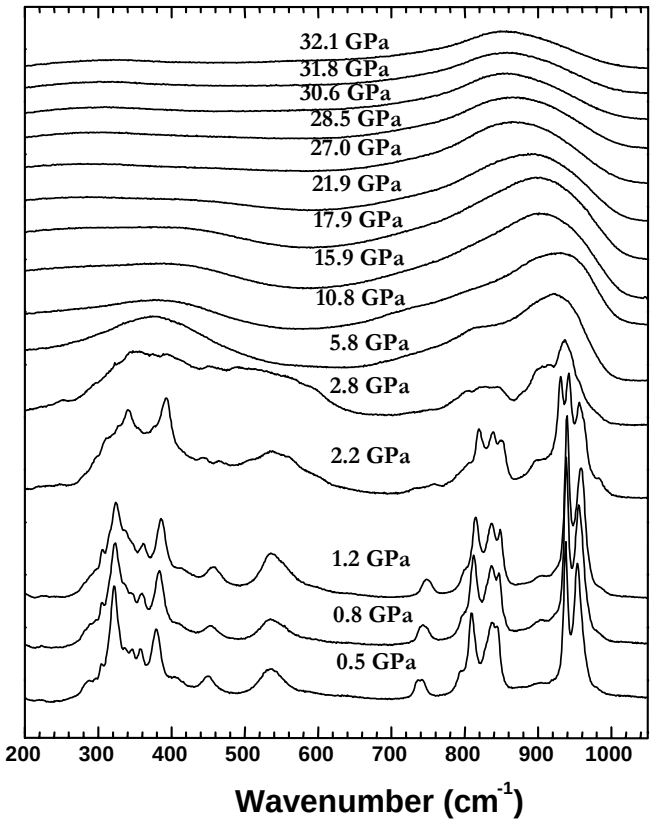

Fig. 3.7-17: Pressure evolution of $Eu_2(MoO_4)_3$ Raman spectra.

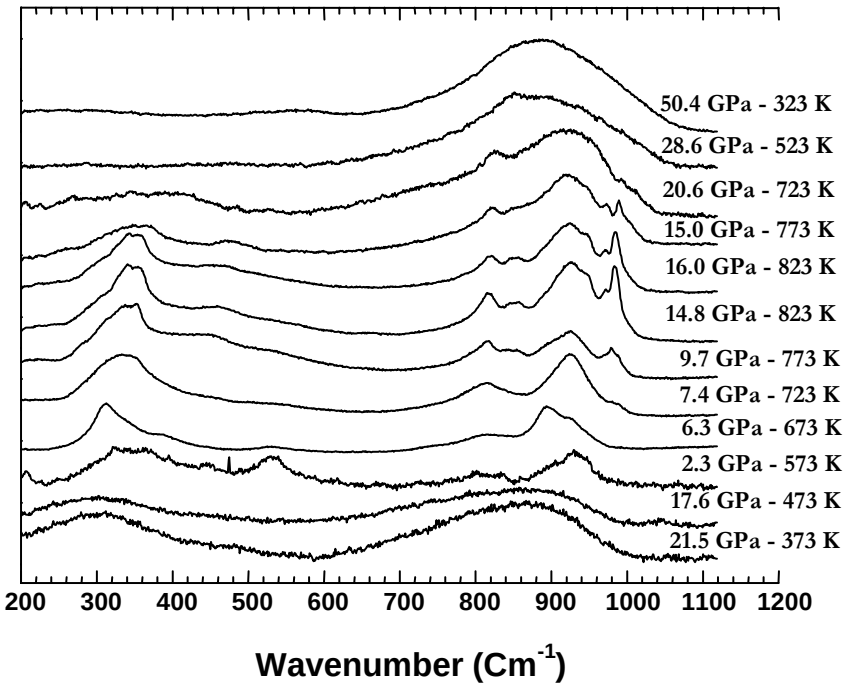

Fig. 3.7-18: Evolution of $Eu_2(MoO_4)_3$ Raman spectra with variation of both P and T.

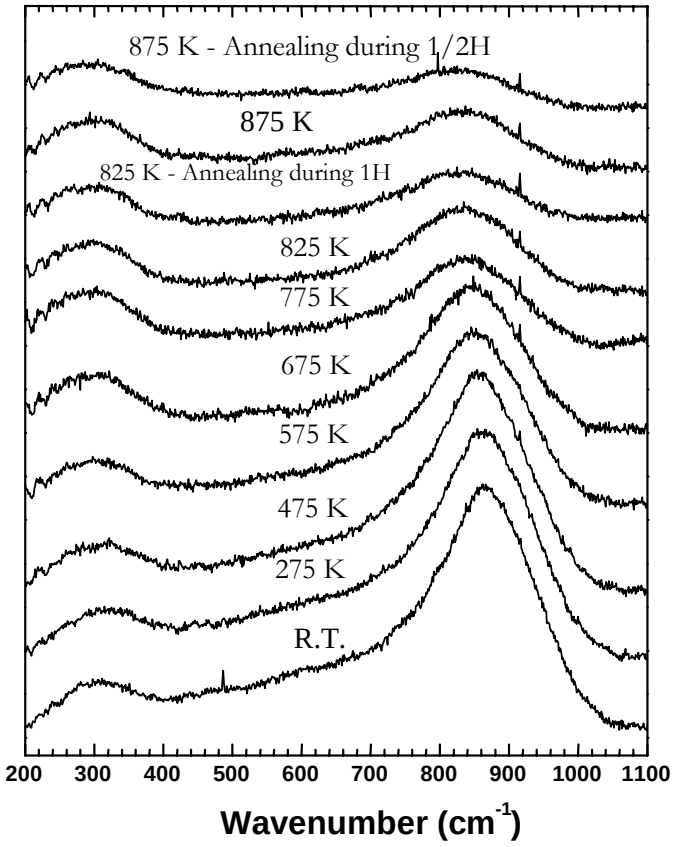

Fig. 3.7-19: Raman spectra from annealing of a pre-pressed sample of $Eu_2(MoO_4)_3$ (32 GPa).

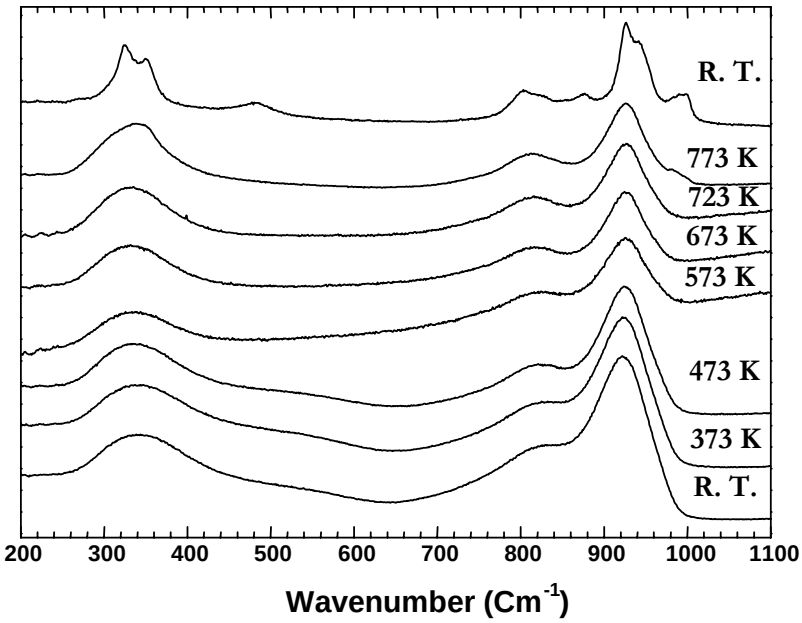

Fig. 3.7-20: Raman spectra from annealing of a decompressed sample of $Eu_2(MoO_4)_3$.

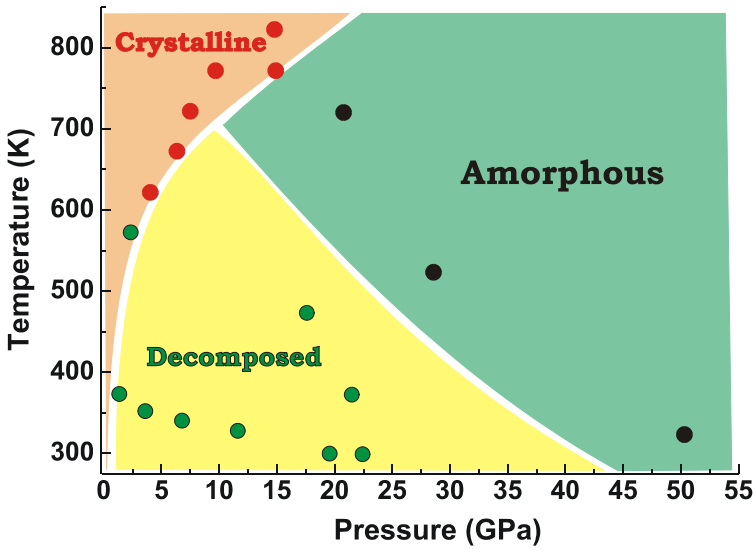

Fig. 3.7-21: Phase diagram of $Eu_2(MoO_4)_3$.

During the course of this study a new effect was observed, namely the change of color and subsequent complete loss of the transparency of the EMO crystal with increasing pressure. This effect points to a considerable shift of the corresponding absorption edge of the crystal, while a discontinuity observed in its pressure behaviour indicates an electronically driven phase transition. The occurrence of this transition in the amorphous state is of special interest; however its precise characterization requires a more detailed study with more specific experimental techniques.

k. *Optical and A.T.E.M. investigations of sintered alumina transformed under excimer laser irradiation (C. Dupas-Bruzek, L.D. Laude, K. Kolev/Mons and F. Langenhorst)*

Laser surface processing of ceramics is important for several structural, tribological, optical and electronic applications (L.D. Laude, European Patent No. 0634502; 18 January 1995). However, little is known on the alumina transformation mechanism under excimer laser irradiation. At low fluxes ($0.5<E<2$ J/cm^2) surface morphological and compositional modifications occur due to melting/resolidification, while at higher fluxes, material is removed by congruent vaporization. In particular, it has been shown by low-angle X-ray diffraction that a so-called crystalline γ-Al_2O_3 phase is formed. However, neither the degree of ordering of the remaining re-solidified material formed at low fluxes, nor the transformation process have been identified to date. The present work addresses the latter point by precisely analyzing all transformation products of an alumina substrate irradiated by an excimer laser source using optical microscopy and analytical transmission electron microscopy (ATEM). In addition, this study reveals the important role of the cooling rate on the morphology and order/disorder degree of the resulting products as well as on nucleation and growth rates. Furthermore, this work provides a clear understanding of the observed activation of the resulting irradiated surface, *e.g.* regarding metal deposition and adhesion.

Sintered alumina substrates (purity 99.6 %, 1-2 µm grain size) have been irradiated in air using an homogenized Kr^+F (248 nm) excimer laser source at a low flux (0.8 J/cm^2). Samples were cooled at two drastically different rates (x 10) using different sample holders.

Optical investigations carried out on the laser-irradiated specimens show that samples cooled at the slowest rate were *partially* transformed (*i.e.* melted and resolidified), whereas samples cooled at the highest rate were *completely* transformed (their irradiated surfaces went completely through the liquid state). Using ATEM, we find for all samples that the transformation product consists of an amorphous matrix containing many elements (C, O, Al, Cu, Si, Mo, Cr, Fe, Ni, Zn, Fig. 3.7-22) which are also found at grain boundaries in virgin (non-irradiated) α-Al_2O_3 samples. This amorphous matrix contains either i) copper grains (size up to 1µm) in samples cooled slowly (Figs. 3.7-23 and 3.7-24) or ii) smaller copper grains (though with a higher concentration), and $CuAl_2O_4$ spinel grains (size up to 100 nm) in samples cooled faster (Figs. 3.7-22 and 3.7-24). Electron diffraction patterns on copper grains from slowly cooled samples ("i") reveal a single <120> lattice preferred orientation perpendicular to the irradiated face. These grains contain two types of planar defects (stacking faults parallel to {110} and/or spinel-type twins parallel to {111}). In some areas of the slower cooled samples ("i"), amorphous elongated cells with approximately 1 µm equal widths are detected (Fig. 3.7-25) and contain very fine copper crystals. These copper grains, which are larger in the valleys between the cells (~ 100-300 nm), contain stacking faults and exhibit the same <120> preferred orientation.

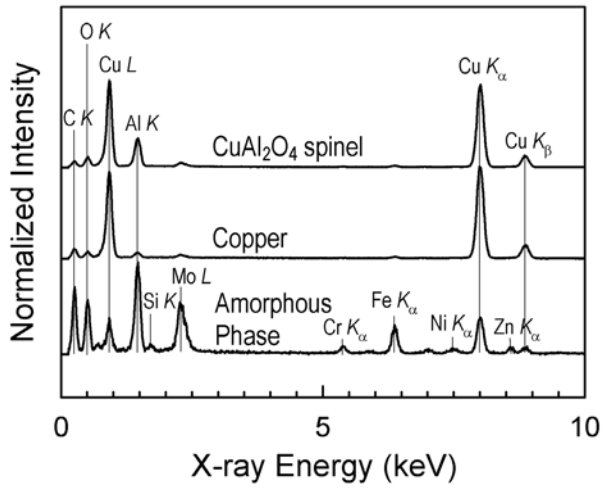

Fig. 3.7-22: Qualitative micro-analysis performed on the amorphous material (bottom), within tiny copper grains (middle) and $CuAl_2O_4$ spinel grains (top).

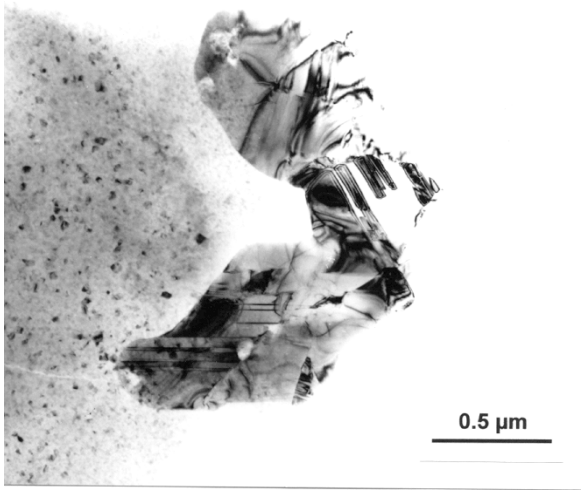

Fig. 3.7-23: TEM bright field image of a copper grain containing {110} stacking faults in a sample cooled slowly. This grain is surrounded by an amorphous phase containing tiny crystallites.

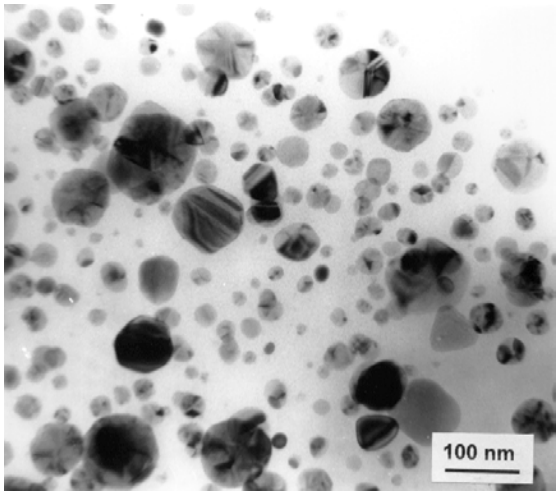

Fig. 3.7-24: TEM bright field image of small (< 100 nm) copper or $CuAl_2O_4$ spinel grains in a fast cooled sample.

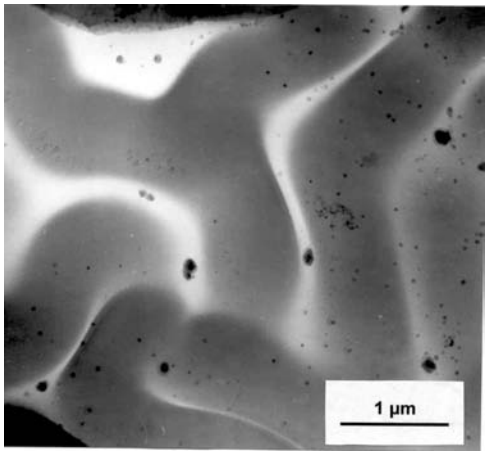

Fig. 3.7-25: TEM bright field image of amorphous elongated cells containing tiny Cu crystals in a slowly cooled sample.

Furthermore, samples were immersed in an autocatalytic bath containing either Ni^{2+}, Cu^{2+}, or $Pt^{2+/4+}$ ions. We observed that metallization starts homogeneously only on samples cooled faster (and completely transformed, "ii") while it develops selectively on the transformed products of samples cooled slowly (partly transformed, "i").

The cement that is present in the starting material at grain boundaries is found to play an important role in the formation of the new amorphous or crystalline materials. Its composition is basically determined by the sintering aids.

The observed Cu grains might stem from the formation of tiny γ-Al_2O_3 nuclei which would integrate Cu ions present in the melt and transform into $CuAl_2O_4$ spinel. Once these tiny $CuAl_2O_4$ spinel grains would be formed, they would further act as nucleation centers for sedimenting further Cu ions, and finally form larger copper-rich grains. Other possibilities exist in order to explain the formation of Cu and $CuAl_2O_4$ grains: these grains might result from a disproportionation reaction with copper being in the 1+ state in the cement such as:

$$Cu_2^{1+}O + Al_2O_3 \rightarrow Cu + Cu^{2+}Al_2O_4$$

The copper grains all have a <120> *common* zone axis perpendicular to the irradiated surface, *i.e.* parallel to the bulk-to-surface thermal gradient that would then appear to drive that preferred orientation.

The amount of transformed products (amorphous and crystalline) is very dependent on the cooling rates. The minimum nucleation rate of crystalline grains is estimated to be equal to 10^{24} cm^{-3} s^{-1}, while the growth rate is of the order of 0.1 m s^{-1} in both samples.

We interpret the elongated cells as being convective cells formed in the melt due to buoyancy-driven convection between bulk (colder) and surface (warmer). Therefore, bulk thermal diffusive transport is not the only process that controls the formation of a new product, but convection is also efficient at least until the end of the heating process.

The crystalline grains favor auto-catalytic metallization. In fact, reducing agents that are included in the autocatalytic bath may provide electrons to these grains, which would thus become electronegative sites. Positive metallic ions that are also present in the solution may then be selectively attracted on such sites. Adhesion of the resulting metallic layer should then be stronger on irradiated samples containing bigger copper grains (samples cooled slower, "i"), because these grains are better anchored to the bulk, and because metallic ions that are included in the auto-catalytic bath are more easily trapped on these larger crystalline surfaces. However, the concentration of Cu grains is lower in samples cooled slower ("i") than in samples cooled faster ("ii"). Optimization of the metallization process may thus proceed in two ways: i) an increase of the Cu content in the cement (or a decrease of the alumina purity) would increase the nucleation rates of $CuAl_2O_4$ grains, thus allowing the concentrations and

the copper grain sizes to increase in slow cooled samples, while ii) a heat treatment after irradiation of rapidly cooled samples would favor grain growth.

This novel, efficient and non-polluting metallization process of sintered alumina can have interesting applications in microelectronics for hybrid circuit configurations (when samples are metallized with copper or nickel) or in biomedicals (when tracks are performed on biocompatible high purity alumina and are metallized with platinum, which is known to be the best biocompatible metal).

3.8 Methodological Developments

Innovation and advances in the understanding of Earth's deep interior depend on the development of new technology and methods for studying mineralogical assemblages at elevated pressures and temperatures. Proper interpretation of geophysical, geochemical, and petrological observations requires the accurate and complex physical, chemical and structural characterization of materials both at ambient and extreme conditions, preferably *in situ*. The emphasis this year was on two new methods: Gigahertz ultrasonic interferometry and acoustic emissions experiments in a multianvil apparatus. These new techniques are giving direct insight into properties and processes occurring in geophysically important materials under high pressures and temperatures. Also, we have continued our efforts to modify, improve, and develop high-pressure – high-temperature devices aimed towards new experimental limits. The new "Drickamer-type" opposed anvil apparatus reaches higher pressures than the usual multianvil press on samples with a volume an order of magnitude larger than that used in conventional diamond anvil cells. Constructed at BGI, the new externally electrically heated diamond anvil system allows us to conduct experiments at pressures above 130 GPa and temperatures above 1200 K. In the piston-cylinder, a novel and elegant method for annealing natural samples at high pressure opens a way to study water in nominally anhydrous minerals subjected to pressures and temperatures of Earth's upper mantle. Advances in analytical techniques are shown in recent studies of Al-bearing silicate perovskite using atom location by channeling-enhanced microanalysis (ALCHEMI) in the transmission electron microscope, and new results are reported in solid-state NMR.

a. *Gigahertz ultrasonic interferometry at Bayerisches Geoinstitut: Where acoustic and optical wavelengths meet (S.D. Jacobsen, H. Schulze, G. Herrmansdörfer, S. Linhardt and K. Klasinski, S.J. Mackwell, in collaboration with K. Müller and H. Ohlmeyer/ZT Uni-Bayreuth, H.-J. Reichmann/Potsdam, H.A. Spetzler and J.R. Smyth/Boulder)*

We have introduced pure ultrasonic shear waves into a diamond anvil cell for the first time. Now, both P and S-wave velocities can be measured at high pressure in single-crystal samples as thin as 20-30 μm, making gigahertz ultrasonic interferometry a powerful new tool for measuring the elastic properties of minerals. The technique is an important compliment to Brillouin light scattering for measuring elasticity in that iron-bearing phases, opaque minerals or metals may be readily studied as there are no optical constraints.

The diamond cell shear wave buffer rod was made from an oriented single-crystal of cubic Yttrium-Aluminium-Garnet (YAG), featured on page 8 of this Annual Report, and shown in schematic in Fig. 3.8-1. An incident P-wave tone burst strikes the conversion facet in the buffer rod so as to produce a shear wave by reflection at exactly 90º from incidence. This allows the shear wave to propagate in pure mode directions of the buffer rod and diamond, but also means the back-reflected echoes are detected by the source transducer so delay-line

ultrasonic interferometry is carried out in the usual manner. A set of PSSP echoes from within the buffer rod and diamond anvil are shown in Fig. 3.8-2.

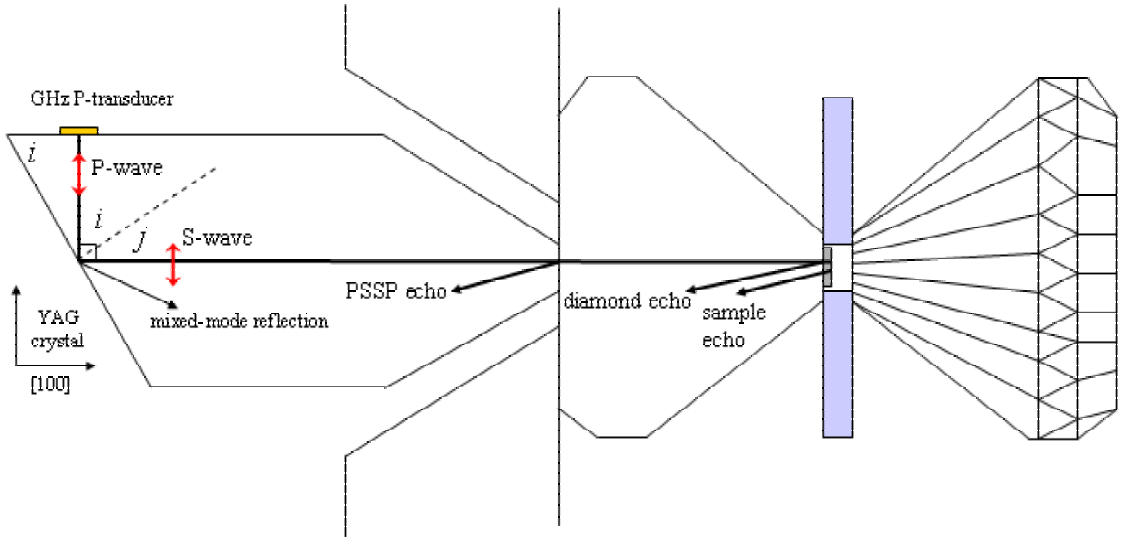

Fig. 3.8-1: The diamond cell shear-wave buffer rod works on the principle of Snell's Law, producing a pure shear wave by P-to-S conversion upon reflection.

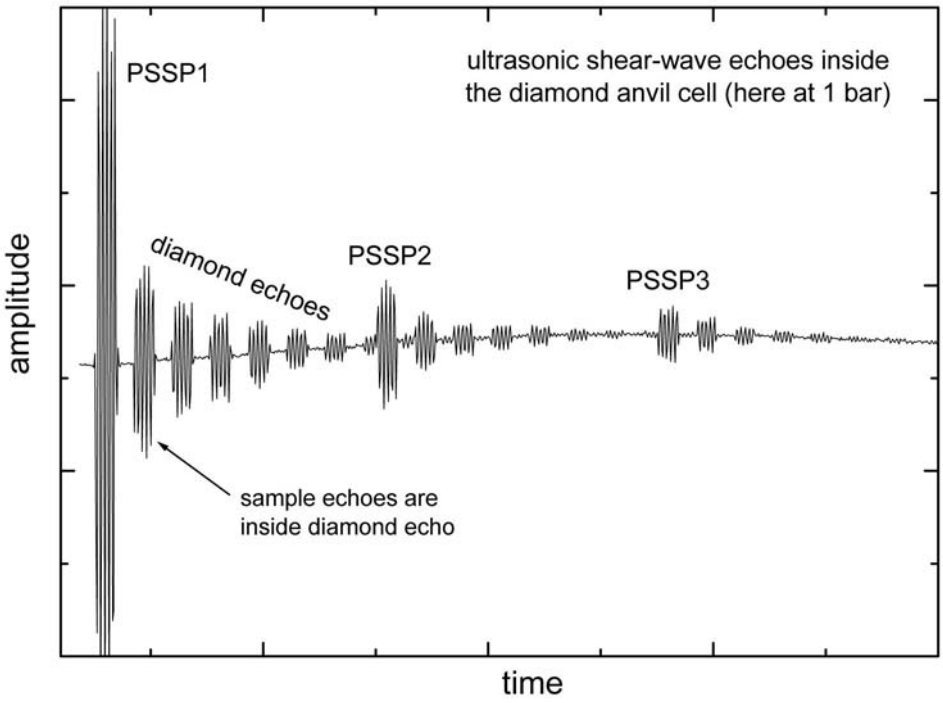

Fig. 3.8-2: Echoes from within the shear buffer rod and diamond anvil cell. Tone bursts labeled PSSP result from round-trips through the buffer rod. Each buffer rod echo transmits shear energy into the diamond, which rings many times. The entire echo train results from the introduction of just one tone burst into the buffer rod.

This year, we also conducted the first high-pressure ultrasonic (P-wave) measurements without the use of an acoustic-transmitting bond between the sample and the diamond anvil. The resulting travel-time-pressure data are of unprecedented quality. Ultrasonics without a glue bond is achieved by adding nanoporous silica aerogel (ρ ~ 0.1 g/cm^3) to the usual methanol-ethanol pressure medium. The low-density gel plus alcohol mixture is hydrostatic to pressures of ~ 10 GPa (based on ruby fluorescence) and acts as a gentle transparent spring to keep the sample against the anvil in a fluid pressure medium.

Using the new ultrasonic pressure medium, an empirical study on the effect of glue bonds was carried out. High-pressure P-wave travel-time data through $(Mg_{0.44}Fe_{0.56})O$ with and without a glue bond was measured up to ~ 8 GPa (Fig. 3.8-3). The travel-time data with a glue bond are slower (but not significantly), and exhibit considerable scatter that would result in a simple linear relationship with pressure. The no-bond data exhibit much higher internal precision with second order curvature, and can thus be more confidently extrapolated to higher pressures.

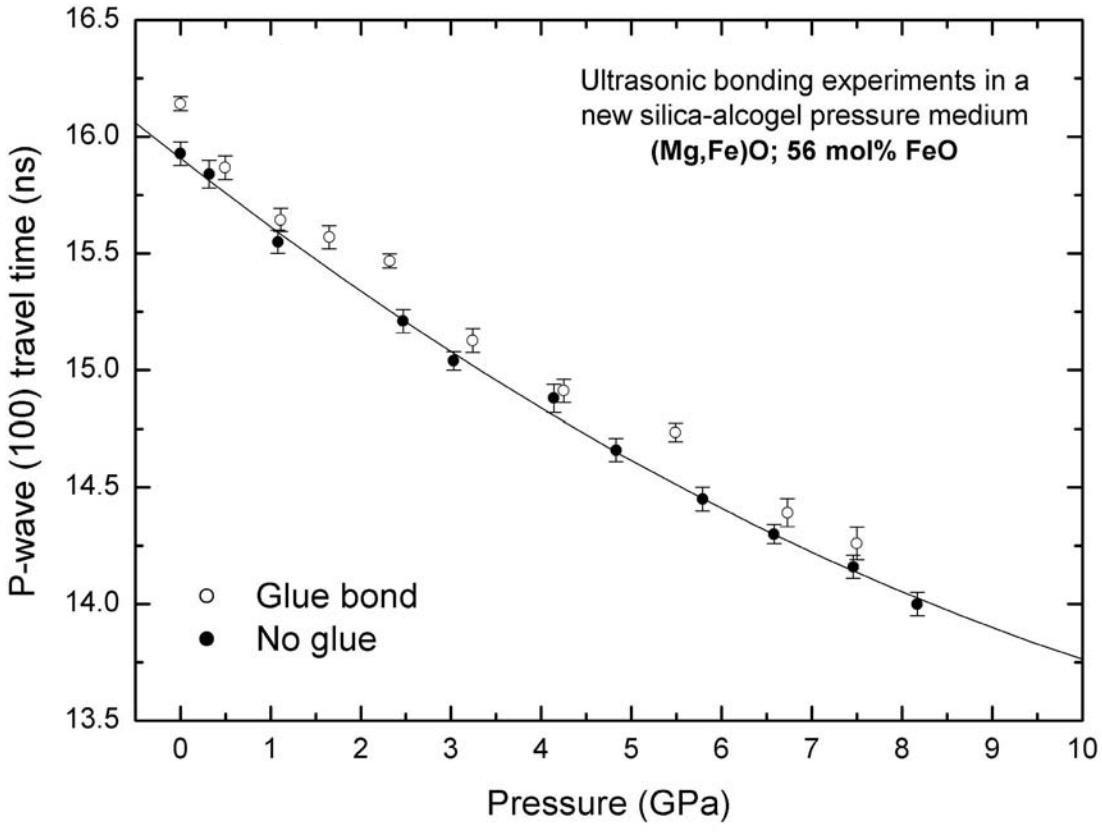

Fig. 3.8-3: P-wave travel-time data for magnesiowüstite-$(Mg_{0.44}Fe_{0.56})O$ with and without a glue bond between the sample and the acoustic diamond anvil. Ultrasonic transmission without a glue bond is achieved using a new silica aerogel alcohol pressure medium, resulting in high-pressure travel time data of unprecedented quality.

b. *A new methodology for multianvil acoustic emissions experiments (D.P. Dobson, in collaboration with P.G. Meredith and S.A. Boon/London)*

Despite several decades of directed research, intermediate and deep-focus earthquakes remain enigmatic. Previous experimental investigations of this anomalously high-pressure brittle process have been hampered by the lack of an effective method for observing seismogenesis at high experimental pressures. We have developed a new methodology to observe microseismicity in multianvil press experiments and applied this technique to serpentine dehydration.

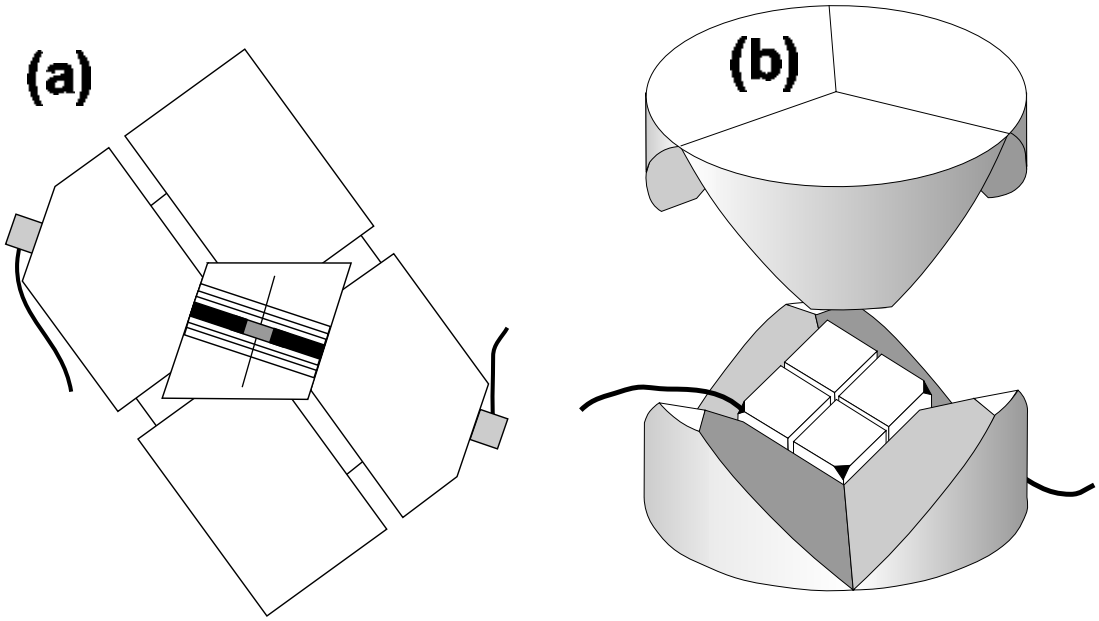

Fig. 3.8-4: Experimental design for multianvil acoustic emissions experiments. a) The high-pressure cell and second-stage anvils showing transducers on opposing anvils, sample (grey) and acoustic waveguides (black). b) The second-stage anvils in the press geometry. The coloured truncations are available for transducers, but anvils on the vertical axis are completely enclosed by the first-stage anvil cradle.

We performed initial tests using two transducers on opposed anvils with corundum or metallic acoustic waveguides. Acoustic emissions (AE) transducers are glued on to the back truncations of anvils as shown in Fig. 3.8-4. Care must be taken to match the compressibility and length of the acoustic waveguides to the pressure-medium to avoid crushing the sample during initial compression. Differences between the arrival times at the transducers of signals from a single event serve as a proxy for the 1-D location of the source. Using 10 MHz transducers gives a spatial resolution of ~ 0.5 mm at an acoustic velocity of 5 km s^{-1} so sources can be located to within, or outside, the sample but fracture propagation cannot be monitored.

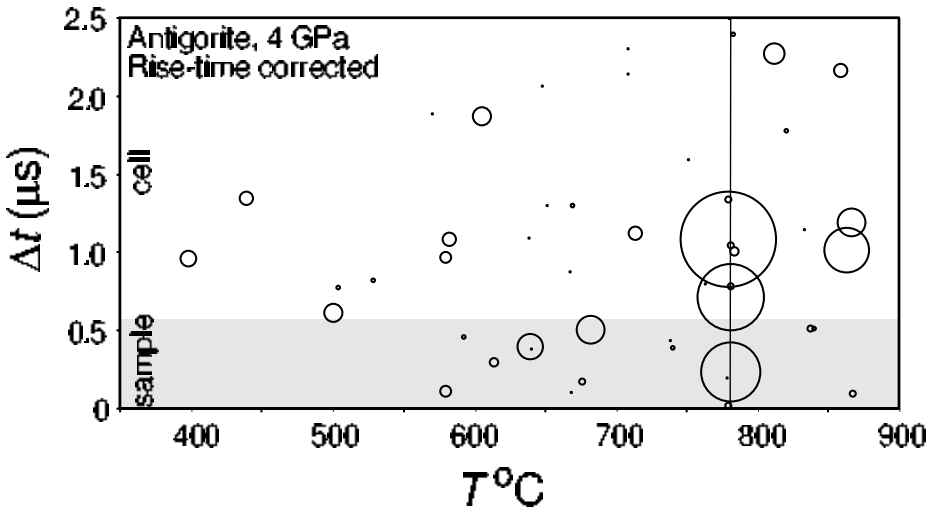

Fig. 3.8-5: Acoustic emissions during dehydration of serpentine at 4 GPa. The area of the symbols represents the energy of the event and Δt is the difference between arrival times at the two transducers. The three largest events occur nearly simultaneously during dehydration, within both the sample and waveguides.

As a proof-of-concept we monitored acoustic emissions during serpentine dehydration at 2-8 GPa. Observations of microseismicity during serpentine dehydration, and analysis of recovered samples shows that dehydration embrittlement and hyfrofracture are viable mechanisms for intermediate depth earthquakes. Figure 3.8-5 shows an acoustic-emissions trace from an experiment at 4 GPa. The spike of high-energy events at ~ 775 °C is associated with dehydration. Dehydration-related acoustic emissions follow of the antigorite dehydration phase diagram closely from 2 to 8 GPa, with some metastable overstep in temperature, which is due to the fast heating rate (5 K/min) used in the experiments.

Further work has focussed on the Olivine-wadsleyite transition. We observe strong AE during transformation of metastable olivine at 16 GPa, but the mechanism for AE generation is currently unclear. Further development work, including true 3-D location and real-time waveform collection, should help to elucidate the mechanisms of ultra-high pressure laboratory AE and deep seismogenesis.

c. *Development of an opposed anvil type high-pressure and high-temperature apparatus using sintered diamond (T. Yagi, D.J. Frost and D.C. Rubie, in collaboration with H. Goto/Tokyo)*

Over the past three years a number of improvements have been made to a “Drickamer-type” opposed anvil apparatus, which uses sintered diamond as the anvil material. (2000 Annual Report). The device can achieve higher pressures than the multianvil apparatus, but has a larger sample volume compared to a diamond anvil. By using a resistance furnace imbedded in the sample chamber, it is possible to heat samples uniformly and stably, which is a great

improvement on the laser heated diamond anvil cell. Here we report further improvements of the technique that allow higher pressures and temperatures to be achieved more stably and easily.

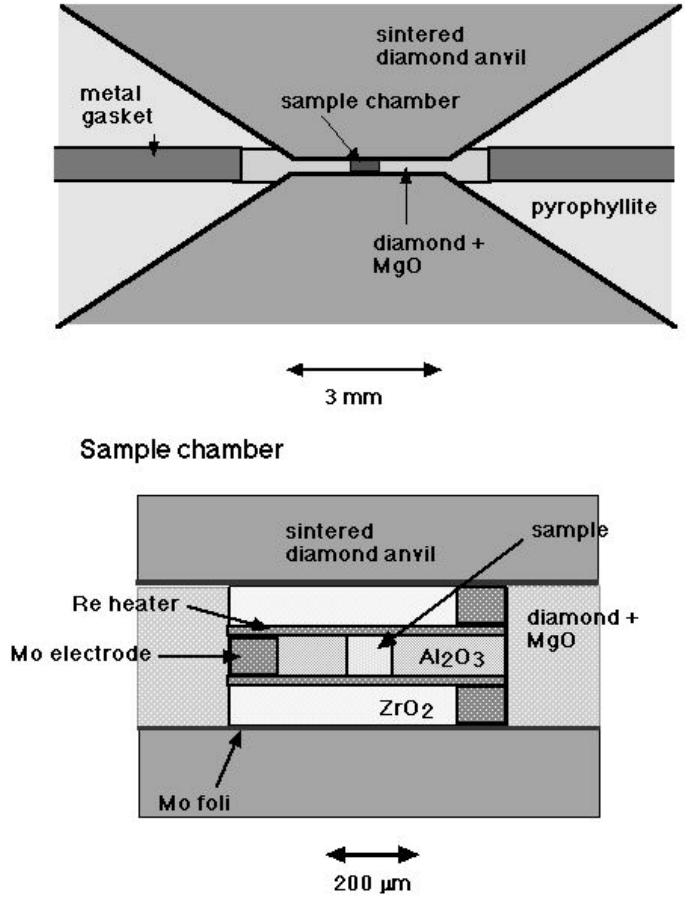

Fig. 3.8-6: The Drickamer apparatus uses two sintered diamond anvils to compress a sample chamber housed in a composite gasket of inner MgO+diamond and outer aluminium alloy (top). The cylindrical sample chamber (bottom) is surrounded by alumina and is heated using a Re foil heater. Zirconia is used as a thermal insulator.

The sample assembly is shown in Fig. 3.8-6. The gasket is made of an aluminium alloy, which is transparent to high energy (> 40 GeV) X-ray, so that we can perform high pressure *in situ* X-ray diffraction studies, when necessary. The pressure-transmitting medium is a 1 to 1 (by weight) mixture of diamond powder and MgO. The sample chamber is made of sintered Al_2O_3 and is sandwiched by two disk heaters made of rhenium foil (30 μm thick). Sintered zirconia (ZrO_2) forms thermal insulating layers between the heater and the anvils. Electrodes are made of either molybdenum or TiC powder. All parts are machined to the desired shape using a laser cutting apparatus, which employs a Q-switched YAG laser. Once the parts are prepared, they can be easily assembled by stacking them one by one in the central hole of the pressure-transmitting medium. The initial size of the sample chamber is 100 μm in diameter and 150 μm in thickness, which is deformed to about 150 μm in diameter and 100 μm in thickness after the experiment.

The assembled parts are compressed using a 50 ton hydraulic press. Pressure calibration using a transition in GaP indicated that 23 GPa could be achieved by applying about 7.5 tonnes at room temperature (2000 Annual Report). This year we have performed heating tests at 12

tonnes by applying an electric power of about 150 W for 10 minutes. After quenching the pressure was released and the recovered sample was imbedded in epoxy resin and ground slowly until the sample appears. Figure 3.8-7 is a cross section through a sample assembly recovered after an experiment. In this experiment, the temperature was raised until the rhenium heater melted. The spherical rhenium beads, which can be seen to the right of the picture, formed as the heater melted. This required temperatures in excess of 3000 °C. The sample can be seen sandwiched between the two remaining parts of the rhenium foil heater. Samples were analysed by Raman spectroscopy. It was found that the starting glass with a composition of $MgSiO_3$ plus 5 % Al_2O_3 was completely transformed to a single phase with the perovskite structure. This indicates that the pressure in the experiment was higher than at least 28 GPa. So far, the temperature has not been measured. We have tried to put a small thermocouple in the sample chamber but because of the large deformation during compression, it is very difficult to avoid electrical contact between heater and thermocouple. We are now trying to establish a technique to estimate the temperature from the resistance change of the heater.

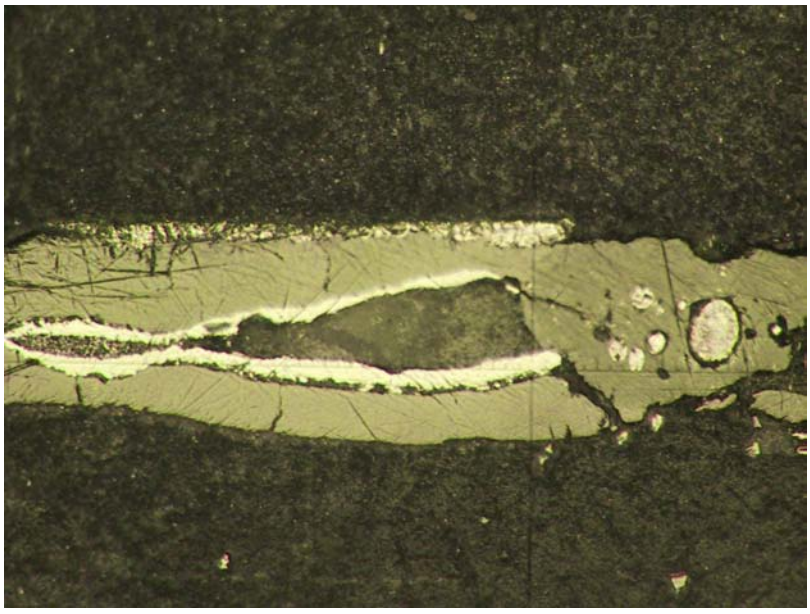

Fig. 3.8-7: A section through a recovered Drickamer sample. The dark regions top and bottom are epoxy resin. The sample is between two horizontal Re foil heater sections in the centre of the picture. The Re foil heater to the right of the picture has melted.

SEM observation of the recovered sample indicates various interesting features of the sample melted at these conditions, such as immiscible liquids of Re and Mo and crystal growth of titanate in molten rhenium during the rapid quench. This implies that the apparatus is eminently suitable for studying the melting behaviour of various materials in a pressure range difficult to achieve using a multianvil apparatus. The recovered charges are much larger that those from the laser heated diamond anvil cell and have experienced a far more even and stable heating regime.

d. *High-temperature heater for diamond anvil cells (N.A. Dubrovinskaia and L.S. Dubrovinsky)*

High-pressure studies provide crucial information for many scientific and industrial applications. Volume changes can produce structural, electronic, magnetic and other phase transitions, initiate chemical reactions, and many other phenomena. During last decades diamond anvil cell (DAC) technique has become the most popular method of pressure generation capable for work in a multimegabar pressure range. However, there still are a number of problems related to high-temperature experiments with DACs.

There are two main methods of heating in DACs-laser and electrical. Laser heating techniques cover a wide P-T field: P > 100 GPa, T = 1300-5000 K. The sample preparation for laser-heating experiments is relatively easy and there is practically no risk to the diamonds due to heating. However, temperature measurements in laser heated DACs is a complex problem which requires multiwavelength spectrometry and a knowledge, particularly, of the pressure and temperature dependence of the emmisivity. Very localised laser heating also creates thermal stress in the DAC, complicating the interpretation of the results. The temperature range below 1200 °C is difficult to handle with laser heating systems. Alternatively, external electrical heating allows one to generate temperatures in a wide range (from 300 K to over 1800 K), which is easy to measure (with thermocouples at T < 2000 K), and which can be maintained at a constant value (±5 K at 1500 K) for several hours. Moreover, in an externally heated DAC at T > 800 K stresses are practically absent and the heating is quite homogeneous. For these reasons, electrical heating is the perfect complement to the laser heating method for studying materials at extreme conditions.

We designed the high-pressure – high-temperature system (Figs. 3.8-8, 3.8-9) which comprises three subunits, namely, the anvil assembly, mechanical loading mechanism, and three heaters – two mounted in the front and back plates, and one placed around the miniature DAC of a cylindrical shape (diameter 23 mm, height 15 mm) made out of a special high-temperature Ti-based alloy (Fig. 3.8-8). The system allows one to conduct experiments in DACs at pressures above 130 GPa and temperatures above 1200 K. It maintains constant pressure (within 1 GPa at megabar pressure range) and temperature (within 5 K at 1000 K) for several hours, allows measuring temperatures accurately with an external thermocouple, fine adjusting of pressure (within 1 GPa) in a whole temperature range. It also does not have measurable temperature gradient within the pressure chamber.

The new heating assembly is easily coupled with experimental set up at synchrotron beam lines (Fig. 3.8-9). It has been used in pilot experiments on Fe-Ni alloys (their behaviour up to 1 Mbar was studied), Fe_3O_4 magnetite (phase transformations and the thermal equation of state), FeO wustite (phase relations to 60 GPa), and H_2O (melting curve to 37 GPa).

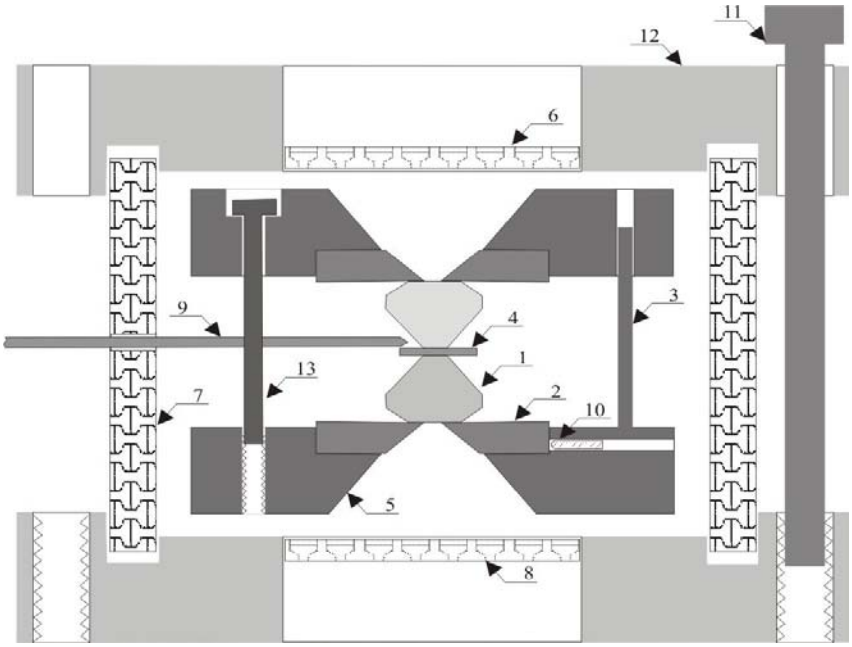

Fig. 3.8-8: Schematic of the high-pressure – high-temperature system: (1) diamond, (2) backing plate, (3) guide pin, (4) gasket, (5) cylindrical platens, (6) front-side heater, (7) cylindrical heater, (8) back-side heater, (9) thermocouple, (10) lateral adjusting screw, (11) one of the six M5 screws with hexagonal heads for applying a load during heating, (12) cylindrical plate, (13) one of the six M3 Allen screws used for room-temperature operations.

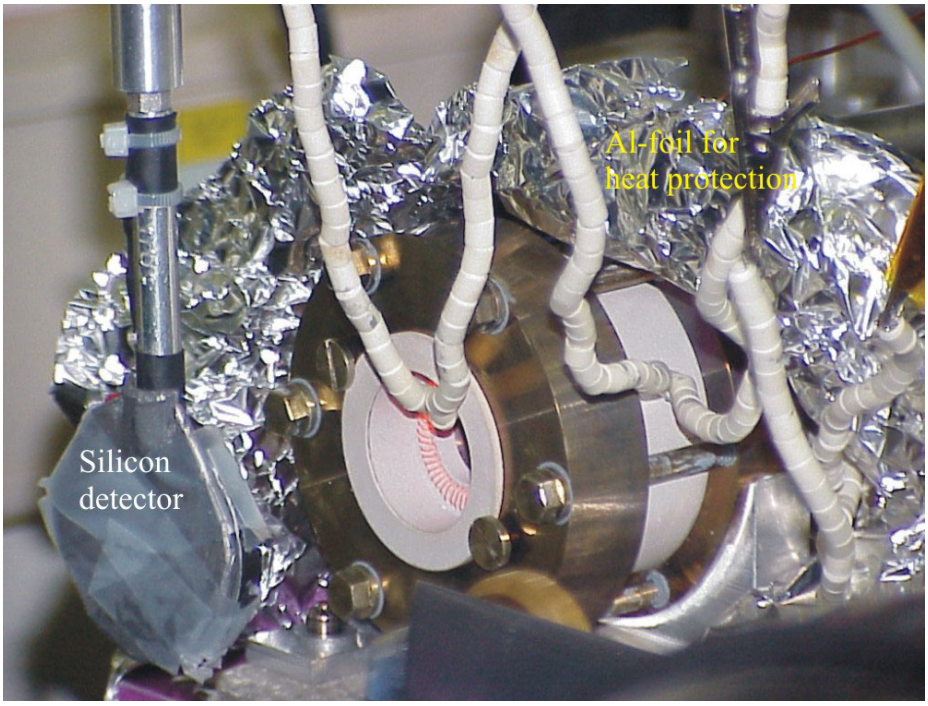

Fig. 3.8-9: High-pressure – high-temperature system mounted for experiments on ID30 beam line at ESRF

e. *Solubility of hydroxyl in pyroxenes under mantle conditions: A novel method for annealing natural samples at high pressure (G.D. Bromiley, H. Keppler, F.A. Bromiley and S.D. Jacobsen)*

Subduction of oceanic lithosphere provides a possible mechanism for the recycling of significant volumes of water back into the Earth's mantle. However, experimental studies suggest that most hydrous phases will breakdown at pressures over 3.0 GPa and temperatures over 700 to 800 °C, leading to slab dehydration. Retention of water in hydrous phases may only occur in the coolest parts of the subducting slab, if at all. In contrast, several recent studies have shown that a number of nominally anhydrous minerals (NAMs) may contain significant volumes of water, in the form of structurally-bound hydrogen, under upper-mantle conditions. Previous studies of natural samples have demonstrated that the pyroxene omphacite contains the most water, and is possibly the most important mineral in terms of recycling water back into the mantle during subduction.

The main tool used in investigating solubility and speciation of hydrogen in NAMs is Fourier-Transform Infrared Spectroscopy (FTIR). However, one drawback of FTIR spectroscopy is the need for large (over 50 μm), good quality, crystalline samples. Previous investigations of hydrogen in omphacitic pyroxenes have focused on characterization of natural samples from mantle xenoliths. Detailed characterization of the effects of pressure and composition on hydroxyl incorporation in synthetic samples have been limited to end-member compositions (jadeite, diopside) due to experimental difficulties in synthesizing crystals of a suitable quality for FTIR examination. An alternative technique, which has been used with some limited success, is to perform annealing experiments using high-quality natural samples. Natural samples are usually cut and polished and sealed in capsules with a suitable buffer mix and source of water. The main problem with such an approach is that experiments are limited to less than 48 hours due to breakdown of the sample. Equilibrium in such experiments is often not attained and thus results are questionable.

A novel technique has been developed to allow long-duration (up to several weeks) high-pressure annealing experiments, using natural samples, to investigate the solubility and speciation of hydroxyl. This method is reliant upon diffusion of hydrogen through platinum at elevated pressures and temperatures. Experiments have been performed using large (cm sized) single crystals of Cr-diopside. Crystals are orientated and cut into blocks with edge lengths of 1, 2 and 3 mm parallel to the crystallographic axes (a, b and c*). Blocks are sealed into small platinum capsules with 5 to 10 wt.% water. These capsules are then pressurized to 2 kb in a hydrothermal bomb to 'shrink-fit' the platinum capsule around the sample, thus forming a protective jacket. The sample (with platinum jacket) is then loaded into a larger Pt-Rh capsule and surrounded by a buffer with the composition of the Cr-diopside. 20 wt.% excess water and 5 wt.% excess silica are also loaded into the capsule. The capsules are then welded shut.

Experiments are performed using the piston-cylinder apparatus at pressures from 0.5 to 4 GPa using a specially constructed, low-friction NaCl cell. After several hundred hours at pressure and temperature, samples, still in platinum jackets, are recovered. The platinum is then removed by polishing. Samples are recovered completely intact, with no cracking in many cases, and with no evidence for chemical breakdown (Fig. 3.8-10). During the experiments, the platinum jacket acts as a semi-permeable membrane, allowing hydrogen diffusion, but prevent diffusion of larger species which would result in reaction with the sample. Hydrogen is effectively buffered throughout the experiments, and the diopside samples are fully saturated with respect to hydrogen.

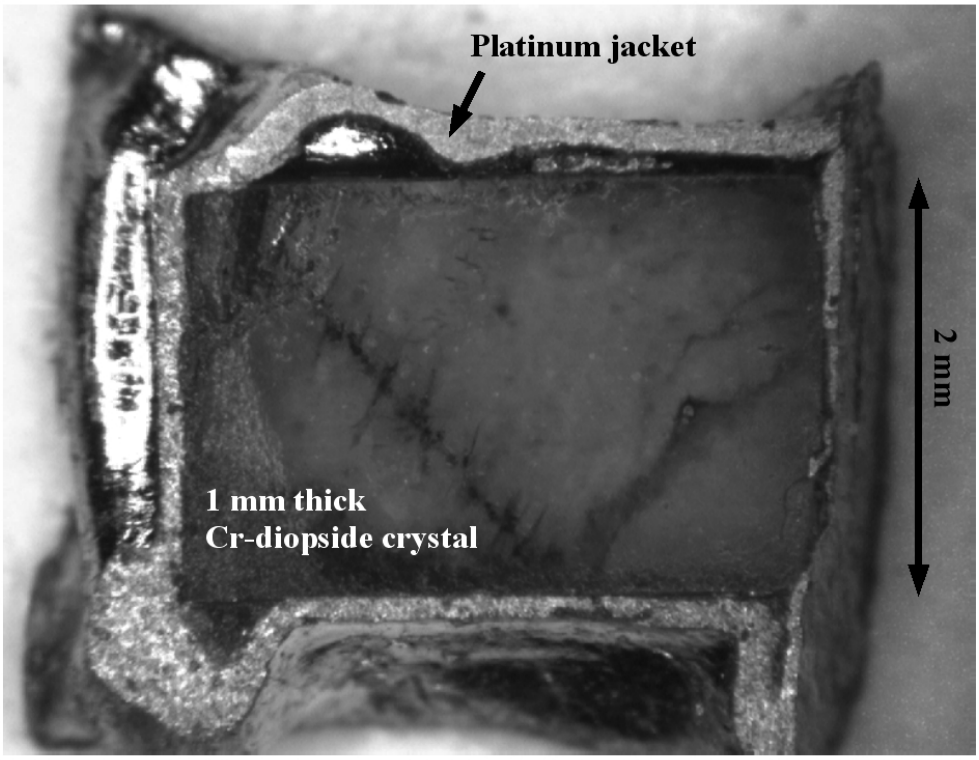

Fig. 3.8-10: Image showing Cr-diopside crystal in platinum jacket after long-duration annealing experiment (prior to preparation for IR analysis, with two sides of capsule removed).

Several experiments have been performed at 1.5 GPa, 1100 °C over different lengths of time to demonstrate attainment of equilibrium. Experiments are now being performed over the full range of pressures possible to study the effects of pressure on hydrogen solubility in Cr-diopside (Fig. 3.8-11). Recovered samples are of suitable quality for use in a number of further studies, such as characterization of the effects of heating on IR absorption band wavelength and an investigation of the effects of varying water contents on P wave velocity using ultrasonic interferometry. The method described will also be used to investigate the effects of pressure on hydroxyl incorporation in more complex, omphacitic compositions.

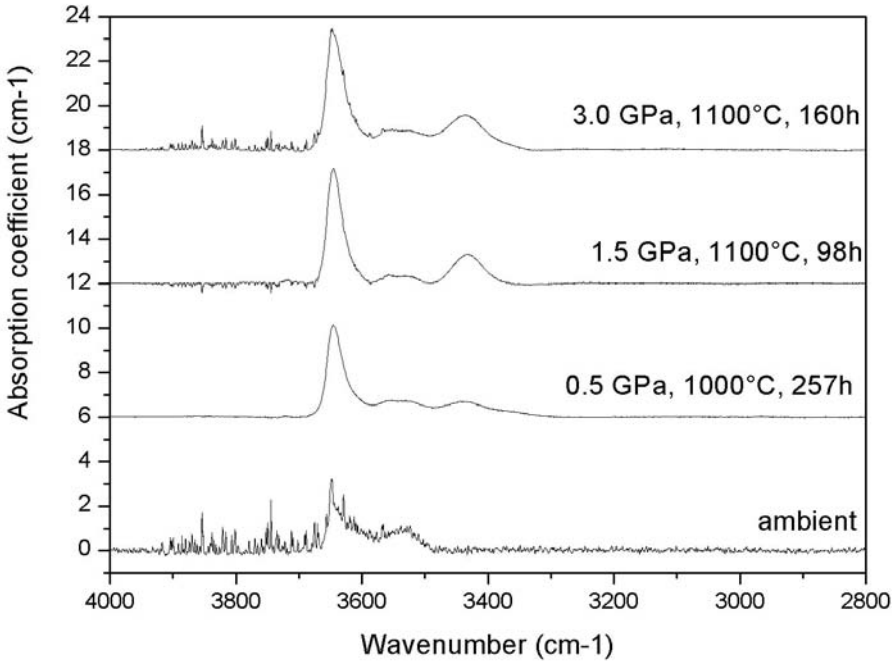

Fig. 3.8-11: FTIR spectra for Cr-diopside annealed at different pressures (offset along y axis with increasing pressure). All absorption bands in wavenumber range due to OH stretching.

f. *ALCHEMI study of perovskite by electron energy dispersive X-ray spectroscopy (EDXS) (N. Miyajima/Tokyo, in collaboration with F. Langenhorst)*

Results from high temperature and pressure experiments indicate that $MgSiO_3$ silicate perovskite is likely the most important carrier mineral phase for trivalent cations such as aluminium and ferric iron in the Earth's lower mantle. Due to their substitution into $A^{2+}B^{4+}O_3$ perovskite, a certain amount of oxygen vacancies might be stable in the crystal structure. The incorporation mechanisms are expected to play a major role in determining the physical and chemical properties of perovskite. The crystal structure has two potential lattice sites for trivalent cations. To clarify the crystal chemistry of Al^{3+} and Fe^{3+}-bearing perovskite, it is necessary to determine the site-specific affinities.

As the first step, we have examined a garnet-perovskite mineral assemblage with the main chemical components $(Mg,Fe,Ca)SiO_3$-Al_2O_3, using atom location by channeling-enhanced microanalysis (ALCHEMI) in a transmission electron microscope (TEM). The probed sample was synthesized using a multianvil press at 26 GPa and 2273 K. The sample was examined using an analytical electron microscope equipped with X-ray energy dispersive detector (XEDS) and electron energy-loss spectrometer (EELS), operating at 200 kV.

The $Fe^{3+}/\Sigma Fe$ ratio in perovskite is 0.28(5), on the basis of the evaluation on Fe $L_{2,3}$-edge electron energy-loss near-edge structure (ELNES) spectra. Results of ALCHEMI (see Fig.

3.8-12) show that the EDS spectra of perovskite display remarkable changes of the peak intensity ratios at systematic tilting conditions along about the <110> direction. The variations in the intensities of Fe-*K* and Ca-*K* peaks relative to Si-*K* in the systematic channeling EDS spectra result from a localized standing electron wave inside the crystal that preferentially causes characteristic ionization processes on either the octahedral site or the pseudo-dodecahedral site. Fe^{2+} appears to occupy the pseudo-dodecahedral site together with Ca. To a certain amount, Al prefers to occupy the octahedral site, charge-balanced by Fe^{3+} in the pseudo-dodecahedral site. This initial result suggests that two different cation sites might be qualitatively distinguished with planer ALCHEMI experiments along the pseudo {110} systematic row orientations of silicate perovskite.

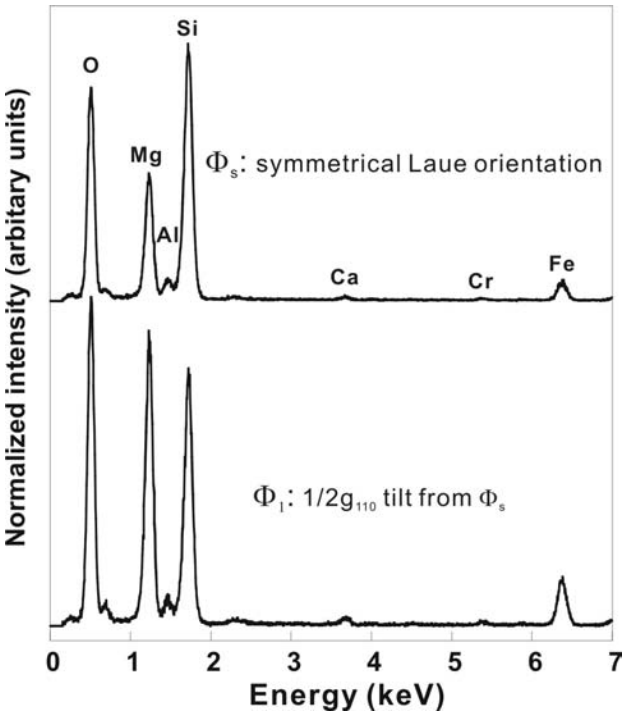

Fig. 3.8-12: Comparison of energy-dispersive X-ray spectra for silicate perovskite oriented pseudo {110} systematic row orientations: the symmetrical Laue orientation, ϕ_s (upper) and slightly inside the Bragg angle for (110), ϕ_1 (lower), normalized with Si intensities. Note the change in relative height of the Fe and Cr peaks, reflecting occupants of pseudo-dodecahedral sites.

g. *New solid-state NMR results (M. Bechmann, X. Helluy and A. Sebald)*

^{29}Si and ^{19}F MAS NMR of samples containing $^{29}Si(^{19}F)_2$ or $^{29}Si(^{19}F)_3$ moieties (X. Helluy and A. Sebald, in collaboration with R. Pietschnig/Graz, H. Foerster and G. Althoff/Rheinstetten)

Samples containing isolated clusters of $^{29}Si(^{19}F)_2$ or $^{29}Si(^{19}F)_3$ spins yield particularly informative straightforward ^{29}Si MAS NMR spectra: under slow spinning conditions, the homo- and heteronuclear dipolar coupling interactions within the cluster are not completely averaged out, leading to complicated ^{29}Si lineshapes reflecting all anisotropic interaction parameters within the cluster and the complete geometry of the SiF_2 or SiF_3 moiety – in the absence of molecular solid-state dynamic effects. Determination of these geometric

parameters involves straightforward MAS NMR experiments in conjunction with extensive numerical simulations. With this approach we could demonstrate, for example, that in an organosilicon compound $RSiF_3$, where R is a bulky organic ligand, the SiF_3 group is rotating rapidly in the crystalline solid material at ambient conditions. Another organosilicon compound R_2SiF_2, again with bulky organic ligands R, was found to display rather unusual ^{19}F chemical shielding tensor properties. These experimental findings should next be completed by a comparison with ab initio calculations of ^{19}F and ^{29}Si shielding parameters in such molecular units.

Double-quantum filtration ^1H MAS NMR techniques (M. Bechmann and A. Sebald, in collaboration with H. Foerster/Rheinstetten)

Amongst the many NMR-active isotopes, ^1H is a particularly attractive target for reasons of sensitivity, at least in principle. In solid-state NMR, however, these favourable properties of the isotope ^1H are often counterbalanced by a lack of spectral resolution, mainly caused by strong linebroadening effects originating from multiple homonuclear dipolar coupling interactions amongst the (usually abundant) ^1H spins. Especially for samples with a rather low natural density of ^1H spins, or for cases where the ^1H spins may be diluted by partial replacement with deuterium, we find that the lineshapes of double-quantum filtered (DQF) ^1H MAS NMR spectra are highly informative. In-depth analyses of these lineshapes by numerical simulations yield information about internuclear ^1H-^1H distances as well as a good estimate of the number of coupled ^1H spins. These ^1H DQF MAS NMR investigations are important for two reasons. We feel that such lineshape analyses can provide a more robust estimate of the number of coupled spins than do conventional so-called multiple-quantum spin-counting experiments. Second, ^1H MAS NMR is a natural complement for diffraction techniques since the precise localisation of hydrogen atoms by means of diffraction techniques is notoriously difficult, sometimes even impossible.

Spin diffusion MAS NMR at and near the so-called n=0 rotational resonance condition (A. Sebald, in collaboration with P. Tekely/Nancy)

Dipolar coupled pairs of spin-1/2 isotopes with large chemical shielding anisotropies and identical or similar isotropic chemical shielding values occur rather commonly in many solid materials. Under suitable MAS conditions, this kind of spin pair gives rise to highly informative lineshapes, encoding information about the internuclear distance as well as shielding tensor orientations. These so-called at, or near, $n = 0$ rotational-resonance lineshape phenomena are useful in many circumstances for purposes of structural analysis where the main emphasis lies on questions regarding short-range distances of less than approximately 300 to 400 pm. When dealing with larger internuclear distances, the lineshapes become increasingly less sensitive to the spin-pair parameters, but many practical applications require

the determination of internuclear distances exceeding 500 pm. Here it becomes necessary to change the experimental approach and to switch from lineshape analysis to MAS NMR experiments with, for example, rotor- or proton-driven spin diffusion characteristics. We could show that MAS NMR experiments of this type permit the quantitative determination of internuclear ^{13}C-^{13}C and ^{31}P-^{31}P distances much larger than 400 pm, even in the presence of considerable chemical shielding anisotropies.

4. Publications, Conference Presentations, Seminars, Visiting Scientists

4.1 Publications (published)

a) Refereed international journals

AHUJA, R.; DUBROVINSKY, L.S. (2002): Cotunnite-structured titanium dioxide and the hardest known oxide. High Pressure Research 22, 429-433

AHUJA, R.; DUBROVINSKY, L.S. (2002): High-pressure structural phase transitions in TiO_2. Journal of Physics: Condensed Matter 14, 10995-10999

AMAMI, M.; VAN SMAALEN, S.; PALATINUS, L.; SALAH, A.B.; HELLUY, X.; SEBALD, A. (2002): Structural investigations of the phase transitions of $[N(CH_3)_4]_2HgCl_4$. Zeitschrift für Kristallographie 217, 532-541

BECERRO, A.I.; REDFERN, S.A.T.; CARPENTER, M.A.; KNIGHT, K.S.; SEIFERT, F. (2002): Displacive phase transitions in and strain analysis of Fe-doped $CaTiO_3$ perovskites at high temperature by neutron diffraction. Journal of Solid State Chemistry 167, 459-471

BECHMANN, M.; HELLUY, X.; MARICHAL, C.; SEBALD, A. (2002): Double-quantum filtered MAS NMR in the presence of chemical shielding anisotropies, direct dipolar and *J* couplings. Solid State Nuclear Magnetic Resonance 21, 71-85

BERNDT, J.; LIEBSKE, C.; HOLTZ, F.; FREISE, M.; NOWAK, M.; ZIEGENBEIN, D.; HURKUCK, W.; KOEPKE, J. (2002): A combined rapid-quench and H_2-membrane setup for internally heated pressure vessels: Description and application for water solubility in basaltic melts. American Mineralogist 87, 1717-1726

BOFFA BALLARAN, T.; MCCAMMON, C.A.; CARPENTER, M.A. (2002): Order parameter behavior at the structural phase transition in cummingtonite from Mössbauer spectroscopy. American Mineralogist 87, 1490-1493

BOLFAN-CASANOVA, N.; KEPPLER, H.; RUBIE, D.C. (2002): Hydroxyl in $MgSiO_3$ akimotoite: A polarised and high-pressure IR study. American Mineralogist 87, 603-608

BOLFAN-CASANOVA, N.; MACKWELL, S.J.; KEPPLER, H.; MCCAMMON, C.A.; RUBIE, D.C. (2002): Pressure dependence of H solubility in magnesiowüstite up to 25 GPa: Implications for the storage of water in the Earth's lower mantle. Geophysical Research Letters 29, No. 10, 10.1029/2001GL014457

COMODI, P.; MONTAGNOLI, M.; ZANAZZI, P.F.; BOFFA BALLARAN, T. (2002): Isothermal compression of staurolite: A single-crystal study. American Mineralogist 87, 1164-1171

CONTRERAS, R.; CAMACHO-CAMACHO, C.; NÖTH, H.; BECHMANN, M.; SEBALD, A.; WRACKMEYER, B. (2002): The molecular structures of organotin complexes with tin coordination numbers 5 to 7, seen by single-crystal X-ray diffraction and solid and solution-state ^{119}Sn NMR. Magnetic Resonance in Chemistry 40, 31-40

CORDIER, P.; THUREL, E.; RABIER, J. (2002): Stress determination in multianvil deformation experiments based on dislocation curvatures measurements: Application to wadsleyite and ringwoodite. Geophysical Research Letters 29, No. 9, 10.1029/ 2001GL014172

DINNEBIER, R.E.; BERNATOWICZ, P.; HELLUY, X.; SEBALD, A.; WUNSCHEL, M.; FITCH, A.; VAN SMAALEN, S. (2002): The structure of compounds $E(SnMe_3)_4$ (E = Si,Ge) as seen by high resolution X-ray powder diffraction and solid-state NMR. Acta Crystallographica B 58, 52-61

DOBSON, D.P. (2002): Self-diffusion in liquid Fe at high pressure. Physics of the Earth and Planetary Interiors 130, 271-284

DOBSON, D.P.; VOČADLO, L.; WOOD, I.G. (2002): A new high-pressure phase of FeSi. American Mineralogist 87, 784-787

DOBSON, D.P.; MEREDITH, P.G.; BOON, S.A. (2002): Simulation of subduction zone seismicity by dehydration of serpentine. Science 298, 1407-1410

DUBROVINSKAIA, N.A.; DUBROVINSKY, L.S.; SWAMY, V.; AHUJA, R. (2002): Cotunnite-structured titanium dioxide. High Pressure Research 22, 391-394

DUBROVINSKY, L.S.; DUBROVINSKAIA, N.A.; PROKOPENKO, V.B.; LE BIHAN, T. (2002): Equation of state and crystal structure of $NaAlSiO_4$ with calcium-ferrite type structure in the conditions of the lower mantle. High Pressure Research 22, 495-499

DUBROVINSKY, L.S.; DUBROVINSKAIA, N.A.; LANGENHORST, F.; RUBIE, D.C.; GEßMANN, C.; FABRICHNAYA, O.; LE BIHAN, T. (2002): Chemical interaction of iron and oxides (Al_2O_3, SiO_2) at high pressure and temperature: Implication for the Earth's deep interior. Electronic Geosciences 7 (http://link.springer.de/link/service/journals/10069/free/conferen/superplu/)

DUBROVINSKY, L.S. (2002): Thermal expansion and equation of state, In: Encyclopedia of Materials: Science and Technology

FROST, D.J.; LANGENHORST, F. (2002): The effect of Al_2O_3 on Fe-Mg partitioning between magnesiowüstite and magnesium silicate perovskite. Earth and Planetary Science Letters 199, 227-241

FUNAKOSHI, K.; SUZUKI, A.; TERASAKI, H. (2002): *In situ* viscosity measurements of albite melt under high pressure. Journal of Physics: Condensed Matter 14, 11343-11347

GAILLARD, F.; SCAILLET, B.; PICHAVANT, M. (2002): Kinetics of iron oxidation-reduction in hydrous silicic melts. American Mineralogist 87, 829-837

GIULI, G.; PARIS, E.; WU, Z.; MOTTANA, A.; SEIFERT, F. (2002): Fe and Mg local environment in the synthetic enstatite-ferrosilite join: An experimental and theoretical XANES and XRD study. European Journal of Mineralogy 14, 429-436

HEUER, M.; HUBER, A.; BROMILEY, G.D.: Crystal structure of calcium iron zinc *catena*-disilicate, $Ca(Fe_{0.52}Zn_{0.48})Si_2O_6$. Zeitschrift für Kristallographie 217, 465-466

IVANOV, B.A.; LANGENHORST, F.; DEUTSCH, A.; HORNEMANN, U. (2002): How strong was impact-induced CO_2 degassing in the K/T event? Numerical modeling of laboratory experiments. – In: KOEBERL, C.; MACLEOD, K.G. (Eds.): "Catastrophic events and Mass Extinctions: Impacts and beyond" – Geological Society of America Special Paper 356, 587-594

JACOBSEN, S.D.; REICHMANN, H.-J.; SPETZLER, H.A.; MACKWELL, S.J.; SMYTH, J.R.; ANGEL, R.J.; MCCAMMON, C.A. (2002): Structure and elasticity of single-crystal (Mg,Fe)O and a new method of generating shear waves for gigahertz ultrasonic interferometry. Journal of Geophysical Research, 107(B2), 2037, 10.1029/2001JB000490

JACOBSEN, S.D.; SPETZLER, H.A.; REICHMANN, H.-J.; SMYTH, J.R.; MACKWELL, S.J.; ANGEL, R.J.; BASSETT W.A. (2002): Gigahertz ultrasonic interferometry at high *P* and *T*: New tools for obtaining a thermodynamic equation of state. Journal of Physics: Condensed Matter 14, 11525-11530

JIANG, J.Z.; LINDELOV, H.; GERWARD, L.; STÅHL, K.; REICO, J.M.; MORI-SANCHEZ, P.; CARLSON, S.; MOHAMED, M.; DOORYHEE, E.; FICHT, A.; FROST, D.J. (2002): Compressibility and thermal expansion of cubic silicon nitride. Physical Review B 65, 161202(R)

KARTASHOV, P.M.; FERRARIS, G.; IVALDI, G.; SOKOLOVA, E.; MCCAMMON, C.A.: Ferriallanite-(Ce), $CaCeFe^{3+}AlFe^{2+}(SiO_4)(Si_2O_7)O(OH)$, a new member of the epidote group: Description, X-ray and Mössbauer study. The Canadian Mineralogist 40, 1641-1648

KLEPPE, A.; JEPHCOAT, A.P.; SMYTH, J.R.; FROST, D.J. (2002): On protons, iron and the high-pressure behavior of ringwoodite. Geophysical Research Letters 29, 10.1029/2002 GL015276

KOHN, S.C.; BROOKER, R.A.; FROST, D.J.; SLESINGER, A.E.; WOOD, B.J. (2002): Ordering of hydroxyl defects in hydrous wadsleyite (β-Mg_2SiO_4). American Mineralogist 87, 293-301

KRAUSE, W.; BERNHARDT, H.J.; MCCAMMON, C.A.; EFFENBERGER, H. (2002): Neustadtelite and cobaltneustadtelite, the Fe^{3+}- and Co^{2+}- analogues of medenbachite. American Mineralogist 87(5-6), 726-738

KUZNETSOV, A.; DMITRIEV, V.; DUBROVINSKY, L.S.; PRAKAPENKA, V.; WEBER, H.-P. (2002): FCC-HCP phase boundary in lead. Solid State Communications 122, 125-127

LANGENHORST, F.; POIRIER, J.-P. (2002): Transmission electron microscopy of coesite inclusions in the Dora Maira high-pressure metamorphic pyrope-quartzite. Earth and Planetary Science Letters 203, 793-803

LANGENHORST, F.; SOLOZCHENKO, V. (2002): ATEM-EELS study of new diamond-like phases of the B-C-N system. Physical Chemistry Chemical Physics 4, 5183-5188

LANGENHORST, F.; BOUSTIE, M.; DEUTSCH, A.; HORNEMANN, U.; MATIGNON, C.; MIGAULT, A.; ROMAIN, J.P. (2002): Experimental techniques for the simulation of shock metamorphism: A case study on calcite. – In: DAVISON, L.; HORIE, Y.; SEKINE, T. (Eds.): "High-Pressure Shock Compression of Solids V - Shock Chemistry with Applications to Meteorite Impacts" – Springer, New York, 1-27

LANGENHORST, F.; POIRIER, J.-P.; DEUTSCH, A.; HORNEMANN, U. (2002): Experimental approach to generate shock veins in single-crystal olivine by shear melting. Meteoritics & Planetary Science 37, 1541-1553

LANGENHORST, F. (2002): Shock metamorphism of some minerals: Basic introduction and microstructural observations. Bulletin of the Czech Geological Survey 77, 265-282

LINNEN, R.L.; KEPPLER, H. (2002): Melt composition control of Zr/Hf fractionation in magmatic processes. Geochimica et Cosmochimica Acta 66, No. 18, 3293-3301

MCCAMMON, C.A. (2002): From diamonds to defects: New ideas about the Earth's interior. Hyperfine Interactions 141/142, 73-81

MCENROE, S.A., HARRISON, R.J., ROBINSON, P., LANGENHORST, F. (2002): Nanoscale hematite-ilmenite lamellae in massive ilmenite rock: An example of "lamellar magnetism" with implications for planetary magnetic anomalies. Geophysical Journal International 151, 890-912

MEYER, H.-W.; CARPENTER, M.A.; BECERRO, A.I.; SEIFERT, F. (2002): Hard-mode infrared spectroscopy of perovskites across the $CaTiO_3$-$SrTiO_3$ solid solution. American Mineralogist 87, 1291-1296

PICHAVANT, M.; MARTEL, C.; BOURDIER, J.-L.; SCAILLET, B. (2002): Physical conditions, structure, and dynamics of a zoned magma chamber: Mount Pelée (Martinique, Lesser Antilles Arc). Journal of Geophysical Research, 107(B5), 10.1029/2001JB000315

POIRIER, J.-P.; LANGENHORST, F. (2002): TEM study of an analogue of the Earth's inner core ε-Fe. Physics of the Earth and Planetary Interiors 129, 347-358

QIN, S.; WU, X.; SEIFERT, F.; BECERRO; A.I. (2002): Micro-Raman study of perovskites in the $CaTiO_3$-$SrTiO_3$ system. Journal of the Chemical Society, Dalton Transactions, 3751-3755

RAUCH, M.; KEPPLER, H. (2002): Water solubility in orthopyroxene. Contributions to Mineralogy and Petrology 143, 525-536

REECE, J.J.; REDFERN, S.A.T.; WELCH, M.D.; HENDERSON, C.M.B.; MCCAMMON, C.A. (2002): Temperature-dependent Fe^{2+}-Mn^{2+} order-disorder behaviour in amphiboles. Physics and Chemistry of Minerals 29, 562-570

ROSS, N.L.; ANGEL, R.J.; SEIFERT, F. (2002): Compressibility of brownmillerite, $Ca_2Fe_2O_5$: Effect of vacancies on the elastic properties of perovskites. Physics of the Earth and Planetary Interiors 129, 145-151

ROZENBERG, G.K.; DUBROVINSKY, L.S.; PASTERNAK, M.P.; NAAMAN, O.; LE BIHAN, T.; AHUJA, R. (2002): High pressure structural studies of hematite (Fe_2O_3). Physical Review B 6506(6), 4112-4120

ROZENBERG, G.K.; PASTERNAK, M.P.; DUBROVINSKY, L.S.; XU, W.M.; LE BIHAN, T. (2002): Structural aspects of Mott transition in FeI_2 compound under high pressure. High Pressure Research 22, 381-384

SCHMIDT, B.C.; KEPPLER, H. (2002): Experimental evidence for high noble gas solubilities in silicate melts under mantle pressures. Earth and Planetary Science Letters 195, 277-290

SCHUBERT, M.; DOLLASE, W. (2002): Generalized ellipsometry for biaxial absorbing materials: Determination of crystal orientation and optical constants of Sb_2S_3. Optics Letters 27, 2073-2075

SHERRIFF, B.; MCCAMMON, C.A.; STIRLING, L. (2002): The colour of Roman pottery from the Leptimus archaeological site, Tunisia. Geoarchaeology 17, 863-874

SILVER, J.; ANANADAN, S.; DAVIES, D.A.; FERN, G.R.; MARSH, P.J.; MILLER, J.R.; TITLER, P.J.; MCCAMMON, C.A. (2002): High pressure Mössbauer spectroscopic studies of molecular solids. The importance of "free" space in molecular lattices. Hyperfine Interactions 141/142, 109-117

SMYTH, J.R.; FROST, D.J. (2002): The effect of water on the 410-km discontinuity: An experimental study. Geophysical Research Letters 29, 10.1029/2001GL014418

SOWERBY, J.R.; KEPPLER, H. (2002): The effect of fluorine, boron and excess sodium on the critical curve in the albite-H_2O system. Contributions to Mineralogy and Petrology 143, 32-37

STÄHLE, V.; KOCH, M.; MCCAMMON, C.A.; MANN, U.; MARKL, G.: Occurrence of low-Ti and high-Ti freudenbergite in alkali syenite dikes from the Katzenbuckel volcano, southwestern Germany. The Canadian Mineralogist 40, 1609-1627

STOYANOVA, R.; ZHECHEVA, E.; BROMILEY, G.D.; BOFFA BALLARAN, T.; ALCANTARA, R.; CORREDOR, J.-I.; TIRADO, J.-L. (2002): High-pressure synthesis of Ga-substituted LiCoO with layered crystal structure. Journal of Materials Chemistry 12, 2501-2506

SUZUKI, A.; OHTANI, E.; FUNAKOSHI, K.; TERASAKI, H.; KUBO, T. (2002): Viscosity of albite melt at high pressure and high temperature. Physics and Chemistry of Minerals 29, 159-165

SWAMY, V.; DUBROVINSKAIA, N.A.; DUBROVINSKY, L.S. (2002): Compressibility of baddeleyite-type TiO_2 from static compression to 40 GPa. Journal of Alloys and Compounds 340, 46-48

TALYZIN, A.V.; DUBROVINSKY, L.S.; LE BIHAN, T.; JANSSON, U. (2002): Pressure-induced polymerization of C-60 at high temperatures: An *in situ* Raman study. Physical Review B 6524(24), 5413

TALYZIN, A.V.; DUBROVINSKY, L.S.; JANSSON, U. (2002): High pressure Raman study of $C_{60}S_{16}$. Solid State Communications 123, 93-96

TARANTINO, S.C.; BOFFA BALLARAN, T.; CARPENTER, M.A.; DOMENEGHETTI, M.C.; TAZZOLI; V. (2002): Mixing properties of the enstatite-ferrosilite solid solution: II. A microscopic perspective. European Journal of Mineralogy 14, 537-547

TEKELY, P.; GARDIENNET, C.; POTRZEBOWSKI, M.J.; SEBALD, A.; REICHERT, D.; LUZ, Z. (2002): Probing molecular geometry of solids by NMR spin exchange at the n = 0 rotational-resonance condition. Journal of Chemical Physics 116, 7607-7616

TERASAKI, H.; KATO, T.; URAKAWA, S.; FUNAKOSHI, K.; SATO, K., SUZUKI, A.; OKADA, T. (2002): Viscosity change and structural transition of molten Fe at 5 GPa. Geophysical Research Letters 29, 10.1029/2001GL014321

TRØNNES, R.G.; FROST, D.J. (2002): Peridotite melting and mineral-melt partitioning of major and minor elements at 21-24 GPa. Earth and Planetary Science Letters 197, 117-131

VOCADLO, L.; BRODHOLT, J.; DOBSON, D.P.; KNIGHT, K.S.; MARSHALL, W.G.; PRICE, G.D.; WOOD, I.G. (2002): The effect of ferromagnetism on the equation of state of Fe_3C studied by first-principles calculations. Earth and Planetary Science Letters 203, 567-575

WU, Z.; PARIS, E.; LANGENHORST, F.; SEIFERT, F. (2002): Oxygen-metal bonding in Ti-bearing compounds from O*1s* spectra and *ab initio* full multiple-scattering calculations. Journal of Synchrotron Radiation 9, 394-400

XU, Y.; MCCAMMON, C.A. (2002): Evidence for ionic conductivity in lower mantle $(Mg,Fe)(Si,Al)O_3$ perovskite. Journal of Geophysical Research 107, 10.1029/ 2001JB000677

ZANG, S.X.; CHEN, Q.Y.; NING, J.Y.; *et al.* (2002): Motion of the Philippine Sea plate consistent with the NUVEL-1A model. Geophysics Journal International 150 (3), 809-819

ZANG, S.X.; CHEN, Q.Y.; NING, J.Y.; *et al.* (2002): Determination of Euler parameters of Philippine Sea plate and the inferences. Science in China (D) 45 (2), 133-142

ZANG, S.X.; LIU, Y.G.; NING, J.Y. (2002): Thermal structure of the lithosphere in North China. Chinese Journal of Geophysics 45 (1), 56-66

ZOTOV, N.; YANEV, Y.; PIRIOU, B. (2002): Time-resolved luminescence of Fe^{3+} and Mn^{2+} ions in hydrous volcanic glasses. Physics and Chemistry of Minerals 29, 291-299

ZOTOV, N.; KEPPLER, H. (2002): Silica speciation in aqueous fluids at high pressures and high temperatures. Chemical Geology 184, 71-82

b) Conference proceedings

MCCAMMON, C.A; BECERRO, A.I.; LAUTERBACH, S.; BLÄß, U.; MARION, S.; LANGENHORST, F.; ANGEL, R.J.; VAN AKEN, P.A.; SEIFERT, F. (2002): Oxygen vacancies in perovskites and related structures: Implications for the lower mantle. Materials Research Society Proceedings 718, D2.3, 109-114

SCHUBERT, M.; KASIC, A.; HOFMANN, T.; GOTTSCHALCH, V.; OFF, J.; SCHOLZ, F.; SCHUBERT, E.; NEUMANN, H.; HODGKINSON, I.; ARNOLD, M.; DOLLASE, W.; HERZINGER, C.M. (2002): Generalized ellipsometry of complex mediums in layered systems. Proceedings SPIE 4806, 264-276

4.2 Publications (submitted, in press)

ANANDAN, S.; SILVER, J.; FERN, G.R.; TITLER, P.J.; MCCAMMON, C.A.: A high pressure Mössbauer spectroscopy study of [^{57}FeOEPCl]. Hyperfine Interactions (in press)

BALOG, P.S.; SECCO, R.A.; RUBIE, D.C.; FROST, D.J.: Equation of state of liquid Fe-10wt.% S: Implications for the metallic cores of planetary bodies. Journal of Geophysical Research (in press)

BECHMANN, M.; HAIN, K.; MARICHAL, C.; SEBALD, A.: X-{^{1}H,^{19}F} triple resonance with a X-{^{1}H} CP MAS probe and characterisation of a ^{29}Si-^{19}F spin pair. Solid State Nuclear Magnetic Resonance (in press)

BOFFA BALLARAN, T.; CARPENTER, M.A.: Line broadening and enthalpy: Some empirical calibrations of solid solution behaviour from IR spectra. Phase Transitions (in press)

BOFFA BALLARAN, T.; ANGEL R.J.: Equation of state and high-pressure phase transitions in lawsonite. European Journal of Mineralogy (in press)

BROMILEY, G.D.; PAWLEY, A.R.: The stability of antigorite in the systems MgO-SiO_2-H_2O (MSH) and MgO-Al_2O_3-SiO_2-H_2O (MASH). The effects of Al^{3+} substitution on the high-pressure stability. American Mineralogist (in press)

BUREAU, H.; MÉTRICH, N.: An experimental study of bromine behaviour in water-saturated silicic melts. Geochimica et Cosmochimica Acta (in press)

BUREAU, H.; TROCELLIER, P.; SHAW, C.; KHODJA, H.; BOLFAN-CASANOVA, N.; DEMOUCHY, S.: Determination of the concentration of water dissolved in glasses and minerals using nuclear microprobe. Nuclear Instrument and Methods, ICNMTA 2002 Meeting, Special Issue (accepted)

CORNELIUS, V.J.; TITLER, P.J.; FERN, G.R.; MILLER, J.R.; SILVER, J.; SNOWDEN, M.J.; MCCAMMON, C.A.: An interesting spin-state transition for [Fe(PPIX)OH] induced by high pressure in a diamond anvil cell. Hyperfine Interactions (submitted)

DEMOUCHY, S.; MACKWELL, S.J.: Water diffusion in synthetic iron-free forsterite. Physics and Chemistry of Minerals (submitted)

DOBSON, D.P.: Oxygen ionic conduction in $MgSiO_3$ perovskite. Physics of the Earth and Planetary Interiors (submitted)

DOBSON, D.P.; CRICHTON, W.A.; BOUVIER, P.; VOCADLO, L; WOOD, I.G.: The equation of state of CsCl-structured FeSi to 40 GPa; implications for silicon in the Earth's core. Geophysical Research Letters (in press)

DOBSON, D.P.; WIEDENBECK, M.: Fe- and C-self-diffusion in liquid Fe_3C to 15 GPa. Geophysical Research Letters (in press)

DUBROVINSKAIA, N.A.; DUBROVINSKY, L.S.: Melting curve of water studied in externally heated diamond anvil cell. High Pressure Research (in press)

DUBROVINSKAIA, N.A.; DUBROVINSKY, L.S.: High-temperature heater for diamond anvil cells. Review of Scientific Instruments (submitted)

DUBROVINSKY, L.S.; DUBROVINSKAIA, N.A.; PRAKAPENKA, V.; SEIFERT, F.; LANGENHORST, F.; DMITRIEV, V.; WEBER, H.-P.; LE BIHAN, V.; High-pressure and high-temperature polymorphism in silica, High Pressure Research (in press)

DUBROVINSKY, L.S.; DUBROVINSKAIA, N.A.; PRAKAPENKA, V.; SEIFERT, F.; LANGENHORST, F.; DMITRIEV, V.; WEBER, H.-P.; LE BIHAN, T.: A class of new high-pressure silica polymorphs. Science (submitted)

DUBROVINSKY, L.S.; DUBROVINSKAIA, N.A.; LANGENHORST, F.; DOBSON, D.P.; RUBIE, D.C.; GEßMANN, C.; LE BIHAN, T.; CRICHTON, W.A.: Iron-silica interaction at core-mantle boundary conditions. Physics of the Earth and Planetary Interiors (submitted)

DUBROVINSKY, L.S.; DUBROVINSKAIA, N.A.; MCCAMMON, C.A.; ROZENBERG, G.K.; AHUJA, R.; OSORIO-GUILLÉN, J.M.; DMITRIEV, V.; WEBER, H.-P.; LE BIHAN, T.; JOHANSSON, B.: Structure of metallic high-pressure Fe_3O_4 polymorph: Experimental and theoretical study. Physical Review B (in press)

DUBROVINSKY, L.S.; DUBROVINSKAIA, N.A.; LANGENHORST, F.; DOBSON, D.P.; RUBIE, D.C.; GESSMANN, C.; ABRIVOSOV, I.; JOHANSSON, B.; BAYKOV, V.I.; VITOS, L.; LE BIHAN, T.; CRICHTON, W.A.: Iron-silica interaction at extreme conditions and the nature of the electrically conducting layer at the base of Earth's mantle. Nature (submitted)

DUPAS-BRUZEK, C.; LAUDE, L.D.; LANGENHORST, F.; KOLEV, K.: Surface structural transformation of sintered alumina induced by excimer laser. Journal of Applied Physics (in press)

FORTENFANT, S.S.; GÜNTHER, D.; DINGWELL, D.B.; RUBIE, D.C.: Temperature dependence of Pt and Rh solubilities in a haplobasaltic melt. Geochimica et Cosmochimica Acta (in press)

FORTENFANT, S.S.; RUBIE, D.C.; REID, J.E.; DALPÉ, C.; GESSMANN, C.K.: Partitioning of Re and Os between liquid metal and magnesiowüstite at high pressure. Physics of the Earth and Planetary Interiors (submitted)

FROST, D.J.: Fe^{2+}-Mg partitioning between garnet, magnesiowüstite and $(Mg,Fe)_2SiO_4$ phases of the transition zone. American Mineralogist (in press)

GAILLARD, F.; PICHAVANT, M.; MACKWELL, S.J.; CHAMPALLIER, R.; SCAILLET, B.; MCCAMMON, C.A.: Chemical transfer during redox exchanges between H_2 and iron-bearing silicate melts. American Mineralogist (in press)

GAILLARD, F.; MACKWELL, S.J.; SCHMIDT, B.C.; MCCAMMON, C.A.: Rate of hydrogen-iron redox exchange in silicate melts and glasses. Geochimica et Cosmochimica Acta (in press)

GAILLARD, F.; PICHAVANT, M.; SCAILLET, B.: Experimental determination of activities of FeO and Fe_2O_3 components in hydrous silicic melts under oxidizing conditions. Geochimica et Cosmochimica Acta (accepted)

GALLARDO, M.C.; ROMERO, F.J.; BECERRO, A.I.; REDFERN, S.A.T.; DEL CERRO, J.; SEIFERT, F.: Cubic-tetragonal phase transition in $Ca_{0.04}Sr_{0.96}TiO_3$: A combined specific heat and neutron diffraction study. Journal of Physics: Condensed Matter (in press)

HEIDELBACH, F.; STRETTON, I.C.; LANGENHORST, F.; MACKWELL, S.J.: Fabric evolution during high shear-strain deformation of magnesiowüstite. Journal of Geophysical Research B (in press)

HELLUY, X.; PIETSCHNIG, R.; SEBALD, A.: ^{29}Si and ^{19}F MAS NMR spectra of isolated $^{29}Si(^{19}F)_2$ and $^{29}Si(^{19}F)_3$ spin systems: Experiments and simulations. Solid State Nuclear Magnetic Resonance (submitted)

HELLUY, X.; SEBALD, A.: Order/disorder phenomena in crystalline phases of compounds $E(XMe_3)_4$ where E = C,Si,Ge and X = Si,Sn. Applied Organometallic Chemistry (in press)

HELLUY, X.; SEBALD, A.: Structure and dynamic properties of solid L-tyrosine-ethylester as seen by ^{13}C MAS NMR. Journal of Physical Chemistry B (in press)

HOLZAPFEL, C.; RUBIE, D.C.; MACKWELL, S.J.; FROST, D.J.: Effect of pressure on Fe-Mg interdiffusion in $(Fe_xMg_{1-x})O$, ferropericlase. Physics of the Earth and Planetary Interiors (submitted)

HUBER, A.; HEUER, M.; FEHR, K.T.; BENTE, K.; SCHMIDBAUER, E.; BROMILEY, G.D.: Characterisation of synthetic hedenbergite ($CaFeSi_2O_6$)-petedunnite ($CAZnSi_2O_6$) solid solution series by X-ray powder diffraction and ^{57}Fe Mössbauer spectroscopy. Physics and Chemistry of Minerals (in press)

JACOBSEN, S.D.; SMYTH, J.R.; SWOPE, R.J.: Thermal expansion of hydrated six-coordinate silicon in thaumasite, $Ca_3Si(OH)_6(CO_3)$ $(SO_4)12$ H_2O. Physics and Chemistry of Minerals (in press)

JACOBSEN, S.D.; SMYTH, J.R.; SPETZLER, H.A.; HOLL, C.M.; FROST, D.J.: Sound velocities and elastic constants of iron-bearing hydrous ringwoodite. Physics of the Earth and Planetary Interiors (submitted)

JING, Z.C.; NING, J.Y.; WANG, S.G.; ZANG, S.X.: Dynamic phase boundaries of olivine-wadsleyite in subduction zones in the western Pacific. Geophysical Research Letters (in press)

LEPORA, A.; GROBETY, B.; MCCAMMON, C.A.: Dehydroxylation of a 3T phengite under reducing and oxidising conditions. European Journal of Mineralogy (submitted)

LIEBSKE, C.; BEHRENS, H.; HOLTZ, F.; LANGE, R.A.: The influence of pressure and composition on the viscosity of andesitic melts. Geochimica et Cosmochimica Acta (in press)

LITASOV, K.; OHTANI, E.; LANGENHORST, F.; YURIMOTO, H.; KUBO, T.; KONDO, T.: Water solubility in Mg-perovskites and water storage capacity in the lower mantle. Earth and Planetary Science Letters (submitted)

LIU, Y.J.; YE, G.Y.; MAO, X.H.; NING, J.Y.: 2-D viscoelastic FEM simulation on stress state in the deep part of a subducted slab. Acta Seismologica Sinica (in press)

MAO, X.H.; LIU, Y.J.; YE, G.Y.; NING, J.Y.: 2-D elastic FEM simulation on stress state in the deep part of a subducted slab. Acta Seismologica Sinica (in press)

MARTEL, C.; SCHMIDT, B.C.: Decompression experiments as an insight into ascent rates of silicic magmas. Contribution to Mineralogy and Petrology (in press, published on the internet: DOI 10.1007/s00410-002-0404-3)

MCCAMMON, C.A.: Mössbauer spectroscopy in the geosciences: Highlights and perspectives. Hyperfine Interactions (submitted)

MCCAMMON, C.A.; ROSS, N.L.: Crystal chemistry of ferric iron in $(Mg,Fe)SiO_3$ majorite. Physics and Chemistry of Minerals (in press)

MECKLENBURGH, J.; RUTTER, E.H.: On the rheology of partially molten synthetic granite. Journal of Structural Geology (in press)

NING, J.Y.; ZANG, S.X.; WANG, S.G.; *et al.*: Coupling between different layers in lithosphere under horizontal drags underneath. Science in China (D) (in press)

O'NEILL, H.S.C.; POWNCEBY, M.; MCCAMMON, C.A.: The magnesiowüstite-iron equilibrium and its implications for the activity-composition relations of $(Mg,Fe)_2SiO_4$ olivine solid solutions. Contributions to Mineralogy and Petrology (submitted)

PADRO, D.; SCHMIDT, B.C.; DUPREE, R.: On the water solubility mechanism in hydrous aluminosilicate glasses: Information from ^{27}Al MAS and MQMAS NMR. Geochimica et Cosmochimica Acta (in press)

PARTZSCH, G.M.; LATTARD, D.; MCCAMMON, C.A.: Mössbauer spectroscopic determination of Fe^{3+}/Fe^{2+} in synthetic basaltic glass: A test of empirical fO_2 equations under superliquidous and subliquidous conditions. Contributions to Mineralogy and Petrology (submitted)

RAKIC, S.; KAHLENBERG, V.; SCHMIDT, B.C.: Hydrothermal synthesis and structural characterization of κ-$Na_2Si_2O_5$ and $Na_{1.84}K_{0.16}Si_2O_5$. Solid State Science (submitted)

RAKIC, S.; KAHLENBERG, V.; SCHMIDT, B.C.: High pressure mixed alkali disilicates in the system $Na_{2-x}K_xSi_2O_5$: Hydrothermal synthesis and crystal structures of $NaKSi_2O_5$-II and $Na_{0.5}K_{1.5}Si_2O_5$. Zeitschrift für Kristallographie (submitted)

RAVNA, E.J.K.; TERRY, M.P.: Geothermobarometry of UHP and HP eclogites and schists – an evaluation of equilibria between garnet-clinopyroxene-kyanite-phengite-coesite/quartz. Journal of Metamorphic Geology (submitted)

REID, J.E.; SUZUKI, A.; FUNAKOSHI, K.; TERASAKI, H.; POE, B.T.; RUBIE, D.C.; OHTANI, E.: The viscosity of $CaMgSi_2O_6$ liquid at pressures up to 13 GPa. Physics of the Earth and Planetary Interiors (submitted)

RUBIE, D.C.; MELOSH, H.J.; REID, J.E.; LIEBSKE, C.; RIGHTER, K.: Mechanisms of metal-silicate equilibration in the terrestrial magma ocean. Earth and Planetary Science Letters (in press)

RUTTER, E.H.; MECKLENBURGH, J.: The extraction of crustal melts from their protolith and the flow behavior of partially molten crustal rocks. – In: BROWN, M.; RUSHMER, T. (Eds.) "Crustal growth processes" – Cambridge University Press (in press)

SIEBERT, J.; GUYOT, F.; GAUTRON, L.; COMBES, R; HAMMOUDA, T.; BORENSZTAJN, S.; FROST, D.J.; MARTINEZ, I.: Experimental study of interactions between silicates and iron-silicon alloys at high pressures and high temperatures. Physics of the Earth and Planetary Interiors (submitted)

SILVER, J.; MCCAMMON, C.A.; DAVIES, D.A.; ANANDAN, S.; TITLER, P.J.; FERN, G.R.; MARSH, P.J.: High pressure Mössbauer spectroscopic studies on two low spin iron porhyrins $[Fe(PPIX)(HIm)_2]Cl$ and $[Fe(OEP)(4\text{-}NH_2Py)_2]Cl$. Journal of the American Chemical Society (submitted)

SMYTH, J.R.; HOLL, C.M.; FROST, D.J.; JACOBSEN, S.D.: High pressure crystal chemistry of hydrous ringwoodite and water in the Earth's interior. Physics of the Earth and Planetary Interiors (submitted)

SMYTH, J.R.; HOLL, C.M.; FROST, D.J.; JACOBSEN, S.D.; LANGENHORST, F.; MCCAMMON, C.A.: Structural systematics of hydrous ringwoodite and water in Earth's mantle. American Mineralogist (in press)

STOYANOVA, R.; ZHECHEVA, E.; ALCANTARA, R.; TIRADO, J.-L.; BROMILEY, G.D.; BOFFA BALLARAN, T.: High-pressure synthesis of layered $Li_{1+x}Ni_{1-x}O_2$ oxides as cathode materials for lithium-ion batteries. Advances in Materials (submitted)

STOYANOVA, R.; ZHECHEVA, E.; ALCÁNTARA, R.; TIRADO, J.L.; BROMILEY, G.D.; BROMILEY, F.; BOFFA BALLARAN, T.: Lithium/nickel mixing in the transition metal layers of lithium nickelate: High-pressure synthesis of layered $Li[LixNi_1-x]O_2$ oxides as cathode materials for lithium-ion batteries. Solid State Ionics (submitted)

SWAMY, V.; DUBROVINSKAIA, N.A.; DUBROVINSKY, L.S.; SIMIONOVICI, A.S.; DRAKOPOULOS, M.; DMITRIEV, V.; WEBER, H.-P.: Compression behavior of nanocrystalline anatase TiO_2. Solid State Communications (in press)

TERRY, M.P.; ROBINSON, P.: Evolution of amphibolite-facies structural features and boundary conditions for deformation during exhumation of HP and UHP rocks, Nordøyane, Western Gneiss Region, Norway. Tectonics (submitted)

TERRY, M.P.; ROBINSON, P.: Eclogite-facies structural features and their bearing on mechanisms for production and exhumation of high-pressure rocks, Western Gneiss Region, Norway. Tectonics (submitted)

TRIBAUDINO, M.; NESTOLA, F.; MENEGHINI, C.; BROMILEY, G.D.: The high temperature $P2_1/c$-$C2/c$ phase transition in iron-free Ca-rich $P2_1/c$ clinopyroxenes. Physics and Chemistry of Minerals (submitted)

WILKINS[†], C.J.; TENNANT, W.C.; WILLIAMSON, B.E.; MCCAMMON, C.A.: Spectroscopic and related evidence on the colouring and nature of New Zealand jade. American Mineralogist (submitted)

[†] *deceased*

4.3 Presentations at scientific institutions and at congresses

BALOG, P.S.; RUBIE, D.C.; FROST, D.J.; SECCO, R.A.: 26.-31.08.2002, 6th High Pressure Mineral Physics Seminar, Verbania, Italy[*3]: "High pressure density measurements of liquid Fe-S"

BECHMANN, M; SEBALD, A.: 28.07.-01.08.2002, 44th Rocky Mountain Conference on Analytical Chemistry, Denver, USA: "Double-quantum filtered MAS NMR at and around the $n = 0$ rotational-resonance condition"

BECHMANN, M; SEBALD, A.: 23.- 27.09.2002, Annual Discussion Group Meeting FG MR, Bremen, Germany: "Double-quantum filtered MAS NMR at and around the $n = 0$ rotational-resonance condition"

BLÄß, U.W.; BOFFA BALLARAN, T.; FROST, D.J.; LANGENHORST, F.; MCCAMMON, C.A.; SEIFERT, F.; VAN AKEN, P.A.: 24.-27.03.2002, EMPG IX, Zürich, Switzerland[*1]: "Silicon-iron exchange in calcium silicate perovskites at transition zone conditions", Journal of Conference Abstracts 7,1, 14

BLÄß, U.W.: 22.-23.06.2002, Arbeitstreffen der Experimentellen Petrologen, Deutsche Mineralogische Gesellschaft, Frankfurt/Main, Germany: "Silizium-Eisen Austausch in $CaSiO_3$-Perowskit"

BLÄß, U.W.; BOFFA BALLARAN, T.; FROST, D.J.; LANGENHORST, F.; MCCAMMON, C.A.; SEIFERT, F.; VAN AKEN, P.A.: 26.-31.08.2002, 6th High Pressure Mineral Physics Seminar, Verbania, Italy[*3]: "Silicon-iron exchange in calcium silicate perovskites at transition zone conditions"

BLÄß, U.W.; BOFFA-BALLARAN, T.; FROST, D.J.; LANGENHORST, F.; MCCAMMON, C.A.; SEIFERT, F.; VAN AKEN, P.A.: 08.-12.09.2002, 80. Jahrestagung der DMG, Hamburg, Germany[*4]: "Silicon-iron exchange in calcium silicate perovskites at transition zone conditions", Beihefte zum European Journal of Mineralogy 14, 22

BOFFA BALLARAN, T.; ANGEL, R.J.: 24.-27.03.2002, EMPG IX, Zürich, Switzerland[*1]: "High-pressure phase transitions in lawsonite", Journal of Conference Abstracts 7,1, 15

BOFFA BALLARAN, T.; CARPENTER, M.A.; KNIGHT, K.S.: 06.-10.12.2002, AGU Fall Meeting, San Francisco, USA[*5]: "Transformation behaviour of cummingtonite: A neutron diffraction study", EOS Trans. AGU, 83(47), Fall Meet. Suppl., Abstract MR72A-1021, 2002

BOTCHARNIKOV, R.; KOEPKE, J.; HOLTZ, F.; MCCAMMON, C.A.: 08.-12.09.2002, 80. Jahrestagung der DMG, Hamburg, Germany[*4]: "An experimental study of the differentiation of a ferro-basaltic system: Effect of water activity and oxygen activity on the phase relations", Beihefte zum European Journal of Mineralogy 14, 25

BROMILEY, G.D.; KEPPLER, H.: 24.-27.03.2002, EMPG IX, Zürich, Switzerland[*1]: "An experimental investigation of hydrogen solubility in pyroxenes along the diopside-jadeite tie-line", Journal of Conference Abstracts 7,1, 19

BROMILEY, G.D.; KEPPLER, H.: 01.-06.09.2002, 18th General Meeting of the International Mineralogical Association, Edinburgh, U.K.: "An experimental investigation of hydrogen solubility in upper-mantle clinopyroxenes"

BYSTRICKY, M.; MACKWELL, S.J.; HEIDELBACH, F.: 24.-27.03.2002, EMPG IX, Zürich, Switzerland[*1]: "Experimental deformation of clinopyroxene aggregates", Journal of Conference Abstracts 7,1, 22

CHAKRABORTY, S.; DOHMEN, R.; HOLZAPFEL, C.; MEISSNER, E.: 28.-31.05.2002, AGU Spring Meeting, Washington, USA[*2]: "Diffusion in olivine-insights from new experimental data", EOS Trans. AGU, 83(19), Spring Meet. Suppl., Abstract V51B-04, 2002

CORNELIUS, V.J.; TITLER, P.J.; FERN, G.R.; SILVER, J.; MCCAMMON, C.A.: 21.-26.05.2002, 5th Seeheim Workshop on Mössbauer Spectroscopy, Seeheim, Germany: "An interesting spin-state transition for [Fe(PPIX)OH] induced by the application of high pressure in a diamond anvil cell"

COUVY, H.; CORDIER, P.; MACKWELL, S.J.; FROST, D.J.: 15.-17.05.2002, Colloque Plasticité 2002, Francheville, France: "Déformation plastique en cisaillement dans la presse multi-enclumes"

COUVY, H.; MACKWELL, S.J.; CORDIER, P.; FROST, D.J.; HEIDELBACH, F.: 26.-31.08.2002, 6th High Pressure Mineral Physics Seminar, Verbania, Italy[*3]: "Plastic deformation of mantle minerals under high pressure: Experimental study in the multianvil apparatus"

COVEY-CRUMP, S.J.; SCHOFIELD, P.F.; STRETTON, I.C.; DAYMOND, M.R.; KNIGHT, K.S.: 06.-10.12.2002, AGU Fall Meeting, San Francisco, USA[*5]: "Neutron diffraction measurements of changes in strain partitioning between the phases during plastic yielding in two phase composites", EOS Trans. AGU, 83(47), Fall Meet. Suppl., Abstract MR72A-1017, 2002

DAHL, P.S.; HAMILTON, M.A.; TERRY, M.P.; ROBERTS, H.J.; KELLEY, S.P.; FREI, R.; JERCINOVIC, M.J.; WILLIAMS, M.L.: 25.-27.03.2002, Northeastern Section – 37th Annual Meeting, Springfield, Massachusetts, USA: "Comparative ion and electron microprobe dating of Wyoming province monazite, with tectonic and analytical implications", Geological Society of America Abstracts with Programs 34(1), A9

DEMOUCHY, S.; MACKWELL, S.J.: 24.-27.03.2002, EMPG IX, Zürich, Switzerland[*1]: "Water diffusion in natural olivine and synthetic forsterite", Journal of Conference Abstracts 7,1, 27

DEMOUCHY, S.; MACKWELL, S.J.: 21-27.09.2002, 2nd "Hydrospec" European Meeting, Vienna, Austria: "Hydrogen diffusion in synthetic forsterite"

DEMOUCHY, S.; MACKWELL, S.J.: 06.-10.12.2002, AGU Fall Meeting, San Francisco, USA[*5]: "Hydrogen diffusion in forsterite", EOS Trans. AGU, 83(47), Fall Meet. Suppl., Abstract T21C-1108, 2002

DOBSON, D.P.: 24.-27.03.2002, EMPG IX, Zürich, Switzerland[*1]: "Oxygen ionic conductivity in $MgSiO_3$ perovskite: Possible pre-melting signal?", Journal of Conference Abstracts 7,1, 28

DOBSON, D.P.: 28.-31.05.2002, AGU Spring Meeting, Washington, USA[*2] *(invited)*: "Diffusion and viscosity in liquid Fe-alloys at high pressures and temperatures", EOS Trans. AGU, 83(19), Spring Meet. Suppl., Abstract V52B-06, 2002

DOBSON, D.P., Meredith, P.G.; Boon, S.A.: 28.-31.05.2002, AGU Spring Meeting, Washington, USA[*2]: "What's all the noise about: Making and measuring deep earthquakes", EOS Trans. AGU, 83(19), Spring Meet. Suppl., Abstract T51A-11, 2002

DUBROVINSKAIA, N.A.; DUBROVINSKY, L.S.: 18.-23.08.2002, 12th Annual V.M. Goldschmidt Conference, Davos, Switzerland: "High-temperature heater for diamond anvil cells. Application for studies of alloys and oxides."

DUBROVINSKAIA, N.A.; DUBROVINSKY, L.S.: 26.-31.08.2002, 6th High Pressure Mineral Physics Seminar, Verbania, Italy[*3]: "High-temperature heater for diamond anvil cells"

DUBROVINSKAIA, N.A.; DUBROVINSKY, L.S.: 04.-07.09.2002, 40th European High-Pressure Research Group Meeting, Edinburgh, U.K.: "High-temperature heater for diamond anvil cells. Melting curve of water."

DUBROVINSKY, L.S.; DUBROVINSKAIA, N.A.; LANGEHORST, F.; RUBIE, D.C.: 28.-31.01.2002, Superplume Workshop, Tokyo, Japan: "Iron-oxides interaction at high pressures and temperatures: Implication for deep Earth's interiors"

DUBROVINSKY, L.S.; DUBROVINSKAIA, N.A.; LANGENHORST, F.; RUBIE, D.C.; MCCAMMON, C.A.; PRAKAPENKA, V.; LE BIHAN, T.: 28.-31.05.2002, AGU Spring Meeting, Washington, USA[*2] *(invited)*: "Study of chemical interaction of iron and complex oxides (Al_2O_3, SiO_2, $MgSiO_3$) at high pressures and temperatures: Combination of synchrotron and in-house facilities", EOS Trans. AGU, 83(19), Spring Meet. Suppl., Abstract M22A-05, 2002

DUBROVINSKY, L.S.; DUBROVINSKAIA, N.A.; LANGENHORST, F.; MCCAMMON, C.A.: 28.-31.05.2002, AGU Spring Meeting, Washington, USA[*2] *(invited)*: "Phase relations and equations of state of solid and liquid in Fe-Ni alloys: Implications for Earth's core", EOS Trans. AGU, 83(19), Spring Meet. Suppl., Abstract M42A-03, 2002

DUBROVINSKY, L.S.; DUBROVINSKAIA, N.A.; ROZENBERG, G.K.; DMITRIEV, V.; WEBER, H.P.: 18.-23.08.2002, 12th Annual V.M. Goldschmidt Conference, Davos, Switzerland: "Fe-O system at extreme conditions"

DUBROVINSKY, L.S.; DUBROVINSKAIA, N.A.; PRAKAPENKA, V.; SEIFERT, F.; LANGENHORST, F.; DMITRIEV, V.; WEBER, H.-P.; LE BIHAN, T.: 26.-31.08.2002, 6th High Pressure Mineral Physics Seminar, Verbania, Italy[*3] *(invited)*: "A class of new high-pressure silica polymorphs"

DUBROVINSKY, L.S.; DUBROVINSKAIA, N.A.; PRAKAPENKA, V.; SEIFERT, F.; LANGENHORST, F.: 04.-07.09.2002, 40th European High-Pressure Research Group Meeting, Edinburgh, U.K.: "A class of new high-pressure silica polymorphs"

EL GORESY, A.; DUBROVINSKY, L.S.; SHARP, T.G.; CHEN, M.: 26.-31.08.2002, 6th High Pressure Mineral Physics Seminar, Verbania, Italy[*3]: "Natural post-stishovite polymorphs of silicia: Their nature versus predictions and relevance to the Earth's mantle"

EL-KHOZONDAR, R.J.; HEIDELBACH, F.: 06.-10.12.2002, AGU Fall Meeting, San Francisco, USA[*5]: "Applications of measurements of physical properties of rocks to large-scale tectonic processes II posters", EOS Trans. AGU, 83(47), Fall Meet. Suppl., Abstract MR52A, 2002

ETSCHMANN, B.; PRING, A.; PUTNIS, A.; GRGURIC, B.; STUDER, A.; MCCAMMON, C.A.: 01.-06.09.2002, 18th General Meeting of the International Mineralogical Association, Edinburgh, U.K.: "Kinetics of exsolution in the pentlandite-pyrrhotite ($(Fe,Ni)_9S_8$-$Fe_{1-x}S$) system"

ETSCHMANN, B.; PRING, A.; PUTNIS, A.; MCCAMMON, C.A.; GRGURIC, B.; STUDER, A.: 06.-15.08.2002, XIX Congress and General Assembly of the International Union of Crystallography, Geneva, Switzerland: "Kinetics of exsolution in the pentlandite-pyrrhotite ($(Fe,Ni)_9S_8$-$Fe_{1-x}S$) system"

FROST, D.J.; LANGENHORST, F.: 18.-23.08.2002, 12th Annual V.M. Goldschmidt Conference, Davos, Switzerland: "The oxidation state of iron in the lower mantle"

FROST, D.J.: 26.-31.08.2002, 6th High Pressure Mineral Physics Seminar, Verbania, Italy[*3] *(invited)*: "The widths of transition zone phase transformations determined from Fe-Mg partitioning"

FROST, D.J.; LIEBSKE, C.; RUBIE, D.C.: 01.-05.10.2002, GEO 2002, Würzburg, Germany: "Element partitioning at lower mantle conditions", Schriftenreihe der Deutschen Geologischen Gesellschaft, Heft 21, 129

FROST, D.J.: 14.11.2002, University of Innsbruck, Austria: "Mineralogy of the Earth's lower mantle"

FUNAKOSHI, K.; TERASAKI, H.: 06.-10.12.2002, AGU Fall Meeting, San Francisco, USA[*5]: "Viscosity measurement of the Fe-FeS melt under high pressure using a high-speed X-ray CCD camera", EOS Trans. AGU, 83(47), Fall Meet. Suppl., Abstract V72B-1315, 2002

GAILLARD, F.; MACKWELL, S.J.; SCHMIDT, B.C.; MCCAMMON, C.A.; PICHAVANT, M.: 24.-27.03.2002, EMPG IX, Zürich, Switzerland[*1]: "Chemical migration associated with iron oxidation-reduction in silicate melts", Journal of Conference Abstracts 7,1, 38

HARTE, B.; HARRIS, J.W.; WILDING, M.; MCCAMMON, C.A.; SAUTTER, V.: 01.-06.09.2002, 18th General Meeting of the International Mineralogical Association, Edinburgh, U.K.: "Eclogite-garnetite inclusions in diamonds from the Saõ Luiz area, Brazil"

HEIDELBACH, F.; STRETTON, I.C.; MACKWELL, S.J.: 20.-22.03.2002, TSK IX, 9. Symposium Tektonik – Strukturgeologie – Kristallingeologie, Erlangen, Germany: "Experimentelle Scherdeformation von Magnesiowüstit ($Mg_{0.8}Fe_{0.2}$)O"

HEIDELBACH, F.; STRETTON, I.C.; LANGENHORST, F.; MACKWELL**,** S.J.: 19.-24.05.2002, Gordon Research Conference on Rock Deformation, Il Ciocco, Barga, Italy: "High strain deformation of magnesiowüstite"

HEIDELBACH, F.: 29.07.-02.08.2002, 51st Annual Denver X-ray Conference, Workshop on Texture Analysis, Colorado Springs, USA: "Texture analysis with synchrotron radiation and geoscience applications"

HEIDELBACH, F.; STRETTON, I.C.; MACKWELL, S.J.: 06.-10.12.2002, AGU Fall Meeting, San Francisco, USA[*5]: "Mechanical behaviour and fabric development in experimentally deformed magnesiowüstite (Mg,Fe)O as a function of Fe-content", EOS Trans. AGU, 83(47), Fall Meet. Suppl., Abstract MR52A-0992, 2002

HEIDELBACH, F.: 18.11.2002, Kolloquium des Geologischen Instituts der Universität Erlangen, Germany: "Gefügeanalyse von Gesteinen: Neue Perspektiven durch Elektronenbeugung im Rasterelektronenmikroskop"

HEINEMANN, R.; KROLL, H.; LANGENHORST, F.; LUEDER, T.: 08.-12.09.2002, 80. Jahrestagung der DMG, Hamburg, Germany[*2]: "Korrelation zwischen Mg,Fe^{2+}-Ordnungs-/ Unordnungskinetik und Entmischungstextur in Orthopyroxenen des Johnstown Meteoriten?", Beihefte zum European Journal of Mineralogy 14, 65

HELLUY, X; SEBALD, A.: 28.07.-01.08.2002, 44th Rocky Mountain Conference on Analytical Chemistry, Denver, USA: "^{1}H-decoupled ^{29}Si and ^{19}F MAS NMR spectra of isolated $^{29}Si(^{19}F)_2$ and $^{29}Si(^{19}F)_3$ spin systems. Experiments and Simulations"

HELLUY, X; SEBALD, A.: 23.-27.09.2002, Annual Discussion Group Meeting FG MR, Bremen, Germany: "^{1}H-decoupled ^{29}Si and ^{19}F MAS NMR spectra of isolated $^{29}Si(^{19}F)_2$ and $^{29}Si(^{19}F)_3$ spin systems. Experiments and simulations"

HOLL, C.M.; SMYTH, J.R.; FROST, D.J.; JACOBSEN, S.D.: 06.-10.12.2002, AGU Fall Meeting, San Francisco, USA[*5]: "High pressure crystal chemistry of hydrous ringwoodite", EOS Trans. AGU, 83(47), Fall Meet. Suppl., Abstract MR62B-1077, 2002

HOLZAPFEL, C.; RUBIE, D.C.; MACKWELL, S.J.; FROST, D.J.; LANGENHORST, F.: 24.-27.03.2002, EMPG IX, Zürich, Switzerland[*1]: "Experimental study of Fe-Mg interdiffusion in lower mantle phases", Journal of Conference Abstracts 7,1, 45

HOLZAPFEL, C.; MIYAJIMA, N.; RUBIE, D.C.; FROST, D.J.; MACKWELL, S.J.; LANGENHORST, F.: 28.-31.05.2002, AGU Spring Meeting, Washington, USA[*2]: "Rates of chemical diffusion in the lower mantle of the Earth", EOS Trans. AGU, 83(19), Spring Meet. Suppl., Abstract V52B-02, 2002

HOLZAPFEL, C.; RUBIE, D.C.; MACKWELL, S.J.; LANGENHORST, F.; CHAKRABORTY, S.: 26.-31.08.2002, 6th High Pressure Mineral Physics Seminar, Verbania, Italy[*3]: "Pressure effect on Fe-Mg interdiffusion: Determination of the activation volumes of mantle minerals in the multianvil press"

HOLZAPFEL, C.; RUBIE, D.C.; CHAKRABORTY, S.; LANGENHORST, F.; FROST, D.J.; MACKWELL, S.J.: 08.-12.09.2002, 80. Jahrestagung der DMG, Hamburg, Germany[*2]: "Modelling the formation of the Earth's core: A kinetic approach", Beihefte zum European Journal of Mineralogy 14, 73

HOLZAPFEL, C.; RUBIE, D.C.; FROST, D.J.; MACKWELL, S.J.; LANGENHORST, F.; CHAKRABORTY, S.: 01.-05.10.2002, GEO 2002, Würzburg, Germany: "Fe-Mg interdiffusion in mantle phases: A first step towards understanding equilibration kinetics of core formation", Schriftenreihe der Deutschen Geologischen Gesellschaft, Heft 21, 169

JACOBSEN, S.D.: 15.2.2002, Universität Karlsruhe, Introductory Meeting of the Alexander von Humboldt Foundation, Karlsruhe, Germany: "Developments in high-pressure mineral physics"

JACOBSEN, S.D.; REICHMANN, H.-J.; SPETZLER, H.A.: 24.-27.03.2002, EMPG IX, Zürich, Switzerland[*1]: "State of a maturing methodology: Gigahertz ultrasonic interferometry", Journal of Conference Abstracts 7,1, 51

JACOBSEN, S.D.; SMYTH, J.R.: 26.-31.08.2002, 6th High Pressure Mineral Physics Seminar, Verbania, Italy[*3]: "Hydration of silicates by Si-OH"

JACOBSEN, S.D.; SPETZLER, H.A.; REICHMANN, H.-J.; MACKWELL, S.J.; SMYTH, J.R.: 06.-10.12.2002, AGU Fall Meeting, San Francisco, USA[*5]: "Effects of iron and pressure on the C_{11} elastic constant of (Mg,Fe)O using a new GHz-ultrasonic diamond cell with *in situ* X-ray diffraction to 10 GPa", EOS Trans. AGU, 83(47), Fall Meet. Suppl., Abstract MR62B-1074, 2002

JACOBSEN, S.D.: 14.11.2002, Sitzung der Kommission für Geowissenschaftliche Hochdruckforschung der Bayerischen Akademie der Wissenschaften, München, Germany: "Gigahertz ultrasonic interferometry at Bayreuth: Where sound and optical wavelengths meet"

KLEMME, S.; FROST, D.J.: 24.-27.03.2002, EMPG IX, Zürich, Switzerland[*1]: "The garnet-spinel transition in the System MgO-Cr_2O_3-SiO_2", Journal of Conference Abstracts 7,1, 55

LANGENHORST, F.: 07.03.2002, Universität Kiel, 5. Workshop des AK Elektronenmikroskopie der DGK, Kiel, Germany: "Röntgenmikroanalyse und Elementverteilungsaufnahme im TEM"

LANGENHORST, F.; SCHERTL, H.-P.; SCHREYER, W.; SOBOLEV, N.; SHATSKY, V.: 24.-27.03.2002, EMPG IX, Zürich, Switzerland[*1]: "Defect microstructures as genetic fingerprint of diamonds", Journal of Conference Abstracts 7,1, 62

LANGENHORST, F.; DEUTSCH, A.; HORNEMANN, U.; IVANOV, B.: 06.-08.06.2002, Universität Potsdam, ICDP-ODP Kolloquium, Potsdam, Germany: "Shock experiments on anhydrite – first results", Abstract Volume, 3

LANGENHORST, F.: 23.-26.09.2002, IX. International Conference on Moldavites, Tektites and Impact Processes, Franzensbad, Czech Republic: "Shock metamorphism of minerals from a microstructural point of view"

LANGENHORST, F.: 20.10.2002, Urweltmuseum, Bayreuth, Germany: "Meteoritenkrater auf der Erde – Zeugen kosmischer Katastrophen"

LANGENHORST, F.: 28.11.2002, Kolloquium, Universität Tübingen, Geowissenschaftliche Fakultät, Tübingen, Germany: "Diamanten aus dem Ries: Eine "himmlische" Gabe"

LIEBERMANN, R.C.; LI, B.; KUNG, J.; WEIDNER, D.J.: 06.-10.12.2002, AGU Fall Meeting, San Francisco, USA[*5]: "Elasticity of mantle minerals and their high-pressure polymorphs at high pressures and temperatures", EOS Trans. AGU, 83(47), Fall Meet. Suppl., Abstract MR11A-11, 2002

LIEBSKE, C.; FROST, D.J.; TRØNNES, R.G.; RUBIE, D.C.: 28.02.-01.03.2002, Workshop "Transport und Reaktionskinetik in Silikatschmelzen", Hannover, Germany: "Melting of mantle material at high pressure"

LIEBSKE, C.; FROST, D.J., TRØNNES; R.G.; RUBIE, D.C.: 24.-27.03.2002, EMPG IX, Zürich, Switzerland[*1]: "Melting of peridotite under lower mantle conditions“, Journal of Conference Abstracts 7,1, 64

LIEBSKE, C.; FROST, D.J.; TRØNNES, R.G.; RUBIE, D.C.: 26.-31.08.2002, 6th High Pressure Mineral Physics Seminar, Verbania, Italy[*3]: "Mantle melting at high pressure"

LIEBSKE, C.; FROST, D.J.; RUBIE, D.C.: 01.-05.10.2002, GEO 2002, Würzburg, Germany: "Melting of mantle material at high pressures and temperatures", Schriftenreihe der Deutschen Geologischen Gesellschaft, Heft 21, 225

LIEBSKE, C.; FROST, D.J.; TRØNNES; R.G.; RUBIE, D.C.: 10.-11.10.2002: 5. Wissenschaftliches Kolloquium zum Schwerpunktprogramm "Bildung, Transport und Differentiation von Silikatschmelzen", Hannover, Germany: "Mantle melting at high pressure"

LITASOV, K.; OHTANI, E.; YURIMOTO, H.; LANGENHORST, F.; KUBO, T.: 26.-31.08.2002, 6th High Pressure Mineral Physics Seminar, Verbania, Italy*3: "Water solubility in Al-Fe-perovskites and water storage capasity of the lower mantle"

MACKWELL, S.J.; BYSTRICKY, M.; HEIDELBACH, F.: 09.-12.07.2002, 2002 Western Pacific Geophysics Meeting, Wellington, New Zealand: "High strain deformation of clinopyroxene and olivine aggregates, and production of seismic anisotropy", EOS Trans. AGU, 83(22), West. Pac. Geophys. Meet. Suppl., Abstract SE31D-11, 2002

MACKWELL, S.J.; KOHLSTEDT, D.L.; BYSTRICKY, M.: 06.-10.12.2002, AGU Fall Meeting, San Francisco, USA*5 *(invited)*: "Rheological constraints on the plastic lithosphere", EOS Trans. AGU, 83(47), Fall Meet. Suppl., Abstract MR51A-01, 2002

MALAVERGNE, V.; SIEBERT, J.; GUYOT, F.; GAUTRON, L.; COMBES, R.; HAMMOUDA, T.; FROST, D.J.: 26.-31.08.2002, 6th High Pressure Mineral Physics Seminar, Verbania, Italy*3: "Experimental study of interactions between silicates and iron-silicon alloys at high pressures and high temperatures"

MARTEL, C.; SCHMIDT, B.C.: 24.-27.03.2002, EMPG IX, Zürich, Switzerland*1: "Decompression experiments as an insight into ascent rates of silicic magmas", Journal of Conference Abstracts 7,1, 68

MARTEL, C.; SCHMIDT, B.C.: 09.-12.04.2002, RST 2002, Nantes, France: "Simulation de l'ascension de magmas rhyollitiques par expériences de décompression"

MARTEL, C.; SCHMIDT, B.C.: 12.-16.05.2002, Montagne Pelee 1902-2002, Explosive Volcanism in Subduction Zones, Saint Pierre, Martinique: "Experimental simulation of plinian and pelean magma ascent"

MARTON, F.C.; MOSENFELDER, J.L.; RUBIE, D.C.: 01.-06.07.2002, Workshop on Structure and Tectonics of Convergent Plate Margins, Castle of Zahrádky, Czech Republic: "Modeling subduction zones: Kinetic and thermal effects on olivine metastability and implications for deep-focus earthquakes"

MARTON, F.C.; XU, Y.; LANGENHORST, F.; RUBIE, D.C.; SHANKLAND, T.J.: 26.-31.08.2002, 6th High Pressure Mineral Physics Seminar, Verbania, Italy*3: "Thermal diffusivity measurements of $(Mg,Fe)_2SiO_4$ polymorphs and modelling subducting slabs"

MARTON, F.C.; RUBIE, D.C.; SHANKLAND, T.J.: 06.-10.12.2002, AGU Fall Meeting, San Francisco, USA*5: "Variable thermal conductivity and thermal and mineralogical structures of subducting slabs", EOS Trans. AGU, 83(47), Fall Meet. Suppl., Abstract T52B-1199, 2002

MARTON, F.C.: 06.11.2002, University of Reading, Department of Classics, Reading, U.K.: "Earthquakes in the ancient world, or, the Graeco-Roman shakedown"

MCCAMMON, C.A.: 25.02.2002, Southampton Oceanography Centre, Southampton, U.K.: "Diamonds are not forever: How compositional zoning in garnets can tell us why"

MCCAMMON, C.A.: 25.02.2002, Southampton Oceanography Centre, Southampton, U.K.: "Oxidation-reduction in the Earth: What old cars and the lower mantle have in common"

MCCAMMON, C.A:: 26.02.2002, Durham University, Durham, U.K.: "Oxidation-reduction in the Earth: What old cars and the lower mantle have in common"

MCCAMMON, C.A.: 27.02.2002, Durham University, Durham, U.K.: "Diamonds are not forever: How compositional zoning in garnets can tell us why"

MCCAMMON, C.A.: 28.02.2002, Edinburgh University, Edinburgh, U.K.: "Oxidation-reduction in the Earth: What old cars and the lower mantle have in common"

MCCAMMON, C.A.: 01.03.2002, Edinburgh University, Edinburgh, U.K.: "Diamonds are not forever: How compositional zoning in garnets can tell us why"

MCCAMMON, C.A.: 04.03.2002, Imperial College, London, U.K.: "Diamonds are not forever: How compositional zoning in garnets can tell us why"

MCCAMMON, C.A.: 06.03.2002, University of Barcelona, Barcelona, Spain: "Diamonds are not forever: How compositional zoning in garnets can tell us why"

MCCAMMON, C.A.: 07.03.2002, University of Barcelona, Barcelona, Spain: "Oxidation-reduction in the Earth: What old cars and the lower mantle have in common"

MCCAMMON, C.A.: 08.03.2002, Institute for Materials Science, Barcelona, Spain: "Oxygen deficient ferrite and silicate perovskites: Structure and physical properties"

MCCAMMON, C.A.; STACHEL, T.; HARRIS, J.: 24.-27.03.2002, EMPG IX, Zürich, Switzerland[*1]: "Ferropericlase from the lower mantle: Oxygen fugacity and diamond genesis", Journal of Conference Abstracts 7,1, 70

MCCAMMON, C.A.; ANGEL, R.J.; BECERRO, A.I.; BLÄß, U.; LANGENHORST, F.; LAUTERBACH, S.; MARION, S.; SEIFERT, F.; VAN AKEN, P.A.: 01.-05.04.2002, Materials Research Society Spring Meeting 2002, San Francisco, USA: "Oxygen vacancies in perovskite and related structures: Implications for the lower mantle"

MCCAMMON, C.A.: 08.04.2002, University of Minnesota at Duluth, Duluth, USA: "Oxidation-reduction in the Earth: What old cars and the lower mantle have in common"

MCCAMMON, C.A.: 10.04.2002, University of Minnesota at Morris, Morris, USA: "Diamonds are not forever: How compositional zoning in garnets can tell us why"

MCCAMMON, C.A.: 10.04.2002, University of Minnesota at Morris, Morris, USA: "Oxidation-reduction in the Earth: What old cars and the lower mantle have in common"

MCCAMMON, C.A.: 11.04.2002, North Dakota State University, Fargo, USA: "Oxidation-reduction in the Earth: What old cars and the lower mantle have in common"

MCCAMMON, C.A.: 12.04.2002, University of North Dakota, Grand Forks, USA: "Diamonds are not forever: How compositional zoning in garnets can tell us why"

MCCAMMON, C.A.: 12.04.2002, University of North Dakota, Grand Forks, USA: "Oxidation-reduction in the Earth: What old cars and the lower mantle have in common"

MCCAMMON, C.A.: 15.04.2002, University of Minnesota at Minneapolis/St. Paul, Minneapolis, USA: "Oxidation-reduction in the Earth: What old cars and the lower mantle have in common"

MCCAMMON, C.A.: 13.05.2002, European Synchrotron Radiation Facility, Grenbole, France: "Diamonds and the dynamics of the Earth's interior"

MCCAMMON, C.A.: 21.-26.05.2002, 5th Seeheim Workshop on Mössbauer Spectroscopy, Seeheim, Germany: "Mössbauer effect studies in the geosciences: Highlights of the past and perspectives for the future"

MCCAMMON, C.A.; LAUTERBACH, S.; VAN AKEN, P.A.; LANGENHORST, F.; SEIFERT, F.: 01.-06.09.2002, 18th General Meeting of the International Mineralogical Association, Edinburgh, U.K.: "EELS studies of lower mantle mineral assemblages: A window to redox conditions"

MECKLENBURGH, J.; HEIDELBACH, F.; MACKWELL, S.J.; SEIFERT, F.: 06.-10.12.2002, AGU Fall Meeting, San Francisco, USA[*5]: "Rheology and Microstructure of (Ca,Sr)TiO_3 perovskite deformed in compression and torsion", EOS Trans. AGU, 83(47), Fall Meet. Suppl., Abstract MR52A-0993, 2002

MIYAJIMA, N.; LANGENHORST, F.; FROST, D.J.; RUBIE, D.C.: 26.-31.08.2002, 6th High Pressure Mineral Physics Seminar, Verbania, Italy[*3]: "Diffusion behaviour of aluminium between perovskite and majoritic garnet"

MIYAJIMA, N.; LANGENHORST, F.; FROST, D.J.; RUBIE, D.C.: 01.-04.10.2002, Annual meeting of the Mineralogical Society of Japan, Osaka, Japan: "Reactive diffusion of aluminium in the garnet-perovskite transformation"

MIYAJIMA, N.; LANGENHORST, F.; FROST, D.J.; RUBIE, D.C.: 27-29.11.2002, Annual meeting of the Japan Society of High Pressure Science and Technology, Matsuyama, Japan: "ATEM analysis of recovered materials from high-pressure and temperature experiments"

NAGY, K.L.; SCHLEGEL, M.L.; FENTER, P.; JACOBSEN, S.D.; STURCHIO, N.C.; CHENG, L.: 06.-10.12.2002, AGU Fall Meeting, San Francisco, USA[*5]: "Illumination of cation sorption mechanisms on muscovite using X-ray reflectivity", EOS Trans. AGU, 83(47), Fall Meet. Suppl., Abstract V61C-03, 2002

NESTOLA, F.; TRIBAUDINO, M.; BOFFA BALLARAN, T.: 24.-27.03.2002, EMPG IX, Zürich, Switzerland[*1]: "The high-pressure $P2_1/c$ - $C2/c$ phase transition for the CMS (CaO-MgO-SiO_2) clinopyroxene", Journal of Conference Abstracts 7,1, 79

NEUFELD, K.; STRETTON, I.C.; MACKWELL, S.J.: 08.-12.09.2002, 80. Jahrestagung der DMG, Hamburg, Germany[*4]: "Deformation and dehydration interactions in serpentinite", Beihefte zum European Journal of Mineralogy 14, 117

NING, J.Y.; JING, Z.C.: 01.-06.07.2002, Workshop on Structure and Tectonics of Convergent Plate Margins, Castle of Zahrádky, Czech Republic: "Understanding deep seismicity from the dynamic olivine-wadsleyite phase boundary"

O'CONNER, B; TERRY, M.P.: 25.-27.03.2002, Northeastern Section – 37th Annual Meeting, Springfield, Massachusetts, USA: "P-T conditions and microstructural analysis of UHP metamorphic rocks during exhumation, Western Gneiss Region, Norway", Geological Society of America Abstracts with Programs 34(1), A67

PARTZSCH, G.M.; LATTARD, D.; MCCAMMON, C.A.: 08.-12.09.2002, 80. Jahrestagung der DMG, Hamburg, Germany[*4]: "Mössbauer spectroscopic determination of Fe^{3+}/Fe^{2+} in synthetic basaltic glasses: A test of empirical fO_2 equations under superliquidus and subliquidous conditions"

PRAKAPENKA, V.; DUBROVINSKY, L.S.; SHEN, G.: 28.-31.05.2002, AGU Spring Meeting, Washington, USA[*2]: "Carbon contamination in diamond anvil cell", EOS Trans. AGU, 83(19), Spring Meet. Suppl., Abstract V51B-08, 2002

PRAKAPENKA, V.; SHEN, G.; RIVERS, M.; SUTTON, S.; DUBROVINSKY, L.S.: 06.-10.12.2002, AGU Fall Meeting, San Francisco, USA[*5]: "Temperature induced crystallization of amorphous silica at high pressures", EOS Trans. AGU, 83(47), Fall Meet. Suppl., Abstract MR61A-1031, 2002

RAKIC, S.; KAHLENBERG, V.; SCHMIDT, B.C.: 08.-12.09.2002, 80. Jahrestagung der DMG, Hamburg, Germany[*4]: "Zur Kristallstruktur der Hochdruckphase $Na_{1.84}K_{0.16}Si_2O_5$", Beihefte zum European Journal of Mineralogy 14, 135

REICHMANN, H.-J.; JACOBSEN, S.D.; BOFFA BALLARAN, T.: 06.-10.12.2002, AGU Fall Meeting, San Francisco, USA[*5]: "Structure and elasticity of natural magnetite", EOS Trans. AGU, 83(47), Fall Meet. Suppl., Abstract MR61A-1024, 2002

REID, J.E.; POE, B.T.; RUBIE, D.C.: 24.-27.03.2002, EMPG IX, Zürich, Switzerland[*1]: "Network modifier and trace element diffusion in diopside liquid at high pressure", Journal of Conference Abstracts 7,1, 89

REID, J.E.; RUBIE, D.C.; MELOSH, J.; POE, B.T.; SUZUKI, A.; SCHMICKLER, B.; LIEBSKE, C.; FUNAKOSHI, K.; RIGHTER, K.: 26.-31.08.2002, 6th High Pressure Mineral Physics Seminar, Verbania, Italy[*3]: "Magma ocean properties and mechanisms of metal-silicate equilibration during core formation"

RUBIE, D.C.: 28.02.-01.03.2002, Workshop "Transport und Reaktionskinetik in Silikatschmelzen", Hannover, Germany: "Transport properties of silicate liquid up to 17 GPa"

RUBIE, D.C.: 08.-09.04.2002, DFG SPP Kolloquium "Mars and the Terrestrial Planets", Münster, Germany: "Mechanisms of core formation"

RUBIE, D.C.; MELOSH, H.J.; REID, J.E.; LIEBSKE, C.; RIGHTER, K.: 18.-23.08.2002, 12th Annual V.M. Goldschmidt Conference, Davos, Switzerland: "Mechanisms of metal-silicate equilibration in the terrestrial magma ocean", Geochimica et Cosmochimica Acta 66, 15A, A654

RUBIE, D.C.; MELOSH, J.; REID, J.E.; LIEBSKE, C.; RIGHTER, K.: 01.-05.10.2002, GEO 2002, Würzburg, Germany: "Mechanisms of metal-silicate equilibration in the terrestrial magma ocean", Schriftenreihe der Deutschen Geologischen Gesellschaft, Heft 21, 284

RUBIE, D.C.: 10.-11.10.2002: 5. Wissenschaftliches Kolloquium zum DFG Schwerpunktprogramm "Bildung, Transport und Differentiation von Silikatschmelzen", Hannover, Germany: "Mechanisms of metal-silicate equilibration in the terrestrial magma ocean"

RUBIE, D.C.: 03.12.2002, Department of Earth and Space Sciences, Osaka University, Japan: "Experimental investigations of magma ocean properties and consequences for the formation of the Earth's core"

SAXENA, S.K.; DUBROVINSKY, L.S.; REKHI, S.; WANG, Z.; SHEN, G.: 28.-31.05.2002, AGU Spring Meeting, Washington, USA[*2] *(invited)*: "Oceans of water in the Earth's core", EOS Trans. AGU, 83(19), Spring Meet. Suppl., Abstract V42A-04, 2002

SCHMIDT, B.C.; DUPREE, R.: 24.-27.03.2002, EMPG IX, Zürich, Switzerland[*1]: "Structural influence of water dissolution in melts and glasses along the join reedmergnerite-albite", Journal of Conference Abstracts 7,1, 95

SCHMIDT, B.C.; DUPREE, R: 08.-12.09.2002, 80. Jahrestagung der DMG, Hamburg, Germany[*4]: "Structure and water dissolution mechanisms of melts and glasses along the join reedmergnerite-albite", Beihefte zum European Journal of Mineralogy 14, 146

SCHMIDT, B.C.; DUPREE, R: 10.-11.10.2002: 5. Wissenschaftliches Kolloquium zum DFG Schwerpunktprogramm "Bildung, Transport und Differentiation von Silikatschmelzen", Hannover, Germany: "On the influence of water on the structure of melts and glasses along the join $NaBSi_3O_8$- $NaAlSi_3O_8$"

SCHMIDT, B.C.; DUPREE, R.: 06.-10.12.2002, AGU Fall Meeting, San Francisco, USA[*5]: "Effect of water on the structure of melts and glasses along the join $NaAlSi_3O_8$-$NaBSi_3O_8$", EOS Trans. AGU, 83(47), Fall Meet. Suppl., Abstract V72B-1318, 2002

SCHOFIELD, P.F.; COVEY-CRUMP, S.J.; STRETTON, I.C.; KNIGHT, K.S.; DAYMOND, M.R.; HOLLOWAY, R.F.: 06.-10.12.2002, AGU Fall Meeting, San Francisco, USA[*5]: "Applications of neutron diffraction measurements in the characterization of the mechanical properties of polycrystalline geological materials", EOS Trans. AGU, 83(47), Fall Meet. Suppl., Abstract MR72A-1024, 2002

SEBALD, A.: 14.-19.04.2002, 43rd ENC, Asilomar, California, USA: "Double-quantum filtered MAS NMR at and around various rotational-resonance conditions"

SEBALD, A.: 22.04.2002, Technische Universität München, Chemisches Institut, München, Germany: "Virtuelles + reales NMR Spektrometer = quantitative Strukturinformation an Festkörpern"

SEBALD, A.: 01.-04.05.2002, Abschlusskolloquium DFG Schwerpunktprogramm "Silicium Chemie", Werfenweng, Austria: "Verbindungen $E(XMe_3)_4$ im festen Zustand – eine dynamische Geschichte"

SEBALD, A.: 25.06.2002, University Nancy, Department of Chemistry, Nancy, France: "Virtual + real NMR spectrometer = quantitative structural information about solids"

SEBALD, A.: 08.-10.10.2002, Conference on Electron Density: Measurement, Calculation, Application, Würzburg, Germany: "Shielding parameters in solid-state NMR – trends in the periodic table of the elements and methodology for the experimental determination of anisotropic NMR interaction parameters"

SEBALD, A.: 17.12.2002, NMRDG Meeting, London, U.K.: "Double-quantum filtration at and near various rotational-resonance conditions"

SHERRIFF, B.L.; JOHNSTON, S.; STIRLING, L.M.; MCCAMMON, C.A.: 27.-29.05.2002, Geological Association of Canada and Mineralogical Association of Canada Joint Annual Meeting, Saskatoon, Canada: "Mineralogical and geochemical study of Roman pottery from Leptimus, Tunisia"

SMYTH, J.R.; FROST, D.J.: 24.-27.03.2002, EMPG IX, Zürich, Switzerland[*1]: "Effects of hydration on the crystal structure of olivine" Journal of Conference Abstracts 7,1, 99

SMYTH, J.R.; HOLL, C.M.; FROST, D.J.; JACOBSEN, S.D.; LANGENHORST, F.; MCCAMMON, C.A.: 26.-31.08.2002, 6th High Pressure Mineral Physics Seminar, Verbania, Italy[*3]: "Structural systematics of hydrous ringwoodite and water in Earth's interior"

STACHEL, T.; HARRIS, J.W.; MCCAMMON, C.A.: 01.-06.09.2002, 18th General Meeting of the International Mineralogical Association, Edinburgh, U.K.: "Inclusions in ultra-deep diamonds – tracers of ancient slabs?"

STEINLE-NEUMANN, G.; MARTON, F.C.; COHEN, R.E.: 28.-31.05.2002, AGU Spring Meeting, Washington, USA[*2]: "Lower mantle elastictiy from molecular dynamics on $MgSiO_3$ perovskite", EOS Trans. AGU, 83(19), Spring Meet. Suppl., Abstract M42A-09, 2002

STOYANOVA, R.; ZHECHEVA, E.; BROMILEY, G.D.; ALCANTARA, R.; CORREDOR, J.-I.; TIRADO, J.-L.; *et al.*: 07.-10.09.2002, 3rd International Conference on Inorganic Materials, Konstanz, Germany: "High-pressure synthesis of Ga-substituted $LiCoO_2$ cathodes for lithium-ion batteries"

TERASAKI, H.; RUBIE, D.C.; FROST, D.J.: 06.-10.12.2002, AGU Fall Meeting, San Francisco, USA[*5]: "Estimation of the timescale for textural equilibrium between liquid iron-sulfide and solid silicate under high pressure", EOS Trans. AGU, 83(47), Fall Meet. Suppl., Abstract MR52A-1007, 2002

TERRY, M.P.; ROBINSON, P.; HAMILTON, M.A.: 25.-27.03.2002, Northeastern Section – 37th Annual Meeting, Springfield, Massachusetts, USA: "U-Th-Pb monazite geochronology in kyanite gneisses, Nordøyane, Norway: Implications concerning thrusting, extension and age of outboard basement in pre-Scandian Baltica", Geological Society of America Abstracts with Programs 34(1), A82

TERRY, M.P.; ROBINSON, P.: 18.-24.08.2002, GSA Penrose Conference "Three-Dimensional Flow, Fabric Development, and Strain in Deformed Rocks and the Significance for Mountain Building Processes: New Approaches", Monte Verita, Ascona, Switzerland: "Boundary conditions and ductile flow associated with exhumation of UHP and HP rocks in the Hinterland of the Scandinavian Caledonides, Western Gneiss Region Norway", GSA Penrose Conference – Monte Verita Abstracts Volume, 77-78

TRØNNES, R.G.; FROST, D.J.; WALTER, M.J.; MCCAMMON, C.A.; NAKAMURA, E.: 06.-09.01.2002, 25th Nordic Geological Winter Meeting, Reykjavik, Iceland: "Peridotite phase relations at 21-24 GPa and variable oxygen fugacity: Implications for plume dynamics"

URAKAWA, S.; TERASAKI, H.; SOMEYA, K.; YOKOSHI, S.; KATSURA, T.; SUEDA, Y.; INOUE, T.; IRIFUNE, T.; FUNAKOSHI, K.; UTSUMI, W.; KATAYAMA, Y.: 26.-31.08.2002, 6th High Pressure Mineral Physics Seminar, Verbania, Italy[*3]: "Phase change and equations of state for high pressure phases of iron sulfide"

XU, Y.; LANGENHORST, F.; SHANKLAND, T.; RUBIE, D.C.: 24.-27.03.2002, EMPG IX, Zürich, Switzerland[*1]: "Thermal diffusivity of upper mantle phases olivine, wadsleyite, and ringwoodite to 20 GPa", Journal of Conference Abstracts 7,1, 108

[*1] EMPG IX: Ninth International Symposium on Experimental Mineralogy, Petrology and Geochemistry, 24.-27.03.2002, Zürich, Switzerland – Journal of Conference Abstracts 7,1

[*2] **AGU: American Geophysical Union Spring Meeting, 28.-31.05.2002, Washington, DC, USA – EOS Transactions, American Geophysical Union, 83(19), AGU Spring Meeting 2002 Supplement**

[*3] **HPMPS-6: 6th High Pressure Mineral Physics Seminar, 26.-31.08.2002, Verbania-Pallanza/Lago Maggiore, Italy, Hotel Castagnola – Collegio Santa Maria**

[*4] **DMG: 80. Jahrestagung der Deutschen Mineralogischen Gesellschaft, 08.-12.09.2002, Hamburg, Germany – Beihefte zum European Journal of Mineralogy 14**

[*5] **AGU: American Geophysical Union Fall Meeting, 06.-10.12.2002, San Francisco, DC, USA – EOS Transactions, American Geophysical Union, 83(47), AGU Fall Meeting 2002 Supplement**

4.4 Lectures and seminars at Bayerisches Geoinstitut

ALI, M.R.: 11.01.2002 "Temperature dependence of crystal structure of $CaTiO_3$ perovskite"

ARMBRUSTER, T.: 28.11.2002 *Mineralogical Society of America Distinguished Lecture*: "Natural zeolites: From structure to applications"

ARMBRUSTER, T.: 29.11.2002 *Mineralogical Society of America Distinguished Lecture*: "From construction kits and building blocks to complex mineral structures: How mineralogists learn what children knew for centuries"

BINA, C.: 26.06.2002 "Seismic signatures and subducted slab mineralogy"

BLÄß, U.: 13.03.2002 "Oxygen deficient perovskite phase in the system $CaSiO_3$-$CaFeO_{2.5}$"

BROMILEY, G.D.: 07.02.2002 "An experimental investigation of hydrogen solubility in pyroxenes along the diopside-jadeite tie-line"

DEMOUCHY, S.: 13.03.2002 "Water diffusion in olivine and forsterite"

DUBROVINSKAIA, N.A.: 04.07.2002 "High-temperature heater for diamond anvil cells"

FROST, D.J.: 17.01.2002 "Fe-Mg partitioning between mantle minerals"

GAILLARD, F.: 31.10.2002 "Rate of redox exchanges between H_2-bearing vapor and iron-bearing melts/glasses"

GANGULY, J.: 25.04.2002 "Solution thermodynamics, diffusion kinetics, and tectono-metamorphic processes"

GANGULY, J.: 08.10.2002 "The puzzle of the Inverted Metamorphic sequence of the Himalayas"

GATTA, G.D.: 02.07.2002 "New insights on HP-behaviour of microporous materials from X-ray single crystal data"

GRZECHNIK, A.: 04.04.2002 "Framework materials at high pressures and high temperatures"

HOLZAPFEL, C.: 07.11.2002 "Diffusion at high pressure: Methods and implications for the mantle of the Earth"

HOLZHEID, A.: 06.06.2002 "Sulfur solubility and separation in silicate melts: Implications to formation of magmatic sulfide ore deposits"

HOSOYA, T.: 02.04.2002 "An in-situ X-ray diffraction study of high-pressure transformation kinetics of enstatite"

IEZZI, G.: 12.03.2002 "Li-bearing amphibole crystal chemistry: An experimental approach"

IVANOV, B.: 17.10.2002 "Impacts do NOT initiate volcanic eruptions: A preliminary study of an impact trigger volcanism"

LANGENHORST, F.: 16.05.2002 "Shock veins in meteorites: Natural observations and experimental simulation"

MCCAMMON, C.A.: 02.05.2002 "Diamonds are not forever"

MECKLENBURGH, J.: 10.01.2002 "High-temperature creep of (Ca,Sr)TiO_3 perovskite"

MEREDITH, P.: 20.06.2002 "Long-term time-dependent rock deformation in a deep-sea laboratory"

NESTOLA, F.: 13.06.2002 "High pressure behaviour of clinopyroxenes"

OKUCHI, T.: 02.09.2002 "Hydrogen in the core"

RUBIE, D.C.: 24.01.2002 "Mechanism of metal-silicate equilibration during core formation"

SATA, N.: 19.11.2002 "High pressure studies on Fe_xO: Quasi–isothermal compression experiments and applications"

SHIRYAEV, A.: 20.09.2002 "Extended defects in diamonds: Insights from small angle X-ray scattering and positron annihilation spectroscopy"

SIMIONOVICI, A.S.: 26.09.2002 "X-ray spectroscopy for micro-imaging at ESRF"

STISHOV, S.M.: 04.06.2002 "Current state of High-Pressure Physics"

TAKAHASHI, E.: 16.09.2002 "Melting phase relations in the system Fe-FeO at 15 to 25 GPa: Introduction of some experiments at the Magma Factory"

TENNANT, C.: 15.01.2002 "New Zealand »Greenstone«/Jade/Nephrite-Myths/Legends and a little science"

UNGAR, T.: 25.06.2002 "Dislocations structure and crystallite size distribution from X-ray diffraction peak profiles"

WOODLAND, A.: 27.06.2002 "Variation of redox state with depth in the Earth's mantle"

YAGI, T.: 01.10.2002 "Development of a new high pressure technique for the study of the deep lower mantle

ZANG, S.X.: 08.08.2002 "Rheological structure of the lithosphere in North Carolina"

4.5 Scientific conferences organized by/with assistance of Bayerisches Geoinstitut

11.-15.02.2002 DMG-Short Course "High-Pressure Experimental Techniques and Applications to the Earth's Interior", Bayerisches Geoinstitut, Universität Bayreuth, Germany (D.C. RUBIE and S.J. MACKWELL)

26.-31.08.2002 6^{th} High Pressure Mineral Physics Seminar, Verbania-Pallanza/Lago Maggiore, Italy, Hotel Castagnola - Collegio Santa Maria (D.C. RUBIE, S. KEYSSNER and P. STAENDNER with D. ANDRAULT, Y. FEI, M. MANGHNANI, E. OHTANI, D. WEIDNER, T. YAGI)

01.-05.10.2002, GEO 2002, Symposium on "Accretion and early differentiation of the Earth", Würzburg, Germany (D.C. RUBIE with H. PALME)

4.6 Visiting scientists

a) Visiting scientists funded by the Bayerisches Geoinstitut

ALETTI, M., Universitá degli Studi di Palermo, Italy: 16.-19.12.2002

ARMBRUSTER, T., Universität Bern, Laboratorium für chemische und mineralogische Kristallographie, Bern, Switzerland: 28.-29.11.2002

BALOG, P., University of Western Ontario, Canada: 11.01.-13.01.2002

BINA, C.R., Northwestern University, Department of Geological Sciences, Evanston, USA: 25.-28.06.2002

CORDIER, P., Université des Sciences et Technologies de Lille, Laboratoire de Structure et Propriétés de l'Etat Solide, Villeneuve d'Ascq, France: 02.-12.04.2002

GATTA, D., Università degli Studi di Perugia, Dipartimento di Scienze della Terra, Perugia, Italy: 02.-04.07.2002

GRZECHNIK, A., Max-Planck-Institut für Festkörperforschung, Stuttgart, Germany: 04.-05.04.2002, 16.-17.06.2002

HOLZHEID, A., Westfälische Wilhelms-Universität Münster, Institut für Mineralogie, Münster, Germany: 05.-07.06.2002, 18.-27.10.2002

IEZZI, G., Universitá degli Studi di Chieti, Italy: 11.-14.03.2002, 11.-20.07.2002

IVANOV, B., Russian Academy of Sciences, Moscow, Russia: 17.10.2002

KANTOR, A., Moscow State University, Russia: 24.07.-06.08.2002

KANTOR, I., Moscow State University, Russia: 24.07.-06.08.2002

KLEMME, S., Universität Heidelberg, Mineralogisches Institut, Heidelberg, Germany: 16.-17.06.2002

KREIDIE, N., Università di Roma Tre, Dipartimento di Scienze Geologiche, Rome, Italy: 21.-27.01.2002

MASHKINA, E., Universität Erlangen, Lehrstuhl für Kristallographie und Strukturphysik, Erlangen, Germany: 09.-14.09.2002

MATTESINI, M., Uppsala University, Department of Physics, Uppsala, Sweden: 04.-07.12.2002

MORGAN, J.P., GEOMAR, Forschungszentrum für marine Geowissenschaften der Christian-Albrechts-Universität zu Kiel, Germany: 26.-27.06.2002

PETERS, L., Christian-Albrechts-Universität zu Kiel, Mineralogie-Kristallographie, Kiel, Germany: 07.-09.10.2002

SATA, N., University of Tokyo, Institute for Solid State Physics, Tokyo, Japan: 17.-21.11.2002

SCHUBERT, M., Universität Leipzig, Fakultät für Physik und Geowissenschaften, Leipzig, Germany: 22.-23.10.2002

SHIRYAEV, A., Russian Academy of Sciences, Institute of Crystallography, Department of Small-Angle X-ray Scattering and Electron Diffraction, Moscow, Russia: 18.-21.09.2002

SIMIONOVICI, A.S., European Synchrotron Radiation Facility, Grenoble, France: 25.-28.09.2002

SMYTH, J.R., University of Colorado at Boulder, Department of Geological Sciences, Boulder, USA: 11.-24.08.2002

SOFFEL, H., Ludwig-Maximilians-Universität München, Institut für Allgemeine und Angewandte Geophysik, München, Germany: 16.-17.06.2002

STEINLE-NEUMANN, G., Northwestern University, Geophysical Laboratory, Evanston, USA: 16.-20.06.2002

STISHOV, S.M., Russian Academy of Sciences, Troitsk, Moscow Region, Russia: 03.-05.06.2002

VELTHUIS, B., University of Amsterdam, The Netherlands: 05.-06.11.2002

TENNANT, C., University of Canterburry, Department of Chemistry, Christchurch, New Zealand: 13.-16.01.2002

UNGAR, T., Eotvos University Budapest, Department of General Physics, Budapest, Hungary: 23.-26.06.2002

WOODLAND, A.B., Universität Frankfurt/Main, Institut für Mineralogie, Frankfurt/Main, Germany: 27.-29.06.2002

ZANG, S.X., Universität Peking, Department of Geophysics, Beijing, China: 05.-09.08.2002

b) Visiting scientists funded by EU Programme "Access to Large-Scale Facilities"

The Bayerisches Geoinstitut is funded by the European Union under the "Access to Research Infrastructure" Programme. Visiting scientists from EU countries who wish to use the experimental (especially high pressure) facilities of the Institute are funded through this programme. Projects and visiting scientists funded during 2002 are as follows (titles of research projects in *italics*):

AITKEN, C.S., Loughborough University, Physics Department, Loughborough, U.K.: *"Raman spectroscopy of diamond like carbon"*, 18.-22.02.2002

AITKEN, C.S., Loughborough University, Physics Department, Loughborough, U.K.: *"Raman spectroscopy of diamond like carbon"*, 04.-08.11.2002

BOLFAN-CASANOVA, N., Université Blaise Pascal CNRS, Laboratoire Magmas et Volcans, Clermont-Ferrand, France: *"Effect of iron content and oxygen fugacity on the hydrogen solubility in magnesiowüstite at high pressure"*, 13.-20.04.2002

BOON, S.A., University College London, Department of Geological Sciences, London, U.K.: *"Acoustic Emissions (AE) study of olivine decomposition"*, 28.01.-03.02.2002

BOON, S.A., University College London, Department of Geological Sciences, London, U.K.: *"Acoustic Emissions (AE) study of olivine decomposition"*, 12.-19.06.2002

BUREAU, H., Laboratoire Pierre Sue, CEA/CNRS, CE Saclay, Gif sur Yvette, France: *"Experimental investigation of diamond growth in high-pressure fluids"*, 11.-22.02.2002

COMBES, R., Université de Marne la Vallée, Laboratoire des Geomateriaux, Marne la Vallée, France: *"High pressure and high temperature metal-silicate interactions in the metal Fe-Si-S and Fe-Si-C systems"*, 28.09.-05.10.2002

CORDIER, P., Université des Sciences et Technologies de Lille, Laboratoire de Structure et Propriétés de l'Etat Solide, Villeneuve d'Ascq, France: *"Plastic deformation experiments under high pressures"*, 15.07.-04.08.2002

CORNELIUS, V., University of Greenwich, School of Chemical and Life Sciences, Woolwich, London, U.K.: *"A high pressure Mössbauer study on porphyrin and iron-sulfur compounds, which are models for active sites in important mammalian and planet proteins. Investigation into pressure dependent spin states"*, 20.03.-03.04.2002

CORNELIUS, V., University of Greenwich, School of Chemical and Life Sciences, Woolwich, London, U.K.: *"A high pressure Mössbauer study on porphyrin and iron-sulfur compounds, which are models for active sites in important mammalian and planet proteins. Investigation into pressure dependent spin states"*, 25.06.-16.07.2002

CUTHBERT, S.J., University of Paisley, Biological & Geological Sciences, School of Engineering & Science, Pailsey, U.K.: *"High pressure to ultrahigh pressure metamorphic transition in the Western Gneiss Complex, Norwegian Caledonides: EMP study of the role of garnet growth and transformation in eclogites"*, 13.-25.10.2002

DMITRIEV, V., Institute National Polytechnique de Grenoble, France: *"In-situ Raman study of pressure induced amorphization in the $Eu_2(MoO_4)_3$ single crystal"*, 15.-23.07.2002

DOBSON, D.P., University College London, Department of Geological Science, London, U.K.: *"Oxygen tracer diffusion in $MgSiO_3$ perovskite"*, 16.-24.09.2002

DONG, Q., Technical University of Denmark, Department of Physics, Lyngby, Denmark: *"Atomic diffusion in bulk metallic glasses and phase transitions in nanocrystals*", 23.-29.06.2002

DONG, Q., Technical University of Denmark, Department of Physics, Lyngby, Denmark: *"Atomic diffusion in bulk metallic glasses and phase transitions in nanocrystals*", 04.-11.08.2002

DONG, Q., Technical University of Denmark, Department of Physics, Lyngby, Denmark: *"Atomic diffusion in bulk metallic glasses and phase transitions in nanocrystals*", 11.-18.11.2002

JEPHCOAT, A.P., University of Oxford, Department of Earth Sciences, Oxford, U.K.: *"(Al,Fe)-$MgSiO_3$ perovskite phases: High resolution synchrotron X-ray diffraction and Rietveld structure refinement"*, 25.02.-03.03.2002

KLEPPE, A.K., University of Oxford, Department of Earth Sciences, Oxford, U.K.: *"(Al,Fe)-$MgSiO_3$ perovskite phases: High resolution synchrotron X-ray diffraction and Rietveld structure refinement"*, 25.02.-03.03.2002

KONZETT, J., Universität Innsbruck, Institut für Mineralogie und Petrographie, Innsbruck, Germany: *"The stability of supersilicic clinopyroxene in simplified and natural bulk compositions"*, 30.09.-21.10.2002

KREIDIE, N., Università degli Studi di Roma Tre, Dipartimento di Scienze Geologiche, Rome, Italy: *"Structural and electrical properties of iron-bearing pyrope-majorite garnets"*, 28.01.-10.02.2002

LUNDEGAARD. L.F., University of Copenhagen, Geological Institute, Copenhagen, Denmark: *"Structural study of Bi_2S_3, Sb_2 and As_2S_3 at high pressure"*, 09.06.-04.07.2002

MACHON, D., Institute National Polytechnique de Grenoble, France: *"In-situ Raman study of pressure induced amorphization in the $Eu_2(MoO_4)_3$ single crystal"*, 15.-23.07.2002

MALAVERGNE, V., Université de Marne la Vallée, Laboratoire des Geomateriaux, Marne la Vallée, France: *"High pressure and high temperature metal-silicate interactions in the metal Fe-Si-S and Fe-Si-C systems"*, 22.-29.09.2002

MCENROE, S.A., Norwegian Geological Survey, Trondheim, Norway: *"Earth analogs for crustal magnetism on Mars: Igneous rocks containing hemoilmenite as discrete grains and as exsolution in pyroxenes"*, 20.01.-03.02.2002

MEREDITH, P.G., University College London, Department of Geological Sciences, London, U.K.: *"Acoustic Emissions (AE) study of olivine decomposition"*, 28.01.-07.02.2002

MEREDITH, P.G., University College London, Department of Geological Sciences, London, U.K.: *"Acoustic Emissions (AE) study of olivine decomposition"*, 17.-24.06.2002

MOLNAR, G., CNRS Toulouse, Laboratoire de Chimie de Coordination, Toulouse, France: *"Spin-crossover phenomena under pressure"*, 20.10.-01.11.2002

POE, B., Istituto Nazionale di Geofisica e Vulcanologia, Rome, Italy: *"In situ determination of mineral electrical properties at high P and T"*, 07.-19.07.2002

POE, B., Istituto Nazionale di Geofisica e Vulcanologia, Rome, Italy: *"In situ determination of mineral electrical properties at high P and T"*, 01.-14.08.2002

RABIER, J., Université de Poitiers, Laboratoire Métallurgie Physique, Futuroscope, France: *"Plastic deformation of 4H - SiC single crystals under confining pressure"*, 21.-26.01.2002

ROBINSON, P., Norwegian Geological Survey, Trondheim, Norway: *"Earth analogs for crustal magnetism on Mars: Igneous rocks containing hemoilmenite as discrete grains and as exsolution in pyroxenes"*, 01.-08.02.2002

ROMANO, C., Università degli Studi di Roma Tre, Dipartimento di Scienze Geologiche, Rome, Italy: *"Structural and electrical properties of iron-bearing pyrope-majorite garnets"*, 16.01.-02.02.2002

ROMANO, C., Università degli Studi di Roma Tre, Dipartimento di Scienze Geologiche, Rome, Italy: *"Structural and electrical properties of iron-bearing pyrope-majorite garnets"*, 13.-28.02.2002

ROZENBERG, G.K., Tel-Aviv University, School of Physics & Astronomy, Tel Aviv, Israel: *"Studies of structural, electronic and magnetic states of Mott insulators at high pressures"*, 06.-18.10.2002

SANLOUP, C., Université Pierre et Marie Curie, Paris, France: *"Preparation and investigation of solid Xe compounds relevant for the Earth"*, 21.05.-01.06.2002

SANLOUP, C., Université Pierre et Marie Curie, Paris, France: *"Preparation and investigation of solid Xe compounds relevant for the Earth"*, 07.-11.10.2002

SCHOFIELD, P., The Natural History Museum, Department of Mineralogy, London, U.K.: *"The influence of microstructure on strain partitioning in two phase olivine-magnesiowüstite aggregates"*, 04.-08.02.2002

SCHOFIELD, P., The Natural History Museum, Department of Mineralogy, London, U.K.: *"The influence of microstructure on strain partitioning in two phase olivine-magnesiowüstite aggregates"*, 06.-10.05.2002

SCHOFIELD, P., The Natural History Museum, Department of Mineralogy, London, U.K.: *"Preparation and characterization of synthetic pyroxenes"*, 27.06.-10.07.2002

SIEBERT, J., Université de Marne la Vallée, Laboratoire des Geomateriaux, Marne la Vallée, France: *"High pressure and high temperature metal-silicate interactions in the metal Fe-Si-S and Fe-Si-C systems"*, 22.09-05.10.2002

STOYANOVA, R., Bulgarian Academy of Sciences, Institute of General and Inorganic Chemistry, Sofia, Bulgaria: *"High pressure synthesis of electrode materials for lithium-ion batteries; II. Stabilization of $LiNi_{1-y}GayO_2$ solid solutions under high-oxygen pressure"*, 16.06.-01.07.2002

TARANTINO, S., Università degli Studi di Pavia, Dipartimento di Scienza della Terra, Pavia, Italy: *"Solid solution and phase transition in columbite-tantalite minerals"*, 10.-20.03.2002

THILLY, L., Université de Poitiers, Laboratoire Métallurgie Physique, Futuroscope, France: *"Plastic deformation of 4H - SiC single crystals under confining pressure"*, 21.-26.01.2002

TITLER, P.J., University of Greenwich, School of Chemical and Life Sciences, Woolwich, London, U.K.: *"A high pressure Mössbauer study on porphyrin and iron-sulfur compounds, which are models for active sites in important mammalian and planet proteins. Investigation into pressure dependent spin states"*, 20.03.-03.04.2002

TSIERKEZOS, N.G., University of Athens, Laboratory of Physical Chemistry, Department of Chemistry, Athens, Greece: *"Ion-solvent interactions of 1:1 electrolytes in N, N-dimethyl-formamide (DMF) – water mixtures"*, 16.-23.06.2002

TRØNNES, R.G., Nordic Volcanological Institute, Reykjavik, Island: *"Peridotite phase relations at 22-25 GPa and variable oxygen fugacity – important geophysical implications"*, 10.-23.11.2002

WEBB, S., Georg-August-Universität Göttingen, Experimentelle und Angewandte Mineralogie, Göttingen, Germany: 27.03.2002

WEBB, S., Georg-August-Universität Göttingen, Experimentelle und Angewandte Mineralogie, Göttingen, Germany: 12.12.2002

c) Visiting scientists supported by other externally funded BGI projects

GÖBBELS, M., Universität Erlangen, Mineralogisches Institut, Erlangen, Germany: 03.01.2002

MAGERL, A., Universität Erlangen, Lehrstuhl für Kristallographie und Strukturphysik, Erlangen, Germany: 03.01.2002

MASHKINA, E., Universität Erlangen, Lehrstuhl für Kristallographie und Strukturphysik, Erlangen, Germany: 15.-28.01.2002

d) Visitors (externally funded)

BYSTRICKY, M., ETH Zürich, Geologisches Institut, Switzerland: 23.09.-04.10.2002
DE RONDE, A., Universität Basel, Geologisch-Paläontologisches Institut, Switzerland: 10.-13.11.2002
DEUTSCH, A., Universität Münster, Institut für Planetologie, Münster, Germany: 19.-20.03.2002, 17.-20.07.2002
DOBMEIER, C., Freie Universität Berlin, Institut für Geologische Wissenschaften, Fachrichtung Geologie, Berlin, Germany: 09.-13.09.2002
DOLLASE, W., University of California, Department of Earth and Space Sciences, Los Angeles, USA: 16.09.-20.11.2002
EL GORESY, A., Max-Planck-Institut für Chemie, Mainz, Germany: 07.-09.10.2002
FUNAMORI, N., University of Tokyo, Department of Earth and Planetary Science, Japan: 23.-24.08.2002
GANICZ, K., Akademie der Wissenschaften, Lodz, Poland: 01.-31.07.2002
GLASER, R., Ben Gurion University, Beer-Sheva, Israel: 19.-24.02.2002
GLICKSMAN, M., Rensselaer Polytechnic Institute, New York, USA: 21.-23.05.2002
HIRAGA, T., University of Minnesota, USA, 03.-06.03.2002
HIRAI, H., University of Tsukuba, Insitute of Geoscience, Tsukuba, Japan: 11.07.-23.08.2002
HIRAO, N., Tohoku University, Japan: 28.03.-01.04.2002
HOLZHEID, A., Universität Münster, Institut für Mineralogie, Münster, Germany: 21.-28.07.2002
HOLTZMAN, B., University of Minnesota, USA: 10.-17.06.2002
HORNEMANN, U., Fraunhofer Institut für Kurzzeitdynamik, Ernst-Mach-Institut, Efringen, Germany: 19.-20.03.2002
HOSOYA, T., Tohoku University, Japan: 28.03.-01.04.2002
KAMENEV, K., University of Edinburgh, Department of Physics & Astronomy, Edinburgh, U.K.: 14.-16.10.2002
KOCH, M., Ruprecht-Karls-Universität Heidelberg, Mineralogisches Institut, Heidelberg, Germany: 02.-04.05.2002, 10.-14.05.2002, 15.-29.07.2002
KOMABAYASHI. T., Tokyo Institute of Technology, Department of Earth & Planetary Sciences, Maruyama & Hirose Laboratory, Tokyo, Japan: 12.09.-31.12.2002
KONDO, T., Tohoku University, Japan: 28.03.-01.04.2002
KUBO, T., Tohoku University, Japan: 31.03.-03.04.2002
LUPULESCU, A., Rensseler Polytechnique, New York, USA: 21.-23.05.2002
MASHKINA, E., Universität Erlangen, Lehrstuhl für Kristallographie und Strukturphysik, Erlangen, Germany: 01.01.-31.05.2002

MASHKINA, E., Universität Erlangen, Lehrstuhl für Kristallographie und Strukturphysik, Erlangen, Germany: 07.-13.10.2002

MIBE, K., Carnegie Institution of Washington, Geophysical Laboratory, USA: 11.07.-02.08.2002

MILHALFFY, P., University of Colorado at Boulder, USA: 18.09.-25.10.2002

MIYAJIMA, N., University of Tokyo, The Institute for Solid State Physics, Chiba, Japan: 25.-28.06.2002, 23.-25.08.2002, 31.08.-08.09.2002

NISHIHARA, Y., Tokyo Institute of Technology, Earth & Planetary Sciences, Tokyo, Japan: 02.-05.09.2002

NOWAK, M., Universität Hannover, Germany: 20.-22.02.2002

OKADA, T., Spring-8, Japan Synchrotron Radiation Research Institute, Hyogo, Japan: 01.-03.09.2002

OKUCHI, T. Nagoya University, Japan: 01.-03.09.2002

PATERSON, M., Australian National University, Canberry, Australia: 31.05.-09.06.2002

RAKIC, S., Universität Bremen, Germany: 20.-26.01.2002

REICHMANN, H.-J., GeoForschungsZentrum Potsdam, Germany: 24.-26.04.2002, 14.-16.08.2002, 18.-20.11.2002

SASWATA, M., University of Minnesota: 19.04.-14.05.2002

SHCHEKA, S., Universität Tübingen, Germany: 05.-15.05.2002, 14.-18.10.2002

TALYZIN, A., Uppsala University, Sweden: 10.03.-12.04.2002, 24.-30.11.2002

TANGE, Y., Tokyo Institute of Technology, Earth & Planetary Sciences, Tokyo, Japan: 02.-05.09.2002

TAKAHASHI, E., Tokyo Institute of Technology, Earth & Planetary Sciences, Tokyo, Japan: 02.-23.09.2002

VANPETEGHEM, C., Tohoku University, Japan: 09.-15.05.2002

4.7 Theses

REID, J.: Transport Properties of Silicate Liquids at High Pressure

FORTENFANT, S.: Experimental Study on the Partitioning Behaviour of the Siderophile Elements (Ni, W, Mo, Pt, Ph, Re and Os) and Geochemical Relevance

4.8 Honours and awards

Dan FROST	received the Max Hey Medal of the Mineralogical Society of Great Britain
Christian HOLZAPFEL	received the Student Paper Award of the American Geophysical Union; Spring Meeting in Boston
Catherine MCCAMMON	elected a Fellow of the Mineralogical Society of America

Joy REID	received the Bernd-Rendel-Prize of the German Research Council (DFG) for young graduated scientists
Friedrich SEIFERT	received the Werner Heisenberg Medal of the Alexander von Humboldt-Foundation

4.9 Editorship of scientific journals

MACKWELL, S.J.	Editorial Board, "Physics and Chemistry of Minerals"
	Editor (Solid Earth), "Geophysical Research Letters"
	Editor-in-Chief, "Geophysical Research Letters"
MCCAMMON, C.A.	Editorial Advisory Board of "Physics and Chemistry of Minerals"
	Advisory Board of "Mössbauer Information Exchange"
RUBIE, D.C.	Editor-in-Chief, Physics of the Earth and Planetary Interiors
SEBALD, A.	Editorial Board of "Solid State Nuclear Magnetic Resonance"
SEIFERT, F.	Editorial Advisory Board of "Physics and Chemistry of Minerals"

4.10 Membership of scientific advisory bodies

MACKWELL, S.J.	Panel for "Universitäre Forschungsinitiativen – Leistungsfähigkeit durch Kooperation", Stifterverband für die Deutsche Wissenschaft
	Panel for Alexander von Humboldt-Foundation Research Fellowships Program
	Panel for "Internationale Qualitäts-Netze", Deutscher Akademischer Austauschdienst (DAAD)
	Panel for Schwerpunktprogramm "Internationales Kontinentales Bohrprogramm (ICDP)", Deutsche Forschungsgemeinschaft
	Member of User’s Selection Panel, EU Large Scale Facility, Bayerisches Geoinstitut
	Member of Forschungskollegium Physik des Erdkörpers e.V.
	Member of AGU Mineral and Rock Physics Committee
	Panel for NASA’s Planetary Geology and Geophysics (PGG) research program
MCCAMMON, C.A.	Member of ESRF Beam Line Review Panel ID-22
	Nominating committee for Officers of the Mineralogical Society of America
	Nominating committee for Committee members of the Mineralogical Society of America

RUBIE, D.C.	Member of AGU Mineral and Rock Physics Executive Committee
	Member of AGU Mineral and Rock Physics Student Award Committee
	Member of AGU Physical Properties of Earth Materials Steering Committee
	Member of Geochemical Society Fellows Committee
	Member of Roebling Medal Committee, Mineralogical Society of America
	Member of User's Selection Panel, EU Large Scale Geochemical Facility, University of Bristol, UK
	Member of SIMS Steering Committee, GFZ, Potsdam
SEBALD, A.	Chairperson of the German Magnetic Resonance Discussion Group, 2001-2004
SEIFERT, F.	Senate and Hauptausschuß of German Science Foundation (DFG)
	Senats-Kommission für geowissenschaftliche Gemeinschaftsforschung (DFG)
	DFG-Senatskommission Perspektiven der Forschung
	Alexander von Humboldt Science Award Committee (until April 2002)
	Committee for Glaciology, Bavarian Academy of Sciences
	Forschungskollegium Mineralogie
	Mitglied des Kuratoriums des Geo-Zentrums an der KTB e. V.
	Academia Europaea, London
	Deutsche Akademie der Naturforscher Leopoldina, Halle
	Bayerische Akademie der Wissenschaften, München
	Akademie der Wissenschaften, Göttingen

4.11 Public relations and press reports

LANGENHORST, F. (2002): Einschlagskrater auf der Erde – Zeugen kosmischer Katastrophen. Sterne und Weltraum 6, 34-44

POIRIER, J.-P.; LANGENHORST, F. (2002): Der innere Aufbau unseres Planeten. Sterne und Weltraum 11, 30-40

5. Scientific and Technical Personnel

Name		Position	Duration in 2002	Funding source
BAILEY, Edward	Dr.	Wiss. Angestellter	to 15.03.	BGI/VP
BALOG, Paul	Dr.	Wiss. Angestellter	from 14.01. to 31.12.	EU, NSERC
BECHMANN, Matthias	Dipl.-Phys.	Wiss. Angestellter		DFG
BLÄß, Ulrich	Dipl.-Min.	Wiss. Angestellter		DFG
BÖHM, Ulrich		Mechaniker		BGI
BÖSS, Wolfgang	RAR	Verwalt. Beamter		BGI
BOFFA BALLARAN, Tiziana	Dr.	Sofia Kovalevskaja-Preisträgerin		AvH
BROMILEY, Fiona	B.Sc.	Stipendiatin		AvH[1]
BROMILEY, Geoffrey	Dr.	Wiss. Angestellter		EU
BYSTRICKY, Misha	Dr.	Wiss. Angestellter	from 01.01. to 31.03.	BGI/VP
COUVY, Hélène	Dipl.-Geol.	Wiss. Angestellte	to 16.11. from 17.11.	BGI/VP EU
DEMOUCHY, Sylvie	Dipl.-Geol.	Wiss. Angestellte		EU
DOBSON, David	Dr.	Forschungsstipendiat	to 31.03.	AvH
DUBROVINSKAIA, Natalia	Dr.	Wiss. Angestellte		BGI
DUBROVINSKY, Leonid	Dr.	Akad. Oberrat		BGI
FISCHER, Heinz		Mechaniker		BGI
FROST, Daniel	Dr.	Akad. Rat z.A.		BGI
GAILLARD, Fabrice	Dr.	Wiss. Angestellter		BGI/VP
GATTA, Giacomo Diego	Dr.	Wiss. Angestellter	from 15.10.	AvH[1]
GOLLNER, Gertrud		Chem.-Techn. Assistentin		BGI
HEIDELBACH, Florian	Ph.D.	Wiss. Assistent		BGI
HELLUY, Xavier	Dr.	Wiss. Angestellter		DFG
HERRMANNSDÖRFER, Georg		Mechaniker		BGI
HOLZAPFEL, Christian	Dipl.-Min.	Wiss. Angestellter		EU
IEZZI, Gianluca	Dr.	Wiss. Angestellter	from 01.11.	AvH[1]
JACOBSEN, Steven	Dr.	Forschungsstipendiat	from 01.01.	AvH
KEYSSNER, Stefan	Dr.	Akad. Oberrat		BGI
KISON-HERZING, Lydia		Sekretärin		BGI
KLASINSKI, Kurt	Dipl.-Ing. (FH)	Techn. Angestellter		BGI
KRAUßE, Detlef	Dipl.-Inform. (FH)	Techn. Angestellter		BGI

KRIEGL, Holger		Haustechniker		BGI
LANGENHORST, Falko	PD Dr.	Akad. Rat		BGI
LEITNER, Oskar		Präparator		BGI
LIEBSKE, Christian	Dipl.-Min.	Wiss. Angestellter		DFG
LINHARDT, Sven		Elektroniker		BGI
MACKWELL, Stephen	Prof. Dr.	Leiter	to 30.11.	BGI
MARKERT, Anke		Techn. Angestellte		EU
MARTON, Fred	Dr.	Wiss. Angestellter		BGI/VP
MCCAMMON, Catherine	Dr.	Akad. Oberrätin		BGI
MECKLENBURGH, Julian	Dr.	Wiss. Angestellter		BGI/VP
MIYAJIMA, Nobuyoshi	Dr.	Wiss. Angestellter	to 28.02.	BGI/VP
NEUFELD, Kai	Dipl.-Geol.	Wiss. Angestellter		BGI/VP
NING, Jie Yuan	Dr.	Stipendiat		UBT
POE, Brent	Dr.	Wiss. Assistent	to 28.02.	BGI
PRINZ, Esther		Wiss. Hilfskraft	to 15.04.	BGI/VP
POIRIER, Jean-Paul	Prof. Dr.	Forschungs-preisträger	from 06.03. to 31.05.	AvH
RAMMING, Gerd		Elektroniker		BGI
RAUSCH, Oliver		Mechaniker		BGI
REID, Joy	M.Sc.	Wiss. Angestellte	to 31.01.	DFG
RUBIE, David C.	Prof. Dr.	Stellvertr. Leiter		BGI
SCHMICKLER, Bettina	Dr.	Wiss. Angestellte	from 01.02.	DFG, EU
SCHMIDT, Burkhard	Dr.	Wiss. Angestellter		BGI/VP
SCHULZE, Hubert		Präparator		BGI
SEBALD, Angelika	PD Dr.	Wiss. Angestellte		DFG
SEIFERT, Friedrich	Prof. Dr.	Stellvertr. Leiter		BGI
SPETZLER, Hartmut	Prof. Dr.	Gastprofessor	01.03.-30.06.	DFG
STÄNDNER, Petra		Fremdsprachen-Sekretärin		BGI
STEINBERGER, Bernhard	Dr.	Wiss. Angestellter	01.09.-31.10.	DFG
STEINLE-NEUMANN, Gerd	Dr.	Juniorprofessor	from 15.12.	BGI
STRETTON, Iona	Dr.	Wiss. Assistentin		BGI
SUZUKI, Akio	Dr.	Wiss. Angestellter	to 03.03.	BGI/VP
		Forschungsstipendiat	from 01.05.	AvH
TERASAKI, Hidenori	Dr.	Wiss. Angestellter	from 01.04.	DFG, BGI/VP
TERRY, Michael	Dr.	Wiss. Angestellter	from 01.06.	BGI/VP
YAGI, Takehiko	Prof. Dr.	Forschungspreis-träger	from 11.07. to 03.10.	AvH

Abbreviations/explanations:

BGI	Staff Position of Bayerisches Geoinstitut
BGI/VP	Visiting Scientists' Program of Bayerisches Geoinstitut
DFG	German Science Foundation
EU	European Union
AvH	Alexander von Humboldt Foundation
UBT	University of Bayreuth, Germany
NSERC	Natural Science and Engineering Research Council of Canada

[1] Sofia Kovalevskaja-Preis

Index

Abrikosov, I. 75
Ahuja, R. 50, 137, 145
Althoff, G. 173
Bechmann, M. 173, 174
Bläß, U.W. 48
Boffa Ballaran, T. 21, 48, 59, 63, 65, 66, 69, 150
Boon, S.A. 164
Boussekso, A. 152
Bromiley, F.A. 59, 115, 170
Bromiley, G.D. 40, 105, 150, 170
Bureau, V 117
Carpenter, M.A. 62
Combes, R. 78
Cordier, P. 28
Couvy, H. 28
Demouchy, S. 111, 113, 115
Deutsch, A. 101, 103
Dmitriev, V. 56, 135, 153
Dobmeier, C. 37, 38
Dobson, D.P. 53, 75, 164
Dubrovinskaia, N.A. 21, 53, 54, 56, 67, 75, 100, 119, 137, 143, 168
Dubrovinsky, L.S. 21, 50, 53, 54, 56, 67, 75, 98, 100, 119, 135,
..... 137, 140, 141, 143, 145, 152, 153, 168
Dupas-Bruzek, C. 157
Dupree, R. 128
El Goresy, A. 98
Feldman, V. 100
Foerster, H. 173, 174
Frost, D.J. 24, 28, 48, 78, 80, 82, 85, 88, 90, 108, 109, 117, 132, 165
Gaillard, F. 113, 115, 124, 126, 129
Gallien, J.-P. 117
Ganguly, J. 88
Gillet, P. 98
Goto, H. 165
Guyot, F. 78
Heidelbach, F. 25, 27, 28, 30, 37, 38, 42, 92
Helluy, X. 173
Herrmansdörfer, G. 161
Holl, C.M. 24, 108
Holzapfel, C. 80
Hornemann, U. 101
Jacobsen, S.D. 20, 21, 24, 108, 113, 161, 170
Jephcoat, A.P. 109
Johansson, B. 75, 137

Kahlenberg, V. 61
Keppler, H. 105, 170
Kitazawa, T. 152
Klasinski, K. 161
Kleppe, A.K. 109
Knight, K. 62
Kohlstedt, D.L. 30
Kolev, K. 157
Konzett, J. 90
Kopylova, M. 84
Kozlov, E. 100
Kreidie, N. 32
Kuznetov, A. 135
Langenhorst, F. 40, 42, 48, 53, 54, 56, 59, 75, 95, 96, 101, 103, 108, 117, 153, 157, 172
Laude, L.D. 157
Liebske, C. 82, 121
Linhardt, S. 161
Lounejeva, E. 103
Lundegaard, L. 66
Machon, D. 153
Mackwell, S.J. 25, 27, 28, 80, 111, 113, 116
Majumder, S. 30
Malavergne, V. 78
Marton, F.C. 34, 35, 36
Masaitis, V.L. 98
Mashkina, E. 148
McCammon, C.A. 32, 44, 47, 48, 53, 84, 108, 126, 127, 148
McEnroe, S.A. 40, 42
Mecklenburgh, J. 25, 116
Melosh, H.J. 73
Meredith, P.G. 164
Miyajima, N. 172
Molnar, G. 152
Müller, K. 161
Nestola, F. 63, 65
Neufeld, K. 116
Ning, J.-Y. 35
Ohlmeyer, H. 161
Osorio Guillen, J.M. 137
Padro, D. 128
Pietschnig, R. 173
Poe, B.T. 32, 121
Poirier, J.-P. 96
Ponyatovsky, E. 153
Prakapenka, V. 56
Rakic, S. 61

Reichmann, H.-J. 21, 161
Righter, K. 73
Ríos, V 69
Robinson, P. 40, 42, 95
Roggensack, K. 115
Romano, C. 32
Ross, N.L. 47
Rozenberg, G.K. 50, 145
Rubie, D.C. 34, 35, 36, 73, 75, 80, 82, 121, 123, 132, 165
Sanloup, C. 89
Sazonova, L. 100
Schertl, H.-P. 96
Schmickler, B. 121
Schmidt, B.C. 61, 89, 126, 128, 129
Schulze, H. 161
Sebald, A. 173, 174
Seifert, F. 25, 48, 54, 56, 148
Shankland, T.J. 34
Shaw, C. 117
Siebert, J. 78
Sinitsin, V. 153
Smyth, J.R. 24, 108, 109, 161
Spetzler, H.A. 24, 161
Steinberger, B. 36
Stern, C. 113
Stoyanova, R. 150
Streck, M. 127
Stretton, I.C. 27, 116
Suzuki, A. 121, 123
Swamy, V. 67, 143
Talyzin, A. 140, 141
Tekely, P. 174
Tennant, W.C. 44
Terasaki, H. 121, 132
Terry, M.P. 92, 95
Tribaudino, M. 63, 65
Trønnes, R.G. 82
Van Aken, P.A. 48
Vocadlo, L. 53
Weber, H.-P. 56, 135
Wilkins, C.J. 44
Williamson, B.E. 44
Wood, I.G. 53
Yagi, T. 165